TKK Dissertations 61
Espoo 2007

STUDY ON NUMERICAL AND MODELLING ERRORS IN LES USING A PRIORI AND A POSTERIORI TESTING

Doctoral Dissertation

Tellervo Brandt

Helsinki University of Technology
Department of Mechanical Engineering
Laboratory of Aerodynamics

TKK Dissertations 61
Espoo 2007

STUDY ON NUMERICAL AND MODELLING ERRORS IN LES USING A PRIORI AND A POSTERIORI TESTING

Doctoral Dissertation

Tellervo Brandt

Dissertation for the degree of Doctor of Science in Technology to be presented with due permission of the Department of Mechanical Engineering for public examination and debate in Auditorium K216 at Helsinki University of Technology (Espoo, Finland) on the 2nd of March, 2007, at 12 noon.

Helsinki University of Technology
Department of Mechanical Engineering
Laboratory of Aerodynamics

Teknillinen korkeakoulu
Konetekniikan osasto
Aerodynamiikan laboratorio

Distribution:
Helsinki University of Technology
Department of Mechanical Engineering
Laboratory of Aerodynamics
P.O. Box 4400
FI - 02015 TKK
FINLAND
URL: http://www.aero.tkk.fi/
Tel. +358-9-451 3505
Fax +358-9-451 3418
E-mail: Tellervo.Brandt@tkk.fi

ISBN 978-951-22-8634-8
ISBN 978-951-22-8635-5 (PDF)
ISSN 1795-2239
ISSN 1795-4584 (PDF)
URL: http://lib.tkk.fi/Diss/2007/isbn9789512286355/

TKK-DISS-2266

Otamedia Oy
Espoo 2007

HELSINKI UNIVERSITY OF TECHNOLOGY
P. O. BOX 1000, FI-02015 TKK
http://www.tkk.fi

ABSTRACT OF DOCTORAL DISSERTATION

Author Tellervo Brandt

Name of the dissertation

Study on numerical and modelling errors in LES using a priori and a posteriori testing

Manuscript submitted 6.10.2006 | Manuscript revised 24.1.2007

Date of the defence 2.3.2007

[X] Monograph | [ ] Article dissertation (summary + original articles)

Department Department of Mechanical Engineering
Laboratory Laboratory of Aerodynamics
Field of research Fluid Dynamics (K103Z)
Opponent(s) Prof. Bernard Geurts
Supervisor Prof. Jaakko Hoffren
Instructor Prof. Jaakko Hoffren

Abstract

Large eddy simulation (LES) is an approach to numerical simulation of turbulent flows. The so-called large scales are solved from the Navier–Stokes equations and the effect of the subgrid scales (SGS) is modelled. This thesis concentrates on the numerical and modelling error of LES where second-order finite-difference schemes and simple SGS models are applied. The work is restricted to these methods because they are often applied in practical LES, and some groups have reported results concerning a large numerical error related to low-order finite-difference-type schemes when compared to the effect of the SGS model. The research work of this thesis is divided into three parts. First, the error components are studied a priori. The focus is on a priori testing of the explicit filtering of the non-linear convection term of the Navier–Stokes equations, which has been suggested as a method to reduce the numerical error. In the second part, explicit filtering is applied in actual LES. The aim is to clarify if it is possible to improve the actual simulation results by explicit filtering as suggested by the a priori studies. In addition, the use of implicit filtering provided by both eddy-viscosity-type models and so-called subfilter-scale (SFS) models are compared to explicit filtering. In the third part, the error components are studied a posteriori using so-called grid-independent LES with and without explicit filtering and the Richardson extrapolation. The aims are related to separating the error components, clarifying the effect of explicit filtering, grid resolution and SGS model parameters on the components and to comparing the approaches. As a test case, a fully developed turbulent channel flow between two parallel walls is applied in all three parts of the thesis. The results of the a priori tests suggest that explicit filtering of the non-linear convection term effectively reduces the numerical error and increases the effect of the SGS model. However, in the actual performed simulations, explicit filtering increased the total simulation error and decreased the effect of the applied SGS models. Based on the performed a posteriori tests, in actual simulations with the standard Smagorinsky model, the numerical and modelling error are of the same magnitude, and explicit filtering with a smooth filter introduces a third error component which is larger than the other two error components. Of the applied approaches, the a posteriori tests using the grid-independent LES explain the behaviour of the actual simulations. The numerical error predicted by the a priori tests is too large and the effect of SGS modelling and explicit filtering are not properly described. The Richardson extrapolation for the numerical error is not valid at the applied grid resolution.

Keywords CFD, LES, a posteriori testing, numerical error, modelling error, explicit filtering

ISBN (printed) 978-951-22-8634-8 | ISSN (printed) 1795-2239

ISBN (pdf) 978-951-22-8635-5 | ISSN (pdf) 1795-4584

Language English | Number of pages 183

Publisher Laboratory of Aerodynamics

Print distribution Laboratory of Aerodynamics

[X] The dissertation can be read at http://lib.tkk.fi/Diss/

TEKNILLINEN KORKEAKOULU
PL 1000, 02015 TKK
http://www.tkk.fi

VÄITÖSKIRJAN TIIVISTELMÄ

Tekijä Tellervo Brandt

Väitöskirjan nimi

Suurten pyörteiden simuloinnissa esiintyvän numeerisen virheen ja mallinnusvirheen tarkastelu a priori ja a posteriori

Käsikirjoituksen päivämäärä 6.10.2006 | Korjatun käsikirjoituksen päivämäärä 24.1.2007

Väitöstilaisuuden ajankohta 2.3.2007

[X] Monografia | [ ] Yhdistelmäväitöskirja (yhteenveto + erillisartikkelit)

Osasto Konetekniikan osasto
Laboratorio Aerodynamiikan laboratorio
Tutkimusala Virtausmekaniikka, (K103Z)
Vastaväittäjä(t) Prof. Bernard Geurts
Työn valvoja Prof. Jaakko Hoffren
Työn ohjaaja Prof. Jaakko Hoffren

Tiivistelmä

Suurten pyörteiden simulointi (LES) on lähestymistapa turbulentin virtauksen numeeriseen simulointiin. Nk. suuret pyörteet ratkaistaan Navier–Stokesin yhtälöistä ja alihilapyörteiden vaikutus mallinnetaan. Tässä väitöskirjassa keskitytään LES:n numeeriseen virheeseen ja mallinnusvirheeseen tilanteessa, jossa käytetään toisen kertaluvun differenssimemetelmää ja yksinkertaisia alihilamalleja. Työ keskittyy näihin menetelmiin, koska ne ovat yleisesti käytössä LES:n käytännön sovelluksissa ja koska kirjallisuudessa on raportoitu alhaisen kertaluvun differenssimenetelmiin liittyvän numeerisen virheen olevan suuri verrattuna alihilamallin vaikutukseen. Väitöskirjan tutkimustyö on jaettu kolmeen osaan. Ensimmäisessä osassa virhekomponentteja tarkastellaan a priori. Pääpaino on Navier–Stokesin yhtälöiden epälineaarisen termin eksplisiittisessä suodatuksessa, jota on kirjallisuudessa ehdotettu käytettäväksi numeerisen virheen pienentämiseen. Toisessa osassa eksplisiittistä suodatusta sovelletaan LES:ssä. Tavoitteena on selvittää, voiko suodatuksella parantaa simulointitulosta kuten a priori -tarkastelujen pohjalta voisi päätellä. Lisäksi sekä pyörreviskositeettimallien että nk. alisuodinmallien implisiittistä suodatusta verrataan eksplisiittiseen suodatukseen. Kolmannessa osassa virhekomponentteja tarkastellaan a posteriori käyttäen nk. hilariippumatonta LES:iä eksplisiitisen ja implisiittisen suodatuksen kanssa sekä Richardsonin ekstrapolointia. Tavoitteet liittyvät virhekomponenttien erottamiseen, suodatuksen, hilaresoluution ja malliparametrien vaikutuksen selvittämiseen sekä lähestymistapojen vertailuun. Kaikissa kolmessa väitöskirjan osassa testitapauksena on täysin kehittynyt turbulentti kanavavirtaus kahden yhdensuuntaisen seinämän välissä. A priori -testien perusteella Navier–Stokesin yhtälöiden epälineaarisen termin suodatus pienentää numeerista virhettä ja kasvattaa alihilamallin vaikutusta. Kuitenkin varsinaisissa simuloinneissa suodatus kasvatti kokonaisvirhettä ja pienensi käytettyjen alihilamallien vaikutusta. Tehtyjen a posteriori -testien perusteella simuloinnissa, jossa käytetään tavallista Smagorinsky-mallia, numeerinen virhe ja mallinnusvirhe ovat suunnilleen saman suuruiset ja suodatus tuo mukaan kolmannen virhekomponentin, joka on kahta muuta suurempi. Käytetyistä virhetarkastelutavoista a posteriori -testit, joissa käytettiin hilariippumatonta LES:iä, selittivät parhaiten simulointituloksia. A priori -testeissä saatu numeerinen virhe on liian suuri ja ne eivät kuvanneet oikein mallin ja suodatuksen vaikutusta. Richardsonin ekstrapoloinnin taustaoletukset eivät ole voimassa käytetyllä hilaresoluutiolla.

Asiasanat CFD, LES, a posteriori -testaus, numeerinen virhe, mallinnusvirhe, eksplisiittinen suodatus

ISBN (painettu) 978-951-22-8634-8 | ISSN (painettu) 1795-2239

ISBN (pdf) 978-951-22-8635-5 | ISSN (pdf) 1795-4584

Kieli englanti | Sivumäärä 183

Julkaisija Aerodynamiikan laboratorio

Painetun väitöskirjan jakelu Aerodynamiikan laboratorio

[X] Luettavissa verkossa osoitteessa http://lib.tkk.fi/Diss/

Preface

The research work presented in this thesis has been done in the Laboratory of Aerodynamics at Helsinki University of Technology (TKK). Prof. Jaakko Hoffren became the supervisor of this work after the retirement of Prof. Seppo Laine. I would like to thank both of them for the opportunity to work at the laboratory and for their encouragement during my post-graduate studies. Prof. Jaakko Hoffren has provided many detailed comments on my work and papers, and during these years I have learned a lot from him.

The thesis work was mainly funded by the Finnish Graduate School in Computational Fluid Dynamics whose director is Prof. Timo Siikonen. This type of research work would not have been possible without the graduate school. Additional funding has been provided by the Finnish Technology Agency (TEKES) within the TURBU-project and the Finnish Cultural Foundation. All these contributions are gratefully acknowledged.

The pre-examiners of this theses were Dr. Jochen Fröhlich and Dr. Jessica Gullbrand. I would like to thank them for the comments I received on the manuscript.

Since this thesis is based on numerical simulations, a working computer system was necessary. Part of the computer capacity was provided by CSC, Scientific Computing Ltd, and part of the simulations were performed on the laboratory's own computer system. Special thanks belong to our laboratory manager, Mr. Mikko Korhonen for all his work and devotion to keeping the computers running. The channel flow code applied in this study is based on a DNS channel flow code written by Dr. Bendiks Jan Boersma from TU Delft. Dr. Geert Brethouwer from KTH Sweden kindly assisted me with this code and taught me the basics of doing DNS.

Since there is no research without colleagues, some people working in the CFD-group of TKK should be mentioned. I would like to thank Dr. Antti Hellsten for all the good conversations we have had and his work for the benefit of our group. Mrs. Katariina Pohjola has given helpful and encouraging comments on my papers, presentations and teaching, and has been a good friend also outside the office. Dr. Petri Majander has provided good comments and advice on LES. In addition, we have many nice people working in the laboratory who keep up

the good spirit. It is not possible to mention all of them by name here, but they are all acknowledged, especially Mr. Timo Sailaranta's funny comments and Ms. Tytti Nyman's and Ms. Mervi Ritvala's help with many practical things.

I should also acknowledge Prof. Jerzy Matusiak who introduced me to CFD when I was an under-graduate student. I would like to thank him and Prof. Eero–Matti Salonen and Prof. Raimo von Hertzen for all the advice I have received during both my under-graduate and post-graduate studies.

Finally, I wish to thank my parents, Eila and Kimmo Juurmaa, for all the love, encouragement and support I have received. Ups and downs belong to research work, and I have been very lucky to be able to share all this and much more with my beloved husband Sami.

Espoo 24.1.2007

Tellervo Brandt

Contents

List of symbols **13**

1 Introduction **17**

1.1 Turbulence 17

1.2 On Numerical Simulation of Turbulent Flows 18

1.3 Previous Research 20

1.4 Formulation of Present Research Problems 23

2 Applied Models and Numerical Methods **27**

2.1 Equations Being Solved in LES 27

2.1.1 Equations Describing the Flow of an Incompressible Fluid 27

2.1.2 Applied Subgrid-Scale Models 29

2.2 Explicit Filtering in LES 36

2.2.1 No Filtering in LES? 36

2.2.2 Different Approaches to Explicit Filtering 37

2.2.3 Properties of Some Filter Functions 40

2.3 Applied Numerical Methods 50

2.3.1 Spatial Grid System and Discretization 50

2.3.2 Pressure Correction Method 51

2.3.3 Time Integration 53

2.3.4 Performing the Actual Simulations 54

2.4 Code Validation in DNS of Channel Flow 55

2.4.1 Flow Statistics 55

2.4.2 Order of the Applied Code 63

3 A Priori Testing of Numerical Error and Explicit Filtering 67
3.1 DNS Data . . . 67
3.2 Explicit Filtering of the Whole Velocity Field . . . 68
3.3 Explicit Filtering of Only the Non-Linear Term . . . 74
3.4 Difference between the Two Approaches . . . 75
3.5 Three-Dimensional Filtering . . . 80
3.6 Conclusions of the a Priori Tests . . . 84

4 Explicit filtering in LES 87
4.1 Comparison between Two Approaches to Explicit Filtering . . . 87
4.2 Effect of Filter Shape . . . 96
4.3 Effect of Filtering versus Effect of SGS Modelling . . . 100
4.4 Explicit and Implicit Filtering . . . 105
4.5 Effect of SFS Modelling with Explicit Filtering . . . 109
4.6 SFS Filtering versus Filtering of Convection Term . . . 116
4.7 Conclusions of Application of Explicit Filtering . . . 122

5 A Posteriori Tests on Numerical and Modelling Error in LES 125
5.1 A Posteriori Tests Using Implicit Filtering . . . 125
5.1.1 Grid-independent LES Using Implicit Filtering . . . 126
5.1.2 Applied Grid Resolutions . . . 127
5.1.3 Effect of Varying Grid Resolution on Numerical and Modelling Error . . . 127
5.1.4 Effect of Varying Model Length Scale on Numerical and Modelling Error . . . 137
5.1.5 Conclusions of Implicit a Posteriori Tests . . . 147
5.2 Approach Using Richardson Extrapolation . . . 149
5.2.1 Numerical and Modelling Error Using Richardson Extrapolation . . . 149
5.2.2 Order of Numerical and Modelling Error in Present LES . 154
5.2.3 Comparison to Tests with Implicit Filtering . . . 160
5.2.4 Conclusions of Using the Richardson Extrapolation . . . 161
5.3 A Posteriori Tests Using Explicit Filtering . . . 162

5.3.1 Grid-Independent LES Using Explicit Filtering 162
5.3.2 Applied Grid Resolutions 163
5.3.3 Error Components and Effect of Filtering 164
5.3.4 Conclusions of a Posteriori Studies with Explicit Filtering 172

6 Summary and Conclusions 173

References 176

List of symbols

$\|\cdot\|_2$	L_2-norm
$\langle\cdot\rangle$	average over time and homogeneous directions
a_l	lth coefficient of a discrete filter
C_S	Smagorinsky coefficient
C_{ij}	cross-stress tensor
E_{uu}	one-dimensional energy spectrum of u
G	filter function
$\widehat{G}$	filter transfer function
h	channel height
I	imaginary unit
$\hat{k}$	wavenumber
L_{ij}	Leonard stress tensor
M^k	kth moment of a filter function
P	mean pressure
p	pressure
R_{ij}	Reynolds stress tensor
Re_τ	Reynolds number based on the friction velocity
S_{ij}	shear-stress tensor
t	time
U	mean streamwise velocity
u	streamwise velocity component
u_i	ith component of the velocity vector, streamwise velocity component evaluated at grid point with index i
u_τ	friction velocity
v	wall-normal velocity component
v_i	wall-normal velocity component evaluated at grid point with index i
w	spanwise velocity component
w_i	spanwise velocity component evaluated at grid point with index i
x	streamwise spatial coordinate
x_i	ith spatial coordinate
y	wall-normal spatial coordinate
z	spanwise spatial coordinate

Greek symbols

Δ	grid spacing, second-order differentiation operation
Δ_f	absolute filter width
Δ_S	Smagorinsky length scale
Δ_{test}	Test-filter width
Δt	timestep
Δx	grid spacing in x direction
δ	Dirac delta function
δ_{ij}	Kronecker delta
ε	error
ϵ	dissipation
ν	kinematic viscosity
ν_t	turbulent viscosity
ρ	density
τ_{ij}	subgrid-scale stress
τ_w	wall-shear stress
ξ	spatial coordinate

Superscripts

$\overline{\cdot}$	test filtering, explicit filtering
$\widetilde{\cdot}$	resolved part, reduction on a discrete grid,
$+$	distance in wall-coordinates $y^+ = yu_\tau/\nu$
$*$	predicted value (pressure correction method)
$'$	SGS part instantaneous value
d	deviatoric part

Subscripts

i	ith coordinate direction, streamwise index of a grid point
j	spanwise index of a grid point
k	wall-normal index of a grid point
x	streamwise component
y	wall-normal component

z spanwise component

Abbreviations

C1	4th-order commutative filter
C2	6th-order commutative filter
CFD	Computational fluid dynamics
CFL	Courant number
DNS	direct numerical simulation
DSM	dynamic Smagorinsky model
LES	large eddy simulation
MKM	Moser, Kim and Mansour (1999)
MM	mixed model
S	Simpson filter
SFS	subfilter scale
SGS	subgrid scale
Smag.	standard Smagorinsky model
SSM	scale-similarity model
T	trapezoidal filter

Chapter 1

Introduction

1.1 Turbulence

In nature, laminar flows are rather an exception, and most of the interesting flows in engineering applications are turbulent. Turbulent flow is three-dimensional, time-dependent, has large Reynolds number, includes a wide range of both time and length scales, and it is diffusive and dissipative (Tennekes and Lumley 1972). Especially the diffusive nature of turbulence is important in engineering applications since in a turbulent flow, momentum, energy, heat, and particles, etc. are mixed effectively, which is seen, for example, in increased drag or enhanced chemical reactions. From the point of view of numerical simulations, the existence of a wide range of characteristic length and time scales is crucial, since for a successful simulation one should be able to capture all these scales.

It follows from the classical theory of Kolmogorov that the length scales describing the eddies in a turbulent flow can be divided into three classes (Pope 2000). The largest scales are of the same size as the characteristic length scales of the geometry, and they depend on external properties of the flow. These scales also contain most of the energy. The size of the smallest scales, or the Kolmogorov scales, is determined by viscosity and by the dissipation rate. In these scales, kinetic energy is dissipated into heat, and the related local Reynolds number is of the order of unity. Between the largest and smallest length scales, there is a range of scales which is characterised by a large local Reynolds number, and the scales are independent of viscosity. At the same time, they are independent of external properties of the flow. These intermediate scales or inertial range of scales depend only on the dissipation rate. According to the theory of Kolmogorov, the intermediate and the Kolmogorov scales are universal, i.e. they are similar in all flows. The three ranges of length scales are illustrated in Figure 1.1 with an energy spectrum, which is plotted on a logarithmic scale as a function of wavenumber. Wavenumber is inversely proportional to wavelength or

to the characteristic length scale of an eddy. The largest scales correspond to the smallest wavenumbers and vice versa. Also the energy cascade process, which was introduced by Richardson (Pope 2000), is illustrated in the figure. Energy is mainly produced at the largest scales, and it is transfered via the inertial range to the Kolmogorov scales where it is dissipated into heat. Dissipation takes place mainly at the smallest scales. The energy transfer from the large scales to inertial range is equal to the energy transferred from the inertial range to the Kolmogorov scales and further into heat. This property is taken advantage of in large eddy simulation of turbulent flows where the effect of the smallest scales on the large ones is often modelled as dissipation (Sagaut 2001).

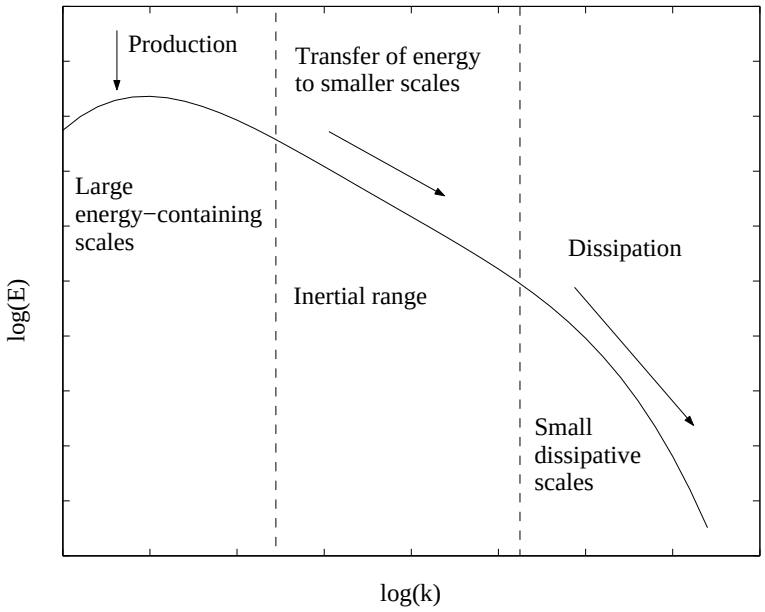

Figure 1.1: Kinetic energy cascade from large turbulent eddy scales to small scales. Vertical axis: logarithm of turbulent kinetic energy. Horizontal axis: logarithm of wavenumber, $k \propto$ inverse of length scale.

1.2 On Numerical Simulation of Turbulent Flows

The numerical simulations of turbulent flows are based on solving a set of non-linear partial differential equations. These equations consist of a continuity equation which simply states that mass is conserved, Navier–Stokes equations or momentum-balance equations which can be derived from Newton's second law of motion and, in the case of compressible flow, an energy equation (see e.g. Pope (2000)). In addition, some constitutive relations, like ideal gas law, may be required. In the momentum and energy equations, there are so-called convective terms which are non-linear. This non-linearity makes it impossible to solve

the equations analytically in a general turbulent flow, and also obtaining numerical solutions becomes difficult. This work concentrates on the numerical error involved in one simulation approach, the large eddy simulation, and the main problem is caused by the non-linear terms.

Direct numerical simulation (DNS) means numerical integration of the governing equations of a fluid flow with such methods that the numerical error is negligible and all the essential length and time scales of the flow field are captured. The features of turbulence, like time-dependency, three-dimensionality and a wide range of length and time scales make it a very challenging task. The smallest scales in a turbulent flow field cannot be ignored since, owing to the non-linear nature of turbulence, they affect the main flow and thus, in a numerical simulation, one has to be able to capture all scales present. It can be shown that the required computer capacity behaves as $\mathcal{O}\left(\mathrm{Re}^3\right)$ with the Reynolds number (Tennekes and Lumley 1972).

While DNS is not a feasible brute-force method for engineering problems, it is, however, a powerful research tool. From simulation results, almost any desired quantity can be evaluated, and once the numerical simulation has succeeded, the flow case can be studied more carefully than possible experimentally. In addition, DNS is not limited by physical constrains like measurements. DNS can also be applied to "thought experiments", which are usually performed by physicists (Moin and Mahesh 1998, Jiménez 2003). Other applications of DNS include, for example, the study of the physics of turbulence, active flow control and validation of computational models. A thorough review of different applications of DNS is provided by Moin and Mahesh (1998). In this thesis, DNS is applied to a priori and a posteriori testing of numerical simulations and to validation of simulation results.

Since DNS requires such large computer capacities, also other simulation methods are required. In large-eddy simulation (LES), the flow field is divided into resolved and unresolved scales. The former are solved from the governing equations and the effect of the latter is modelled (see e.g. Sagaut (2001)). The equations which are used to describe a flow field in LES are formally obtained from the Navier–Stokes equations using a filtering procedure, and the resulting equations together with a model for the unresolved scales are solved on a discrete computational grid. The cutoff wavenumber, which divides the length scales into resolved and unresolved scales, should be located in the inertial range of Figure 1.1, and the unresolved scales should be universal scales having large wavenumbers.

Using explicit filtering in a simulation means that a filtering procedure with a low-pass filter is explicitly applied to the resolved flow field during the simulation. This divides the flow field into resolved scales, subfilter scales and subgrid scales (Carati, Winckelmans and Jeanmart 2001, Gullbrand and Chow 2003). Subfilter-scales (SFS) are smaller than the applied filter width but larger that the grid

resolution. An SFS model is applied to reconstruct these scales from the resolved flow field (Gullbrand and Chow 2003). Subgrid scales (SGS) are smaller than the grid spacing and an SGS model is applied to model their effect. In traditional LES, no explicit filtering is applied, and the grid resolution defines the separation between resolved and SGS scales. The damping introduced to the flow field is a combination of the reduction on a discrete grid and SGS modelling. This approach is often referred to as implicit filtering. In most practical simulations, this concept of implicit filtering is applied, and a Smagorinsky model (Smagorinsky 1963) or its dynamic version (Germano, Piomelli, Moin and Cabot 1991) is applied.

In engineering applications of computational fluid dynamics (CFD), Reynolds-Averaged Navier–Stokes (RANS) simulations have been the traditional approach. In RANS, an average flow field is solved, and the effect of turbulence is modelled. Although RANS performs well in cases with attached boundary layers, LES is superior in cases with large-scale time-dependent structures like in massively separated flows. LES is becoming a more and more popular approach in engineering applications, and e.g. in CFD conferences arranged by European Congress on Computational Methods in Applied Sciences and Engineering (ECCOMAS), more applied studies are performed with LES than with RANS. As discussed in the next section, numerical methods and the effect of numerical error can have a large effect in LES. In LES, their role is more pronounced than in RANS. As LES is becoming a more popular approach also in engineering applications, there is also a growing need for analysing the quality of the results and the effect of numerics on the simulation results.

1.3 Previous Research

In a simulation with no turbulence modelling, the error is due to numerics and it can be controlled by applying a fine computational grid. When the grid is refined, it will finally be able to describe all the length scales present in the flow field and the simulation becomes DNS. In LES, the concept is not as clear. Since the idea is to model the effect of the subgrid motion on the larger scales, there are dynamically important scales in the flow field that are of the same size as the grid spacing. Usually, when LES is applied in complex geometries, finite-difference-type schemes are applied. However, especially with low-order, i.e. second or fourth-order finite-difference schemes, the effect of numerical error becomes more pronounced than in spectral methods. There are not as many grid points for the description of the small-wavelength components as for the high-wavelength components, and thus, the smallest motions present in the solution are most badly affected by the numerical error. When the frequency components of the resolved flow field are studied, spectral methods treat all the frequency components in the same manner. However, finite-difference-type schemes introduce so-called modi-

fied wavenumbers and they produce accurately only the small-frequency components and damp the high-frequency components (see e.g. Kravchenko and Moin (1997)). When the grid resolution is increased in a simulation with no explicit filtering, the numerical error related to the resolved scales of the coarser grid diminishes, but at the same time, there will be new small scales present, and these scales are again contaminated by numerical error. In addition, the effect of the SGS model will diminish with increased resolution. Thus, even after grid refinement, the dominance of the SGS model over the numerical error is not necessarily clear.

The numerical error involved with low-order finite-difference schemes has been studied a priori by using both actual finite-difference methods (Vreman, Geurts and Kuerten 1994*a*, Vreman, Geurts and Kuerten 1995, Majander and Siikonen 2002) and spectral schemes with modified wavenumbers, which mimic the behaviour of the difference scheme, (Ghosal 1996, Kravchenko and Moin 1997, Chow and Moin 2003). In a priori tests, the numerical error and the SGS term of an LES grid are calculated from DNS data. The DNS data are filtered and restricted on a coarser grid and the derivatives evaluated there represent an LES result. This result is then compared to the derivatives evaluated on the DNS grid, which represents the exact solution. In all these studies, it was noticed that the numerical error involved with the low-order finite-difference scheme can be larger than the effect of the SGS model. Applying high-order methods would improve the situation, but as the truncation error is reduced, aliasing error may become a problem (Kravchenko and Moin 1997). In the above mentioned a priori studies, explicit filtering was noticed to decrease the numerical error (Vreman et al. 1994*a*, Ghosal 1996), and they recommended using an explicit filter with a filter width four times the grid spacing when a second-order scheme is applied.

Explicit filtering has also been applied in actual LES. Lund and Kaltenbach (1995) applied explicit filtering in a simulation of a fully developed turbulent channel flow between two infinite parallel walls. They filtered the velocity field in the streamwise and spanwise directions using the spectral cutoff filter. This filter is applied in the spectral space and it is sharp, i.e. multiple filtering does not affect the resolved flow field. To keep the effective grid resolution constant, Lund and Kaltenbach increased the grid resolution as the filtering was applied. They noticed that the filtering improved the simulation results, but it was computationally quite demanding. It was easier to obtain improved simulation results by increasing the grid resolution than by filtering.

In practical applications of LES, increasing the grid resolution or transformation into the spectral space is not possible owing to limited computer capacity and complex geometries, respectively. Thus, filtering has to be performed in the physical space. However, the filters applied in the physical space are smooth in the spectral space and multiple filtering of the flow field produces extra damping to all frequency components of the resolved flow field. Lund (1997) suggested

that, when smooth filters are applied, filtering should be performed only for the non-linear convection term of the Navier–Stokes equations.

Gullbrand studied the use of explicit filtering of the non-linear convection term with different SGS models and a fourth-order scheme in several publications (Gullbrand 2001, Gullbrand 2002, Gullbrand and Chow 2003). As a test case, she used turbulent channel flow. She concluded that explicit filtering improved the simulation results when compared to the traditional implicit filtering and that when explicit filtering was applied, the contribution from the SGS model increased (Gullbrand 2001). In addition, she found that in simulations with explicit filtering, the use a SFS model for scales smaller than filter width and larger than grid spacing improved the results when compared to using the dynamic Smagorinsky model (Gullbrand 2002). Amiri, Hannani and Mashayek (2005) applied explicit filtering also in the channel flow but at a lower Reynolds number with a compact fourth-order scheme and the dynamic Smagorinsky model. They obtained somewhat improved results when compared to the simulations with no filtering. However, in all actual applications of explicit filtering, the improvement of the simulation results was not as large as could be expected based on the a priori tests. There are also alternative approaches to explicit filtering, and we will discuss some of them in the next chapter.

In a priori tests, the interaction of numerics and SGS modelling is unclear. Most SGS models are dissipative and they smooth out the resolved LES field, thus affecting the numerical error. It is difficult to include this phenomenon in a priori testing. In a posteriori tests, actual LES results are compared to DNS and to so-called grid-independent LES or fine-grid LES to separate the effect of the numerical and modelling error. Vreman, Geurts and Kuerten (1996) studied different numerical methods, second and fourth-order and a spectral scheme, in a turbulent mixing layer using a dynamic mixed model and found that the effect of the numerical and modelling errors can be of different sign, and thus they can partially cancel out each other. In addition, they noticed that also in the actual simulation, the numerical error was larger than the modelling error if the filter width was equal to the grid spacing and the situation was reversed when a filter with the width of two grid spacings was applied. Geurts and Fröhlich (2002) proposed a method for predicting the error components, where different combinations of grid resolutions and filter widths are characterised by quantities named as SGS resolution and SGS activity. Geurts and Fröhlich (2002) and Meyers, Geurts and Baelmans (2003) applied this approach with the standard Smagorinsky model in a turbulent mixing layer and in homogeneous turbulence, respectively. In both studies, the numerical error of a fourth-order scheme and the modelling error related to the standard Smagorinsky model were of the same size and they partially cancelled out each other, as in the study of Vreman et al. (1996).

Grid-independent or fine-grid LES means an LES simulation where the grid res-

olution is increased to a level where the effect of numerics is negligible while the effect of the SGS model is preserved. Thus, the effect of the SGS model is not decreased with increasing resolution. There are different approaches to obtain grid-independent LES and to analyse the error components of LES. An approach using explicit filtering was applied in the a posteriori tests of Vreman et al. (1996) and in the studies involving the behaviour of different SGS models of Gullbrand (2002). They kept the absolute width of the explicit filter constant while increasing the grid resolution. This means that the frequency content of the resolved flow field is controlled explicitly by applying a low-pass filter that removes the high-frequency components. Geurts and Fröhlich (2002) and Meyers et al. (2003) applied implicit filtering provided by the standard Smagorinsky model, and the grid-independent LES was approached by increasing the grid resolution while keeping the model length scale constant. The model length scale is a parameter controlling the size of the smallest resolved length scales. In this approach, the LES equations are interpreted as a set of equations with one externally defined parameter, the model length scale. Traditionally, the model length scale is a priori tied to the grid resolution. In addition, there are methods for quality assessment of LES which do not require DNS data or grid-independent LES (Klein 2005, Celik, Cehreli and Yavuz 2005). These methods are based on the Richardson extrapolation. It has been suggested that 80 per cent of the energy should be resolved in LES (Pope 2000), and Celik, Cehreli and Yavuz (2005) proposed an index of resolution quality for LES, which is based on approximating the resolved turbulent kinetic energy using Richardson extrapolation. Klein (2005) applied the Richardson extrapolation to evaluate the numerical and modelling error in LES, and he strongly criticises the use of the concept of grid-independent LES.

1.4 Formulation of Present Research Problems

The present thesis work concentrates on error analysis of LES and on explicit and implicit filtering. The test case applied is fully developed turbulent channel flow between two infinite parallel walls. An incompressible case at a relatively low Reynolds number, where accurate DNS is possible, is chosen. The research is divided into three parts: First, a priori studies are performed, then filtering is applied in actual simulations and finally, a posteriori tests are performed and the different error analysing methods are compared.

In the previous a priori studies described above, explicit filtering of the whole velocity field was studied, while in actual simulations, filtering of the non-linear convection term has been applied. In the a priori tests of this thesis, the filtering of the non-linear convection term is studied and the differences between the two approaches are first analysed a priori. After the a priori tests, filtering is applied

to actual LES. As described above, the previous studies where explicit filtering was applied in actual simulations concentrated mainly on SGS and SFS modelling. Here, besides testing the hypothesis based on the a priori tests, the aim is to find out how the choice of the filter function and model parameters affect the total simulation error and what the pure effect of filtering is when compared to SGS modelling. In addition, results obtained using explicit filtering are compared to simulations with implicit filtering, and the differences between these approaches are described. In this thesis, Smagorinsky-type and scale-similarity SGS and SFS models are applied to study explicit filtering. These models were chosen because they are not computationally too heavy, and the aims of the work are not related to improved modelling but rather to a fundamental study on explicit filtering. On the other hand, the use of more advanced models, like a dynamic mixed model and a reconstruction model, has already been studied in the context of explicit filtering by Gullbrand (2002).

Both implicit and explicit filtering are applied in the present a posteriori tests and in addition, the use of the Richardson extrapolation in LES is studied. The aims are to quantify the numerical and modelling error as well as the effect of filtering, to explain the behaviour of simulation results by the two error components and to compare the different approaches to obtaining the errors. A comparison between these three approaches has not been previously presented and in addition, the approach to a posteriori testing using implicit filtering has not been applied in a wall-bounded flow before.

In this thesis, it is shown that according to a priori tests, filtering of the whole velocity field leads to an unphysical situation, while filtering of the nonlinear convection term decreases the numerical error effectively. However, when comparing these results to the actual simulations, it is noticed that the numerical error predicted by a priori tests for the second-order methods is too pessimistic at least when the standard Smagorinsky model is applied. In a posteriori studies, the numerical and modelling errors are estimated and it is demonstrated that their magnitude can be of the same size, which has been noticed also in other test cases in previous studies. In addition, the use of explicit filtering with smooth filters is studied and it is shown in both actual simulations and in a posteriori studies that this approach can introduce a large additional error component.

The contents of the thesis is organised as follows. A description of the applied numerical and modelling methods is given in Chapter 2. In Chapters 3, 4 and 5, the results a priori studies, simulations with explicit and implicit filtering and a posteriori tests are presented, respectively. The conclusions are drawn in the last chapter.

The results of the a priori studies in Chapter 3 were published in Brandt (2006*a*) and they also formed the main part of the author's licentiate thesis (Brandt 2004). The results of simulations with explicit and implicit filtering in Chapter 4 were

published in Brandt (2006*b*) and Brandt (2006*d*). The results of the a posteriori tests obtained using implicit and explicit filtering were published in Brandt (2007) and Brandt (2006*c*), respectively, and the study on the Richardson extrapolation in Brandt (2006*e*).

Chapter 2

Applied Models and Numerical Methods

In Section 2.1, we briefly review the equations being solved in direct numerical simulation (DNS) and large eddy simulation (LES) and discuss the subgrid-scale (SGS) model applied in LES in this thesis. One of the focuses of this thesis is explicit filtering in LES, and the filter functions and the different approaches to explicit filtering are discussed in Section 2.2. The numerical implementation of the applied methods is discussed in Section 2.3, and a grid-convergence study with no SGS modelling is presented in Section 2.4.

2.1 Equations Being Solved in LES

2.1.1 Equations Describing the Flow of an Incompressible Fluid

In the case of an incompressible flow, the continuity equation and Navier–Stokes equations may be written in a non-dimensional form as

$$\frac{\partial u_j}{\partial x_j} = 0 \tag{2.1}$$

$$\frac{\partial u_i}{\partial t} = -\frac{\partial p}{\partial x_i} + \frac{\partial}{\partial x_j}\left(- u_i u_j + \frac{1}{\mathrm{Re}_\tau}\left(\frac{\partial u_i}{\partial x_j} + \frac{\partial u_j}{\partial x_i}\right)\right), \tag{2.2}$$

where $u_i\,(i = 1, 2, 3)$ is the non-dimensional velocity component in the ith coordinate direction, p is the non-dimensional pressure and Re_τ is the Reynolds number based on the friction velocity. This thesis concentrates on the fully developed turbulent channel flow between two parallel walls, and the reference scales are thus

chosen to be appropriate for this flow case. We scale the equations by channel half-height, $h/2$, and by friction velocity, u_τ, and the Reynolds number is here defined as

$$\mathrm{Re}_\tau = \frac{u_\tau h/2}{\nu}, \tag{2.3}$$

where ν kinematic viscosity. Hereafter, u_i refers to velocity field scaled by the friction velocity, u_τ, x_i to a coordinate scaled by the channel half-height, t to time scaled by h/u_τ and p to pressure scaled by ρu_τ^2, where ρ is the density. Friction velocity is defined via wall-shear stress, τ_w, as

$$u_\tau = \sqrt{\frac{\tau_w}{\rho}}. \tag{2.4}$$

In large eddy simulation (LES), the idea is to solve only the largest scales of motion and to model the effect of the smaller scales. The equations being solved are formally derived by applying a low-pass filter to the continuity and Navier–Stokes equations (2.1 and 2.2). This filter separates the large and small scales. A one-dimensional filtering operation for the velocity field is defined in the physical space as

$$\tilde{u}_i(x) = \int G(x-\xi, \Delta_f, x)\, u_i(x)\, \mathrm{d}\xi, \tag{2.5}$$

where Δ_f is the filter width, x and ξ are spatial coordinates and G is the filter function. Extending the filtering to three dimensions is straightforward. The obtained equations may be written as

$$\frac{\partial \tilde{u}_j}{\partial x_j} = 0 \tag{2.6}$$

$$\frac{\partial \tilde{u}_i}{\partial t} = -\frac{\partial \tilde{p}}{\partial x_i} + \frac{\partial}{\partial x_j}\left(-\tilde{u}_i\tilde{u}_j - \tau_{ij} + \frac{1}{\mathrm{Re}_\tau}\left(\frac{\partial \tilde{u}_i}{\partial x_j} + \frac{\partial \tilde{u}_j}{\partial x_i}\right)\right) \tag{2.7}$$

where $\tilde{u}_i$ is the resolved velocity component and τ_{ij} is a subgrid-scale (SGS) stress defined as

$$\tau_{ij} = \widetilde{u_i u_j} - \tilde{u}_i\tilde{u}_j. \tag{2.8}$$

τ_{ij} stress appears in the equations from the filtering of the non-linear convection term $\widetilde{u_i u_j}$. It cannot be determined using only the resolved flow field $\tilde{u}_i$, and thus it requires modelling. The subgrid-scale models applied for modelling of τ_{ij} in this thesis are discussed in Subsection 2.1.2. Often when finite-volume-type schemes are applied, implicit filtering concept is applied and filtering is present only in the derivation of the equations, and not in the actual implementation. If explicit filtering is applied during the simulation, the form of the equations changes, and often a subfilter scale is applied to model the effect of scales that are smaller than the filter width but larger than the grid spacing. This is discussed in more detail in Section 2.2.

In the channel flow, there are two homogeneous directions, the streamwise and the spanwise. In these directions, periodic boundary conditions are applied. The no-slip condition is forced on the top and bottom walls. In the applied coordinate system, the x-axis points in the streamwise direction, the z-axis in the spanwise and the y-axis in the wall-normal direction. Correspondingly, the streamwise velocity component u_1 is referred to as u, the wall-normal component u_2 as v, and the spanwise component u_3 as w.

2.1.2 Applied Subgrid-Scale Models

Smagorinsky Model

The models that work in physical space are very often based on the eddy-viscosity concept, which assumes that the energy transfer mechanism from the resolved scales to the subgrid scales is analogous to the molecular mechanism represented by the diffusion term. The subgrid-scale shear stress is written using the Boussinesq approximation as

$$\tau_{ij} - \frac{1}{3}\tau_{kk}\delta_{ij} = -2\nu_T\tilde{S}_{ij}, \tag{2.9}$$

where ν_T is the eddy viscosity and $\tilde{S}_{ij}$ is the resolved shear-stress tensor

$$\tilde{S}_{ij} = \frac{1}{2}\left(\frac{\partial\tilde{u}_i}{\partial x_j} + \frac{\partial\tilde{u}_j}{\partial x_i}\right). \tag{2.10}$$

Since the trace of $\tilde{S}_{ij}$ is zero, only the deviatoric part of the subgrid-scale stress can by modelled using the eddy-viscosity concept. The trace of τ_{ij} is included in the pressure term as

$$\Pi = \tilde{p} + \frac{1}{3}\tau_{kk}. \tag{2.11}$$

Eddy-viscosity models can be based on resolved scales, on energy at the cutoff wavenumber, which should be located in the area of intermediate scales in Figure 1.1, or on a reconstruction of the subgrid scales (Sagaut 2001). The first alternative is the simplest one. The existence of the subgrid scales then follows from the structure of the resolved field. Eddy viscosity is assumed to be a function of the characteristic length scale of the subgrid scales, Δ_S, and of the energy flux through the cutoff, $\tilde{\epsilon}$:

$$\nu_T = \nu_T\left(\Delta_S, \tilde{\epsilon}\right). \tag{2.12}$$

If one makes an assumption of local equilibrium, i.e. the production of turbulent kinetic energy, $\mathscr{P}$, equals the energy transfer through the cutoff and further the energy dissipated to heat, ϵ, at the small scales as discussed in Chapter 1:

$$\mathscr{P} = \tilde{\epsilon} = \epsilon, \tag{2.13}$$

the following equation for the eddy viscosity can be obtained (Sagaut 2001):

$$\nu_T = (C_S \Delta_S)^2 \, |\tilde{S}|, \tag{2.14}$$

where

$$|\tilde{S}| = \sqrt{2 \tilde{S}_{ij} \tilde{S}_{ij}}, \tag{2.15}$$

and C_s is the model parameter, which has to be fixed a priori. The Smagorinsky model for SGS stress may now be written as

$$\tau_{ij} - \frac{1}{3} \tau_{kk} \delta_{ij} = -2 \, (C_S \Delta_S)^2 \, |\tilde{S}| \, \tilde{S}_{ij} \tag{2.16}$$

This model was first proposed by Smagorinsky (1963) and it is the most commonly used SGS model.

The usual choice for the length scale in the Smagorinsky model is to make it equal to a representative grid spacing as

$$\Delta_S = \Delta = (\Delta_x \Delta_y \Delta_z)^{1/3}, \tag{2.17}$$

where Δx, Δz and Δy refer to grid spacings in different coordinate directions. There are also other possibilities like

$$\Delta_S = \Delta = \left(\Delta_x^2 + \Delta_y^2 + \Delta_z^2\right)^{1/2}. \tag{2.18}$$

There is no universal value for the model parameter, but assuming isotropic turbulence there are several ways to predict a value for it. These values are all close to $C_S \approx 0.2$ (Sagaut 2001). Smagorinsky (1963) assumed the value of $C_S = 0.23$. However, in shear flows this value is usually adjusted. Deardorff (1970) used a value of $C_S = 0.1$ for channel flow and even smaller values have been applied. Usually the values are between 0.08 and 0.11 (Najjar and Tafti 1996). However, also the use of values close to $C_S \approx 0.2$ in the channel flow have been suggested (Mason and Callen 1986). In the present study, the value $C_S = 0.085$ was used because it was previously noticed that in the present code this value produces the best results (Brethouwer 2002).

The product of the model coefficient and the model length scale, $C_S \Delta_S$, has been shown to be the equivalent of the Kolmogorov dissipation length for the LES flow generated by Equations (2.7) (Muschinski 1996) and thus, it controls the size of the smallest resolved flow structures. Thus, actually varying either C_S or Δ_S results in changing the dissipation or damping provided by the model. Increasing the product $C_S \Delta_S$ has also been called implicit filtering (e.g. Geurts and Fröhlich (2002)). In the present study, the model coefficient C_S is fixed and the model length scale is varied.

In wall-bounded flows, the size of the smallest length scales of the flow field reduces as the wall is approached, and thus it is necessary to reduce the model

length scale and the length of the implicit filter provided by the model in the near-wall region (Moin and Kim 1982). With the standard Smagorinsky model, van Driest damping is usually applied to obtain

$$C_S = C_{S0}\left(1 - \exp\left(y^+/25\right)\right)^2, \tag{2.19}$$

where $y^+ = \mathrm{Re}_\tau y$ is the distance from the wall in wall-coordinates and C_{S0} the value of the model parameter in the bulk flow. However, there are other possibilities. Ferziger and Peric (1999) suggests that by choosing a proper length scale, the use of van Driest damping could be avoided. In the present study, the van Driest damping is applied both in actual simulations and in a posteriori tests.

Besides the flow-dependent model coefficient, the Smagorinsky model has other drawbacks. It predicts incorrect asymptotic behaviour in near-wall regions or in laminar flows (Zang, Street and Koseff 1993). The use of wall functions improves the behaviour near walls, but the model still yields non-zero SGS stresses in laminar flows. It has also been found to overpredict dissipation in transitional flows (Piomelli, Zang, Speziale and Hussaini 1990, Vreman, Geurts and Kuerten 1997). The Smagorinsky model is purely dissipative and it does not allow energy backscatter from small scales to large scales. Because it is an eddy-viscosity model, it assumes that SGS stresses are aligned with the strain-rate tensor. This gave low correlations with the exact SGS stress in the a priori tests of Bardina, Ferziger and Reynolds (1980) (see e.g. Ferziger (1996)).

Dynamic Smagorinsky Model

Germano et al. (1991) suggested a dynamic procedure for the calculation of the parameter in the Smagorinsky model. A second filter, a test filter, that is wider than the original filter applied to the governing equations, is used to define two levels of stress tensors: subgrid scale and subtest scale. It is assumed that both the SGS stress and subtest-scale stress can be modelled using the same functional form of the Smagorinsky model.

Here, the test-filtered quantities are denoted by the overbar, $\overline{u}$. This test filtering is a different procedure from explicit filtering applied in deriving the LES equations.

The dynamic procedure is described as follows. The SGS stress is defined as

$$\tau_{ij} = \widetilde{u_i u_j} - \tilde{u}_i \tilde{u}_j \tag{2.20}$$

and modelled using the Smagorinsky model as in Equation (2.16):

$$\tau_{ij} - \frac{1}{3}\tau_{kk}\delta_{ij} = -2\nu_T \tilde{S}_{ij} = -2C\Delta^2 |\tilde{S}|\ \tilde{S}_{ij} \tag{2.21}$$

The subtest-scale stress, $\mathscr{T}_{ij}$, is defined as

$$\mathscr{T}_{ij} = \widetilde{\overline{u_i u_j}} - \overline{\tilde{u}_i}\,\overline{\tilde{u}_j} \tag{2.22}$$

and the Smagorinsky model is applied to it as

$$\mathscr{T}_{ij} - \frac{1}{3}\mathscr{T}_{kk}\delta_{ij} = -2C\Delta_{\text{test}}^2|\overline{\tilde{S}}|\;\overline{\tilde{S}}_{ij} \tag{2.23}$$

where Δ_{test} is the width of the test filter and

$$\overline{\tilde{S}}_{ij} = \frac{1}{2}\left(\frac{\partial\overline{\tilde{u}}_i}{\partial x_j} + \frac{\partial\overline{\tilde{u}}_j}{\partial x_i}\right). \tag{2.24}$$

The subgrid-scale stress, τ_{ij}, and subtest-scale stress, $\mathscr{T}_{ij}$, can be related to each other through the resolved turbulent stress and Germano identity (Germano 1992). The resolved turbulent stress, the Leonard stress, which represents the energy scales between the grid filter and the test filter, is defined as

$$L_{ij} = \overline{\tilde{u}_i\tilde{u}_j} - \overline{\tilde{u}_i}\,\overline{\tilde{u}_j} \tag{2.25}$$

and it can be written in the form (Germano identity)

$$L_{ij} = \widetilde{\overline{u_i u_j}} - \overline{\tilde{u}_i}\,\overline{\tilde{u}_j} - \left(\widetilde{\overline{u_i u_j}} - \overline{\tilde{u}_i\tilde{u}_j}\right) = \mathscr{T}_{ij} - \overline{\tau_{ij}}. \tag{2.26}$$

L_{ij} contains only the resolved scales and it can thus be evaluated from the resolved flow field. If we substitute Equations (2.21) and (2.23) into Equation (2.26), we obtain an equation where the only unknown is the parameter of the Smagorinsky model C:

$$L_{ij} - \frac{1}{3}L_{kk}\delta_{ij} = -2C\Delta_{\text{test}}^2|\overline{\tilde{S}}|\;\overline{\tilde{S}}_{ij} + 2\overline{C\Delta^2|\tilde{S}|\;\tilde{S}_{ij}} \tag{2.27}$$

If it is assumed that C varies slowly enough to be removed from the filtering operation, it could, in principle, be solved from Equation (2.27), but in the a priori tests of Germano et al. (1991), it turned out that the right-hand side can be zero. In addition, there are five independent equations in (2.27), and C is thus over-determined.

In the channel flow case, C can be assumed to be a function of time and the wall-normal direction only ($C = C\,(t, y)$), and it can be extracted from the filtering operator. Germano et al. (1991) contracted Equation (2.27) with $\tilde{S}_{ij}$ and obtained the equation

$$C = -\frac{1}{2}\,\frac{\langle\left(L_{ml} - \frac{1}{3}L_{kk}\right)\delta_{ij}\tilde{S}_{ml}\rangle_{xz}}{\Delta_{\text{test}}^2\langle|\overline{\tilde{S}}|\;\overline{\tilde{S}}_{ij}\tilde{S}_{ij}\rangle_{xz} - \Delta^2\langle\overline{|\tilde{S}|\;\tilde{S}_{pq}}\tilde{S}_{pq}\rangle_{xz}}, \tag{2.28}$$

where $\langle u\rangle_{xz}$ denotes averaging over the planes parallel to the walls. Averaging is performed to avoid the situations when the denominator becomes small or zero.

Without averaging, there would also be some mathematical inconsistency in the model. To remove C from the filtering operator, one has to assume that it varies slowly in the directions where filtering is performed. Without the averages in Equation (2.28) C would, however, vary strongly in space. Zang et al. (1993) note that these fluctuations might be due to putting too much burden on the parameter. The parameter is forced to be a scalar, although it actually is a tensor.

Lilly (1992) criticised the contracting procedure leading to Equation (2.28) since it ignores many other possible projections of Equation (2.27). In addition, the physical meaning of the procedure is not obvious. Lilly (1992) suggested solving Equation (2.27) in the least squares sense, which leads to (it is assumed $C = C(t, y)$)

$$C = \frac{1}{2}\frac{L_{ij}M_{ij}}{M_{nm}M_{nm}}, \tag{2.29}$$

where

$$M_{nm} = \Delta_{\text{test}}^2 |\overline{\tilde{S}}|\overline{\tilde{S}}_{nm} - \Delta^2 \overline{|\tilde{S}|\tilde{S}_{nm}}. \tag{2.30}$$

Equation (2.29) allows negative values for the constant C and thus also the eddy viscosity ν_T may obtain negative values. Negative eddy viscosity is usually interpreted as energy backscatter from the subgrid scales to the resolved scales. However, Sagaut (2001) notes that the backward energy transfer obtained using this type of model is not based on the physical description of the process and it should be taken with caution.

It has turned out that the eddy viscosity obtained by the dynamic Smagorinsky model can have large negative values, which makes the simulation unstable. Usually, eddy viscosity is limited by the molecular viscosity, and values smaller than $\nu_T < -\nu$ are set equal to $-\nu$ (Sagaut 2001). However, even if limitation is applied, the dynamic Smagorinsky model has turned out to be unstable in some complex flows, while the standard Smagorinsky model still provides enough dissipation to keep the computation stable (Majander and Siikonen 2004).

In cases where there are homogeneous directions, as in the channel flow, the numerator and denominator of Equation (2.29) are usually averaged over these directions to obtain

$$C = \frac{1}{2}\frac{\langle L_{ij}M_{ij}\rangle_{xz}}{\langle M_{nm}M_{nm}\rangle_{xz}}. \tag{2.31}$$

which leads to the subgrid model

$$\begin{aligned}\tau_{ij} - \frac{1}{3}\tau_{kk}\delta_{ij} = -2C\Delta^2|\tilde{S}|\ \tilde{S}_{ij} = -\frac{\langle L_{pq}M_{pq}\rangle_{xz}}{\langle M_{nm}M_{nm}\rangle_{xz}}\Delta^2|\tilde{S}|\ \tilde{S}_{ij} = \\ = \frac{\langle L_{pq}\left(\left(\Delta_{\text{test}}/\Delta\right)^2 |\overline{\tilde{S}}|\overline{\tilde{S}}_{pq} - \overline{|\tilde{S}|\tilde{S}_{pq}}\right)\rangle_{xz}}{\langle\left(\left(\Delta_{\text{test}}/\Delta\right)^2 |\overline{\tilde{S}}|\overline{\tilde{S}}_{nm} - \overline{|\tilde{S}|\tilde{S}_{nm}}\right)^2\rangle_{xz}}|\tilde{S}|\ \tilde{S}_{ij}\end{aligned} \tag{2.32}$$

In Equation (2.32), only the ratio $\Delta_{\text{test}}/\Delta$ is required and thus, there is no problem in determining the model length scale. A very typical choice is to use the value of $\Delta_{\text{test}}/\Delta = 2$. However, the exact form of the discrete test filter affects the filter width, and this should be taken into account (Lund 1997). The a priori study and simulations of Piomelli, Moin and Ferziger (1988) with the standard version of the model suggested that the spectral cutoff filter should be preferred to other filters with the Smagorinsky model, and this was confirmed in simulations with the dynamic model by Gullbrand (2001). In both studies, the channel flow was used as the test case. Lund (1997) demonstrated that the choice of the test filter does not affect the decay of turbulent kinetic energy. However, Meyers, Geurts and Baelmans (2005) noticed that the width of the test filter affects the total simulation error, and with the trapezoidal filter the total error diminished when the ratio $\Delta_{\text{test}}/\Delta$ was increased.

Usually, with the dynamic model, filtering is performed only in the homogeneous directions. However, in most practical application of LES, these directions do not exist. Gullbrand (2004) studied the use of three-dimensional test filtering in the channel, and found that, when a smooth test filter is applied, test filtering in the wall-normal direction improves the simulation results. However, the best results with the dynamic Smagorinsky model were produced when the sharp spectral cutoff filter was applied in the homogeneous directions.

The dynamic evaluation of the model parameter removes some of the problems that have arisen with the standard Smagorinsky model. The bulk flow value of the constant is automatically suitable and needs no tuning. Also, damping near the solid walls becomes unnecessary. However, the dynamic Smagorinsky model is still an eddy-viscosity model, and the deficiencies of this formulation remain. For example, Bogey and Bailly (2005) noticed in a compressible turbulent jet flow that the use of eddy-viscosity-type models decreases the effective Reynolds number of the resolved flow field, and in Visbal and Rizzetta's (2002) simulations of isotropic turbulence, Smagorinsky models dissipated energy over a wide range of scales, including the resolved scales. In addition, the application of the dynamic model in complex flow geometries is not straightforward. To improve the behaviour of the dynamic models in these situations, localised models have been proposed. In a general flow case, there are no homogeneous directions and averaging is thus not always a feasible approach. Gullbrand (2004) studied the use of three-dimensional local averaging which improved the prediction of the turbulent channel flow. Sagaut (2001) provides a review on other types of localised models. Some of the models are computationally quite expensive.

Scale-Similarity Model and Mixed Models

The scale-similarity model (SSM) models the SGS stresses rather than their effect on the large scales. When explicit filtering is applied, SSM provides a first-

order reconstruction of the subfilter-scale stresses. The model is based on the so-called scale similarity hypothesis, which states that the largest unresolved scales are similar to the smallest resolved scales (Sagaut 2001). The starting point in deriving the model is the Leonard decomposition of the SGS stress (Leonard 1974). When the velocity field is written as the sum of the resolved component and SGS component as

$$u_i = \tilde{u}_i + u_i', \tag{2.33}$$

we may write for the SGS stress

$$\begin{aligned}\tau_{ij} &= \widetilde{u_i u_j} - \tilde{u}_i\tilde{u}_j = \widetilde{(\tilde{u}_i + u_i')\left(\tilde{u}_j + u_j'\right)} - \tilde{u}_i\tilde{u}_j = \\ &= \underbrace{\widetilde{\tilde{u}_i\tilde{u}_j} - \tilde{u}_i\tilde{u}_j}_{=L_{ij}} + \underbrace{\widetilde{\tilde{u}_i u_j'} + \widetilde{u_i'\tilde{u}_j}}_{=C_{ij}} + \underbrace{\widetilde{u_i' u_j'}}_{=R_{ij}} = \\ &= L_{ij} + C_{ij} + R_{ij},\end{aligned} \tag{2.34}$$

where L_{ij} is the Leonard stress that describes the interaction between the resolved scales, C_{ij} is the cross-stress tensor that represents the interaction between the resolved and SGS motions, and R_{ij} is the Reynolds stress tensor that describes the interaction between the SGS motions. The Leonard stress involves only the resolved velocities and needs no modelling. In the scale-similarity model, the assumption of the scale-similarity is applied and an additional filtering is applied to the resolved flow field to separate the smallest and largest resolved scales. The subgrid scales are approximated by the largest subgrid scales, which are further approximated by the smallest resolved scales as (Ferziger 1996)

$$u_i' \approx \overline{u_i'} \approx \tilde{u}_i - \overline{\tilde{u}}_i, \tag{2.35}$$

where the overbar refers to an additional filtering that has to be applied explicitly to the resolved field. Additionally, it is assumed in C_{ij} and R_{ij} that $\widetilde{uv} \approx \tilde{u}\tilde{v}$. The following approximations are then obtained for the cross-stress and Reynolds stress tensors:

$$\begin{aligned}C_{ij} &\approx \overline{\tilde{u}}_i\overline{u_j'} + \overline{u_i'}\,\overline{\tilde{u}}_j \approx \overline{\tilde{u}}_i\left(\tilde{u}_j - \overline{\tilde{u}}_j\right) + \left(\tilde{u}_i - \overline{\tilde{u}}_i\right)\overline{\tilde{u}}_j \\ R_{ij} &\approx \overline{u_i'}\,\overline{u_j'} \approx \left(\tilde{u}_i - \overline{\tilde{u}}_i\right)\left(\tilde{u}_j - \overline{\tilde{u}}_j\right).\end{aligned} \tag{2.36}$$

Once these approximations are combined with the Leonard stress tensor, one obtains the scale-similarity model for the SGS stress:

$$\tau_{ij} = \overline{\tilde{u}_i\tilde{u}_j} - \overline{\tilde{u}}_i\overline{\tilde{u}}_j. \tag{2.37}$$

The model was proposed by Bardina et al. (1980), and their form of the model required that two identical filter functions were applied to the flow quantities. Liu, Meneveau and Katz (1994) generalized the model to be used with two different filters.

Germano (1986) noted that the Leonard and cross-stresses defined in Equation (2.34) are not Galilean invariant. When the Leonard stress is evaluated explicitly, this forms a problem, since the model for cross and Reynolds stresses should also not be Galilean invariant. Germano (1986) suggested modified definitions for these stresses as

$$\begin{aligned} L_{ij} &= \widetilde{\tilde{u}_i\tilde{u}_j} - \tilde{\tilde{u}}_i\tilde{\tilde{u}}_j \\ C_{ij} &= \widetilde{\tilde{u}_i u'_j} + \widetilde{u'_i\tilde{u}_j} - \tilde{\tilde{u}}_i\tilde{u'}_j - \tilde{u'}_i\tilde{\tilde{u}}_j \\ R_{ij} &= \widetilde{u'_i u'_j} - \tilde{u'}_i\tilde{u'}_j. \end{aligned} \tag{2.38}$$

In terms of these definitions, the scale-similarity model evaluates only the Leonard stress and involves no model for the cross-stress or for the Reynolds stress.

In practice, it has turned out that the SSM model dissipates hardly at all (see e.g. Ferziger (1996)). A class of models called mixed models combines a scale-similarity type model and an eddy-viscosity model. Owing to the eddy-viscosity part, they include more dissipation than the scale-similarity model. Both the original scale-similarity model and the first mixed model were proposed by Bardina et al. (1980) (see e.g. Sagaut, (2001)). They combined the scale-similarity model with the Smagorinsky model as

$$\tau_{ij} - \frac{1}{3}\tau_{kk}\delta_{ij} = -2\left(C_S\Delta\right)^2 |\tilde{S}|\ \tilde{S}_{ij} + \left(\widetilde{\tilde{u}_i\tilde{u}_j} - \tilde{\tilde{u}}_i\tilde{\tilde{u}}_j\right) - \frac{1}{3}\left(\widetilde{\tilde{u}_k\tilde{u}_k} - \tilde{\tilde{u}}_k\tilde{\tilde{u}}_k\right)\delta_{ij}. \tag{2.39}$$

Also other choices than the Smagorinsky model are possible, and dynamic versions of the mixed model have been proposed, e.g. by Zang et al. (1993) and Vreman, Geurts and Kuerten (1994*b*).

2.2 Explicit Filtering in LES

When low-order finite-difference-type schemes are applied, the use of explicit filtering is usually justified by damping of the high-frequency components and thus the reduction of the numerical error and the expected improved simulation results. This has been supported by a priori tests (Ghosal 1996, Kravchenko and Moin 1997) and some actual simulations using finite-differences and explicit filtering (Lund and Kaltenbach 1995, Gullbrand 2001). In addition, explicit filtering is a tool in a posteriori testing of LES (Clark, Ferziger and Reynolds 1979, Vreman et al. 1996, Gullbrand 2002). In this section, we discuss the continuous filter functions and the different approaches to explicit filtering applied in this thesis.

2.2.1 No Filtering in LES?

Usually in LES applying finite-volume-type schemes, no explicit filtering is applied, and formally, the difference between the equations being solved (2.7) and

the Navier–Stokes equations (2.2) is the SGS term or SGS model. Even though the filter is not necessarily explicitly present in the simulation, there is a built-in filter associated with the chosen SGS model (Mason and Callen 1986, Magnient and Sagaut 2001), and with dissipative models, the built-in filter damps down the high-frequency components.

In finite-volume-type approximations, reduction on a discrete grid is often interpreted as filtering over a small control volume. Thus, the computational grid and SGS modelling are tied together. This approach was originally presented by Schumann (1975) and it is widely applied. However, as discussed in Chapter 1, there have been suggestions that, owing to the large truncation errors in finite-difference-type schemes, grid filtering is not sufficient from the point of view of the numerical error.

It has also been proposed that, in finite-difference calculations, discrete approximations of derivatives introduce a sort of implicit filter (Rogallo and Moin 1984). The discrete differentiation operator applied in finite-difference schemes can be written for the streamwise velocity component at grid point i as

$$\left.\frac{\Delta u}{\Delta x}\right|_i = \frac{u_{i+1} - u_i}{\Delta x} = \frac{\mathrm{d}}{\mathrm{d}x}\int_{x_i}^{x_{i+1}} u\,\mathrm{d}x = \left.\frac{\mathrm{d}\tilde{u}}{\mathrm{d}x}\right|_i, \tag{2.40}$$

where the subscripts refer to positions in space. However, Lund (1997) criticises this interpretation. While the filter applied to Navier–Stokes equations should be an average over a small volume in space, the interpretation in Equation (2.40) is a one-dimensional operator and the direction of filtering is determined by the differentiation. Navier–Stokes equations involve derivatives with respect to all three spatial coordinates, and thus, all the terms in the equations will be filtered with a different filter. Lund (1997) concludes that although there is an implicit filtering operation related to a finite-difference approximation, owing to multi-dimensionality, this is not a well-defined three-dimensional filter.

2.2.2 Different Approaches to Explicit Filtering

The idea in explicit filtering is to insure that the frequency content of all the terms in the equations is the same and to explicitly remove the high frequencies that are badly described by the discrete grid. The explicitly filtered equations are often written as

$$\frac{\partial \overline{\tilde{u}}_i}{\partial t} = -\frac{\partial \overline{\tilde{p}}}{\partial x_i} + \frac{\partial}{\partial x_j}\left(- \overline{\tilde{u}}_i\overline{\tilde{u}}_j - \tau_{ij} + \frac{1}{\mathrm{Re}_\tau}\left(\frac{\partial \overline{\tilde{u}}_i}{\partial x_j} + \frac{\partial \overline{\tilde{u}}_j}{\partial x_i}\right)\right), \tag{2.41}$$

where tilde refers to the implicit filtering induced by the reduction of the flow quantities on the discrete grid and the overbar to the explicit filter and the SGS term is

$$\tau_{ij} = \overline{\widetilde{u_i u_j}} - \overline{\tilde{u}}_i\overline{\tilde{u}}_j. \tag{2.42}$$

The most straightforward approach to implement explicit filtering would be to filter the velocity field at the end of each timestep as done by Lund and Kaltenbach (1995), where the spectral cutoff filter was applied in the homogeneous directions of the turbulent channel flow. However, when finite-difference-type methods are applied, filtering is usually performed in physical space and the filter function is not a projection like the spectral cutoff filter, i.e. filtering a quantity twice further damps down the high frequencies. This is a problem especially when an explicit time-integration method is applied (Lund 1997). One timestep of an explicit time-integration method for the resolved velocity field $\tilde{u}_i$ may be written as:

$$\tilde{u}_i^{n+1} = \tilde{u}_i^n + \Delta t^n \left(c_1 \Delta \tilde{u}_i^n + c_2 \Delta \tilde{u}_i^{n-1} \right), \tag{2.43}$$

where the superscript n refers to time levels, Δt is the timestep, c_1 and c_2 are the coefficients of the method and $\Delta \tilde{u}_i$ is the change of the velocity at one timestep. If $\tilde{u}_i^{n+1}$ is filtered at the end of each timestep, the resulting equation will look like

$$\begin{aligned} \overline{\tilde{u}_i^{n+1}} &= \overline{\overline{\tilde{u}_i^n} + \Delta t^n \left(c_1 \Delta \tilde{u}_i^n + c_2 \Delta \tilde{u}_i^{n-1} \right)} = \\ &= \overline{\overline{\tilde{u}_i^{n-1}} + \Delta t^{n-1} \left(c_1 \Delta \tilde{u}_i^{n-1} + c_2 \Delta \tilde{u}_i^{n-2} \right)} + \Delta t^n \left(c_1 \Delta \tilde{u}_i^n + c_2 \Delta \tilde{u}_i^{n-1} \right), \end{aligned} \tag{2.44}$$

where the overbar refers to explicit filtering. It is noticed that if the filter is not a projection, i.e. $\overline{\overline{u}}_i \neq \overline{u}_i$, the results from the previous time levels will be multiply filtered and damped further as the time integration proceeds. This is the case with all the filters defined in the physical space. However, the high-order commutative filters, which are discussed in Section 2.2.3, have a shape close to the spectral cutoff filter, and thus the damping is reduced.

In the implementation of an explicit time-integration method, the change of the velocity field $\Delta \tilde{u}_i$ is usually stored in its own variable. One way to avoid the excessive filtering is to filter $\Delta \tilde{u}_i$ as it is stored. In this case, each $\Delta \tilde{u}_i$ is filtered only once, and all the terms of Equation (2.43) will have the same frequency content. One timestep of an explicit time-integration method is then written as

$$\begin{aligned} \tilde{u}_i^{n+1} &= \tilde{u}_i^n + \Delta t^n \left(c_1 \overline{\Delta \tilde{u}_i^n} + c_2 \overline{\Delta \tilde{u}_i^{n-1}} \right) \\ &= \tilde{u}_i^{n-1} + \Delta t^{n-1} \left(c_1 \overline{\Delta \tilde{u}_i^{n-1}} + c_2 \overline{\Delta \tilde{u}_i^{n-2}} \right) + \Delta t^n \left(c_1 \overline{\Delta \tilde{u}_i^n} + c_2 \overline{\Delta \tilde{u}_i^{n-1}} \right), \end{aligned} \tag{2.45}$$

and we see that each term is now filtered only once.

Since the non-linear convection term of the Navier–Stokes equations is the term that generates frequencies beyond the characteristic frequency that defines the resolved flow field, it is sufficient to filter only this term (Lund 1997). In these approaches, the momentum equations being solved are written as

$$\frac{\partial \tilde{u}_i}{\partial t} = -\frac{\partial}{\partial x_j} \left(\overline{\tilde{u}_i \tilde{u}_j} + \overline{\tau}_{ij} \right) - \frac{\partial \tilde{p}}{\partial x_i} + \frac{\partial}{\partial x_j} \left(\frac{1}{\mathrm{Re}_\tau} \left(\frac{\partial \tilde{u}_i}{\partial x_j} + \frac{\partial \tilde{u}_j}{\partial x_i} \right) \right), \tag{2.46}$$

where the overbar again means explicit filtering. In this approach, the definition of the SGS term is written as

$$\overline{\tau}_{ij} = \widetilde{u_i u_j} - \overline{\tilde{u}_i \tilde{u}_j}, \tag{2.47}$$

which differs from the definition of Equation (2.8). If only the non-linear convection term is filtered, the Leonard stress (Eq. 2.34) is included implicitly in the convective term (Gullbrand 2001). Filtering of the non-linear convection term was successfully applied in the channel flow by Gullbrand (2001), Gullbrand (2002) and Amiri et al. (2005) with fourth-order finite-difference schemes. This approach is studied in the present work a priori, in actual simulations with a second-order scheme and a posteriori. In this type of filtering approach, a subfilter-scale model is often applied to reconstruct the scales that are smaller than the filter width but larger than the grid resolution (Gullbrand and Chow 2003).

In Equation (2.46), notation $\tilde{u}_i$ is used for the resolved velocity field. No overbar is visible since this term is not explicitly filtered. However, the resolved velocity field is affected by the filtering and it is not the same as the resolved velocity of Equation (2.7) where no explicit filtering is applied.

There are also alternative approaches to explicit filtering which stress the role of modelling. When explicit filtering is applied, in addition to subgrid-scale (SGS) stresses there are subfilter-scale (SFS) stresses which also require modelling. Carati et al. (2001) proposed an alternative formulation for explicit filtering where filtering and discretization processes are distinguished, and the SGS and SFS stresses are modelled separately. In this formulation, the actual filtering operation is performed only in the SFS model. They write the filtered Navier–Stokes equations as

$$\frac{\partial \overline{\tilde{u}}_i}{\partial t} = -\frac{\partial}{\partial x_j}\left(\widetilde{\overline{\tilde{u}}_i \overline{\tilde{u}}_j} + \widetilde{T_{ij}}\right) - \frac{\partial \overline{\tilde{p}}}{\partial x_i} + \frac{\partial}{\partial x_j}\left(\frac{1}{\mathrm{Re}_\tau}\left(\frac{\partial \overline{\tilde{u}}_i}{\partial x_j} + \frac{\partial \overline{\tilde{u}}_j}{\partial x_i}\right)\right), \tag{2.48}$$

where tilde refers to reduction to the discrete grid and the notation $\overline{\tilde{u}}_i$ stresses the indirect effect of explicit filtering on the resolved velocity field. T_{ij} represents both SGS and SFS stresses and it is defined as

$$\begin{aligned} T_{ij} &= \overline{u_i u_j} - \overline{\tilde{u}}_i \overline{\tilde{u}}_j = \left(\overline{u_i u_j} - \overline{\tilde{u}_i \tilde{u}_j}\right) + \left(\overline{\tilde{u}_i \tilde{u}_j} - \overline{\tilde{u}}_i \overline{\tilde{u}}_j\right) = \\ &= \overline{\tau}_{ij} + \left(\overline{\tilde{u}_i \tilde{u}_j} - \overline{\tilde{u}}_i \overline{\tilde{u}}_j\right), \end{aligned} \tag{2.49}$$

where the first term is the SGS stress and the second one the SFS stress. If this decomposition is substituted in Equation (2.48), an equation similar to Equation (2.46) is obtained. However, the velocity field $\overline{\tilde{u}}_i$ is being solved in the simulation, not $\tilde{u}_i$ which represents the resolved velocity field when no filtering is applied. Despite the formal similarity of the equations, a clear difference of the two approaches is that in the approach of Carati et al. (2001), the actual explicit

filtering appears only in the SFS model. The simplest possible SFS model for the last term of Equation (2.49) would be to approximate $\tilde{u}_i$ by $\overline{\tilde{u}}_i$, which means using the scale-similarity model. The approach of Carati et al. (2001) was applied by Winckelmans, Wray, Vasilyev and Jeanmart (2001) with a tensor-diffusivity model and by Gullbrand and Chow (2003) with dynamic mixed model and with dynamic reconstruction model. Winckelmans et al. (2001) noticed that in the turbulent channel flow, the results were similar to the ones obtained with no filtering and Gullbrand and Chow (2003) that the simulation results were improved when compared to a case with no filtering when a high-order reconstruction was applied to the SFS stresses. In both studies, the results with explicit filtering were compared to a simulation with the dynamic Smagorinsky model with the spectral cutoff as the test filter.

Stolz, Adams and Kleiser (2001) presented an approximative deconvolution model (ADM) for the description of the scales that are smaller than the applied filter width. The use of this model can be interpreted as explicit filtering, and it has also been applied in compressible flows together with high-order filters which are very close to the spectral cutoff filter (Mathew, Lechner, Foysi, Sesterhenn and Friedrich 2003, Mathew, Foysi and Friedrich 2006).

In addition, there are groups who do not apply any SGS modelling and let high-order filters eliminate the high-order modes from the resolved flow field. Visbal and Rizzetta (2002) applied compact schemes and high-order filters, and Bogey and Bailly (2006) low-dissipative schemes and selective explicit filtering. In both studies, it was concluded that using the high-order filtering instead of eddy-viscosity-type SGS modelling avoided the damping of the low frequencies and the reduction of the effective Reynolds number, which occur with eddy viscosity models.

2.2.3 Properties of Some Filter Functions

In this section, we interpret the resolved flow field $\tilde{u}_i$ as being obtained from a numerical simulation where the reduction on a discrete grid acts as a filter and no explicit filtering is applied. This is the commonly applied interpretation in simulations applying finite-difference-type approaches. An explicitly filtered velocity field is obtained by explicitly applying the filtering operation Eq. (2.5) during the simulation:

$$\overline{\tilde{u}}_i(x) = \int G(x-\xi, \Delta_f, x)\, \tilde{u}_i(x)\, \mathrm{d}\xi. \tag{2.50}$$

The idea of filtering is to damp the high frequencies in the resolved flow field, and thus the filter function is often studied in the spectral space. There filtering is performed as a product of the filtered function and the filter transfer function

as

$$\overline{\hat{u}}_i = \hat{u}_i \, \widehat{G}, \tag{2.51}$$

where hat refers to the Fourier transform and the filter transfer function, $\widehat{G}$, is the Fourier transform of the filter function

$$\widehat{G}\left(\hat{k}\right) = \int_{-\infty}^{\infty} G\left(x\right) e^{-I\hat{k}x} \mathrm{d}x, \tag{2.52}$$

where $\hat{k}$ refers to the wavenumber.

In this thesis, basically two types of filters are applied. In the first category, there are the filters that are discrete approximations to the so-called top-hat filter, and in the second category, the filters that are discrete approximations of the spectral cutoff filter. The top-hat filter is depicted in Figure 2.1, and it is sharp in the physical space. Its filter function is written as

$$G\left(x-\xi, \Delta_f\right) = \begin{cases} \frac{1}{\Delta_f}, & \text{for} \quad |x-\xi| < \Delta_f/2 \\ 0, & \text{otherwise} \end{cases} \tag{2.53}$$

and the corresponding transfer function as

$$\widehat{G}\left(\hat{k}\right) = \frac{\sin\left(\hat{k}\Delta_f/2\right)}{\hat{k}\Delta_f/2}. \tag{2.54}$$

As seen in the lower part of Figure 2.1, the top-hat filter is non-local in spectral space, and the frequencies close to the grid cutoff frequency $\hat{k}_\mathrm{c} = \pi/\Delta_f$ are damped but they are still included in the filtered field. The spectral cutoff filter, see Figure 2.2, has the opposite behaviour to the top-hat. Its filter transfer function is sharp:

$$\widehat{G}\left(\hat{k}\right) = \begin{cases} 1, & \text{for} \quad |\hat{k}| < \hat{k}_\mathrm{c} \\ 0, & \text{otherwise} \end{cases} \tag{2.55}$$

and the filter function is written as

$$G\left(\frac{x-\xi}{\Delta_f}\right) = 2\frac{\sin\left(\pi\frac{x-\xi}{\Delta_f}\right)}{\pi\left(x-\xi\right)/\Delta_f}, \tag{2.56}$$

where the filter width and the cutoff wavenumber are related via $\Delta_f = \pi/\hat{k}_\mathrm{c}$. There are also other possible filter functions and a thorough review on filters commonly applied in LES has been provided, e.g. by Sagaut (2001).

There are several ways to determine the width of a filter (Lund 1997), and in this thesis two of them are applied. For a positive-definite filter function G, the effective filter width is usually described by the standard deviation (Lund 1997):

$$\Delta_f = \sqrt{12 \int_{-\infty}^{\infty} x^2 G\left(x\right) \, \mathrm{d}x}, \tag{2.57}$$

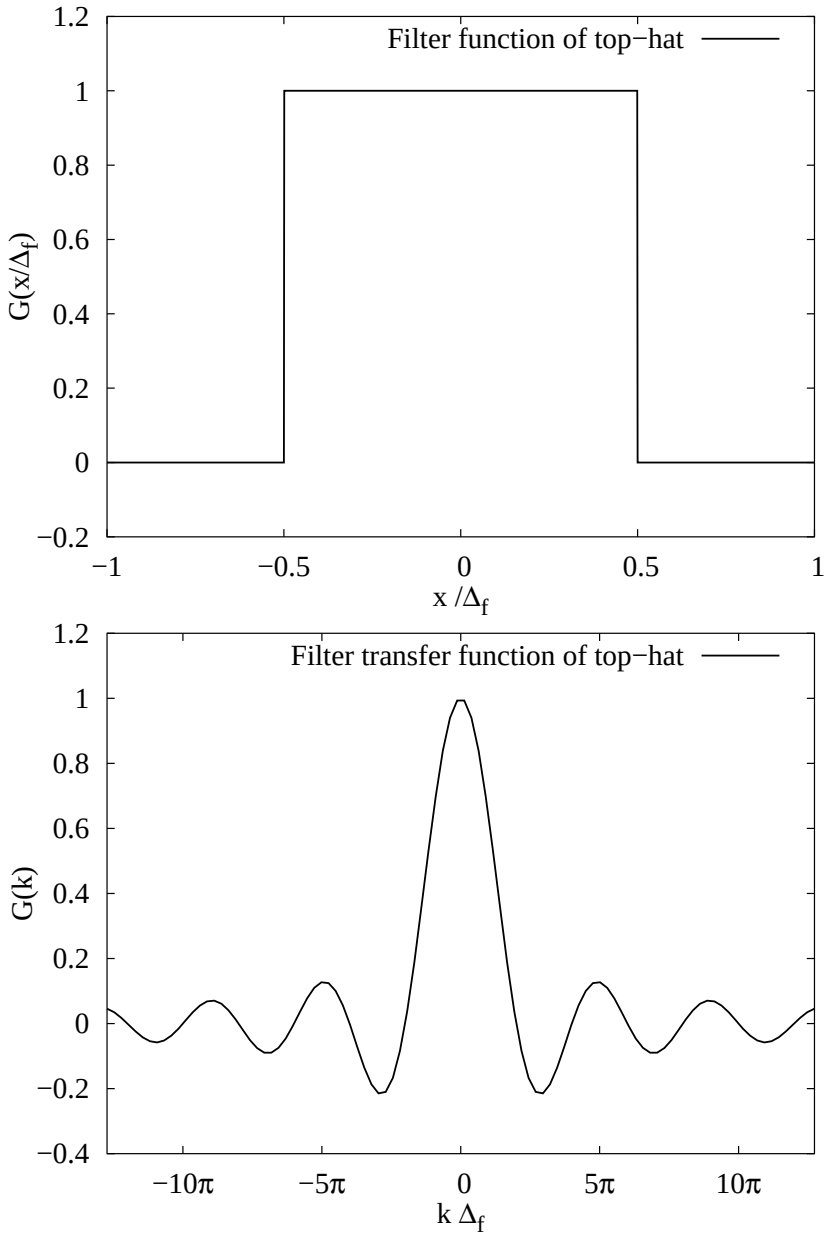

Figure 2.1: Filter function, G, (upper) and filter transfer function, $\widehat{G}$, (lower) of top-hat filter.

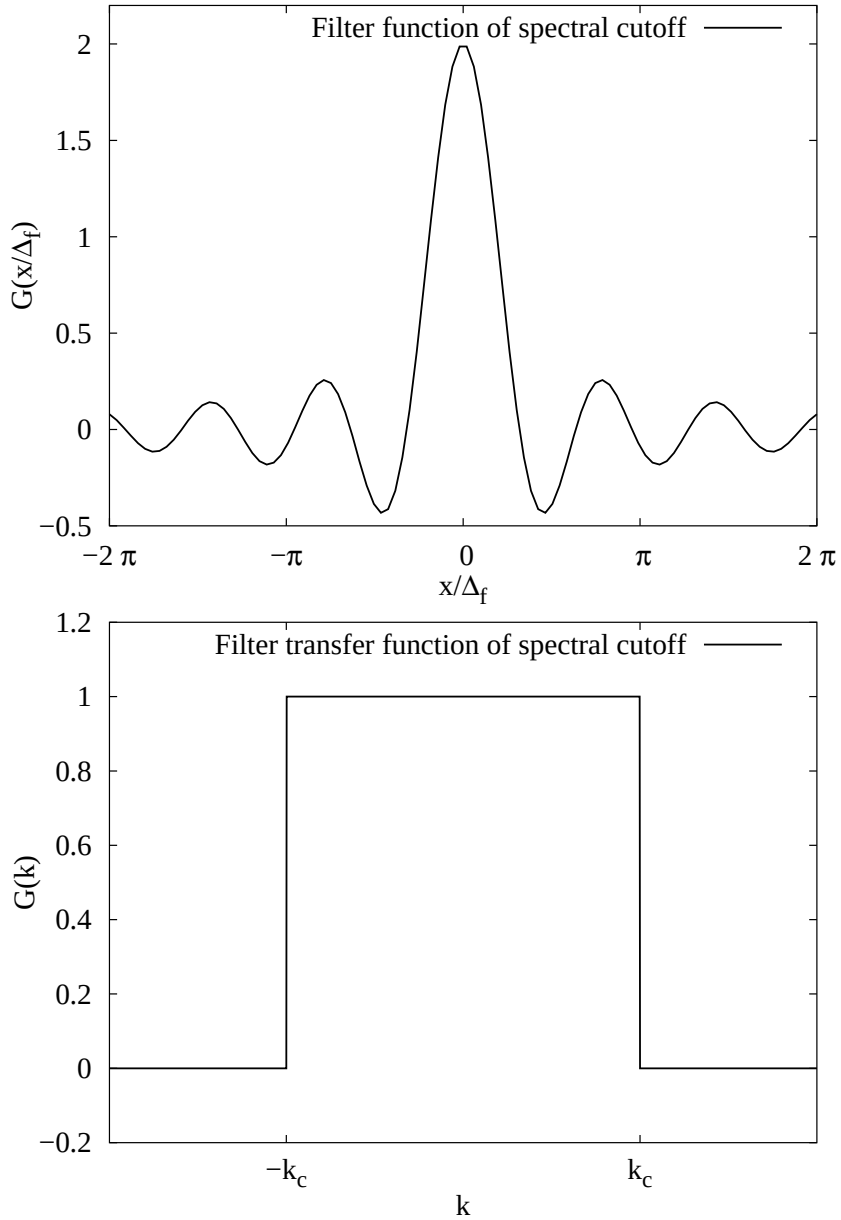

Figure 2.2: Filter function, G, (upper) and filter transfer function, $\widehat{G}$, (lower) of spectral cutoff filter.

where factor 12 assures that the filter width of the top-hat filter equals the length of the interval over which the filter function is non-zero. For some filters the second moment is zero, and this definition is then not valid. An alternative approach, which is natural for the spectral cutoff filter, is to interpret the wavenumber at which the filter transfer function obtains the value 0.5 as the effective cutoff frequency (Lund 1997, Vasilyev, Lund and Moin 1998). The filter width in the physical space is then related to this effective cutoff frequency via $\Delta_f = \pi/k_c$.

In numerical simulations, all the flow quantities are known only at discrete points in space, and a discrete counterpart is required for the continuous filtering operator (2.5). This is obtained by applying a numerical integration scheme to Equation (2.5). The Simpson and trapezoidal filters, commonly applied in LES using finite-difference schemes, are discrete counterparts of the top-hat filter (2.53) with the width of two grid spacings. The Simpson filter is obtained by assuming that the filter function is of Equation (2.53) form with $\Delta_f = 2\Delta$ and then approximating the integrand in Equation (2.5) by a Lagrange polynomial on each two adjacent subintervals. The resulting scheme is second-order accurate (Kreyszig 1993). The trapezoidal filter is obtained when the integrand is approximated by a piecewise linear function. In addition to Simpson and trapezoidal rules, also higher-order methods have been applied (Najjar and Tafti 1996). The resulting discrete filtering operation may be written as

$$\widetilde{u}_i\left(x_j\right) = \sum_{l=-K}^{K} a_l u_i\left(x_{j+l}\right), \tag{2.58}$$

where subscript j refers to a point in space and the coefficients a_l and the number of applied nodal points $2K+1$ are determined by the chosen numerical integration method and the assumed form of the filter function. The one-dimensional filter function corresponding to the discrete filtering operator may be written as (Lund 1997)

$$G\left(x\right) = \sum_{l=-K}^{K} a_l \delta\left(x - l\Delta\right), \tag{2.59}$$

where δ is the Dirac delta function and Δ the grid spacing. A multidimensional discrete filter is obtained by applying the one-dimensional filter sequentially to each coordinate direction. The filter transfer function corresponding to the discrete filter is written as

$$\widehat{G} = \sum_{l=-K}^{K} a_l \int \delta\left(x + l\Delta\right) e^{I\hat{k}x} \mathrm{d}x = \sum_{l=-K}^{K} a_l e^{I\hat{k}l\Delta} \tag{2.60}$$

If the filter is symmetrical, the imaginary part of the filter transfer function vanishes.

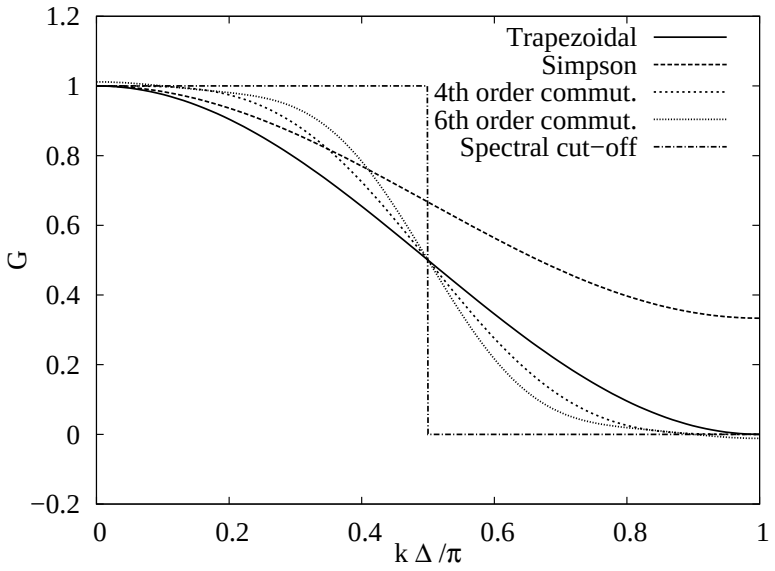

Figure 2.3: Transfer function $\widehat{G}$ of Simpson, trapezoidal and two commutative filters.

The coefficients of the one-dimensional Simpson and trapezoidal filters are given in Table 2.1, and the filter transfer functions are depicted in Figure 2.3. Two- or three-dimensional filters can be obtained by applying filtering sequentially to each coordinate direction. We notice that the Simpson filter does not obtain the value zero at the grid cutoff. The two other filters appearing in the figure, the commutative filters, are discussed later in this section.

Table 2.1: Coefficients of discrete filter with $\Delta_f = 2\Delta$. S = Simpson, T = Trapezoidal, C1 = 4th order commutative filter, C2 = 6th order commutative filter.

	a_0	$a_{\pm1}$	$a_{\pm2}$	$a_{\pm3}$	$a_{\pm4}$	$a_{\pm5}$
S	2/3	1/6				
T	1/2	1/4				
C1	1/2	9/32	0	−1/32		
C2	1/2	75/256	0	−25/512	0	3/256

Since the chosen numerical method determines the exact form of the discrete filter function (Eq. 2.59), it also affects the properties of the discrete filter like the filter width. The discrete counterpart of the standard-deviation-based definition of the filter width (Eq. 2.57) is written as (Lund 1997)

$$\Delta_f = \sqrt{12 \sum_{l=-K}^{K} l^2 a_l}. \tag{2.61}$$

The Simpson rule yields the intended filter width $\Delta_f = 2\Delta$, but with the trapezoidal rule, a larger effective filter width, $\Delta_f = 2.45\Delta$, is obtained.

The LES equations were derived from the Navier–Stokes equations assuming that the filtering operator commutes with differentiation. This is true for all filters if the grid is equally spaced. On a stretched grid, the discussed filters will introduce additional terms in the equations, which result from the lack of commutation. In the channel flow, this happens in the wall-normal direction where the grid is usually stretched. For example, a straightforward application of the top-hat filter (2.53) to an inhomogeneous direction

$$\overline{u}(x) = \frac{1}{\Delta_{f+}(x) + \Delta_{f-}(x)} \int_{x-\Delta_{f-}(x)}^{x+\Delta_{f+}(x)} u(y)\, \mathrm{d}y, \tag{2.62}$$

where $\Delta_{f+}(x) + \Delta_{f-}(x)$ is the effective filter width at location x, introduces a commutation error which is not necessarily small in comparison to the discretization error (Ghosal and Moin 1995).

Ghosal and Moin (1995) presented an approach to filtering that is based on mapping the non-uniform domain to an equally spaced one. The filtering operation for function $u(x)$ on the non-uniform grid is written as

$$\begin{aligned} \overline{u}(x) &= \frac{1}{\Delta_f} \int_{-a}^{b} G\left(\frac{f(x) - f(y)}{\Delta_f}\right) u(y) \frac{\mathrm{d}f}{\mathrm{d}y}\, \mathrm{d}y = \\ &= \frac{1}{\Delta_f} \int_{-a}^{b} \widetilde{G}(x, y, \Delta_f)\, u(y)\, \mathrm{d}y, \end{aligned} \tag{2.63}$$

where G is the filter function on the uniform grid and $\xi = f(x)$ is the mapping from the non-uniform grid, where the spatial coordinate is labelled as x, into the uniform grid, where the spatial coordinate is labelled as ξ. Interval $[-a, b]$ defines the area over which the filtering is applied in the physical space. This generalisation of the filter function to a non-uniform grid can be performed for any filter function. Since the grid becomes finer near solid boundaries, the support of the new filter function $\widetilde{G}$ automatically contracts when a wall is approached. In addition, owing to $\mathrm{d}f/\mathrm{d}y$, the filter function becomes asymmetrical near walls and gives more weight to those points that are close to the walls (Ghosal and Moin 1995).

Vasilyev et al. (1998) applied the approach of Ghosal and Moin (1995) to construct discrete higher-order commutative filters that avoid the inclusion of extra terms in the governing equations. They showed that, if a filter has vanishing moments for $k = 1, \ldots, n-1$, the commutation error is of the order Δ^n. The kth-order filter moment is defined as

$$M^k(\xi) = \int \zeta^k G(\xi, \zeta)\, \mathrm{d}\zeta, \tag{2.64}$$

and Vasilyev et al. (1998) thus discuss a class of filters that satisfy

$$\begin{aligned} M^0(\xi) &= 1 \quad \text{for} \quad \xi \in [f(-a), f(b)] \\ M^k(\xi) &= 0 \quad \text{for} \quad k = 1, \ldots, n-1 \quad \text{and} \quad \xi \in [f(-a), f(b)] \\ M^k(\xi) & \quad \text{exist for} \quad k \geq n \end{aligned} \tag{2.65}$$

The first requirement actually states that if a constant is filtered its value does not change. This is common to all filters.

In the approach of Vasilyev et al. (1998), the constructed filters are discrete filters defined in the computational space. This is convenient since the computational space, where the filters are actually applied in the implementation, is always uniformly distributed, and from the construction it then follows that the error owing to commutation is automatically of the desired order in the physical space.

A possibly asymmetrical discrete filtering operation on a uniform grid may be written as

$$\overline{u}_j = \sum_{l=-K_j}^{L_j} a_l^j u_{j+l}, \tag{2.66}$$

where the index j refers to a point in space. The corresponding discrete filter function is written as

$$G(x_j) = \sum_{l=-K_j}^{L_j} a_l^j \delta(x_j - x_l), \tag{2.67}$$

and the discrete filter transfer function as

$$\widehat{G}\left(\hat{k}\right) = \sum_{l=-L_j}^{K_j} a_l^j e^{-I\Delta\hat{k}l}. \tag{2.68}$$

The index j stresses the possibility that the number of used nodal points and filter coefficients may vary in space. Thus, a symmetrical filter could be applied in the middle of the domain and an asymmetrical one near the walls. For the discrete filter function to satisfy properties (2.65), the coefficients a_l^j should satisfy the equations

$$\int G(x)\, \mathrm{d}x = \sum_{l=-L_j}^{K_j} a_l^j = 1 \tag{2.69}$$

$$\int x^k G(x)\, \mathrm{d}x = \sum_{l=-L_j}^{K_j} l^k a_l^j = 0, \quad k = 1, \ldots, n-1. \tag{2.70}$$

The larger the number of vanishing moments, the closer the filter transfer function $\widehat{G}$ is to the spectral cutoff filter at the low wavenumbers.

To obtain a reasonable filter, one has to state some additional requirements involving the shape of the filter transfer function. Vasilyev et al. (1998) set the value of $\widehat{G}$ to zero at the grid cutoff wavenumber, $\hat{k}_c = \pi/\Delta$, to remove the high-frequency components. As we saw in Figure (2.3), there are filters like the Simpson filter which do not satisfy this requirement. Thus, just damping the high frequencies might be sufficient. The filter should also have the desired effective filter width for which Vasilyev et al. (1998) apply the definition based on the effective cutoff wavenumber. If in addition, a number of derivatives of $\widehat{G}$ is fixed to zero at the grid cutoff, its shape at the high frequencies becomes closer to the spectral cutoff. The wider the desired filter, the more derivatives one has to fix at the grid cutoff. Otherwise, the filter transfer function can obtain large negative or positive values at high frequencies. As equations, these requirements are written as:

$$\widehat{G}\left(\frac{\pi}{\Delta}\right) = \sum_{l=-L_j}^{K_j} a_l^j e^{-I\pi l} = \sum_{l=-L_j}^{K_j} (-1)^l a_l^j = 0 \tag{2.71}$$

$$\widehat{G}\left(\frac{\pi}{\Delta_f}\right) = \sum_{l=-L_j}^{K_j} e^{-I\pi\Delta/\Delta_f l} a_l^j = 0.5 \tag{2.72}$$

$$\frac{\mathrm{d}^m}{\mathrm{d}\hat{k}^m}\widehat{G}\left(\hat{k}\right)|_{\hat{k}=\pi/\Delta} = (-I\Delta)^m \sum_{l=-L_j}^{K_j} l^m (-1)^l a_l^j = 0 \tag{2.73}$$

where m has values from 1 to the maximum number of derivatives set to zero. If the filter is symmetrical, i.e. $L_j = K_j$ and $a_{-i} = a_i$, the equations the discrete filter needs to satisfy simplify further since for a symmetrical filter, the odd moments in Equation (2.70), the imaginary part of Equation (2.72) and odd derivatives at the grid cutoff (Eq. 2.73) vanish automatically.

In this thesis, several filters were constructed following the method of Vasilyev et al. (1998). In Table 2.1, labels C1 and C2 refer to 4th and 6th-order commutative filters which both have two vanishing derivatives at the grid cutoff and the width of $\Delta_f = 2\Delta$. These filters are depicted in Figure 2.3, and we notice that they are closer to the spectral cutoff than the Simpson and trapezoidal filters. Thus, besides the small commutation error, the benefit of these commutative filters is their shape. Actually, the trapezoidal filter is an example of a second-order commutative filter. In addition, filters with the widths of three, four and six grid spacings were constructed. Their coefficients are given in Table 2.2, and the filter transfer functions are depicted in Figure 2.4. The properties of all the applied filters are collected in Table 2.3. As the filter width was increased to avoid large negative and positive values of the filter transfer function, more derivatives had to be fixed to zero at the grid cutoff. In order to keep the number of nodal points the filter applies and thus the computational cost reasonable, the number of zero moments and the order of the commutation error had to be decreased.

Table 2.2: Coefficients of wider discrete filters.

Δ_f/Δ	a_0	$a_{\pm1}$	$a_{\pm2}$	$a_{\pm3}$	$a_{\pm4}$	$a_{\pm5}$	$a_{\pm6}$
3	373/1152	911/3456	203/1728	-11/2304	-203/6912	-61/6912	
4	0.2606	0.2134	0.1146	0.0370	0.0053	-0.0004	-0.0002
6	0.1564	0.1539	0.1332	0.0866	0.0375	0.0095	0.0011

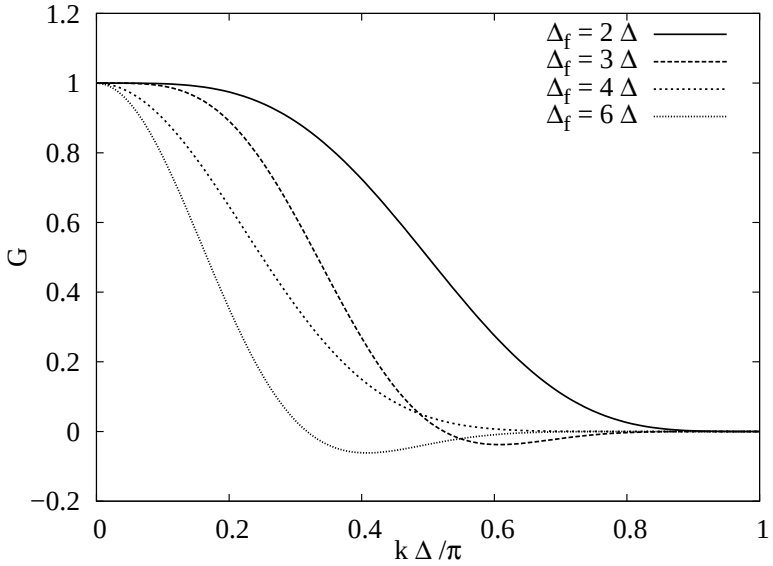

Figure 2.4: Transfer functions $\widehat{G}$ of commutative filters with different widths.

The approaches for filtering on non-uniform grids discussed by Ghosal and Moin (1995) and Vasilyev et al. (1998) can be extended to three dimensions. Also, the corresponding error estimates hold in the three-dimensional case. The three-dimensional discrete filter is obtained by sequential application of the one-dimensional discrete filter to all coordinate directions. The filters discussed above apply quite many grid points, and this constitutes a problem in the near-wall region when the filter is applied in the wall-normal direction. Thus, in the points near solid walls, filters with fewer zero moments that also apply fewer grid points, or asymmetrical versions of the filters were applied.

Besides high-order filtering, there are also other approaches to deal with the commutation error related to filtering on non-uniform grids. van der Bos and Geurts (2005) show that the commutation error can be associated with the apparent local creation or destruction of resolved turbulent flow scales. Based on a priori studies, they propose Lagrangian modelling for the effect of non-uniform filter width on the kinetic energy. The model is written in terms of the material derivate of

the filter width.

Table 2.3: Properties of filter and filter transfer functions of the applied filters. S = Simpson, T = Trapezoidal, C = Commutative.

	filter width Δ_f/Δ	commut error $\mathcal{O}(\Delta^n)$	zero derivatives at k_c N
S	2	2	1
T	2	2	1
C	2	4	3
C	2	6	3
C	3	4	3
C	4	2	9
C	6	2	9

2.3 Applied Numerical Methods

2.3.1 Spatial Grid System and Discretization

In the simulations presented in this thesis, the second-order central-difference scheme was applied on a staggered grid system. This grid system was first proposed by Harlow and Welch (1965). On a staggered grid, the pressure point is located in the middle of a computational cell and the velocity points on the boundaries. The streamwise velocity point is on the boundary normal to the streamwise component, etc. The staggered grid system is illustrated in Figure 2.5, where u refers to the streamwise velocity component and v to the wall-normal one. The spanwise velocity component is denoted with w. The pressure points are marked with black squares and the streamwise and wall-normal velocity points with arrows. Also the numbering of the p, u and v points is marked.

The staggered grid system has two advantages over the collocated system where all flow quantities are located in the middle of the computational cell. Firstly, there is a strong coupling between velocity and pressure and thus, oscillating pressure modes are readily avoided (Ferziger and Peric 1999). Secondly, when the non-linear convection term of the Navier–Stokes equations (2.2) is written in the divergence form as in Equation (2.2), the central-difference scheme conserves kinetic energy only on the staggered system (Morinishi, Lund, Vasilyev and Moin 1998). At high Reynolds numbers, SGS models do not usually dissipate enough energy to stabilise the simulation, and schemes that do not conserve kinetic energy may be unstable (Mahesh, Constantinescu and Moin 2004). When the resolution

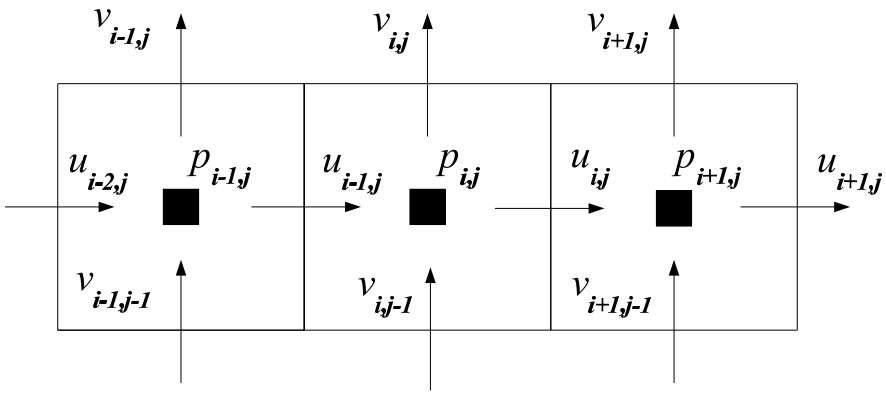

Figure 2.5: p, u and v points on a staggered grid.

is fine enough to resolve the viscous dissipation, as in DNS, it is not as crucial that the numerical scheme conserves kinetic energy (Mahesh et al. 2004).

The applied grid was equally spaced in the streamwise and spanwise directions. We label the grid resolution in these directions as Δx and Δz. In the wall-normal direction, the applied grid was stretched using the hyperbolic tangent function:

$$y_j = \frac{1}{2}\left(1 + \frac{\tanh\left(\gamma\left(1 + 2\left(j_{\max} - j\right)/j_{\max}\right)\right)}{\tanh\left(\gamma\right)}\right), \tag{2.74}$$

where j is the index of each grid point in the wall-normal direction and values 2 and 2.2 were applied for the parameter γ which controls the grid stretching. The wall-normal grid spacing is defined as $\Delta y_j = y_j - y_{j-1}$.

The details of the applied discretization method, the classical analysis of the involved truncation error and the conservation properties were discussed in the author's licentiate thesis (Brandt 2004).

2.3.2 Pressure Correction Method

In the Navier–Stokes equations (2.1) and (2.2), there is no independent equation for pressure. A usual choice for incompressible flows is to interpret the pressure gradient as a parameter that is used to force the continuity condition (2.1).

When an explicit time-integration method is applied, the temporally discretized form of the momentum equation may by written as

$$\tilde{u}_i^{n+1} = \tilde{u}_i^n + \Delta t^n\left(-\frac{\partial \tilde{p}}{\partial x_i} + \frac{\partial}{\partial x_j}\left(-\tilde{u}_i\tilde{u}_j - \tau_{ij} + \frac{1}{\mathrm{Re}_\tau}\left(\frac{\partial \tilde{u}_i}{\partial x_j} + \frac{\partial \tilde{u}_j}{\partial x_i}\right)\right)\right), \tag{2.75}$$

where Δt^n is the timestep and the superindices refer to time levels. The integration of the momentum equation is performed in two steps. First, only the convective and diffusive terms are integrated, and the resulting field is called the predicted velocity field u_i^*:

$$\tilde{u}_i^* = \tilde{u}_i^n + \Delta t^n \left(\frac{\partial}{\partial x_j} \left(-\tilde{u}_i \tilde{u}_j - \tau_{ij} + \frac{1}{\mathrm{Re}_\tau} \left(\frac{\partial \tilde{u}_i}{\partial x_j} + \frac{\partial \tilde{u}_j}{\partial x_i} \right) \right) \right). \tag{2.76}$$

The final velocity field is obtained from the predicted field by including the pressure gradient term using the explicit Euler method:

$$\frac{\partial u_i^{n+1}}{\partial x_i} = \frac{\partial u_i^*}{\partial x_i} - \Delta t^n \frac{\partial^2 p}{\partial x_i \partial x_i}. \tag{2.77}$$

When it is required that the final field is divergence-free, a Poisson equation is obtained for pressure as

$$\frac{\partial u_i^*}{\partial x_i} - \Delta t^n \frac{\partial^2 p}{\partial x_i \partial x_i} = 0 \quad \Rightarrow \quad \frac{\partial^2 p}{\partial x_i \partial x_i} = \frac{1}{\Delta t} \frac{\partial u_i^*}{\partial x_i}. \tag{2.78}$$

The final velocity is obtained by correcting the predicted velocity field by pressure gradient as

$$u_i^{n+1} = u_i^* - \Delta t \frac{\partial p}{\partial x_i}. \tag{2.79}$$

One interpretation of this method is that the convective and diffusive terms are integrated using a chosen time-integration method and the pressure gradient is integrated using the explicit Euler method. When a multi-step method, like the Runge–Kutta, is applied, the Poisson equation for pressure is solved and the continuity equation is forced on each intermediate timestep.

In the channel flow, periodic boundary conditions are applied to pressure in the streamwise and spanwise directions, and thus only the fluctuating pressure, which has a zero mean value, is solved from Equation (2.78). In the channel flow, there is a mean-pressure gradient only in the streamwise direction, and in the non-dimensional form applied here, this non-dimensional mean-pressure gradient has the value 2. Thus, after the pressure correction step (2.79), the velocity field is once more corrected by the mean-pressure gradient as

$$u = u^{n+1} - \Delta t \underbrace{\frac{\partial P}{\partial x}}_{=2}. \tag{2.80}$$

In this correction, only a constant (constant in space) is added to the streamwise velocity component. Thus, after this second pressure correction step, the velocity field is still divergence-free.

Solving the discrete counterpart of the Poisson equation (2.78) for pressure is time consuming. When this equation is discretized with the second-order central-difference scheme, pressure will be connected with its six neighbouring values. We can, however, decouple the derivatives by transforming the homogeneous directions into Fourier space, and thus speed up the computation. This method for easing the integration of the Poisson equation was first applied by Orszag (1969). After the transformation, the Poisson equation may be written as

$$\left(-\hat{k}_x^2 - \hat{k}_z^2\right)\hat{p} + \frac{\partial^2 \hat{p}}{\partial y^2} = \mathcal{F}\left(\frac{1}{\Delta t}\frac{\partial u_i^*}{\partial x_i}\right), \tag{2.81}$$

where $\hat{p}$ denotes the Fourier-transform of p, $\hat{k}_x$ and $\hat{k}_z$ the modified wavenumbers corresponding to the second-order central-difference scheme in the x and z-directions respectively, and $\mathcal{F}$ the Fourier-transform operator.

Periodic boundary conditions for pressure are applied in the streamwise and spanwise directions. Velocity is fixed at the solid walls, and as noted by Moin and Kim (1980), no boundary conditions are required there for pressure.

This type of pressure-correction approach is very typical in channel flow simulations, and it has been applied, e.g. in Moin and Kim (1982), Eggels, Unger, Weiss, Westerweel, Adrian, Friedrich and Nieuwstadt (1994) and Gullbrand and Chow (2003).

2.3.3 Time Integration

In this thesis, a low-storage third-order three-stage explicit Runge–Kutta method is applied to time integration. In Runge–Kutta methods, the increased accuracy is gained by taking intermediate timesteps inside physical ones. Runge–Kutta methods thus require information only from one previous time level and maintain their accuracy even when the timestep varies. The cost is extra computational effort. The equations have to be integrated several times in one physical timestep. However, the large Courant number 1.7 allowed by the applied method (Lundbladh, Berlin, Skote, Hildings, Choi, Kim and Henningson 1999) compensated for the extra effort when compared to a third-order Adams–Bashforth method (Brandt 2004). Also a four-stage version of this Runge–Kutta method is available, and in DNS, it was found to be more efficient than the three-stage version (Brandt 2004). However, in some parts of the the present work, explicit filtering is applied on each intermediate timestep, and then the four-stage method became too heavy.

The applied Runge–Kutta method may be written as

$$\begin{aligned} u_i^{n+1/3} &= u_i^n + \Delta t^n \frac{8}{15} \Delta u_i^n \\ u_i^{n+2/3} &= u_i^{n+1/3} + \Delta t^n \left(\frac{5}{12} \Delta u_i^{n+1/3} - \frac{17}{60} \Delta u_i^n \right) \\ u_i^{n+1} &= u_i^{n+2/3} + \Delta t^n \left(\frac{3}{4} \Delta u_i^{n+2/3} - \frac{5}{12} \Delta u_i^{n+1/3} \right) \end{aligned} \tag{2.82}$$

where the superscripts refer to time levels, Δt is the timestep, $u_i^{n+1/3}$, $u_i^{n+2/3}$ and u_i^{n+1} to resolved flow fields on the first, second and third intermediate timestep, respectively, and Δu_i is the change of u_i, which includes the space-discretized convection, diffusion and SGS terms from Equation (2.7). This Runge–Kutta method has the advantage that between the intermediate timesteps, we have to store only the result from the previous intermediate timestep. The Poisson equation (2.78) is solved at each intermediate timestep, and the pressure correction steps (2.79) and (2.80) are applied to each intermediate velocity field. When explicit filtering is applied, also filtering is performed on each intermediate step.

In the simulations, the timestep varied in time and the maximum Courant number was fixed to the value 1.2 or below to assure that the error owing to temporal discretization remains small. The timestep was determined from the condition

$$\Delta t = \min \left(\mathrm{CFL} \left(\frac{|u_i|}{\Delta x_i} + \nu \frac{1}{\Delta x_i^2} \right)^{-1} \right), \tag{2.83}$$

where CFL is the Courant number, $|u_i|$ is the absolute value of ith velocity component and Δx_i the grid spacing in the ith coordinate direction.

2.3.4 Performing the Actual Simulations

The channel flow code used in the simulations is based on a DNS code written by Dr. Bendiks Jan Boersma from TU Delft. In the present work, Runge–Kutta schemes for time integration, subgrid-scale models and explicit filtering were implemented to the code. The numerical methods, models and filters included in the present version of the code were described in the previous sections.

The initial condition for the present simulations was obtained using a random field or by interpolating the velocity field of another simulation. The simulations were first run for $30 - 40$ non-dimensional time units to let the initial disturbances edge away, and no statistics were collected during this time. After the first $30 - 40$ time units, the simulations were continued for about 60 time units, and during this time the statistics were updated after each 0.1 or 0.2 time units. One indication of converged statistics is the coincidence of the profiles evaluated

from top and bottom walls. Usually, once the profiles of the root mean squares of the fluctuating velocity components matched on both walls, the statistics were converged. In some simulations with large explicit filter widths, some asymmetry remained between the top and bottom walls. In these cases, the studied Reynolds stress profile is the average between the two walls. Most of the simulations were run as serial jobs in CSC's (Scientific Computing Ltd) computer "sepeli" which is a cluster of 2.2 GHz AMD Opteron-processors.

2.4 Code Validation in DNS of Channel Flow

In this section, DNS results for the fully developed turbulent channel flow between two infinite parallel walls are presented at two Reynolds numbers, $\mathrm{Re}_\tau = 180$ and $\mathrm{Re}_\tau = 395$. The aim is to verify the performance of the code and the actual order of the numerical methods. We first study the mean flow quantities at the highest applied resolutions for both Reynolds numbers, and then the behaviour of the total error at the $\mathrm{Re}_\tau = 395$ case.

2.4.1 Flow Statistics

The dimensions of the channel and the highest applied grid resolution in DNS for the $\mathrm{Re}_\tau = 180$ case are given in Table 2.4 and for the $\mathrm{Re}_\tau = 395$ case in Table 2.5. For both cases, the grid convergence was studied in the author's licentiate's thesis (Brandt 2004). For the $\mathrm{Re}_\tau = 180$ case, good grid convergence was obtained there, and thus the study is not repeated here and only the results with the highest resolution are presented. In the present work, the simulations at $\mathrm{Re}_\tau = 395$ were repeated using higher resolutions, and the grid-convergence study is presented here.

Table 2.4: Dimensions of the channel and grid resolution in the DNS at $\mathrm{Re}_\tau = 180$.

	streamwise	spanwise	wall-normal
extent of the domain / channel height	4.0	2.0	1.0
extent in wall units	1440	720	360
number of grid points	120	150	100
size of grid cells in wall units	12	5	6 (max) 0.5 (min)

wall units: $x^+ = \mathrm{Re}_\tau x$, where x is scaled by the channel half-width.

The mean-velocity profile and the diagonal Reynolds stress components scaled by the friction velocity from the simulation at $\mathrm{Re}_\tau = 180$ are given in Figures 2.6 and

Table 2.5: Dimensions of the channel and grid resolution in the DNS at $\mathrm{Re}_\tau = 395$.

	streamwise	spanwise	wall-normal
extent of the domain / channel height	3.0	1.6	1.0
extent in wall units	2370	1264	790
number of grid points	216	216	216
size of grid cells in wall units	11	6	8 (max) 0.5 (min)

wall units: $x^+ = \mathrm{Re}_\tau x$, where x is scaled by the channel half-height.

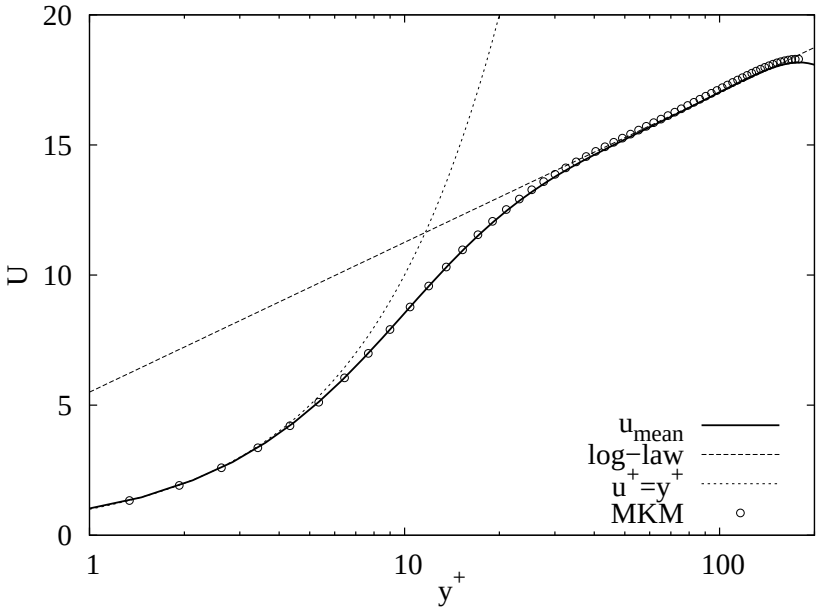

Figure 2.6: Mean-velocity profile. $\mathrm{Re}_\tau = 180$.

2.7, respectively, and the turbulent, viscous and total stresses in Figure 2.8. The reference data is from the simulations of Moser et al. (1999) (MKM). The one-dimensional energy spectra of the streamwise velocity component in streamwise and spanwise directions are plotted in Figure 2.9. The spectra were obtained as Fourier transforms of the streamwise and spanwise two-point self-correlation functions of the velocity component. The streamwise one-dimensional spectrum is plotted in the middle of the channel and the spanwise in the near-wall region. These are the restricting areas for the spectra. In addition, spectra from $y^+ \approx 36$ are included. They are required in the next chapter. We see that the spectra drop off several orders of magnitude, and thus the grid resolution seems adequate.

In Figure 2.10, the mean-velocity profile is plotted from the $\mathrm{Re}_\tau = 395$ case. To study the grid convergence, three coarser grid results obtained on grids with 126^3,

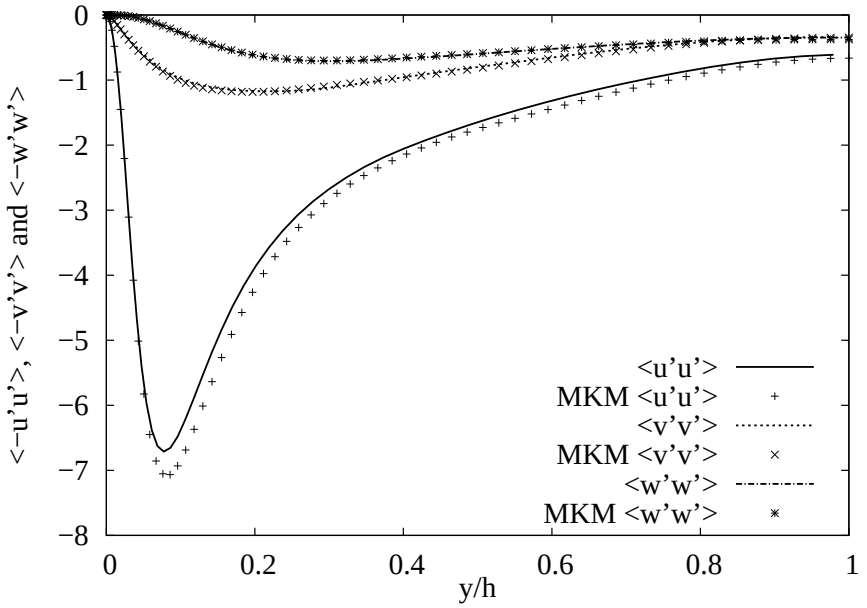

Figure 2.7: Diagonal Reynolds stress components $\langle u_i' u_i' \rangle$. $\mathrm{Re}_\tau = 180$.

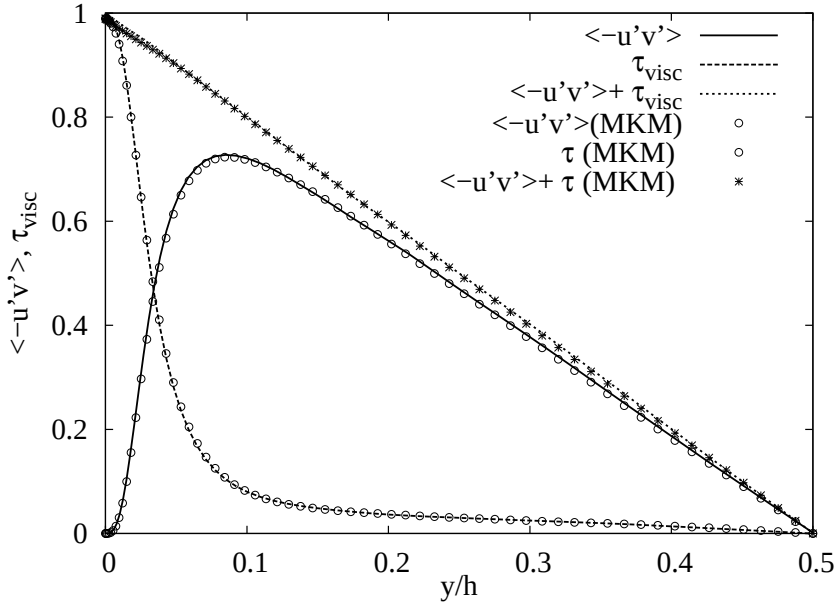

Figure 2.8: Turbulent, viscous and total stresses. $\mathrm{Re}_\tau = 180$.

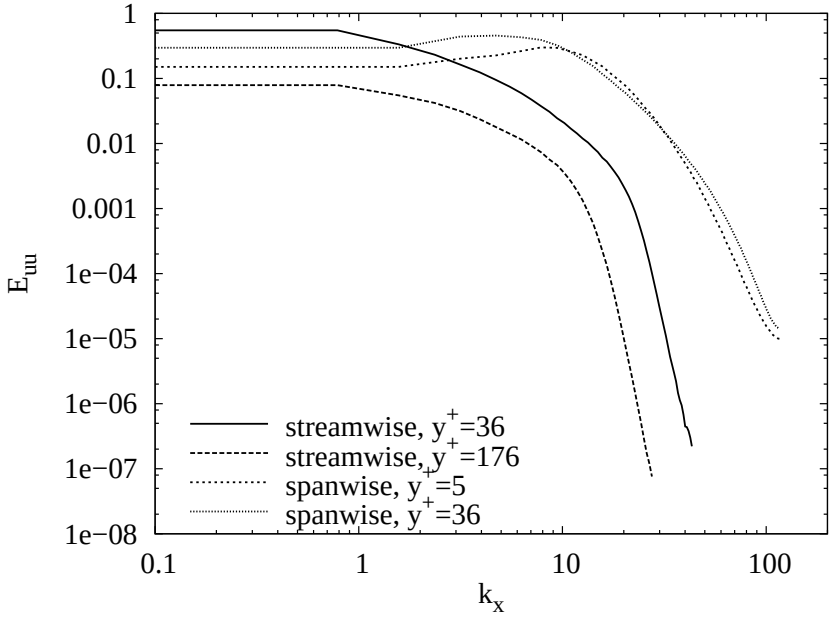

Figure 2.9: One-dimensional energy spectra in streamwise and spanwise directions. $\mathrm{Re}_\tau = 180$.

150^3 and 180^3 grid points and the same computational domain as in the 216^3 case are included. The mean velocity is underpredicted compared to the reference data. The diagonal Reynolds stress components are given in Figures 2.11–2.12. Here, all the stress components remain slightly underpredicted. The turbulent shear stress is depicted in Figure 2.14, and there we see good grid convergence. The total, viscous and turbulent stresses for the highest resolution case are depicted in Figure 2.15. The one-dimensional energy spectrum of the streamwise velocity component in the streamwise direction is plotted in Figure 2.16 in the middle of the channel, and the spanwise spectrum in the near-wall region ($z^+ \approx 5$). The spectra drop off, but in the spanwise direction, the resolution could be further improved. At this larger Reynolds number, the simulation is thus not as well resolved as at the lower Reynolds number.

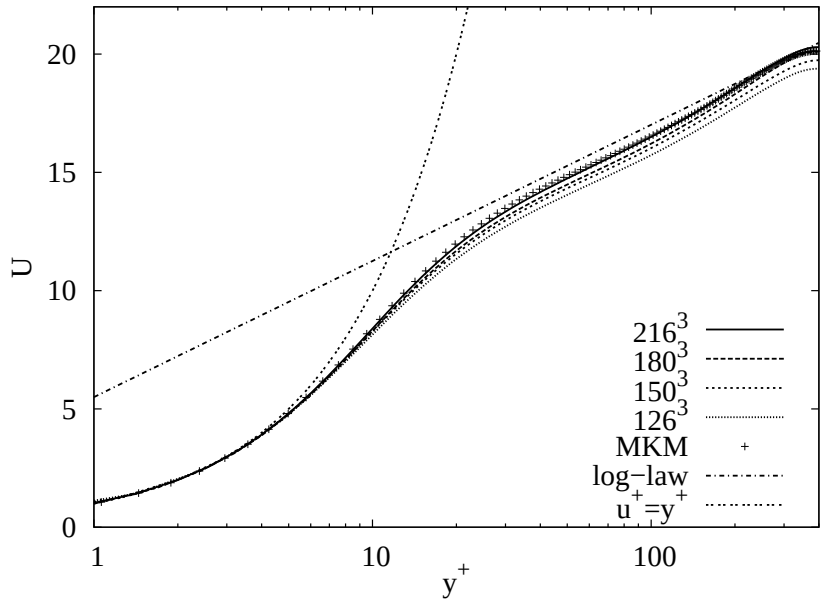

Figure 2.10: Mean velocity profile. $\mathrm{Re}_\tau = 395$.

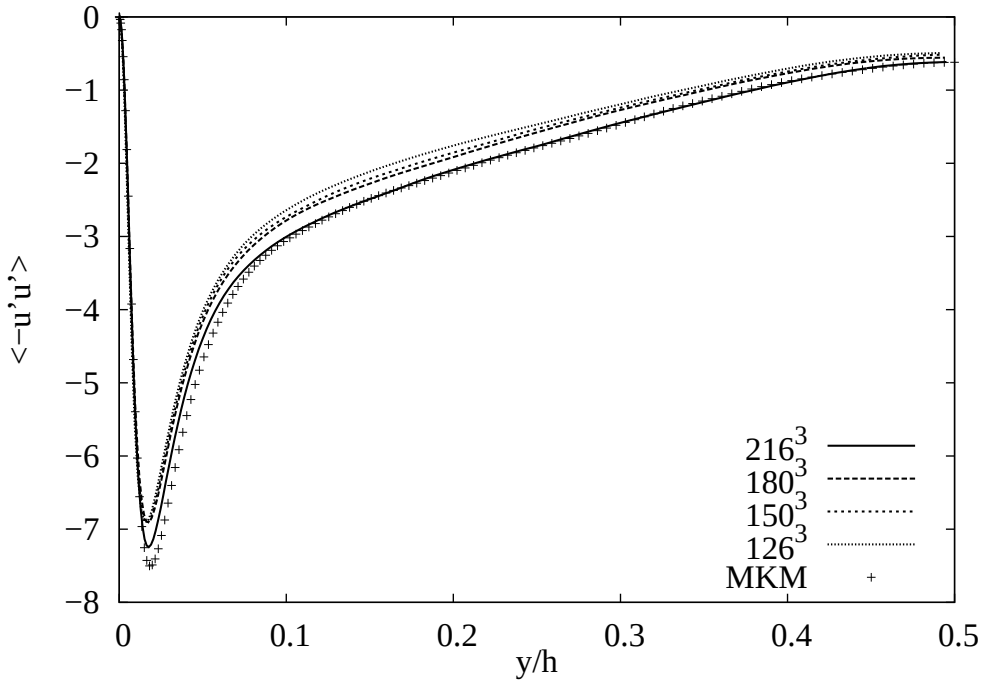

Figure 2.11: Streamwise Reynolds stress component $\langle u'u' \rangle$. $\mathrm{Re}_\tau = 395$.

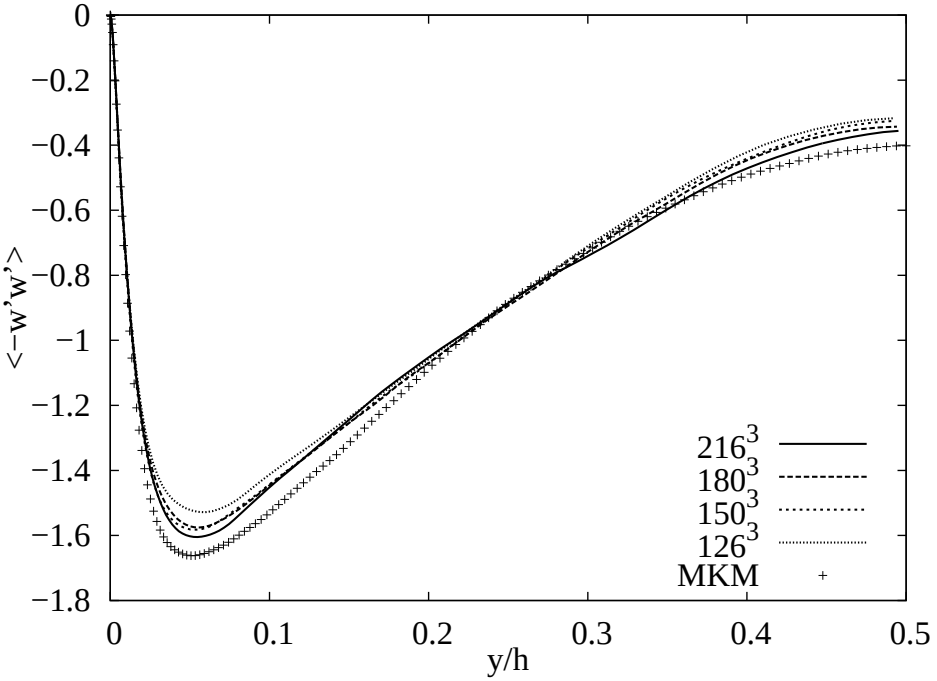

Figure 2.12: Spanwise Reynolds stress component $\langle w'w' \rangle$. $\mathrm{Re}_\tau = 395$.

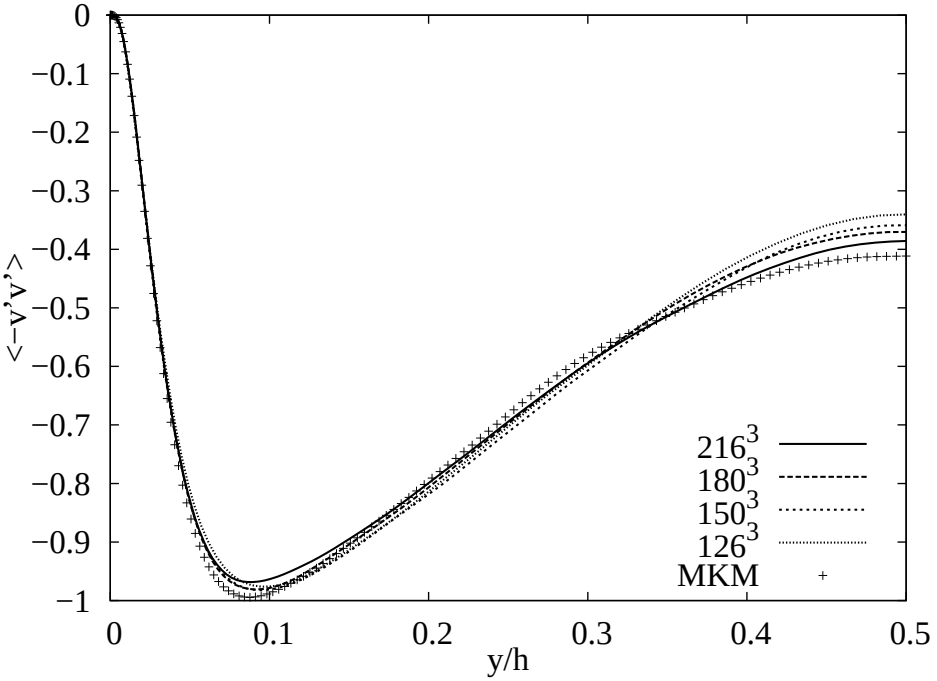

Figure 2.13: Wall-normal Reynolds stress component $\langle v'v' \rangle$. $\mathrm{Re}_\tau = 395$.

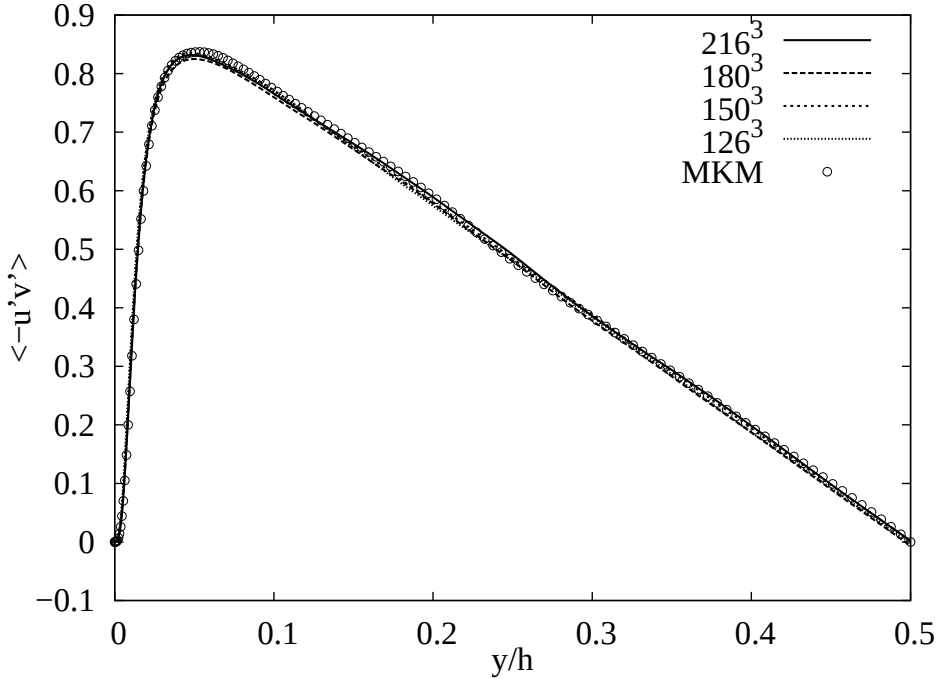

Figure 2.14: Turbulent shear stress $\langle u'v' \rangle$. $\mathrm{Re}_\tau = 395$.

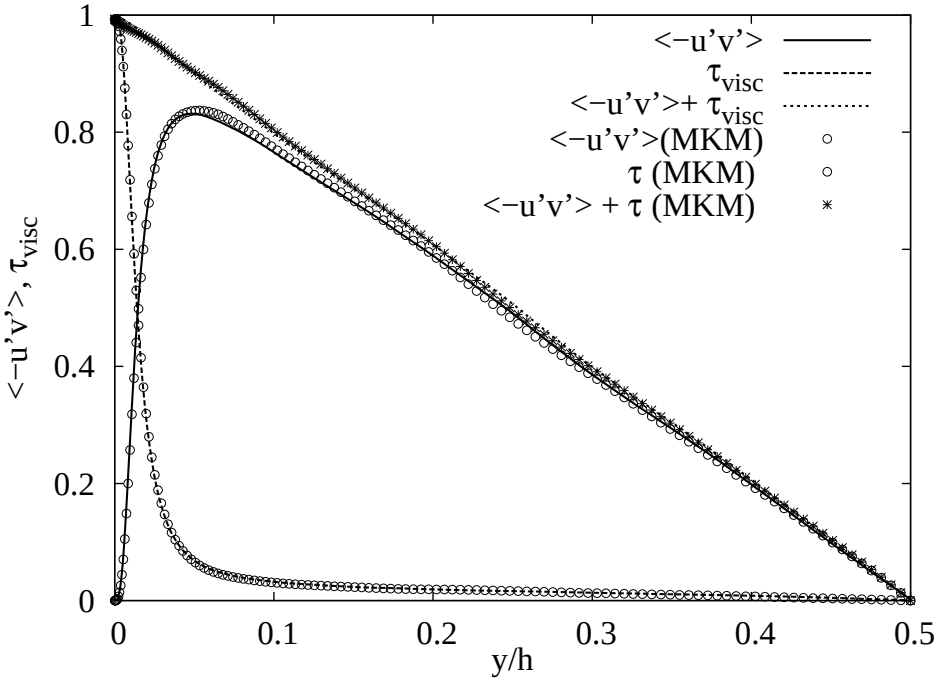

Figure 2.15: Total, viscous and turbulent stresses for 216^3 case. $\mathrm{Re}_\tau = 395$.

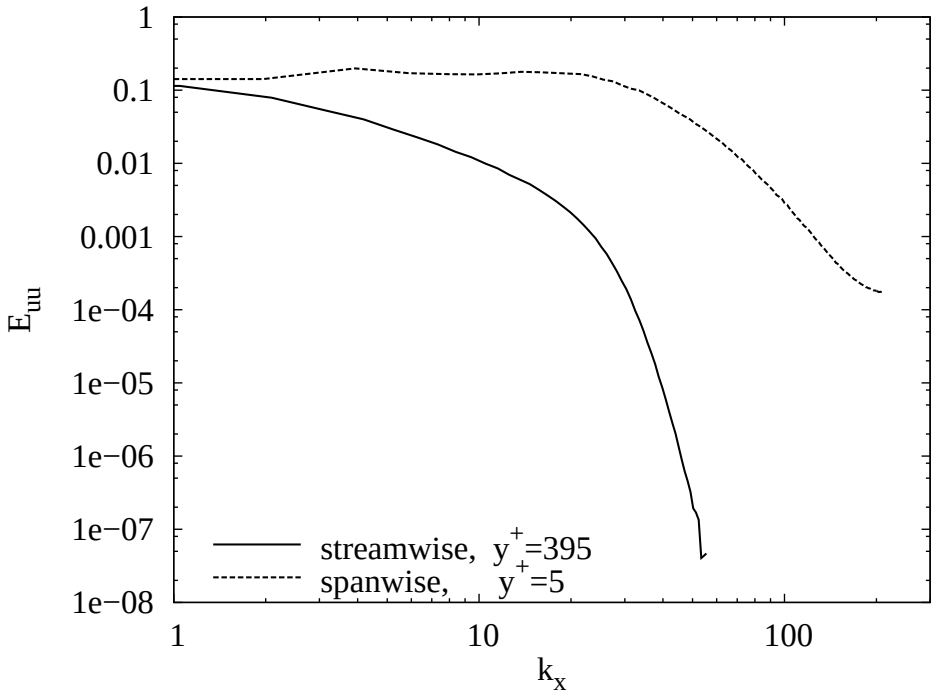

Figure 2.16: One-dimensional energy spectra in streamwise and spanwise directions. $\mathrm{Re}_\tau = 395$.

2.4.2 Order of the Applied Code

Nominally, the applied numerical methods are of second order in space, as discussed in Section 2.3. Here, we verify this by inspecting the decrement of numerical error as the grid resolution is increased. By the use of the Taylor series one obtains the following formula for the numerical error of a pth-order scheme:

$$\tilde{u} - u_{\mathrm{DNS}} = c\Delta^p + \mathcal{O}\left(\Delta^{p+1}\right), \tag{2.84}$$

where $\tilde{u}$ is the numerical solution, c is a constant which depends on the exact solution and Δ is grid spacing. Here, u_{DNS} is a grid-converged DNS result that represents the exact solution. In the so-called asymptotic range, the first term in the expansion should dominate.

Four simulations of the channel flow at $\mathrm{Re}_\tau = 395$ were run using grids of 126^3, 150^3, 180^3 and 216^3 cells. The actual numerical error was evaluated for each case using the DNS data of Moser et al. (1999) (u_{DNS}). The flow statistics from these cases have already been presented in the previous section, and the obtained error for the mean-velocity profile is depicted as a function of the wall distance in Figure 2.17. Also, theoretical error for the three finer grid cases, which is obtained by scaling the error of the coarsest grid by the square of the grid refinement factor, is included in the figure. We notice that the convergence is not completely monotonic. In the middle of the channel, the error first decreases faster than the theoretical one, but at the largest resolution it starts to increase. In the viscous sublayer, the error first decreases and then increases. This makes the use of the Richardson extrapolation difficult (Celik, Li, Hu and Shaffer 2005). However, the numerical error decreases faster than the theoretical one for each case, and we can claim that the code is second-order accurate.

For the error in the streamwise, spanwise and wall-normal Reynolds stress components, the corresponding plot is given in Figures 2.18, 2.19 and 2.20, respectively. In the middle of the channel, the obtained error decreases first slightly slower than the the theoretical one, while in the near-wall region, the grid-convergence rate is clearly slower than the theoretical one.

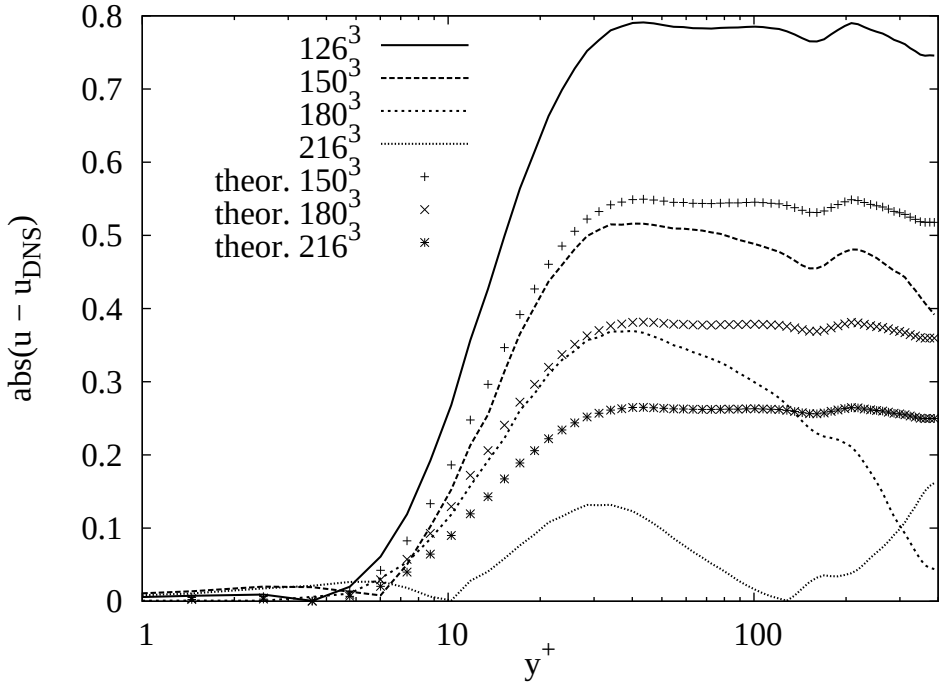

Figure 2.17: Obtained and theoretical numerical error in mean velocity of simulations with no modelling.

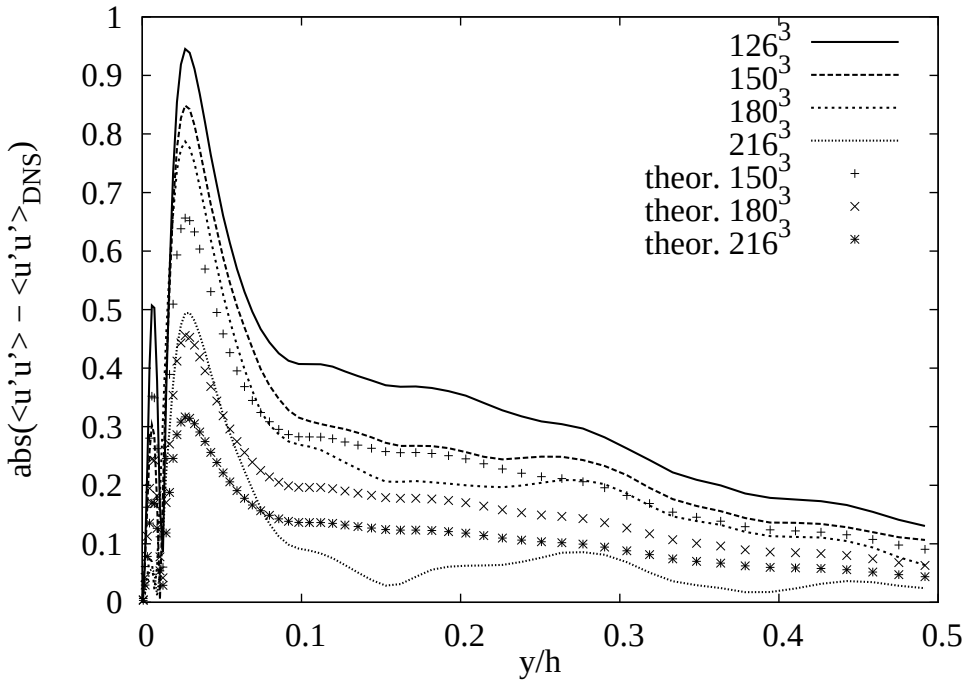

Figure 2.18: Obtained and theoretical numerical error in the streamwise diagonal Reynolds stress of simulations with no modelling.

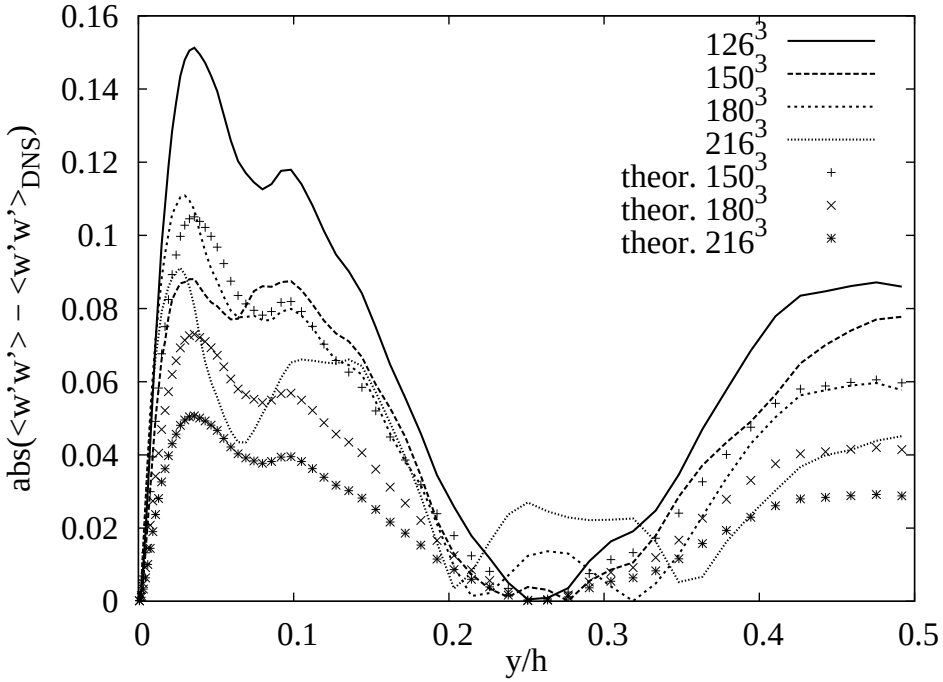

Figure 2.19: Obtained and theoretical numerical error in the spanwise diagonal Reynolds stress of simulations with no modelling.

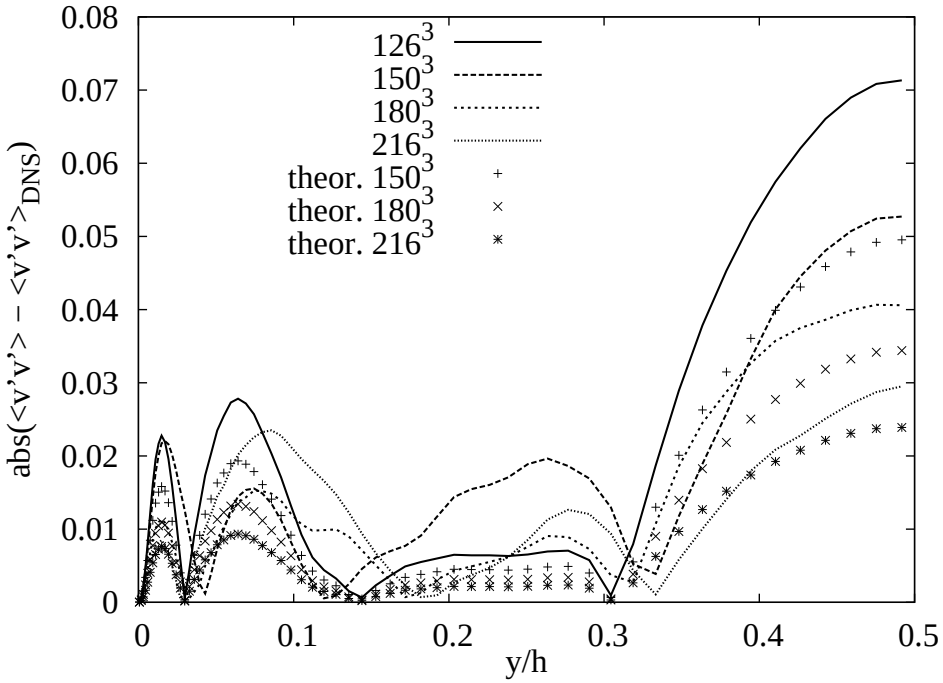

Figure 2.20: Obtained and theoretical numerical error in the wall-normal diagonal Reynolds stress of simulations with no modelling.

Chapter 3

A Priori Testing of Numerical Error and Explicit Filtering

*The results of this chapter were presented in Brandt (2006*a*).*

In this chapter, the numerical error involved in LES and the possibilities to affect it via explicit filtering are studied a priori using filtered DNS data. Here, we focus only on the numerical error involved with the non-linear convection term. The error is evaluated using several instantaneous velocity fields obtained on different timesteps and then averaged over time. Thus, the situation is studied on average on one timestep. The tests are performed for two Reynolds numbers, $\mathrm{Re}_\tau = 180$ and $\mathrm{Re}_\tau = 395$. In Section 3.1, the applied DNS data is briefly reviewed. In Section 3.2, the traditional approach, where the whole velocity field is filtered, is applied, and in Section 3.3, only the non-linear convection term of the Navier–Stokes equations is filtered explicitly. In Section 3.4, we discuss the differences between the two approaches, and finally in Section 3.5, three-dimensional filtering is discussed.

3.1 DNS Data

DNS results obtained using the numerical methods discussed in the previous chapter were presented in Section 2.4. For the Reynolds number $\mathrm{Re}_\tau = 180$, the same DNS data is used here for a priori testing and the resolution of the DNS was given in Table 2.4. For the $\mathrm{Re}_\tau = 395$ case, the resolution of the applied DNS data, shown in Table 3.1, is lower than that discussed in the previous chapter. The DNS data at this resolution was discussed in the author's licentiate thesis (Brandt 2004) and in Brandt (2006*a*). When the grid resolution was varied, the conclusions of the a priori tests were not sensitive to it and thus, the resolution of the DNS is considered adequate for these a priori tests.

Table 3.1: Dimensions of the channel and grid resolution in the DNS at $\mathrm{Re}_\tau = 395$.

	streamwise	spanwise	wall-normal
length / channel height	3.0	1.6	1.0
length in wall units	2370	1264	790
number of grid points	160	160	120
size of grid cells in wall units	15	8	15 (max) 0.7 (min)

wall units: $x^+ = \mathrm{Re}_\tau x$, where x is scaled by the channel half-width.

3.2 Explicit Filtering of the Whole Velocity Field

In the a priori tests, we follow the approach suggested by Vreman et al. (1994*a*). The explicitly filtered LES equations that are being solved in the incompressible case are written as

$$\frac{\partial \overline{\tilde{u}}_i}{\partial t} + \frac{\partial \overline{\tilde{u}}_i \overline{\tilde{u}}_j}{\partial x_j} = -\frac{\partial \overline{\tilde{p}}}{\partial x_i} + \frac{\partial}{\partial x_j}\left(\frac{1}{\mathrm{Re}_\tau}\left(\frac{\partial \overline{\tilde{u}}_i}{\partial x_j} + \frac{\partial \overline{\tilde{u}}_j}{\partial x_i}\right)\right) - \varepsilon_{\mathrm{SGS}i}, \tag{3.1}$$

where tilde refers to the implicit grid filter, overbar to the explicit filter and $\varepsilon_{\mathrm{SGS}i}$ is the ith component of the SGS term that requires modelling, i.e. the divergence of the SGS stress τ_{ij} in Equation (2.42). The relation between the exact filtered non-linear term and its discrete counterpart may be written as

$$\frac{\partial \overline{\widetilde{u_i u_j}}}{\partial x_j} = \frac{\Delta \overline{\tilde{u}}_i \overline{\tilde{u}}_j}{\Delta x_j} + \underbrace{\frac{\partial \overline{\widetilde{u_i u_j}}}{\partial x_j} - \frac{\partial \overline{\tilde{u}}_i \overline{\tilde{u}}_j}{\partial x_j}}_{=\varepsilon_{\mathrm{SGS}i}} + \underbrace{\frac{\partial \overline{\tilde{u}}_i \overline{\tilde{u}}_j}{\partial x_j} - \frac{\Delta \overline{\tilde{u}}_i \overline{\tilde{u}}_j}{\Delta x_j}}_{=\varepsilon_{\mathrm{num}i}}, \tag{3.2}$$

where the product $\overline{\tilde{u}}_i \overline{\tilde{u}}_j$ can be evaluated from the resolved flow field, $\Delta/\Delta x_j$ is the difference approximation to the first derivative with respect to variable x_j and $\varepsilon_{\mathrm{num}i}$ represents the numerical error related to the spatial discretization of the non-linear convection term of the ith momentum equation. The numerical error related to the viscous dissipation term is assumed to be small in comparison with that of the convection term. In addition, the numerical error related to time integration is assumed to be small owing to the small timestep applied in the explicit time-integration method. This choice to study only the numerical error related to the convection term was also made by Vreman et al. (1994*a*) and Majander and Siikonen (2002).

The exact SGS term and the numerical error can be estimated from DNS data using Equation (3.2). One assumes that the DNS velocity field u_i is a good approximation to the exact solution. The DNS field is filtered using a filter with

the width, Δ_f, equal to the assumed LES grid spacing, Δ_{LES}, to obtain the field $\tilde{u}_i$ corresponding to the LES velocity field. In this study, a fourth-order commutative filter with the width of three grid spacings (see Table 2.2) was applied as the grid filter. When explicit filtering is studied, $\tilde{u}_i$ is filtered again applying a wider filter to obtain the explicitly filtered field $\overline{\tilde{u}}_i$. In this study, the trapezoidal filter was applied as the explicit filter. If the filter width of the trapezoidal filter is based on the standard deviation, it is slightly wider than the region over which the quantity being filtered is integrated (Lund 1997).

Both terms appearing in the definition of the SGS term, $\varepsilon_{\mathrm{SGS}i}$, and the first term in the definition of the numerical error, $\varepsilon_{\mathrm{num}i}$, are evaluated on the DNS grid, and a fourth-order central-difference scheme is applied. The fourth-order scheme is used to make the numerical error related to these terms as small as possible. Since the DNS result was obtained using a second-order scheme, the accuracy of the prediction of these terms is, however, not of fourth order.

The second term in the definition of the numerical error $\varepsilon_{\mathrm{num}i}$ is evaluated on the LES grid. The grid-filtered velocity field $\tilde{u}_i$ is restricted to the LES grid, it is filtered explicitly on the LES grid, products $\overline{\tilde{u}}_i\overline{\tilde{u}}_j$ are evaluated on the cell boundaries using a second-order interpolation and finally, the second-order central-difference scheme is applied on this coarser grid. The points of the LES grid match the DNS grid, and thus no interpolation is applied when the filtered field is restricted to the DNS grid. Explicit filtering is performed here on the LES grid because this term represents the derivative evaluated in LES, and in actual LES, the velocity field is filtered on the LES grid. This differs somewhat from the choice made by Vreman et al. (1994*a*) and Majander and Siikonen (2002), but this approach was considered more consistent. In the present work, the different approaches were compared, but this had no effect on the conclusions.

The resolutions of the studied LES grids at the two Reynolds numbers are given in Tables 3.2 and 3.3. The finer wall-normal resolution in Table 3.2 is applied in this section, and the coarser one is used later when the three-dimensional filtering is studied. The grid spacing of the studied LES grid in the streamwise and spanwise direction, Δ_{LES}, was three times the grid spacing of the corresponding DNS grid. Actual channel flow simulations applying similar resolutions have been performed by Piomelli et al. (1988), Majander and Siikonen (2002) and Gullbrand (2001). In the first set of the a priori tests, both filters are applied only in the homogeneous directions, and the LES grid has the same resolution in the wall-normal direction as the original DNS grid does. This approach was applied in the a priori tests of Majander and Siikonen (2002).

Only the SGS term and the numerical error of the streamwise momentum equation are studied here. The spanwise and wall-normal momentum equations were studied by Majander and Siikonen (2002), and the behaviour was similar to the streamwise equation.

Table 3.2: Dimensions of the channel and resolution of the studied LES grid in the a priori tests at $\mathrm{Re}_\tau = 180$.

	streamwise	spanwise	wall-normal	
extent of the domain / channel height	4.0	2.0	1.0	1.0
number of grid points	40	50	100	32
resolution in wall units	36	14	0.5 (min)	1.8 (min)

wall units: $x^+ = \mathrm{Re}_\tau x$, where x is scaled by the channel half-width.

Table 3.3: Dimensions of the channel and resolution of the studied LES grid in the a priori tests at $\mathrm{Re}_\tau = 395$.

	streamwise	spanwise	wall-normal
extent of the domain / channel height	3.0	1.6	1.0
number of grid points	53	53	120
resolution in wall units	45	24	15 (max) 0.7 (min)

wall units: $x^+ = \mathrm{Re}_\tau x$, where x is scaled by the channel half-width.

The L_2-norms of the numerical error, $\varepsilon_{\mathrm{num}}$, and of the exact SGS term, $\varepsilon_{\mathrm{SGS}}$, of the streamwise momentum equation from the a priori tests at $\mathrm{Re}_\tau = 180$ are depicted in Figure 3.1 across the channel half-height. L_2-norm of a function u on a domain Ω is defined as

$$\|u\|_{L_2} = \sqrt{\int_\Omega u^2 \,\mathrm{d}\Omega}. \tag{3.3}$$

The L_2-norms were first evaluated over the homogeneous directions. To insure that the results are not due to statistical variation, the norms were averaged also over time. The L_2-norm was evaluated after each 0.2 non-dimensional time-units during a period of 30 non-dimensional time-units. Thus, we are studying the average situation on one timestep. In Figure 3.1, we see that in the cases where explicit filtering is not applied, the L_2-norms $\|\varepsilon_{\mathrm{num}}\|_2$ and $\|\varepsilon_{\mathrm{SGS}}\|_2$ are of the same magnitude only in the near-wall region. For the most part, $\|\varepsilon_{\mathrm{num}}\|_2$ is much larger than $\|\varepsilon_{\mathrm{SGS}}\|_2$. As the explicit filter of the width of two LES grid spacings ($\Delta_f = 2\Delta_{\mathrm{LES}}$) is applied, the magnitude of the numerical error diminishes. However, the SGS term $\varepsilon_{\mathrm{SGS}}$ does not grow as fast as the numerical error $\varepsilon_{\mathrm{num}}$ diminishes, and the numerical error still dominates the SGS term in most part of the channel. The same type of behaviour was also noticed by

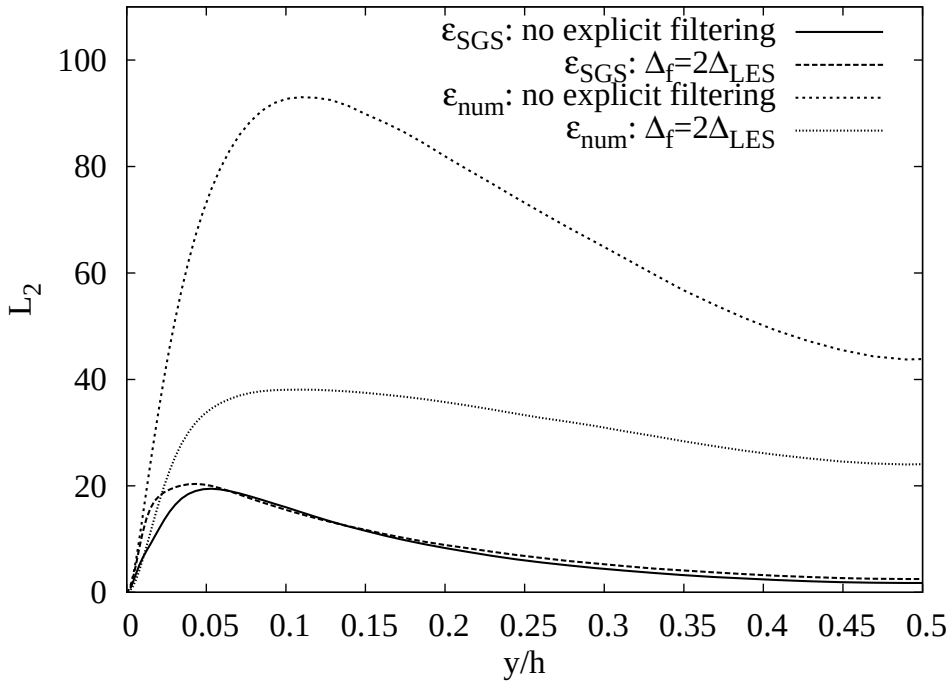

Figure 3.1: L_2-norms of the SGS term, $\varepsilon_{\mathrm{SGS}}$, and numerical error, $\varepsilon_{\mathrm{num}}$. The whole velocity field is filtered. $\mathrm{Re}_\tau = 180$.

Majander and Siikonen (2002).

In principle, increasing the filter width further would lead to a situation where $\|\varepsilon_{\mathrm{num}}\|_2$ is smaller than $\|\varepsilon_{\mathrm{SGS}}\|_2$. However, on a fixed grid resolution, this situation would not be physically meaningful and in addition, it would be computationally inefficient. In Figure 3.2, we see the behaviour of $\|\varepsilon_{\mathrm{SGS}x}\|_2$ from the cases where larger filter widths are applied. We notice that when the filter width is large enough, the growth of the SGS term stops and it actually begins to diminish. This happens first only in a small area, but later in the whole channel. This behaviour is in contradiction with the idea of explicit filtering. However, it is to be expected by studying the energy spectra and the cutoff wavenumber. The minimum wavelength that the grid is able to describe is two times the grid spacing, Δ. Thus, the maximum wavenumber scaled by the channel half-height, δ, is

$$\hat{k}_{\max}\delta = \frac{2\pi}{2\Delta/\delta}. \tag{3.4}$$

In the current DNS, the maximum wavenumbers in the streamwise and spanwise directions were $\hat{k}^x_{\max}\delta \approx 47$ and $\hat{k}^y_{\max}\delta \approx 118$, respectively. On the studied LES grid with no explicit filtering, these wavenumbers are 12 and 30, respectively. When the spectra in Figure 2.9 are considered, these cutoff wavenumbers seem to be reasonable. When explicit filtering is applied, the effective resolution is determined by the filter width Δ_f. Thus, also the cutoff wavenumber is determined

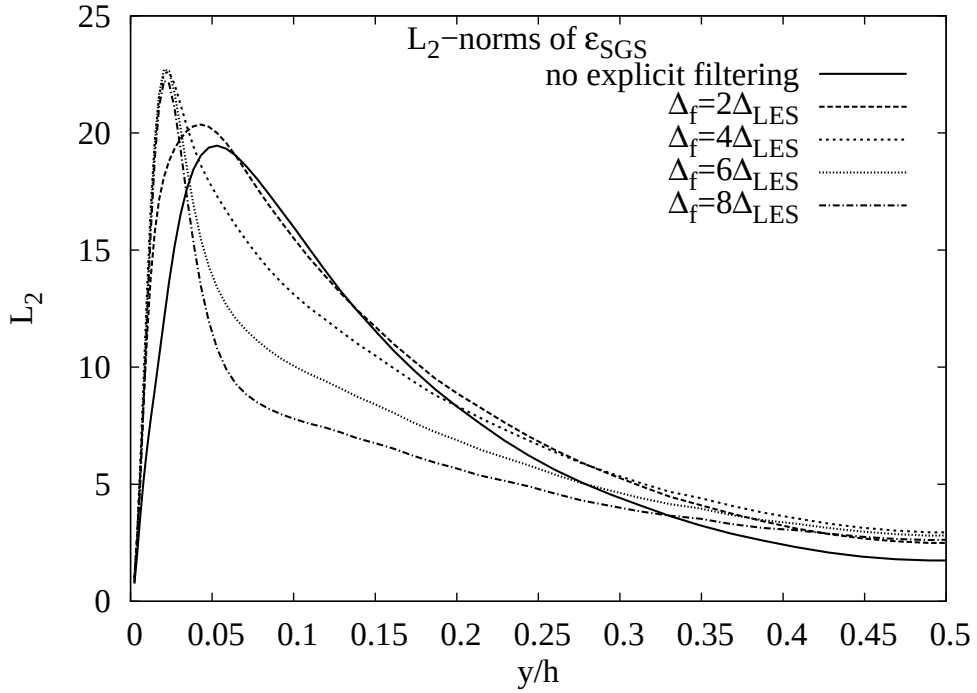

Figure 3.2: L_2-norm of the SGS term using filters of different widths. The whole velocity field is filtered. $\mathrm{Re}_\tau = 180$.

by Δ_f. When the explicit filter of the width of $\Delta_f = 4\Delta_{\mathrm{LES}} = 12\Delta_{\mathrm{DNS}}$ was applied, the cutoff wavenumber in the streamwise direction was approximately $\hat{k}^x_{\mathrm{max}}\delta \approx 3$ and in the spanwise direction $\hat{k}^y_{\mathrm{max}}\delta \approx 10$. The energy spectra from the area where the undesired behaviour of the SGS term began ($y/h \approx 0.05$, $y^+ \approx 36$) are also included in Figure 2.9. We notice that, as the explicit filter is applied, both the streamwise and spanwise cutoff wavenumbers are quite low. As the filter width is increased further, the cutoff wavenumbers become even smaller. Therefore, one reason for the unphysical behaviour of the SGS term is that the filter width had become too large and also the large energy-bearing scales were affected by the filter. This means that the assumptions made in the derivation of the LES equations were contradicted.

When the SGS term is considered, there are two alternatives for the interpretation of the results. First, the obtained SGS term can be seen as the SGS term of a simulation on a reasonable LES grid applying explicit filtering. The other possibility is to interpret it as the SGS term of an LES performed on a grid with spacing equal to the filter width Δ_f and with no explicit filtering. Similar interpretation cannot be made for the numerical error. The resolution at which the magnitude of the SGS term started to diminish also gives a limit for the minimum resolution necessary in LES simulation of the channel flow at this Reynolds number. At a lower resolution, the grid-filtered momentum equations would no longer be

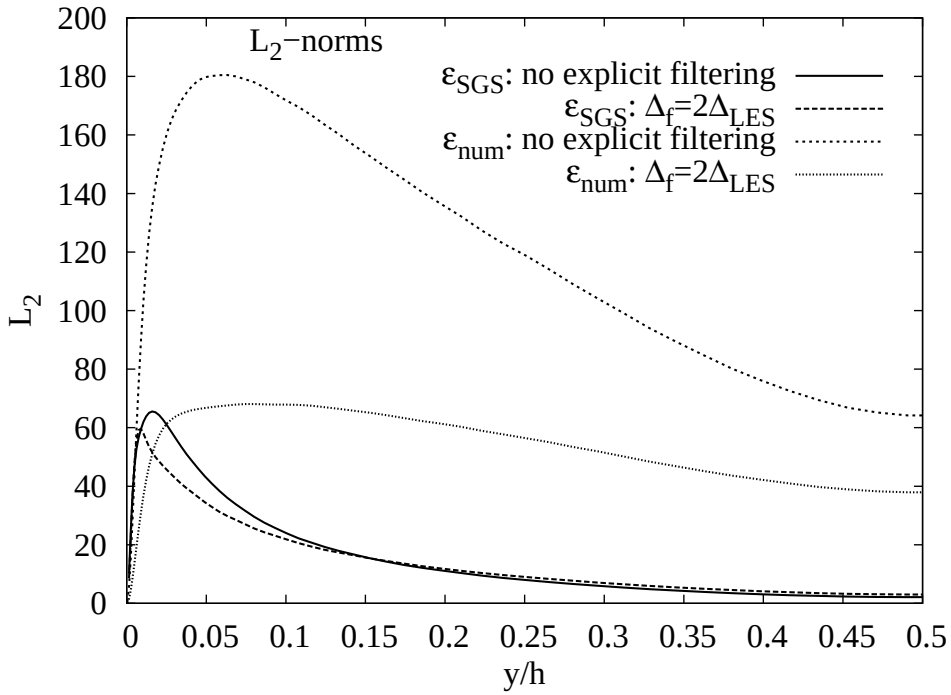

Figure 3.3: L_2-norms of the SGS term, $\varepsilon_{\mathrm{SGS}}$, and numerical error, $\varepsilon_{\mathrm{num}}$. The whole velocity field is filtered. $\mathrm{Re}_\tau = 395$.

meaningful. At this Reynolds number ($\mathrm{Re}_\tau = 180$), the behaviour started when the grid spacing was eight times our DNS grid spacing. Thus, the LES grid would have the nominal resolution of $\Delta x^+ = 144$ and $\Delta y^+ = 56$. This would be quite a coarse LES grid.

In Figure 3.3, we see the behaviour of the L_2-norms of the SGS term and of the numerical error from the a priori tests performed at $\mathrm{Re}_\tau = 395$. Here, the results were averaged over the homogeneous directions and 20 non-dimensional time units. As expected, in this case the magnitude of the SGS term is larger in the near-wall region than at the lower Reynolds number. However, the numerical error still dominates the SGS term. Explicit filtering diminishes the numerical error, and in the near-wall region, $\|\varepsilon_{\mathrm{SGS}}\|_2$ and $\|\varepsilon_{\mathrm{num}}\|_2$ are about the same size. However, the applied LES grid is quite coarse for explicit filtering and thus, the SGS term does not grow with the filter width. In Figure 3.4, we have the L_2-norms of the SGS term from tests where also wider filters were applied. In this case, the L_2-norm of the SGS term starts to diminish already when the filter width is $\Delta_f = 2\Delta_{\mathrm{LES}} = 6\Delta_{\mathrm{DNS}}$. Thus, the LES results on this grid could not be improved using explicit filtering because the nominal resolution becomes too low.

Based on the results of this section, we can say that if one applies explicit filtering to the whole velocity field, one has to increase the grid resolution. Otherwise, the nominal resolution becomes too low and the SGS term starts to behave in

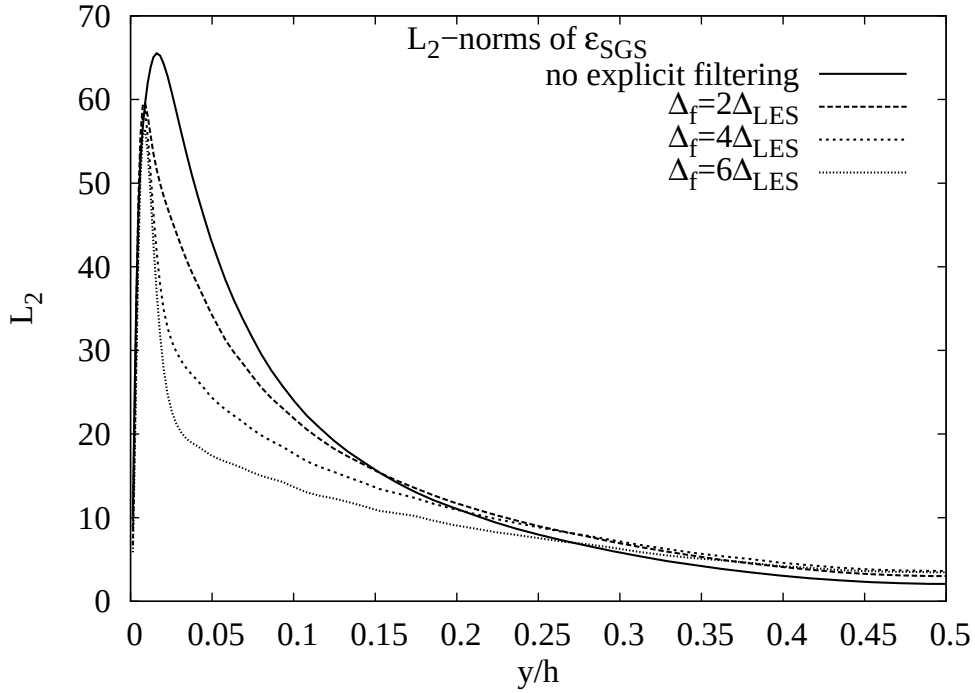

Figure 3.4: L_2-norm of the SGS term using also wider filters. The whole velocity field is filtered. $\mathrm{Re}_\tau = 395$.

an unphysical manner. However, in large eddy simulation, the computational capacity usually sets limits on the grid resolution. Thus, it seems that on a reasonable LES grid, explicit filtering of the whole velocity field is not a reasonable approach to reducing the numerical and total errors.

3.3 Explicit Filtering of Only the Non-Linear Term

Next, we consider the approach to explicit filtering where the explicit filter is applied only to the non-linear convection term. This approach was suggested by Lund (1997). The equations being solved are written as

$$\frac{\partial \tilde{u}_i}{\partial t} + \frac{\partial \overline{\tilde{u}_i \tilde{u}_j}}{\partial x_j} = -\frac{\partial \tilde{p}}{\partial x_i} + \frac{\partial}{\partial x_j}\left(\frac{1}{\mathrm{Re}_\tau}\left(\frac{\partial \tilde{u}_i}{\partial x_j} + \frac{\partial \tilde{u}_j}{\partial x_i}\right)\right) - \varepsilon_{\mathrm{SGS}i}, \tag{3.5}$$

where the overbar again refers to the explicit filter and the tilde to the implicit filter. The difference from Equation (3.1) is that the explicit filter is applied only on the left side, and the other terms are affected only by the implicit filter. The

SGS term $\varepsilon_{\mathrm{SGS}i}$ in Equation (3.5) is defined as

$$\varepsilon_{\mathrm{SGS}i} = \frac{\partial \widetilde{u_i u_j}}{\partial x_j} - \frac{\partial \overline{\tilde{u}_i \tilde{u}_j}}{\partial x_j} \tag{3.6}$$

and the numerical error $\varepsilon_{\mathrm{num}i}$ related to the spatial discretization of the convection term as

$$\varepsilon_{\mathrm{num}i} = \frac{\partial \overline{\tilde{u}_i \tilde{u}_j}}{\partial x_j} - \frac{\Delta \overline{\tilde{u}_i \tilde{u}_j}}{\Delta x_j}. \tag{3.7}$$

Both definitions differ from Equation (3.2). We will see that the differences in the definition of the SGS term $\varepsilon_{\mathrm{SGS}i}$ are crucial.

Explicit filtering of only the non-linear term was tested using the same methods as discussed in the previous section. The essential difference is that the explicit filter is applied only to the product of the velocity components and not to the individual velocity components.

In Figure 3.5, we depict the L_2-norms of $\varepsilon_{\mathrm{SGS}}$ and $\varepsilon_{\mathrm{num}}$ of the streamwise momentum equation from the case at $\mathrm{Re}_\tau = 180$ and in Figures 3.6 from the $\mathrm{Re}_\tau = 395$ case. We notice that this filtering approach has indeed the desired effect on both the numerical error and the SGS term. The numerical error rapidly diminishes and, in addition, the magnitude of the SGS term grows fast with the filter width. The SGS term is everywhere clearly larger than the numerical error. The undesired diminishing of the SGS term as the filter width grows is not noticed in this approach.

3.4 Difference between the Two Approaches

In this section, we further discuss some of the differences between the two applied approaches to explicit filtering. Firstly, we discuss the sum of the numerical error and the SGS term, and secondly the two definitions of the SGS term.

The sum of the SGS term and the numerical error can be interpreted as the difference between a sufficiently resolved and a coarse-grid DNS solution, i.e. an LES without an SGS model. For the case, where the whole velocity field is filtered, the sum is written as

$$\varepsilon_{\mathrm{SGS}i} + \varepsilon_{\mathrm{num}i} = \frac{\partial \overline{\widetilde{u_i u_j}}}{\partial x_j} - \frac{\partial \overline{\tilde{u}_i}\,\overline{\tilde{u}_j}}{\partial x_j} + \frac{\partial \overline{\tilde{u}_i}\,\overline{\tilde{u}_j}}{\partial x_j} - \frac{\Delta \overline{\tilde{u}_i}\,\overline{\tilde{u}_j}}{\Delta x_j} = \frac{\partial \overline{\widetilde{u_i u_j}}}{\partial x_j} - \frac{\Delta \overline{\tilde{u}_i}\,\overline{\tilde{u}_j}}{\Delta x_j}. \tag{3.8}$$

If only the non-linear term is filtered explicitly, the sum of $\varepsilon_{\mathrm{SGS}i}$ and $\varepsilon_{\mathrm{num}i}$ is written as

$$\varepsilon_{\mathrm{SGS}i} + \varepsilon_{\mathrm{num}i} = \frac{\partial \widetilde{u_i u_j}}{\partial x_j} - \frac{\partial \overline{\tilde{u}_i \tilde{u}_j}}{\partial x_j} + \frac{\partial \overline{\tilde{u}_i \tilde{u}_j}}{\partial x_j} - \frac{\Delta \overline{\tilde{u}_i \tilde{u}_j}}{\Delta x_j} = \frac{\partial \widetilde{u_i u_j}}{\partial x_j} - \frac{\Delta \overline{\tilde{u}_i \tilde{u}_j}}{\Delta x_j}. \tag{3.9}$$

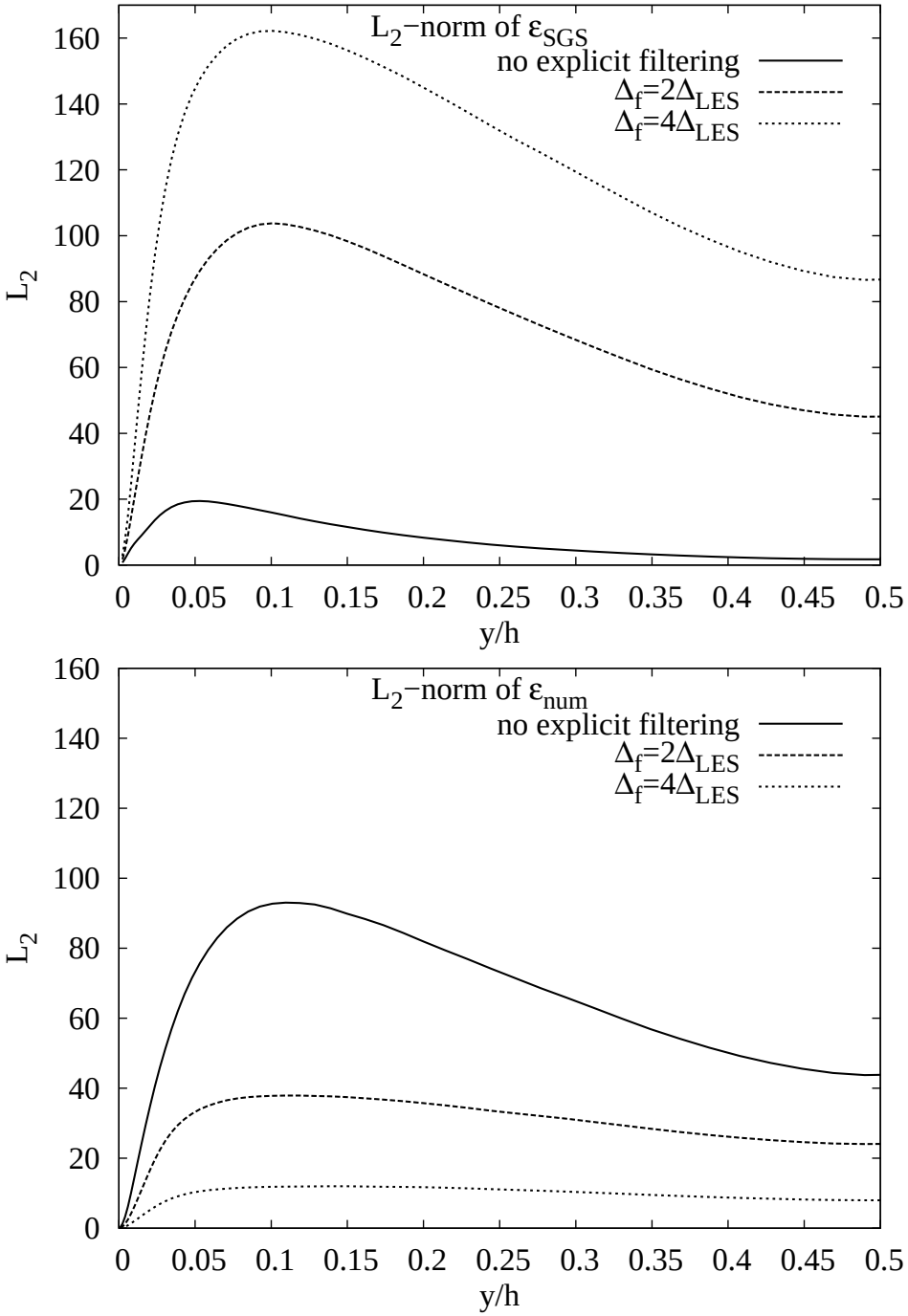

Figure 3.5: Upper: L_2-norm of the SGS term, $\varepsilon_{\mathrm{SGS}}$. **Lower:** L_2-norm of numerical error, $\varepsilon_{\mathrm{num}}$. Explicit filters of widths 2 and 4 LES grid spacings. Only the non-linear term is filtered. $\mathrm{Re}_\tau = 180$.

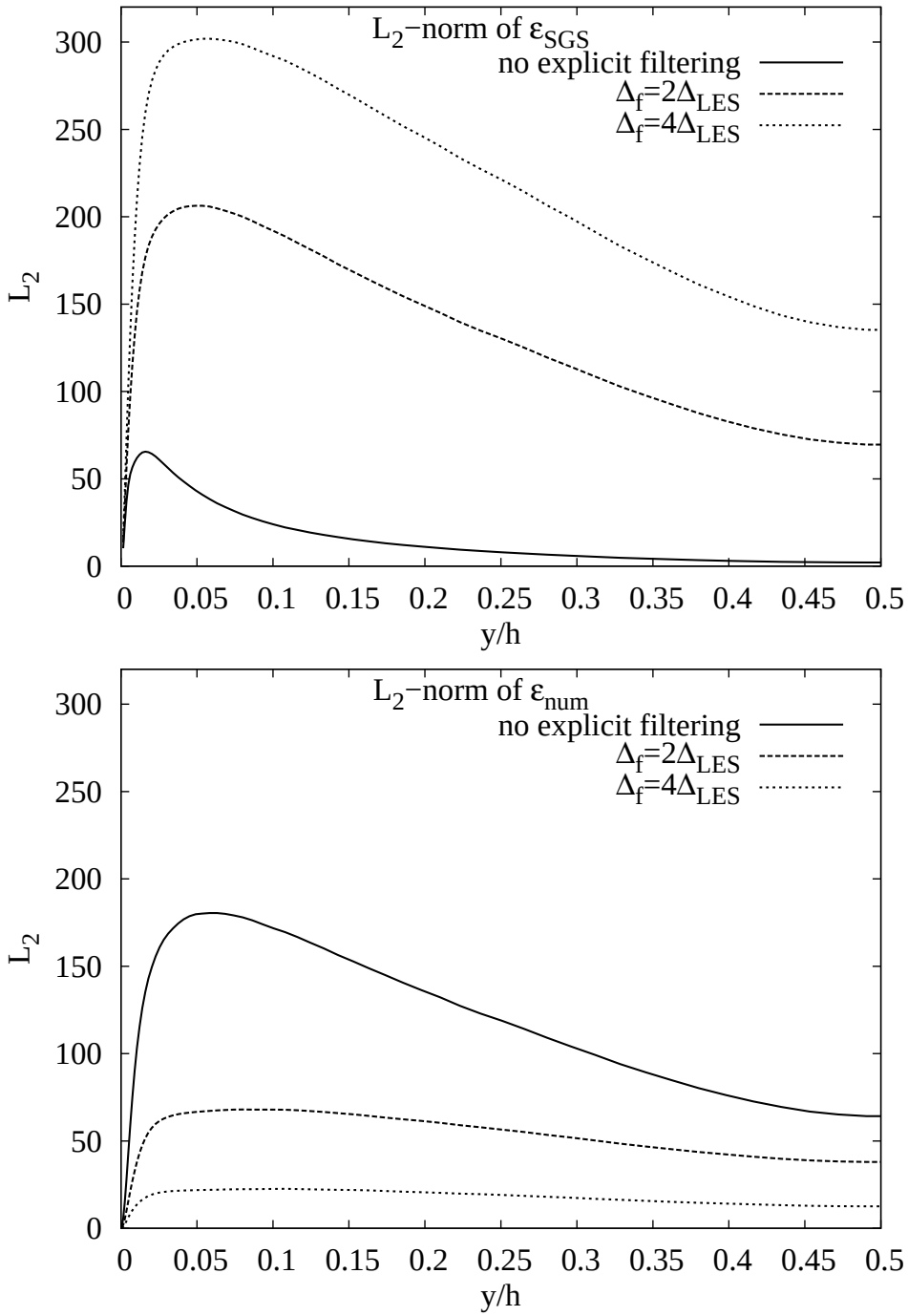

Figure 3.6: Upper: L_2-norm of the SGS term, $\varepsilon_{\mathrm{SGS}}$. **Lower:** L_2-norms of numerical error, $\varepsilon_{\mathrm{num}}$. Explicit filters of widths 2 and 4 LES grid spacings. Only the non-linear term is filtered. $\mathrm{Re}_\tau = 395$.

This sum for both approaches at Reynolds number $\mathrm{Re}_\tau = 180$ is plotted in Figures 3.7. We notice that in the first approach, the difference between the sufficiently resolved and the coarse-grid DNS appears to diminish when explicit filtering is applied. This suggests, somehow misleadingly, that the results of a coarse-grid DNS could be improved simply by applying an explicit filter to the whole velocity field. In this case, the numerical error is effectively diminished, which leads to the apparent decreased difference between the sufficiently resolved and the coarse-grid DNS. Applying an SGS model could not improve these coarse-grid results, since the effect of the SGS term also diminishes. The upper part of Figure 3.7 thus demonstrates the fact that when the whole velocity field is filtered, some information is lost, and we cannot recover it by modelling.

The lower part of Figure 3.7 is from the case where only the non-linear term is filtered. In this case, the behaviour of the difference is the opposite. Increasing the filter width increases the difference between the sufficiently resolved and the coarse-grid DNS results. This indicates that, at the same time as the numerical error decreases, the scales filtered out are shifted to the SGS term, and using an SGS model could improve the results. This supports the conclusion that the latter method may lead to improved large eddy simulation results.

Depending on whether the explicit filter was applied to the whole velocity field or only to the non-linear term, the behaviour of the SGS term $\varepsilon_{\mathrm{SGS}i}$ was clearly different. We next consider more carefully the origin of this difference. We label the SGS term of the first approach, where the whole velocity field is filtered explicitly, with the superscript 1

$$\varepsilon^1_{\mathrm{SGS}i} = \frac{\partial \overline{\widetilde{u_i}\widetilde{u_j}}}{\partial x_j} - \frac{\partial \overline{\tilde{u}_i}\,\overline{\tilde{u}_j}}{\partial x_j}, \tag{3.10}$$

and the SGS term of the second approach, where explicit filtering is applied only to the non-linear term, with the superscript 2

$$\varepsilon^2_{\mathrm{SGS}i} = \frac{\partial \widetilde{u_i u_j}}{\partial x_j} - \frac{\partial \overline{\tilde{u}_i \tilde{u}_j}}{\partial x_j}. \tag{3.11}$$

In both definitions for the SGS term $\varepsilon_{\mathrm{SGS}i}$, tilde refers to the grid filter and overbar to the explicit filter. The first term of $\varepsilon_{\mathrm{SGS}i}$ represents the non-linear term that appears in the filtered Navier–Stokes equations. The second term represents the quantity that is evaluated using only the resolved field. There are differences between the two definitions in both of these terms, and $\varepsilon^2_{\mathrm{SGS}i}$ and $\varepsilon^1_{\mathrm{SGS}i}$ are related to each other via the equation

$$\varepsilon^2_{\mathrm{SGS}i} = \varepsilon^1_{\mathrm{SGS}i} + \underbrace{\frac{\partial \widetilde{u_i u_j}}{\partial x_j} - \frac{\partial \overline{\widetilde{u_i}\widetilde{u_j}}}{\partial x_j}}_{=\mathrm{DIFF1}} + \underbrace{\frac{\partial \overline{\tilde{u}_i}\,\overline{\tilde{u}_j}}{\partial x_j} - \frac{\partial \overline{\tilde{u}_i \tilde{u}_j}}{\partial x_j}}_{=\mathrm{DIFF2}}. \tag{3.12}$$

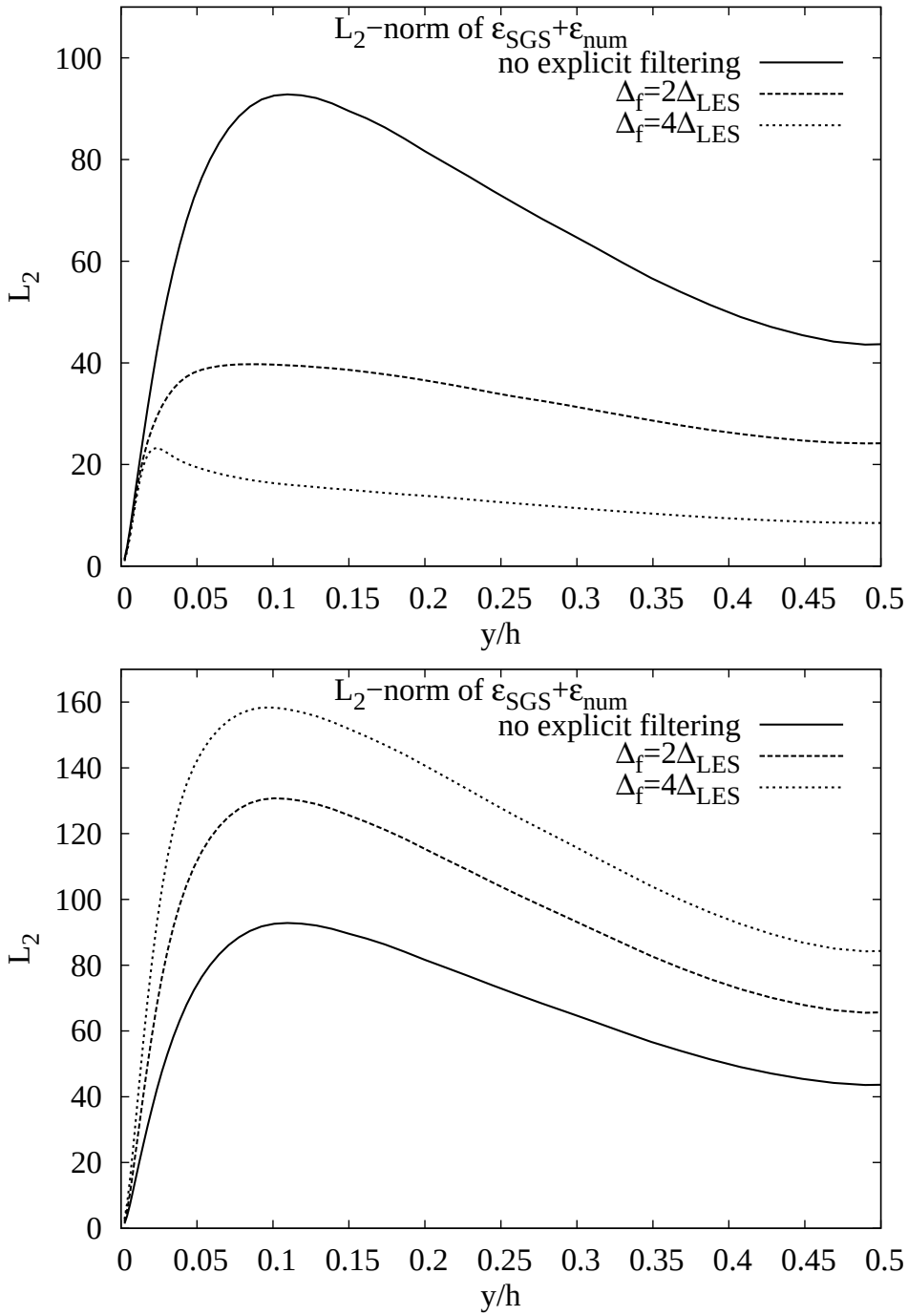

Figure 3.7: L_2-norm of the sum of the SGS term, $\varepsilon_{\mathrm{SGS}}$, and numerical error, $\varepsilon_{\mathrm{num}}$. **Upper:** The whole velocity field is filtered. **Lower:** Only the non-linear term is filtered. $\mathrm{Re}_\tau = 180$.

The difference between $\varepsilon^1_{\mathrm{SGS}i}$ and $\varepsilon^2_{\mathrm{SGS}i}$ consists of two parts: the difference in the resolved non-linear term in the filtered Navier-Stokes equations (DIFF1) and the quantity being evaluated from the resolved field (DIFF2). DIFF1 represents the sub-filter part of $\partial\widetilde{u_i u_j}/\partial x_j$, and DIFF2 is the divergence of the sub-filter scale stress or Leonard stress. The L_2-norms of these two terms are depicted in Figure 3.8 with varying explicit filter widths. Both of these terms increase in magnitude with increasing filter width, but the difference in the resolved non-linear term (DIFF1) forms the major part of the difference between the two definitions of $\varepsilon_{\mathrm{SGS}i}$. It seems that, in the behaviour of the SGS term, the crucial point is the interpretation of the non-linear term of the filtered Navier–Stokes equations.

3.5 Three-Dimensional Filtering

In the a priori tests discussed in the previous sections, filtering was applied only in the homogeneous directions, and the wall-normal resolution of the LES grid was the same as the resolution of the DNS grid. In this section, we discuss a priori tests in which filtering is applied also in the wall-normal direction, and the resolution in this direction corresponds to a resolution of a normal LES grid (see Table 3.2). Both filtering of the whole velocity field and filtering of the non-linear term only are studied here at the Reynolds number $\mathrm{Re}_\tau = 180$. Filtering in inhomogeneous directions is an important issue, since in real applications of LES, homogeneous directions are rather an exception. The aim of these tests is to verify that the results of the previous sections are not restricted to cases with only homogeneous directions.

Applying filtering in the wall-normal direction is not as straightforward as in the homogeneous directions, because the grid spacing varies and changing the order of the derivative and the filter tends to introduce commutation errors. Commutative filters have been proposed (Vasilyev et al. 1998) and applied in actual simulations (Gullbrand 2001), and they can also be applied in the a priori tests. The same symmetrical fourth-order commutative filter as applied in the homogeneous directions was used in the wall-normal direction in the middle of the domain. In the near-wall region, asymmetrical commutative filters were constructed following the method discussed in Section 2.2.3. Since these filters are applied as grid filters, they should have the effective filter width of three DNS grid spacings. In addition, they should have as low a commutation error as possible, since the commutation error adds to the error in evaluation of the SGS term $\varepsilon_{\mathrm{SGS}i}$ and of the numerical error $\varepsilon_{\mathrm{num}i}$ on the DNS grid. However, in order to avoid large negative and positive values of the filter function in the near-wall region, the order of the filter was reduced at the three points of the DNS grid that were closest to the walls.

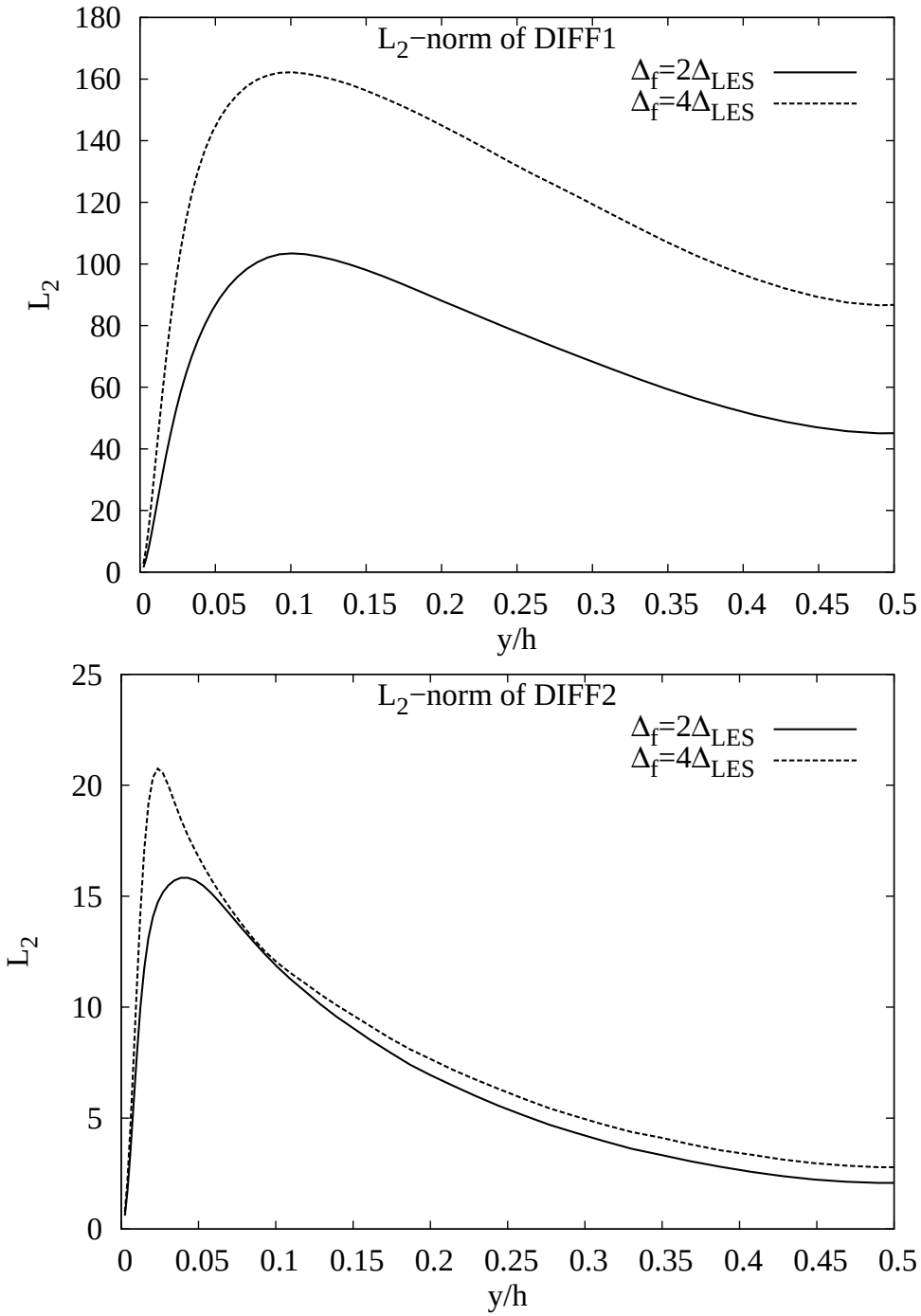

Figure 3.8: The difference between the definitions $\varepsilon^1_{\mathrm{SGS}}$ and $\varepsilon^2_{\mathrm{SGS}}$ for the SGS term. See Eq. (3.12). **Upper:** The difference in the resolved non-linear term. **Lower:** The difference in the term evaluated from the resolved field. $\mathrm{Re}_\tau = 180$.

The last term of the numerical error $\varepsilon_{\mathrm{num}i}$ (Eq. 3.7) is evaluated on the LES grid, and also the explicit filtering is performed there. The trapezoidal filter has the commutation error of second order, and since the second-order central-difference scheme is applied on the LES grid, it is a suitable choice also for the three-dimensional filtering.

The other three terms in $\varepsilon_{\mathrm{SGS}i}$ and $\varepsilon_{\mathrm{num}i}$ are evaluated on the DNS grid (Eqs. (3.2), (3.6) and (3.7)). Thus, the velocity field is filtered, but it is not restricted to the LES grid, and also the explicit filter has to be applied on the DNS grid. The explicit filter applied on the DNS grid has to have a filter width of six DNS grid spacings. The derivatives on the DNS grid were evaluated using the fourth-order central-difference scheme and the grid filter was of fourth order. Therefore, we would also like to have a fourth-order explicit filter. This makes the construction of the explicit filter somewhat problematic on the DNS grid. To obtain a filter transfer function that has that long a filter width and behaves well, i.e. does not have large negative or positive values, one has to fix at least four derivatives of the filter transfer function at the grid cutoff frequency. This is why a filter that is only of second order was applied as the explicit filter on the DNS grid. This introduces a commutation error of the order Δ_{DNS}^2 to the corresponding terms of $\varepsilon_{\mathrm{SGS}i}$ and $\varepsilon_{\mathrm{num}i}$. However, the error on the LES grid is of the order Δ_{LES}^2, and the numerical error on the DNS grid is still too small to affect the conclusions of the a priori tests.

The results from the a priori tests applying three-dimensional filtering to the whole velocity field are given in the upper part of Figure 3.9. Here, the L_2-norms were evaluated on a single timestep. In the case with label "2D", only the grid filter is three-dimensional and the explicit filter is two-dimensional, and in case "3D", both the grid and the explicit filters are three-dimensional. Applying the three-dimensional explicit filter reduces further the numerical error, which is natural, since the LES velocity field becomes somewhat smoother owing to the filtering performed in the wall-normal direction. When the three-dimensional explicit filter is applied, the SGS term diminishes slightly. This again is undesired behaviour, and it is a result of the damping of the large-scale eddies.

The numerical error and the SGS term from the tests where only the non-linear term is filtered are depicted in the lower part of Figure 3.9. We notice the same behaviour of the numerical error as in the previous case, while here the SGS term grows when the three-dimensional explicit filter is applied. In addition, the SGS term is everywhere much larger than the numerical error. Thus, also explicit three-dimensional filtering of only the non-linear term leads to the desired result.

The results presented in this section verify that applying filtering only in homogeneous directions in the a priori testing did not affect the overall conclusion of Sections 3.2–3.4. When three-dimensional filtering was applied, filtering of the whole velocity field seemed to lead to an unphysical situation. The desired

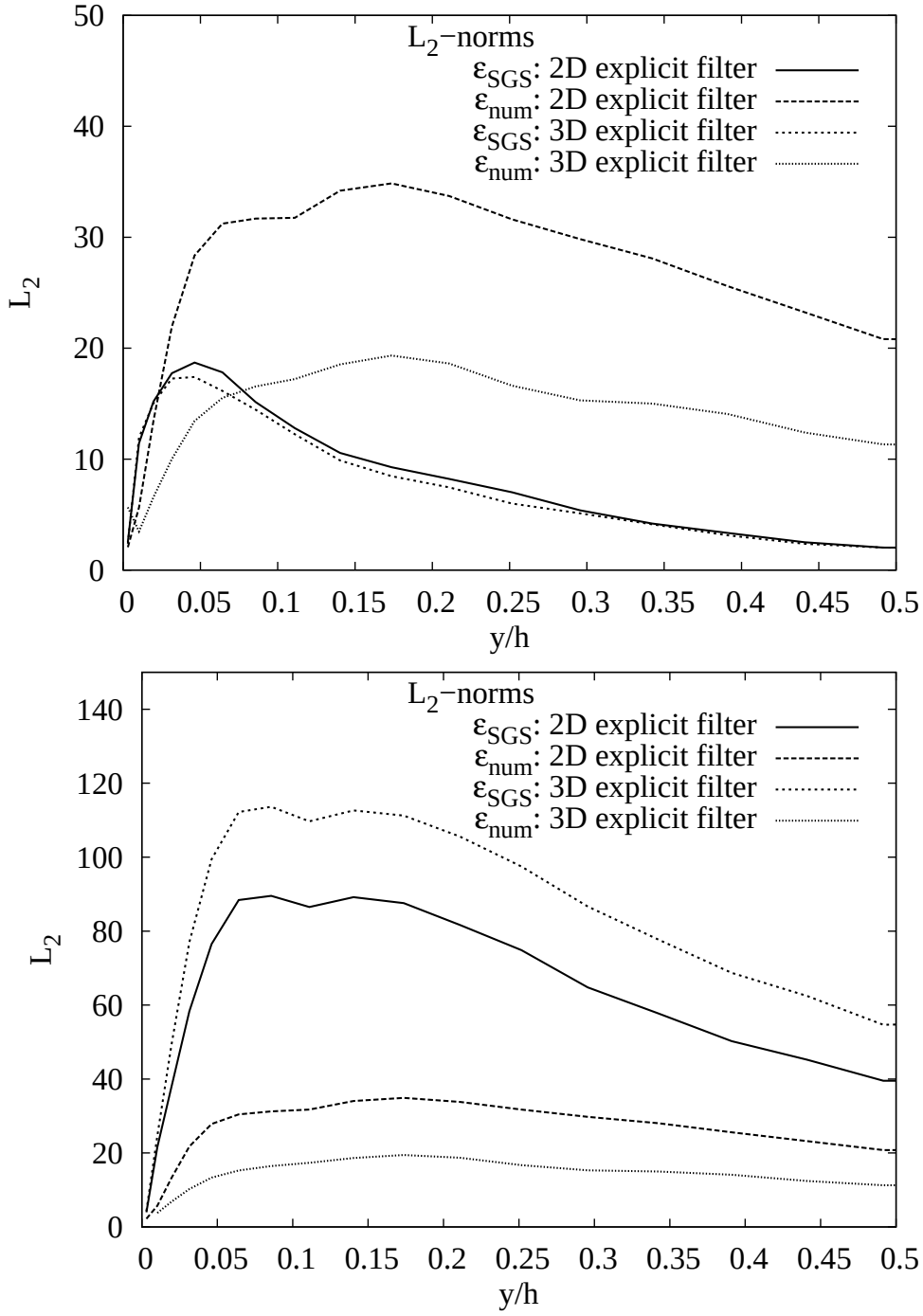

Figure 3.9: Numerical error and SGS term using three-dimensional grid filter and two- and three-dimensional explicit filters. **Upper:** The whole velocity field is filtered explicitly. **Lower:** Only the non-linear term is filtered explicitly. $\Delta_f = 2\Delta_{\mathrm{LES}}$. "2D": three-dimensional grid filter and two-dimensional explicit filtering. "3D": both filters were three dimensional. $\mathrm{Re}_\tau = 180$.

behaviour of filtering only the non-linear term was further reinforced when the three-dimensional filter was applied.

3.6 Conclusions of the a Priori Tests

In this chapter, the aim was to clarify how well explicit filtering is suited to potentially improving the simulation results by reducing numerical errors in a practical large eddy simulation, where low-order finite-difference schemes are applied, and where the grid resolution is not increased as the explicit filter is applied.

When the whole velocity field was filtered while the grid resolution was kept constant, filtering did not increase the SGS term and finally, when the filter width was increased further, the SGS term started to diminish. One reason for this unphysical behaviour is that the large energy-bearing eddies were affected by the filter. This began already when a filter width of four grid spacings was applied. This filter width combined with the second-order central-difference scheme has been previously suggested by some groups (Vreman et al. 1994*a*, Ghosal 1996). Based on the results presented in this chapter, it seems that to increase the effect of the SGS model using this approach, one would have to increase also the grid resolution. Usually, this is not possible because of the increased computational demands.

When only the non-linear term was filtered, the desired behaviour was obtained. As the filter width was increased, the L_2-norm of the numerical error diminished and that of the SGS term increased. The numerical error was clearly smaller than the SGS term. The increased SGS term indicates that in an actual simulation, the role of the chosen SGS model is pronounced, and the responsibility for scales being filtered out is shifted to the model. Thus, an SGS model can improve the simulation results. By studying the sum of the numerical error and the SGS term, it was further demonstrated that while filtering of the whole velocity field leads to loss of information, subfilter-scale motions are effectively shifted to the SGS term if the non-linear convection term in filtered.

The main difference between the two discussed approaches to explicit filtering is the interpretation of the resolved non-linear term in the filtered Navier–Stokes equations. In the first approach, where the whole velocity field is filtered, one tries to approximate the non-linear term that has been explicitly filtered. In the second approach, where the explicit filter has been applied only to the non-linear terms, one tries to approximate the grid-filtered term.

In the previously published a priori studies of the channel flow, filtering has been applied only in the homogeneous directions. However, in many applications, there are no homogeneous directions. In this thesis, a priori tests applying filtering in the wall-normal direction were presented. We noticed that including this filtering

reinforced the overall conclusion. The unphysical behaviour of the SGS term in the case, where the whole velocity field was filtered explicitly, remained. The desired behaviour when only the non-linear term was filtered was even stronger with the three-dimensional filtering. Thus, the conclusions from the tests with filtering in homogeneous directions can be extended to cases with inhomogeneous directions. This suggests that explicit filtering is an effective method for reducing numerical errors also in practical applications with inhomogeneous directions.

In cases where there are homogeneous directions, there is the possibility to apply the filtering only in these directions. Based on the present results, it seems that filtering also in inhomogeneous directions further increases the difference between the numerical error and the SGS term. On the other hand, filtering in inhomogeneous directions further increases the computational cost, while improved results can be obtained with filtering applied only in the homogeneous directions.

Based on these a priori tests, it seems that explicit filtering of the non-linear term could be an efficient way to control the level of numerical errors in large eddy simulation. In this approach, the responsibility for the subfilter scales is effectively shifted to the SGS model, and in simulations applying explicit filtering, advanced SGS models are probably required.

Chapter 4

Explicit filtering in LES

*The results of Sections 4.1–4.4 were published in Brandt (2006*b*) and the results of Sections 4.5 and 4.6 in Brandt (2006*d*).*

In this chapter, explicit filtering is applied in actual LES of the turbulent channel flow at $\mathrm{Re}_\tau = 395$. In Section 4.1, we discuss some different approaches to explicit filtering. In Section 4.2, the effect of the filter function is studied. In Section 4.3, the effect of explicit filtering is separated from the effect of SGS modelling, and in Section 4.4 explicit filtering is compared to the implicit filtering provided by the Smagorinsky model. In Section 4.5, also the dynamic Smagorinsky and scale-similarity models are applied together with explicit filtering, and finally in Section 4.6, explicit filtering of the convection term is compared to filtering via subfilter-scale modelling.

4.1 Comparison between Two Approaches to Explicit Filtering

In Section 2.2, we discussed different approaches to explicit filtering in LES, in Chapter 3 these approaches were studied a priori, and in this section, they are applied in actual LES. The equations being solved in the case where the non-linear convection term is filtered are Equations (2.46) and the term that needs modelling is given in Equation (2.47). When the change of the velocity field is filtered, Equations (2.41) are solved and the SGS term is defined in Equation (2.42). In this section, the same SGS models are used in both cases, and no reconstruction is applied to the SFS stresses. The effect of this choice is studied in Section 4.5.

The applied grid resolution is given in Table 4.1, and the applied filter function is the 4th-order commutative filter C1 with the width of two grid spacings (see Table 2.1 and Figure 2.3), which was applied in all three coordinate directions.

The grid resolution is almost the same as in the a priori tests of the previous chapter (see Table 3.3), but the extent of the computational domain is doubled in the homogeneous directions. Filtering connects the neighbouring points explicitly to each other, and by increasing the domain it was assured that the domain did not restrict the largest flow structures in the homogeneous flow directions. However, it turned out that the obtained flow statistics would have been the same also in a smaller domain.

Table 4.1: Applied resolution and domain size.

	streamwise	spanwise	wall-normal
extent of the domain (scaled by h)	6.0	3.2	1.0
number of grid points	108	108	90
resolution in wall units (Δ^+)	44	23	min 1.0, max 20

wall units: $x^+ = \mathrm{Re}_\tau x$, where x is scaled by the channel half-height.

There are several differences between an actual LES and a priori testing. In actual simulations, the effect of the applied SGS model, the modelling error and the dynamical behaviour of the solution are included, while they were not visible in a priori testing. In the previous section, the situation was studied in one average timestep. However, if in an actual simulation the whole velocity field is filtered in the end of each timestep, the damping of the results from the previous timesteps becomes worse in each timestep as the simulation proceeds, and this makes the approach impossible to apply. In the present work, this approach was tested in a simulation, and the mean velocity and Reynolds stress components were overpredicted by more than 100 per cent. In the a priori test of the previous section, the case where the whole velocity field was filtered probably corresponds better to an actual simulation where the change of the velocity field is filtered in the end of a timestep, since in this approach, all the terms of the LES equations are filtered and the effect of time-integration is avoided. This approach corresponding to Equation (2.45) was discussed in Section 2.2.2. In both cases, all the components affecting the flow field are filtered. In this section, we discuss the filtering of the non-linear convection term and the filtering of the change of the velocity field.

In this section, we compare the results from simulations with explicit filtering to results of LES performed using the same code without explicit filtering and to the DNS of Moser et al. (1999). The standard Smagorinsky model (see Section 2.1.2) was applied to SGS modelling. The value $C_S = 0.085$ was used for the model coefficient, and in the cases with no explicit filtering, the model length scale, Δ_S, was equal to the grid spacing, as in Equation (2.17). Explicit filtering reduces the effective resolution of the grid, and it is necessary to model the effect of the length scales that are smaller than the filter width instead of scales smaller than the grid spacing. In the standard Smagorinsky model, the size of the largest

modelled scales is controlled via the model length scale. Thus, in the cases with explicit filtering, the model length scale was set equal to the explicit filter width.

The computational cost of explicit filtering was studied in simulations where filtering was performed only in the homogeneous directions. Here, filtering increased the CPU-time consumed during one timestep by a factor of 2.6. In the simulations presented in this section, filtering was applied in all three coordinate directions and therefore the cost was even larger. However, the efficiency of the implementation could probably be improved.

The mean-velocity profiles from the cases with no filter and with filtering of the non-linear convection term and of the change of the velocity field are plotted in Figure 4.1. When no filtering is applied, the slope of the velocity profile is too low, and the mean bulk velocity is underpredicted. When the non-linear convection term $\tilde{u}_i\tilde{u}_j$ is filtered, the viscous sublayer becomes thicker, and the mean bulk velocity is overpredicted. When $\Delta\tilde{u}_i$ is filtered, the velocity profile changes only slightly. In both cases with explicit filtering, the slope of the profile decreases. The deviatoric diagonal streamwise Reynolds stress component

$$\langle u'u'\rangle^d = \langle u'u'\rangle - 1/3\Big(\langle u'u'\rangle + \langle v'v'\rangle + \langle w'w'\rangle\Big), \tag{4.1}$$

where the brackets refer to the average over homogeneous directions and time, are given in Figure 4.2. The corresponding Reynolds stress components in the spanwise and wall-normal directions are presented in Figure 4.3 and 4.4, respectively. Only the deviatoric part is studied as suggested by Winckelmans, Jeanmart and Carati (2002) since the Smagorinsky model is traceless. In Figures 4.2–4.4, we see that the filtering further increases the overprediction of the Reynolds stress – filtering of $\tilde{u}_i\tilde{u}_j$ slightly more than filtering of $\Delta\tilde{u}_i$. The results are similar for all the stress components.

In Figures 4.5, 4.6 and 4.7, we have the one-dimensional energy spectra evaluated in the streamwise direction for the streamwise, spanwise and wall-normal velocity components respectively, from the near-wall region ($y^+ \approx 5$). The reference results are DNS and not filtered DNS and thus in the reference results, there are high-frequency components which cannot in any case be present in LES where the frequency content of the resolved flow field is always limited. In cases with explicit filtering, the high frequency motions are efficiently damped down, when compared to simulation with no explicit filtering, as they should, and this suggests that the numerical error decreases. However, also the low frequencies, which the grid is able to describe accurately, are damped. The energy spectra in the spanwise direction for the streamwise velocity component are depicted in Figure 4.8, where explicit filtering has only a small effect on the low frequencies. The situation is similar for the other velocity components. In Figure 4.9, we see that in the middle of the channel, explicit filtering does not have that large an effect on the energy spectra. The situation is similar for the other velocity components and in

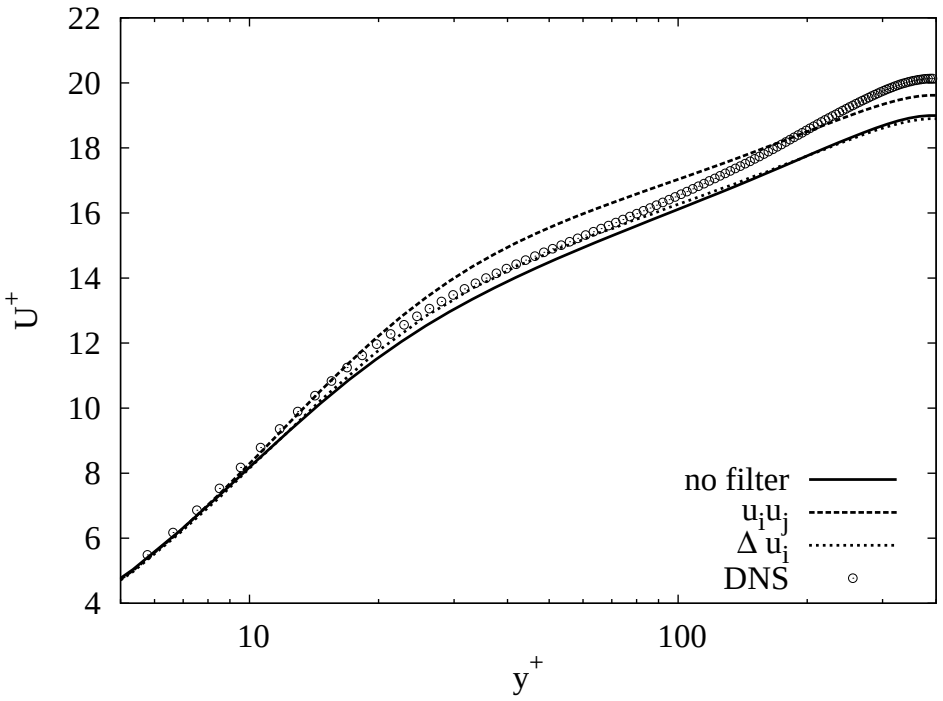

Figure 4.1: Comparison between filtering approaches: $u_i u_j$ or Δu_i is filtered. Mean-velocity profile.

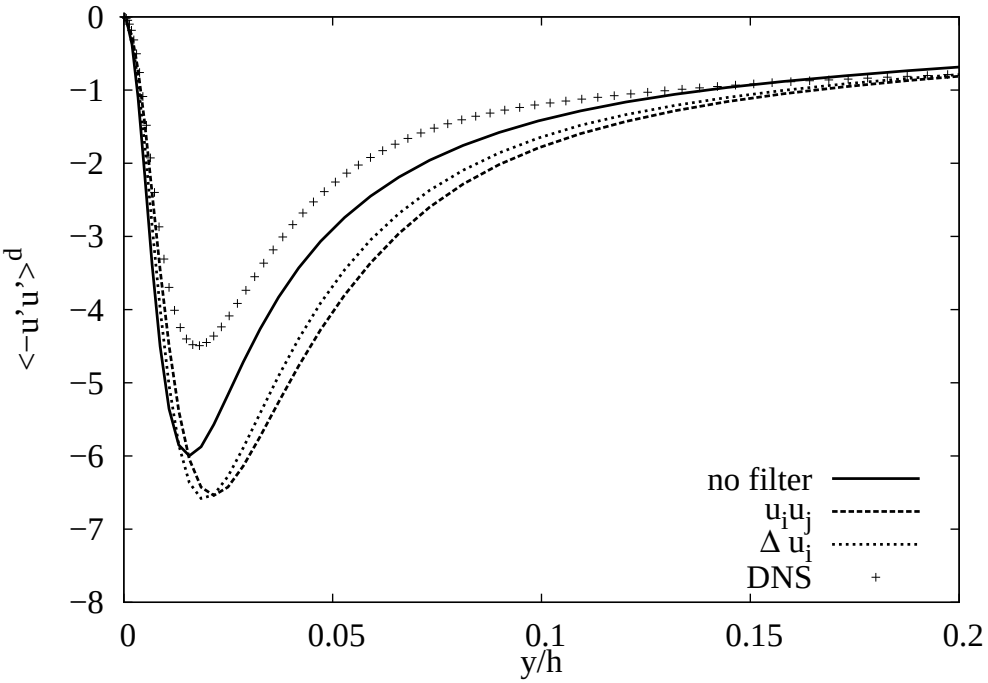

Figure 4.2: Comparison between filtering approaches: $u_i u_j$ or Δu_i is filtered. Deviatoric streamwise Reynolds stress.

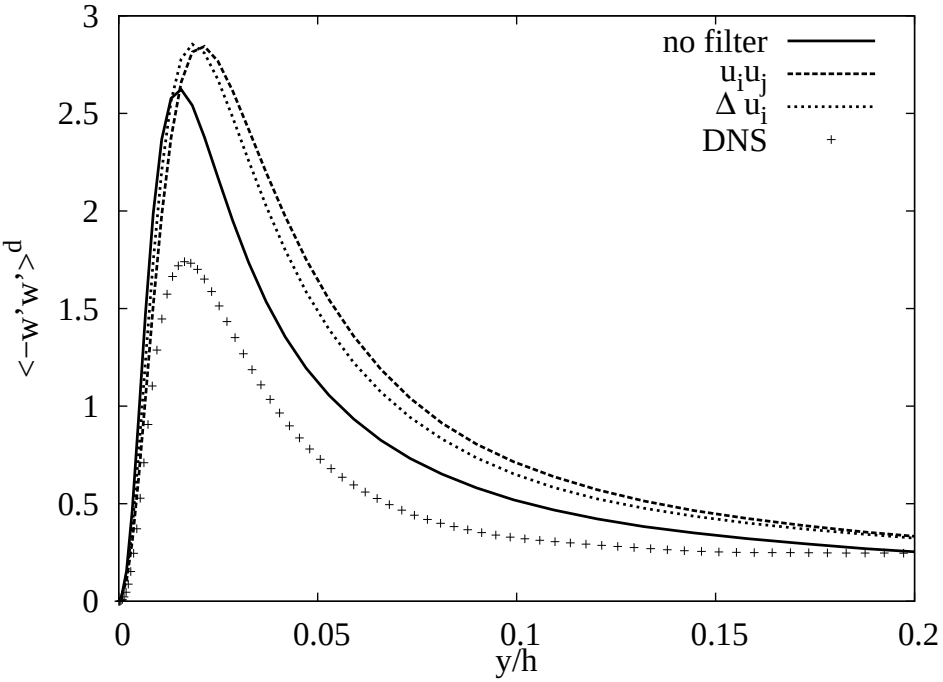

Figure 4.3: Comparison between filtering approaches: $u_i u_j$ or Δu_i is filtered. Deviatoric spanwise Reynolds stress.

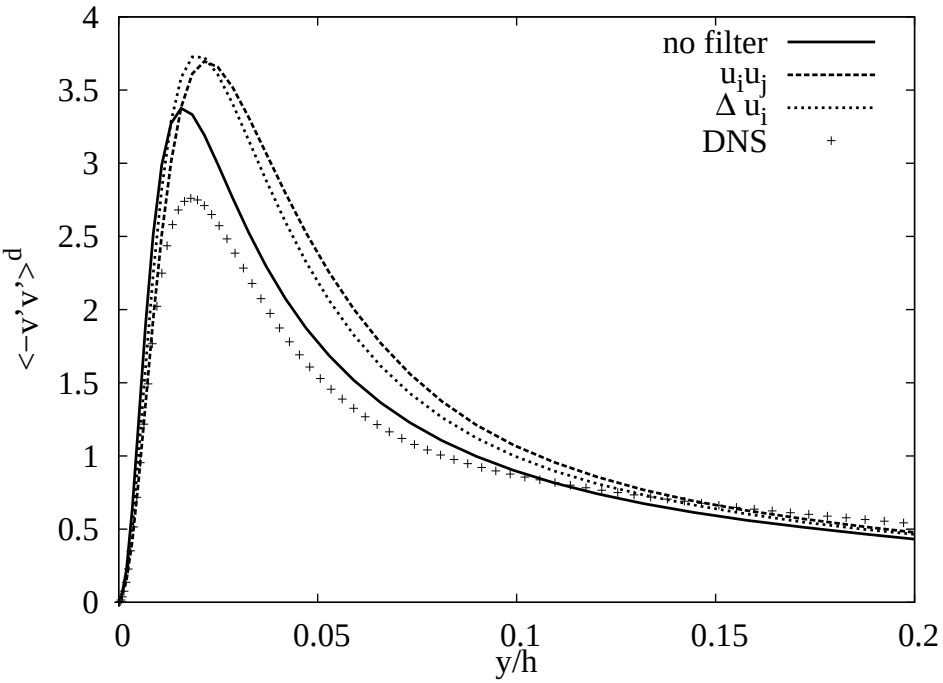

Figure 4.4: Comparison between filtering approaches: $u_i u_j$ or Δu_i is filtered. Deviatoric wall-normal Reynolds stress.

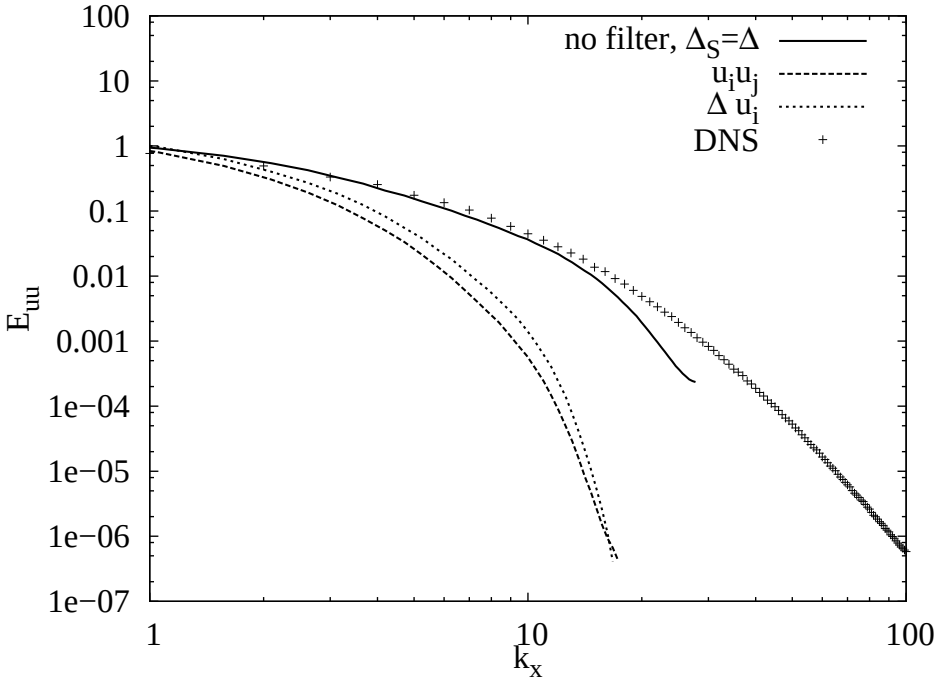

Figure 4.5: Comparison between the filtering approaches: u_iu_j or Δu_i is filtered. One-dimensional energy spectra for u at $y^+ \approx 5$. Streamwise direction.

the spanwise direction.

The SGS shear stress τ_{12} is depicted in Figure 4.10. When explicit filtering is applied, the SGS shear stress increases. Probably this is mainly owing to the increased model length scale which directly controls the level of eddy viscosity and the SGS stress. Also in the other presented flow quantities, the results obtained with explicit filtering are affected by both filtering and modelling.

Although there were only small differences between the two studied filtering approaches at the filter width applied here, their differences became more evident when the filter width was increased: filtering of the change of the velocity became unstable. This is why, for the rest of the thesis, only filtering of the non-linear convection term is considered.

Since filtering damped down the badly described high frequencies and an increase of the model length scale adds more dissipation in the solution, the numerical error in the present simulations should be effectively diminished when compared to the case with no filtering. However, in cases where explicit filtering was applied, the total simulation error was increased. In the next sections, we discuss in more detail the factors behind this.

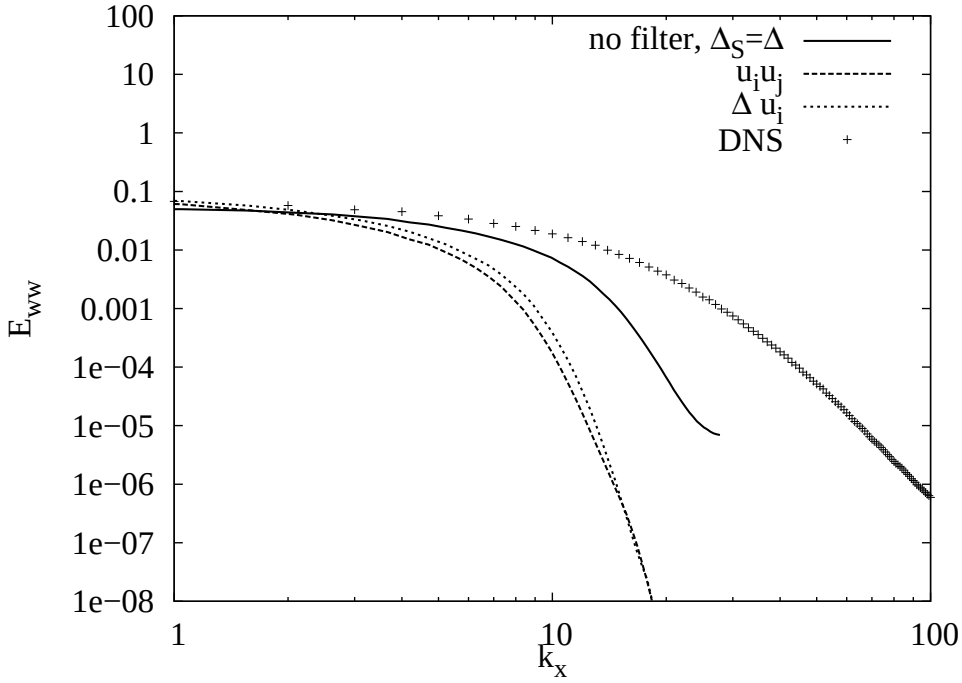

Figure 4.6: Comparison between the filtering approaches: u_iu_j or Δu_i is filtered. One-dimensional energy spectra for w at $y^+ \approx 5$. Streamwise direction.

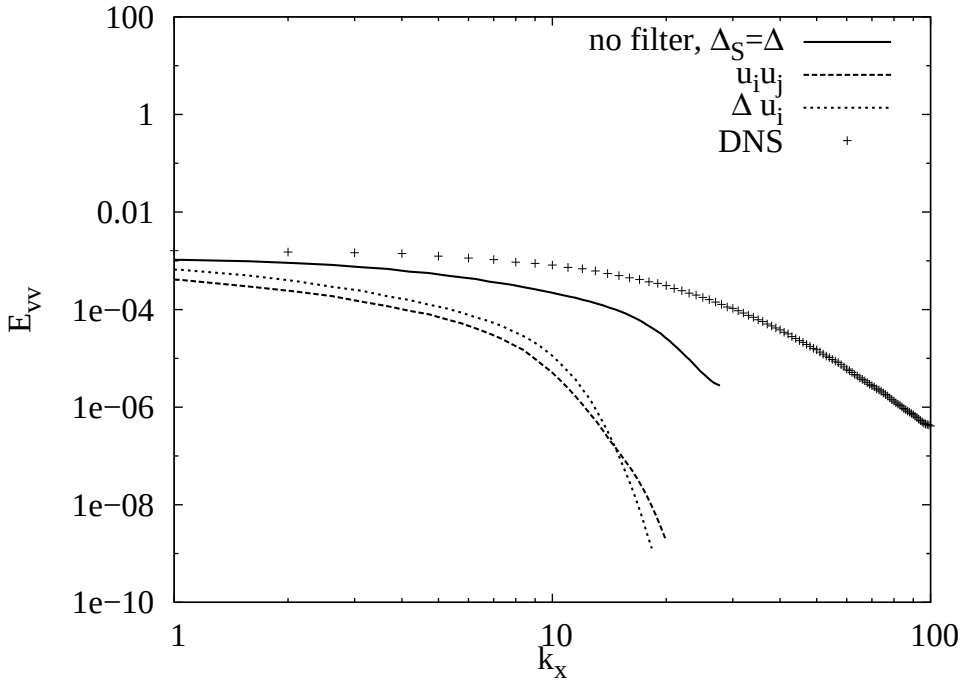

Figure 4.7: Comparison between the filtering approaches: u_iu_j or Δu_i is filtered. One-dimensional energy spectra for v at $y^+ \approx 5$. Streamwise direction.

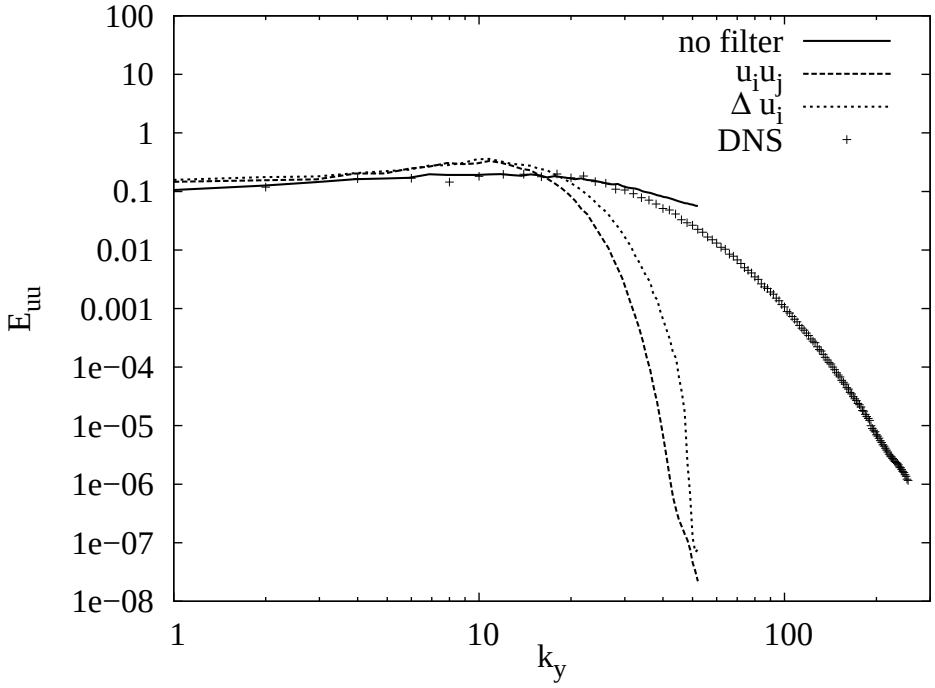

Figure 4.8: Comparison between the filtering approaches: $u_i u_j$ or Δu_i is filtered. One-dimensional energy spectra for u at $y^+ \approx 5$. Spanwise direction.

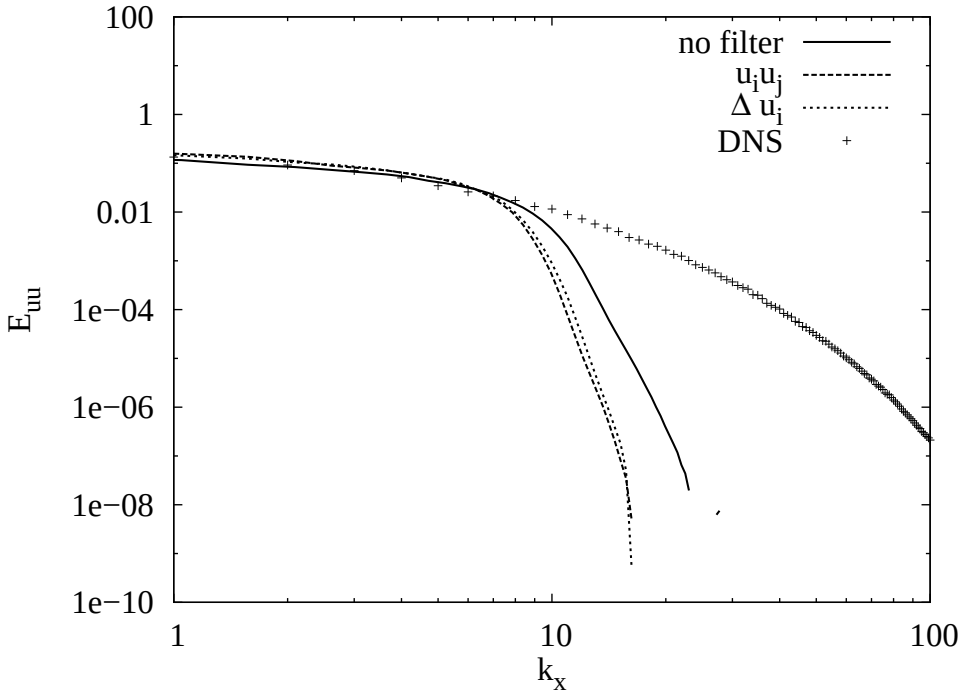

Figure 4.9: Comparison between the filtering approaches: $u_i u_j$ or Δu_i is filtered. One-dimensional energy spectra for u in the middle of the channel. Streamwise direction.

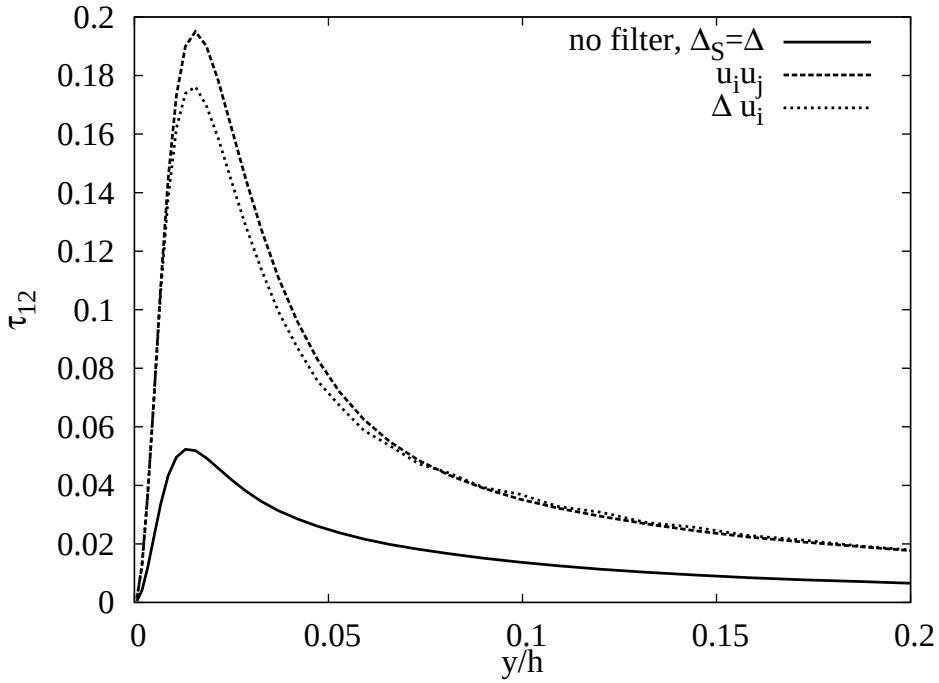

Figure 4.10: Comparison between the filtering approaches: $u_i u_j$ or Δu_i is filtered. SGS shear stress τ_{12}.

4.2 Effect of Filter Shape

In this section, we study the effect of the shape of the chosen explicit filter function on LES. Here, the non-linear convection term $\tilde{u}_i\tilde{u}_j$ is filtered explicitly using the Simpson, trapezoidal and fourth- and sixth-order commutative filters, which were discussed in Section 2.2.3. The filter transfer functions of these filters were depicted in Figure 2.3 and the coefficients were given in Table 2.1. There are three main differences between these filters: the commutation error, the shapes of the filter functions, and the effective filter widths. The commutation error related to changing the order of differentiation and filtering is the smallest with the 6th-order filter and largest with the trapezoidal and Simpson filters (2nd order). The shape of the filter transfer function affects the error in the conservation of kinetic energy and in the Galilean invariance, which are broken in this formulation of explicit filtering (Lund 1997). The 6th-order commutative filter is closest to the spectral cutoff filter, and thus these errors should be the smallest with this filter. In the high-frequency part, the Simpson filter and in the low-frequency area, the trapezoidal filter are furthest away from the spectral cutoff. As discussed in Section 2.2.3, the effective filter widths of the commutative and Simpson filters are two grid spacings, but the width of the trapezoidal filter is 2.45. In this section, we study the effect of these differences between the filters on the obtained flow statistics.

The mean-velocity profiles obtained using different discrete filters are plotted in Figure 4.11 and the streamwise deviatoric Reynolds stress in Figure 4.12. All the filters produce the same slope in the logarithmic layer, but the trapezoidal and Simpson filters overpredict the mean bulk velocity more than the commutative filters. Also, the Reynolds stress is most overpredicted with these filters. The total error obtained as a difference to the DNS data is smaller with the Simpson filter than with the trapezoidal filter, whereas there are no essential differences between the two commutative filters. The situation is similar for the other Reynolds stress components.

The one-dimensional energy spectra E_{uu} for the streamwise velocity component from the near-wall region ($y^+ \approx 5$) are evaluated in the streamwise direction in Figure 4.13. The commutative filters follow the DNS curve slightly closer than the others and damp down the high frequencies most efficiently. The trapezoidal filter affects the lower frequencies most, which could also be expected based on the shape of the filter. The Simpson filter transfer function obtains quite large values near the grid cutoff (see Figure 2.3), but still it damps the high frequencies as efficiently as the other filters. The situation is similar for the other velocity components. In Figure 4.14, the spectra are evaluated in the spanwise direction, and here the Simpson filter does not damp down the high frequencies very efficiently.

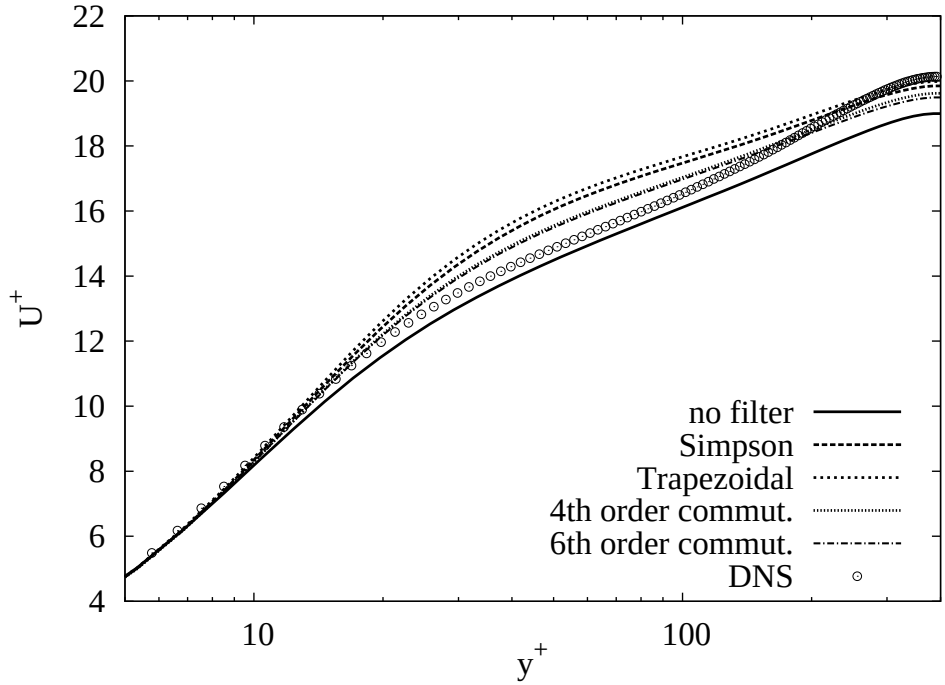

Figure 4.11: Comparison between filter functions. Mean-velocity profile.

As noticed in the previous subsection, the SGS shear stress increases in the present simulations via the model length scale. In Figure 4.15, we see that the filter function has only a small effect on this quantity.

Based on the results of this section, there are no essential differences in the behaviour of the two commutative filters, and these filters produce results closer to the DNS data than the Simpson and trapezoidal filters. The 6th-order filter requires slightly more computational effort than the 4th-order filter, and thus, for the rest of thesis, the 4th-order filter is applied as the explicit filter. The first mentioned difference between the filters was the order of the commutation error. However, this probably does not explain the differences between the simulation results, since they remain also in cases where there is no filtering in the wall-normal direction (not shown here) and thus no commutation error. The second difference was the shape of the filter transfer functions. Since the Simpson filter produces results closer to the DNS data than the trapezoidal, the shape in the low-frequency area is probably crucial. The third difference was the filter width, which explains some of the behaviour of the trapezoidal filter. Owing to the larger filter width, this filter affects a larger range of wavelengths and damps the simulation results most.

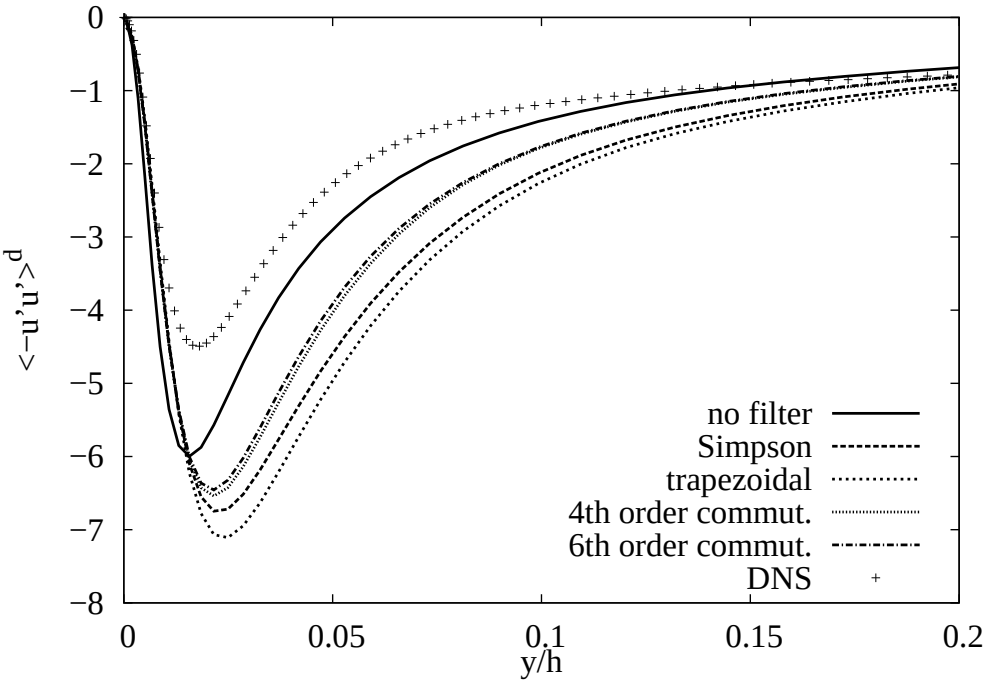

Figure 4.12: Comparison between filter functions. Deviatoric streamwise Reynolds stress.

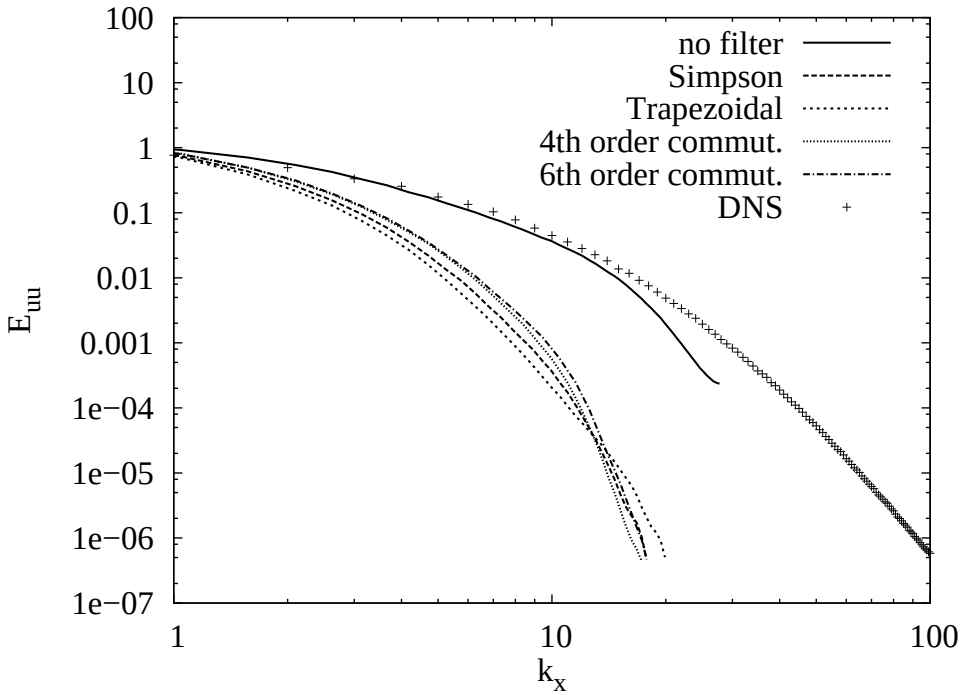

Figure 4.13: Comparison between filter functions. One-dimensional energy spectra E_{uu} at $y^+ \approx 5$. Streamwise direction.

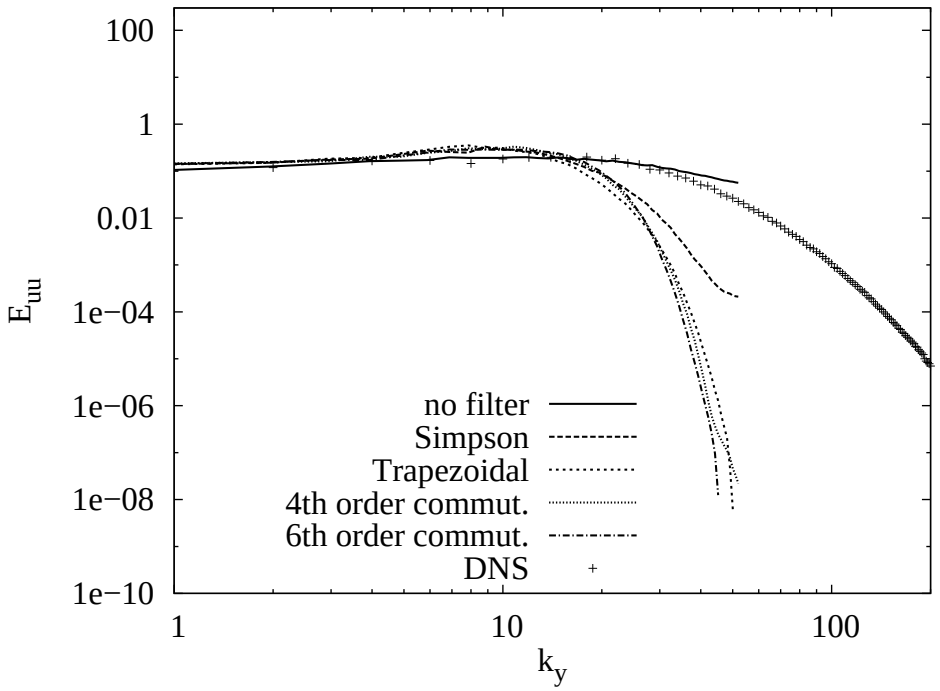

Figure 4.14: Comparison between filter functions. One-dimensional energy spectra E_{uu} at $y^+ \approx 5$. Spanwise direction.

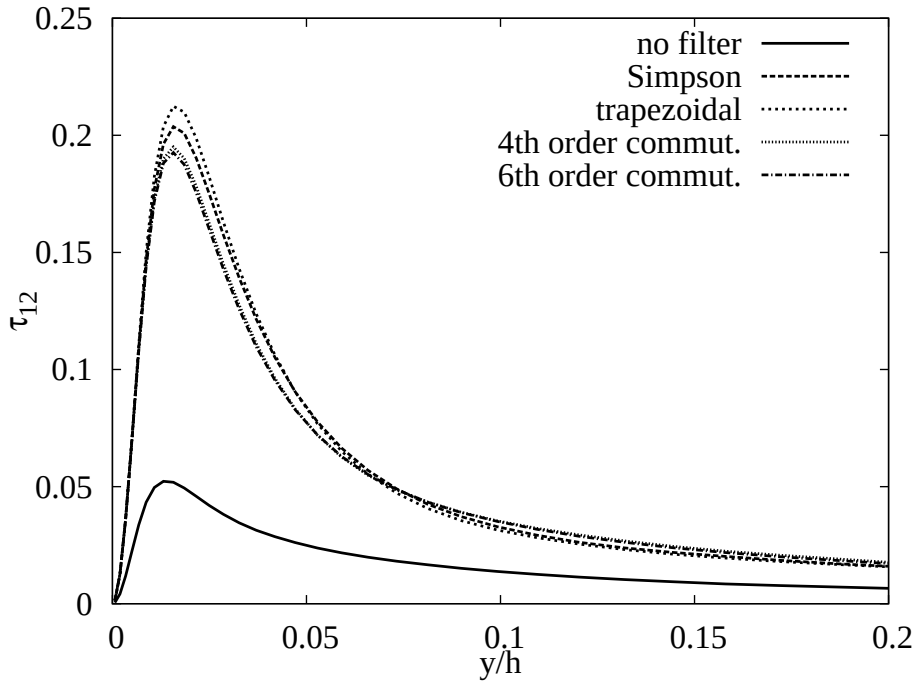

Figure 4.15: Comparison between filter functions. SGS shear stress τ_{12}.

4.3 Effect of Filtering versus Effect of SGS Modelling

In the previous section, the Smagorinsky length scale, Δ_S, was kept equal to the filter width, Δ_f, i.e. two grid spacings, in all cases with explicit filtering, and it was equal to the grid spacing in the cases with no filtering. Thus, in cases with explicit filtering, the quality of the results was a combination of filtering and modelling. Here, we compare cases with and without filtering using no model, and using the model length scale equal to grid spacing, and length scale equal to filter width. Firstly, the aim is to describe the effect of mere filtering on the simulation results. Secondly, we wish to compare the effect of modelling in cases with and without explicit filtering. Thirdly, the interaction between modelling and filtering is demonstrated. In this section, when explicit filtering is applied, we filter the non-linear convection term using the 4th-order commutative filter.

In the upper part of Figure 4.16, we have the mean-velocity profiles from simulations with explicit filtering, and in the lower part, from simulations without explicit filtering. In both cases, the simulations were repeated with different values of the model length scale. If we compare the two figures, we notice that, when explicit filtering is applied, the effect of modelling is reduced. In the lower part of Figure 4.16, where no explicit filtering is applied, the increase of the model length scale rapidly increases the mean bulk velocity and the thickness of the viscous sublayer. In the upper part of the figure, this influence of modelling is clearly diminished. In addition, we notice that most of the changes obtained in the previous section when explicit filtering was applied are already present in the case with no model in the upper part of the figure. Thus, the changes were mainly the result of filtering itself. However, we further see in the same figure that, when the Smagorinsky length scale is increased, the prediction of the mean-velocity profile slightly improves. The viscous sublayer becomes better captured and the slope of the profile improves slightly. Thus, the model is able to compensate somewhat for the effect of filtering.

In Figure 4.17, corresponding plots are given for the streamwise deviatoric Reynolds stress. Most of the overprediction of the Reynolds stress that was noticed in the previous section is actually the result of filtering and the model again has a rather small effect on the results. When the model length scale is increased, the peak value reduces and moves towards the middle of the channel. As seen in the lower part of the figure, this is owing to modelling, and in the upper part, the use of explicit filtering prevents the profile from widening too much. The results are similar for the other Reynolds stress components. Thus, a similar conclusion as drawn for the mean-velocity profile can be stated here: most of the overprediction of the Reynolds stress noticed in the previous sections was owing to filtering itself, and increasing the model length scale again slightly improves the results.

The one-dimensional energy spectra in the streamwise direction are depicted in the near-wall region (at $y^+ \approx 5$) in Figure 4.18. We notice that the main difference between explicit filtering and the damping provided by the model is their effect on the high frequencies. The model affects the low and high frequencies in a similar manner, whereas explicit filtering damps the high frequencies much stronger than the low frequencies. Also Visbal and Rizzetta (2002) and Bogey and Bailly (2006) noticed that eddy-viscosity-type models can affect a wider range of scales than explicit filtering. In Figure 4.18, in the case with explicit filtering and the large model length scale, the low frequencies are damped in a similar manner as with only modelling, but the high frequencies are damped more. However, in the spectra evaluated in the spanwise direction, the effect of modelling is not that strong (not shown here).

In the previous sections, we noticed that the total error, obtained as the difference to DNS data, increased when explicit filtering was applied, and the choice of the filter function did not have a large effect on this. Based on the results of this subsection, there seem to be two factors behind this behaviour: the effect of filtering itself and the behaviour of the applied SGS model with filtering. With the current numerical methods, explicit filtering alone had a large affect on the flow statistics, and it was the major factor behind the large total error. This new error introduced by explicit filtering overshadows the possible positive effect filtering might have on the numerical error. When SGS modelling was applied, filtering decreased the effect of modelling, but as the model length scale was increased, the model was able to improve the prediction of the flow statistics compared to the case with no model. In addition, in cases with the large model length scale, the results with explicit filtering were better than the results without explicit filtering. Thus, despite the large effect of filtering itself on the total simulation error, there was some desirable interaction between filtering and SGS modelling.

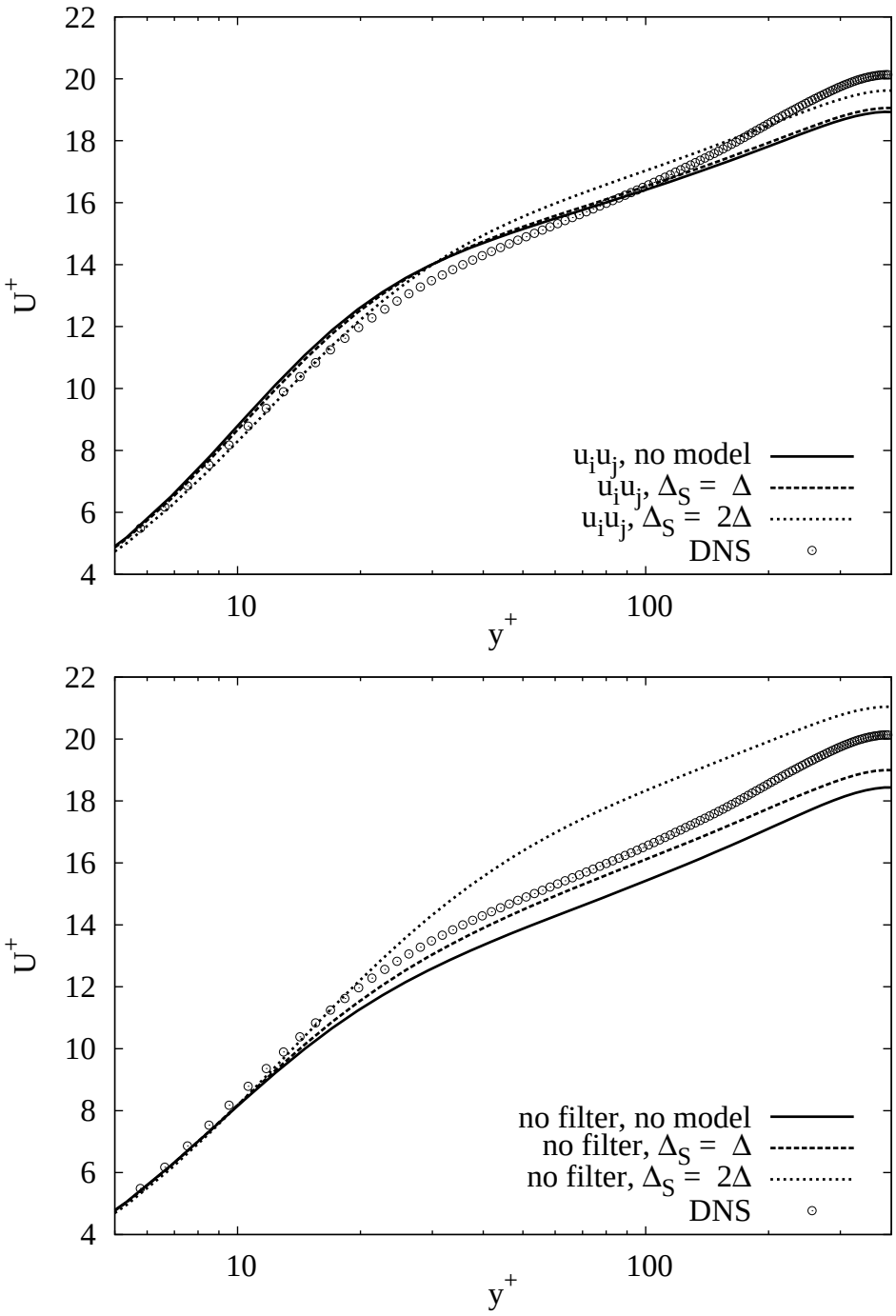

Figure 4.16: Effect of model and filtering. Mean-velocity profile. **Upper:** Explicit filtering is applied. **Lower:** No explicit filtering is applied.

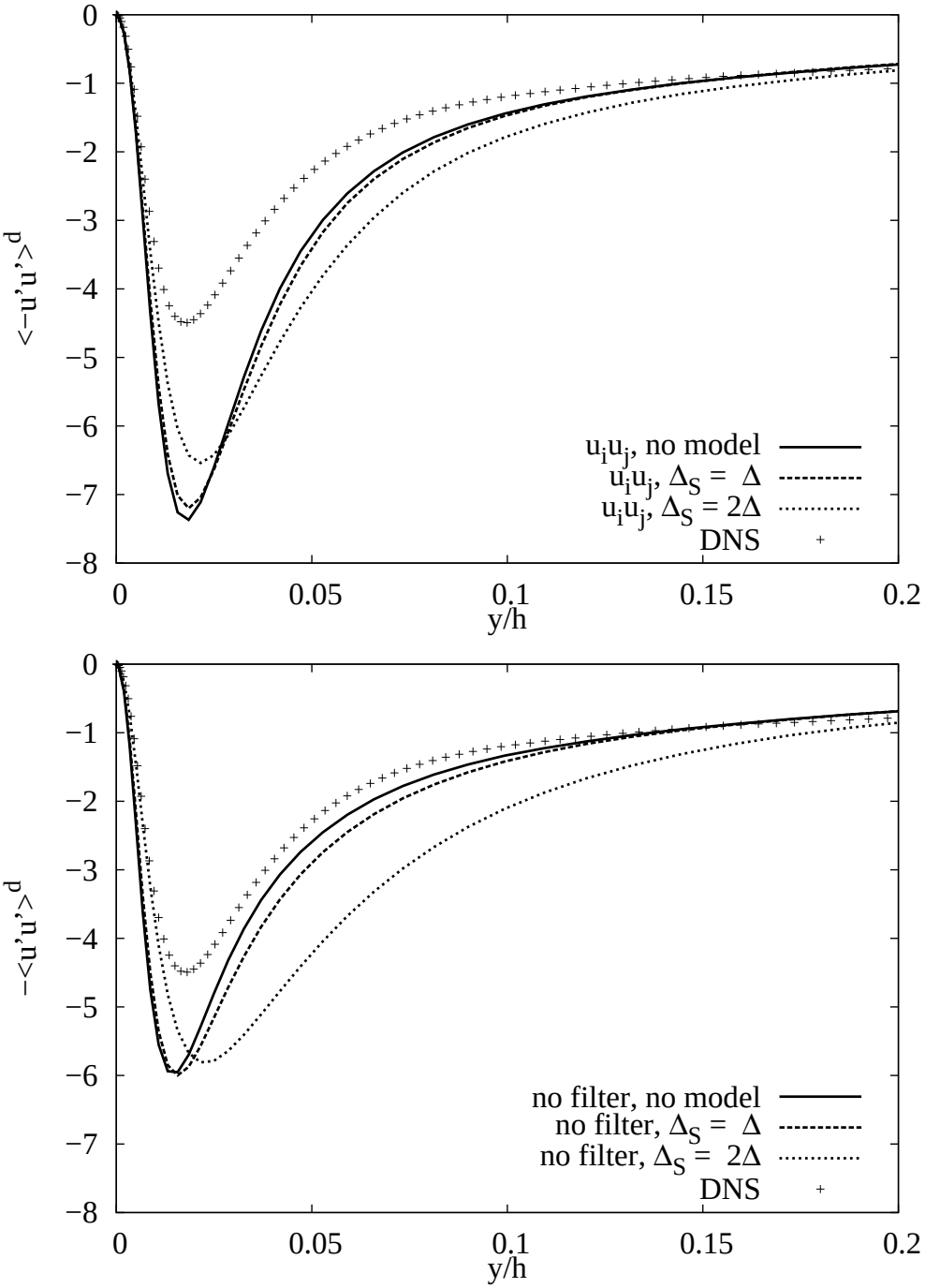

Figure 4.17: Effect of model and filtering. Deviatoric streamwise Reynolds stress. **Upper:** Explicit filtering is applied. **Lower:** No explicit filtering is applied.

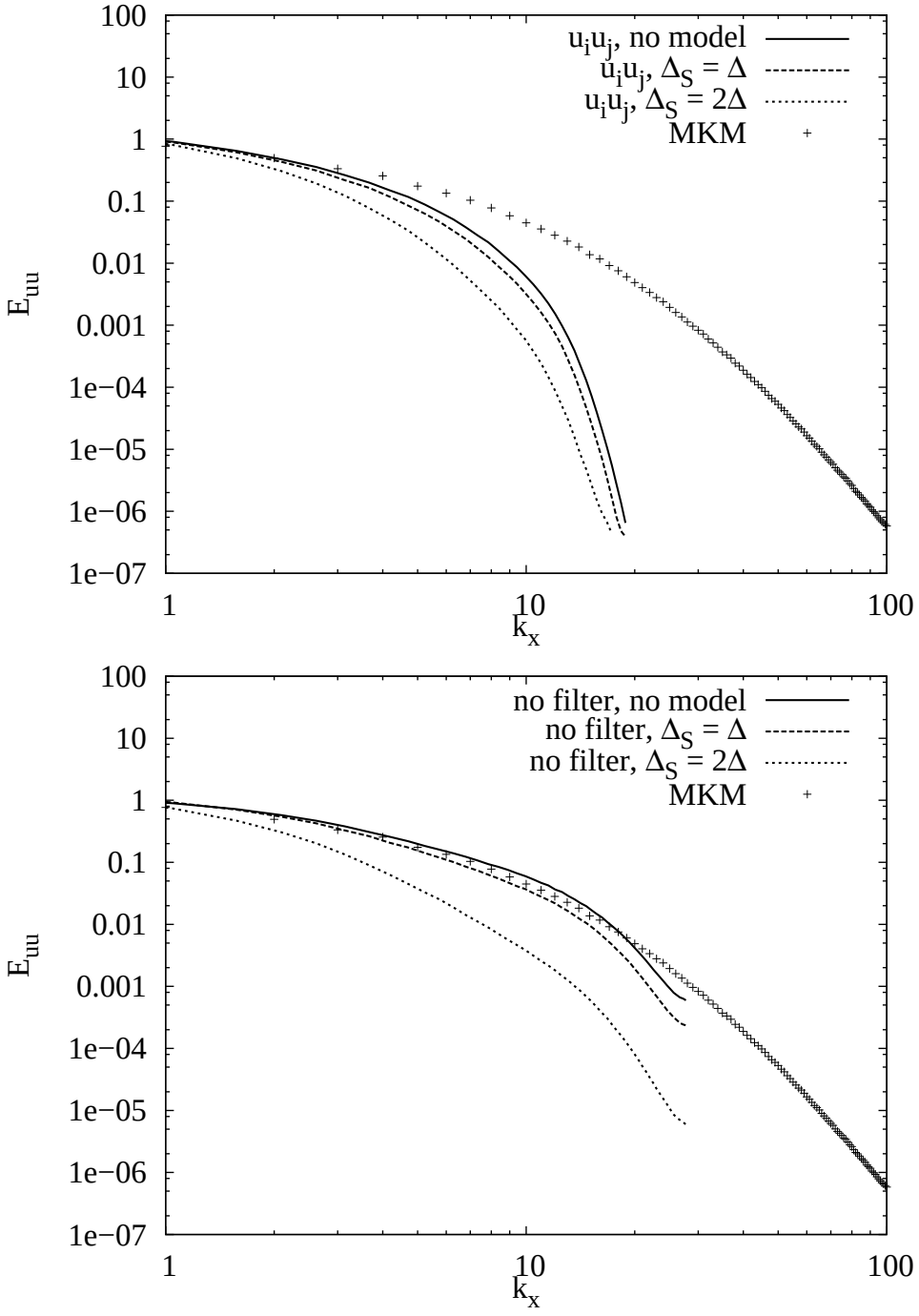

Figure 4.18: Effect of model and filtering. One-dimensional energy spectra at $y \approx 5$. Streamwise direction. **Upper:** Explicit filtering is applied. **Lower:** No explicit filtering is applied.

4.4 Explicit and Implicit Filtering

The use of explicit filtering was suggested as a method to reduce the numerical error in LES via damping the badly described low-frequency components of the resolved flow field. This is not the only possible way to smooth out the flow field. The standard Smagorinsky model is a purely dissipative model, and adding dissipation to the simulation should also make the resolved flow field smoother and reduce the numerical error. Usually, the model length scale is set equal to the grid spacing, but at the same time the model coefficient is varied. Here, we fix the model coefficient and interpret varying the product $C_S\Delta_S$ as varying the model length scale Δ_S. This type of approach has been applied by Muschinski (1996).

In this section, we study the differences between explicit filtering of the non-linear convection term and the implicit filtering provided by the SGS model. The differences are emphasised by the use of wider explicit filter widths in cases with explicit filtering and wider model length scales, i.e. implicit filter widths, in cases with implicit filtering. In cases with explicit filtering, the filter widths of 1.5Δ, 2Δ, 3Δ and 4Δ are applied, and to separate the effect of explicit filtering from modelling, the model length scale is kept equal to the grid spacing. These results are compared to cases with no explicit filtering and larger model length scales. It is actually not physically correct to increase the explicit filter width and not to increase the effect of the SGS model, because when the resolved field is filtered explicitly, SGS or SFS modelling should be used to model the scales affected by filtering. However, this comparison is done to study the differences and similarities between the explicit and implicit procedures, and to complete the study of the previous section.

In Figure 4.19, we have the mean-velocity profiles from cases with increasing explicit filter widths. To compare this to the case where implicit filter width is increased, two curves from the lower part of Figure 4.16 are included. We notice that in the mean bulk velocity, the effects of implicit and explicit filtering are similar to each other. However, explicit filtering does not increase the mean bulk velocity as rapidly as implicit filtering. The main difference is in the viscous sublayer. When explicit filtering is applied, the velocity near the end of the layer increases, but the thickness of the logarithmic layer remains constant. Increased velocity near the end of the viscous sublayer makes the slope in the logarithmic layer incorrect. With implicit filtering, the viscous sublayer thickens.

The deviatoric streamwise Reynolds stresses from the different cases are plotted in Figure 4.20, and two curves from the lower part of Figure 4.17 are included. As the explicit filter width is increased, the peak of the Reynolds stresses becomes more overpredicted, and the distribution widens. When only implicit filtering is applied, the peak of the Reynolds stress becomes less overpredicted, but the

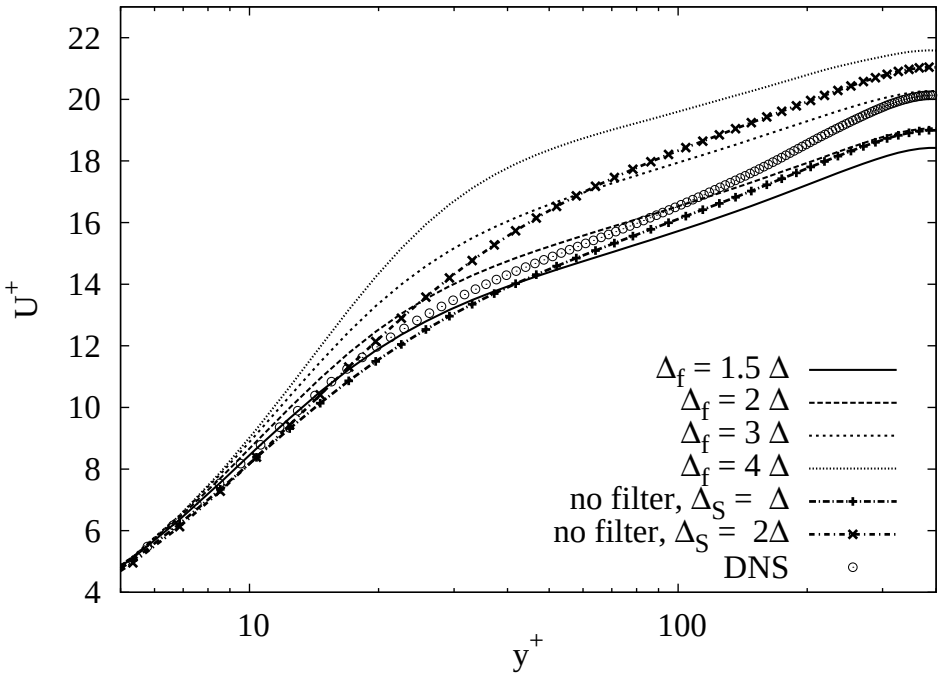

Figure 4.19: Explicit filter width is increased. Mean-velocity profile.

distribution widens more rapidly than with explicit filtering. These differences between the filtering approaches were also visible in the previous section, where explicit filtering increased the peak value and prevented the profile from widening.

As seen in Figure 4.21, increasing the width of the explicit filter affects the behaviour of the Smagorinsky model. The peak value of the SGS shear stress is increased with the filter width although the model length scale was not varied between the simulations, and thus the effect of the SGS model on the turbulent shear stress increases in the near-wall region. However, in the middle of the channel, the level of the SGS shear stress decreases. The SGS shear stress is increased in comparison to the case with no filtering only when large explicit filter widths are applied. This supports the conclusion of the previous section, where we noticed that, when the explicit filter width equals two grid spacings, the effect of the model decreases compared to the case with no explicit filtering. Since the product $C_S\Delta_S$ is kept constant, the changes in the SGS shear stress are caused by the changes in the strain-rate tensor (see Equation 2.16).

The one-dimensional energy spectra evaluated in the near-wall region ($y^+ \approx 5$) from cases with explicit filtering are depicted in the streamwise direction in Figure 4.22. Two curves where no filtering is applied and the model length scale is varied are included from the lower part of Figure 4.18. We see that as the explicit filter width is increased, also the lower frequencies are damped down. Since the

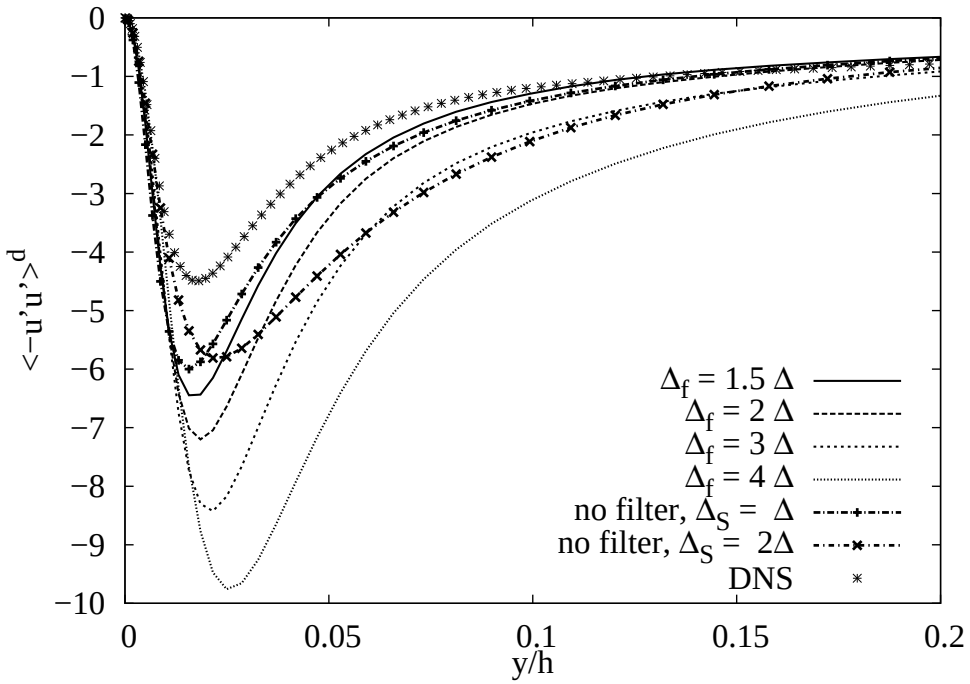

Figure 4.20: Explicit filter width is increased. Deviatoric diagonal streamwise Reynolds stress.

applied filters are not sharp, the use of wide filters affects the whole spectrum. This is similar to the behaviour of the cases with implicit filtering. However, all the explicit filters damp down the high frequencies more efficiently than implicit filtering, which affects all frequencies in a similar manner even if the model length scale is increased. Damping of the high frequencies can be considered as a desirable feature, because it reduces the numerical error.

In the previous section, the effect of filtering with a smooth filter was separated from the effect of SGS modelling. In this section, these differences where further emphasized by comparing results with explicit and implicit filtering with larger filter widths. We saw that wide smooth filters have some similar effects on the flow quantities as implicit filtering provided by the Smagorinsky model. These wide explicit filters damp also the low-frequency components of the resolved flow field, and thus the effect is similar to the effect of extra dissipation introduced by implicit filtering.

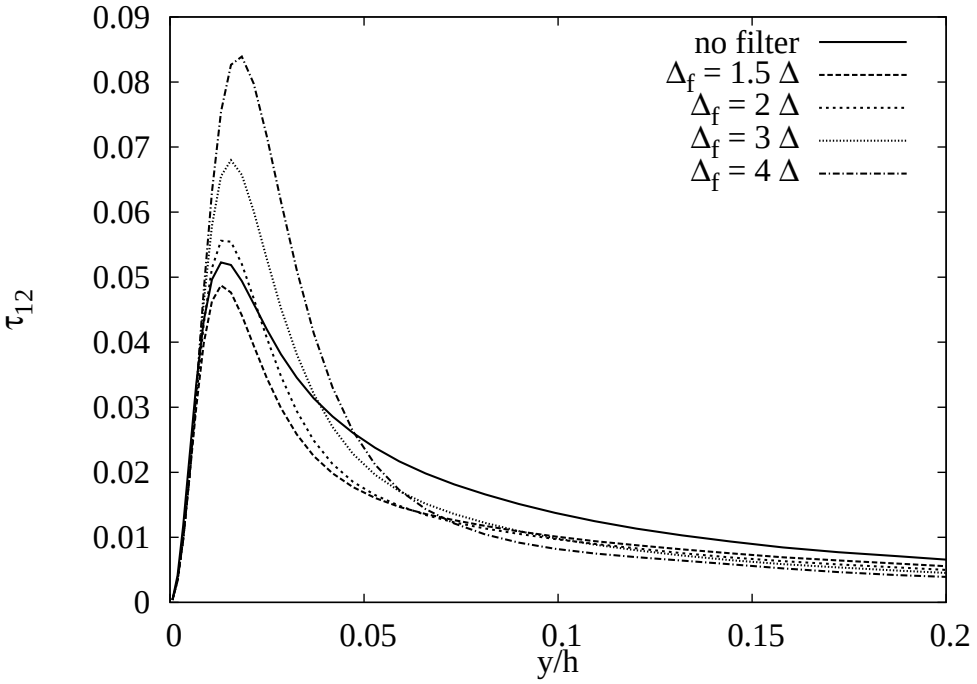

Figure 4.21: Explicit filter width is increased. SGS shear stress τ_{12}.

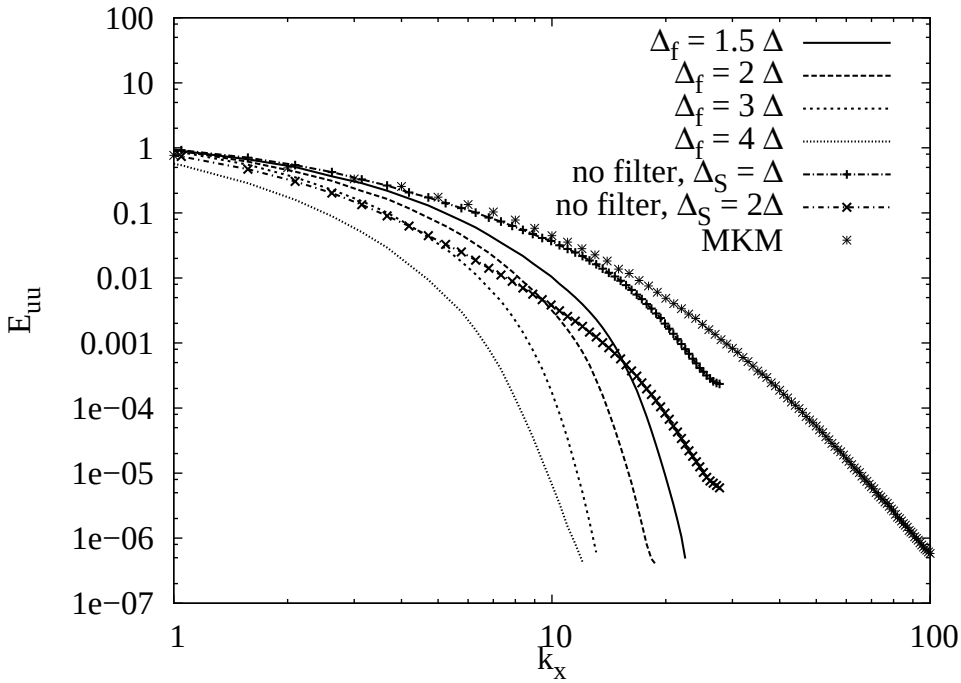

Figure 4.22: Explicit filter width is increased. One-dimensional energy spectra at $y^+ \approx 5$. Streamwise direction.

4.5 Effect of SFS Modelling with Explicit Filtering

The results of the previous subsections were obtained using the standard Smagorinsky model, which is one of the simplest subgrid-scale models. It is a dissipative model which is usually used to model SGS stresses. In the previous sections, no separate modelling or reconstruction was applied to the subfilter-scale stresses, which are related to scales smaller than filter width but larger than grid spacing. To verify that the results were not caused by poor SGS or SFS modelling, these simulations are repeated here using the dynamic version of the Smagorinsky model (DSM) for the SGS stresses, the scale-similarity model (SSM) for the SFS stresses and a mixed model (MM), where the Smagorinsky model is used to model subgrid-scale stresses and SSM to model subfilter-scale stresses. These models were discussed in Section 2.1.2. They are selected for use here because they are still rather simple to implement and the extra computation time is not too large. As noticed in Section 4.1, explicit filtering increases the computation time, and it is not realistic to assume that it could be applied in complex applications together with a complex SGS model.

In the simulations of this section, the grid resolution is the same as given in Table 4.1. The fourth-order commutative filter with the width of two grid spacings is applied as the explicit filter as well as the filter of the scale-similarity model. In simulations with explicit filtering, the test filter of the dynamic model is the commutative filter with the width of four grid spacings, and in simulations with no explicit filtering the test filter is the commutative filter with the width of two grid spacings. These filters were discussed in Section 2.2.3 and the filter transfer functions were depicted in Figure 2.4. In simulations with explicit filtering and the standard Smagorinsky model, the length scale of the Smagorinsky models is set equal to the filter width as in Sections 4.1 and 4.2. In simulations with the mixed model, the length scale of the Smagorinsky model was equal to grid spacing, because the scale-similarity part models the subfilter-scales.

The mean-velocity profiles from simulations with different models with and without explicit filtering are given in Figure 4.23. In the upper part of the figure, no explicit filtering is applied, and in the lower part, the non-linear convection term and the SGS and SFS models are filtered explicitly using the filter width of two grid spacings. When no explicit filtering is applied, there are clear differences between the mean bulk velocities obtained using different models, and the dynamic Smagorinsky model (DSM) produces the value closest to the reference data of the DNS of Moser et al. (1999). With both Smagorinsky models, the viscous sublayer is slightly too thick. When compared to the case with no model, SSM has almost no effect on the mean-velocity profile. The mixed model (MM) falls in between the SSM and Smagorinsky models.

In the lower part of Figure 4.23, we notice that explicit filtering reduces the differences between the models and the curves are closer to the case with no modelling, meaning that the effect of modelling is decreased. As noticed in the previous section with the standard Smagorinsky model, filtering changes the slope of the profile, which becomes too low. Here, we notice that despite the use of somewhat better models and inclusion of the first-order reconstruction for the SFS stresses, the slope still changes by the same amount. With DSM, the decreased slope decreases the mean bulk velocity. In the case with the standard Smagorinsky model, SSM and MM, filtering improves the prediction of the mean bulk velocity. In the standard Smagorinsky model, the coupling between the model and filtering is forced via the model length scale, which is here equal to the explicit filter width. The increased model length scale is visible in the increased thickness of the viscous sublayer. With the two other models, the thickness of the viscous sublayer slightly improves compared to the case with no filtering.

The resolved deviatoric streamwise Reynolds stress obtained using no explicit filtering is plotted in the upper part of Figure 4.24. The ones obtained with SSM and MM are underpredicted, whereas the ones produced by the Smagorinsky models are overpredicted. When we compare the results to the case with no modelling, we see that the effect of modelling is largest with SSM. The corresponding results for cases where explicit filtering was applied to the non-linear convection term and to the SGS and SFS stresses, are shown in the lower part of Figure 4.24. Here, we first notice that filtering increases the overprediction of the Reynolds stress with all models. In the previous section, it was noticed that this results from filtering itself, and here the trend continues also with DSM, SSM and MM. With DSM, SSM and MM, filtering slightly decreases the effect of modelling, whereas with the standard Smagorinsky model, the effect of modelling is increased because it is directly controlled via the model length scale.

The SGS or SFS shear stresses, τ_{12}, obtained with and without explicit filtering are plotted in the upper and lower parts of Figure 4.25, respectively. We notice that with DSM, SSM and MM, τ_{12} clearly decreases when filtering is applied, which is in agreement with the results obtained for the mean-velocity profile and for the Reynolds stress. With the standard Smagorinsky model, τ_{12} increases because of the increased model length scale.

The one-dimensional energy spectra from the near-wall region ($y^+ \approx 5$) are evaluated in the streamwise direction in Figure 4.26. In the upper part of the figure where no explicit filtering is applied, the differences between the models are rather small, whereas in the lower part, the standard Smagorinsky model damps down the spectrum most. It was noticed in the previous section that damping of the low frequencies mainly results from the implicit filtering provided by the model. Here, we see that with SSM, which introduces no extra dissipation to the simulation, the low frequencies are least affected. The benefit of using a model or reconstruction for subfilter-scales is also demonstrated here: when an SFS model

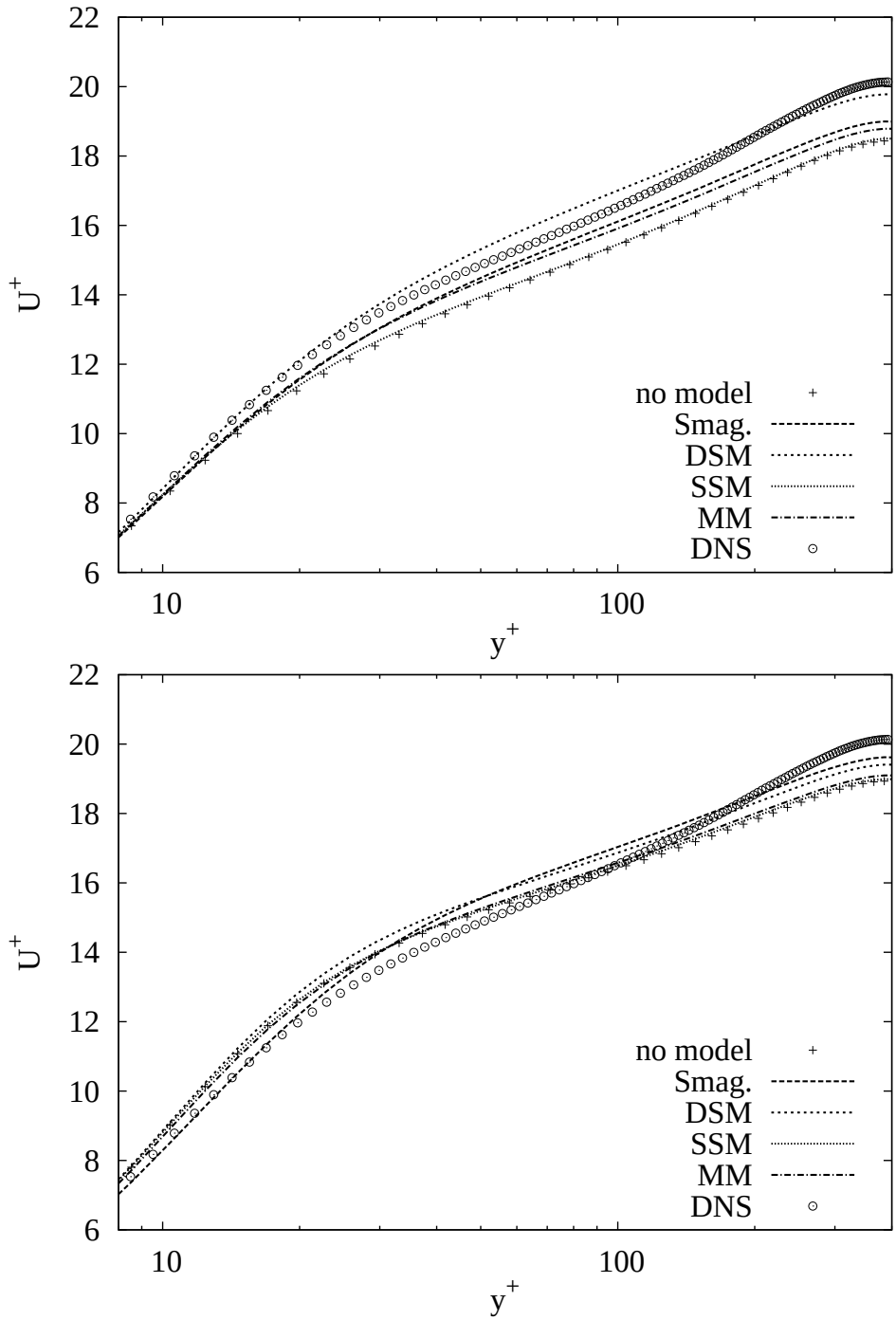

Figure 4.23: Mean-velocity profile. Explicit filtering of the convection term with different SGS models. **Upper:** No explicit filtering. **Lower:** Explicit filtering with $\Delta_f = 2\Delta$.

is used as in SSM or MM, the damping of the low frequencies is diminished. When explicit filtering is applied, the high frequencies are efficiently damped with all the models, which suggests that although the total error was not decreased, the numerical error is probably smaller.

Based on the results of this subsection, it seems that although in SSM and MM a simple reconstruction is used to model the subfilter scales, the same deficiency as noticed with the Smagorinsky models is seen with these models when the non-linear convection term is filtered. In SSM, there is no direct interaction between the model and explicit filtering. In DSM, modelling and explicit filtering are coupled via the increased test-filter width. It has been noticed that as long as the width of the explicit filter is correctly treated, the results are not sensitive to the choice of the test filter (Lund 1997). Since, in addition, explicit filtering reduces the effect of the model, it is understandable that the effect of the model did not increase. With the standard Smagorinsky model, the coupling between the model and filtering is easily set via the model length scale, but the modelling error limits the accuracy of the results.

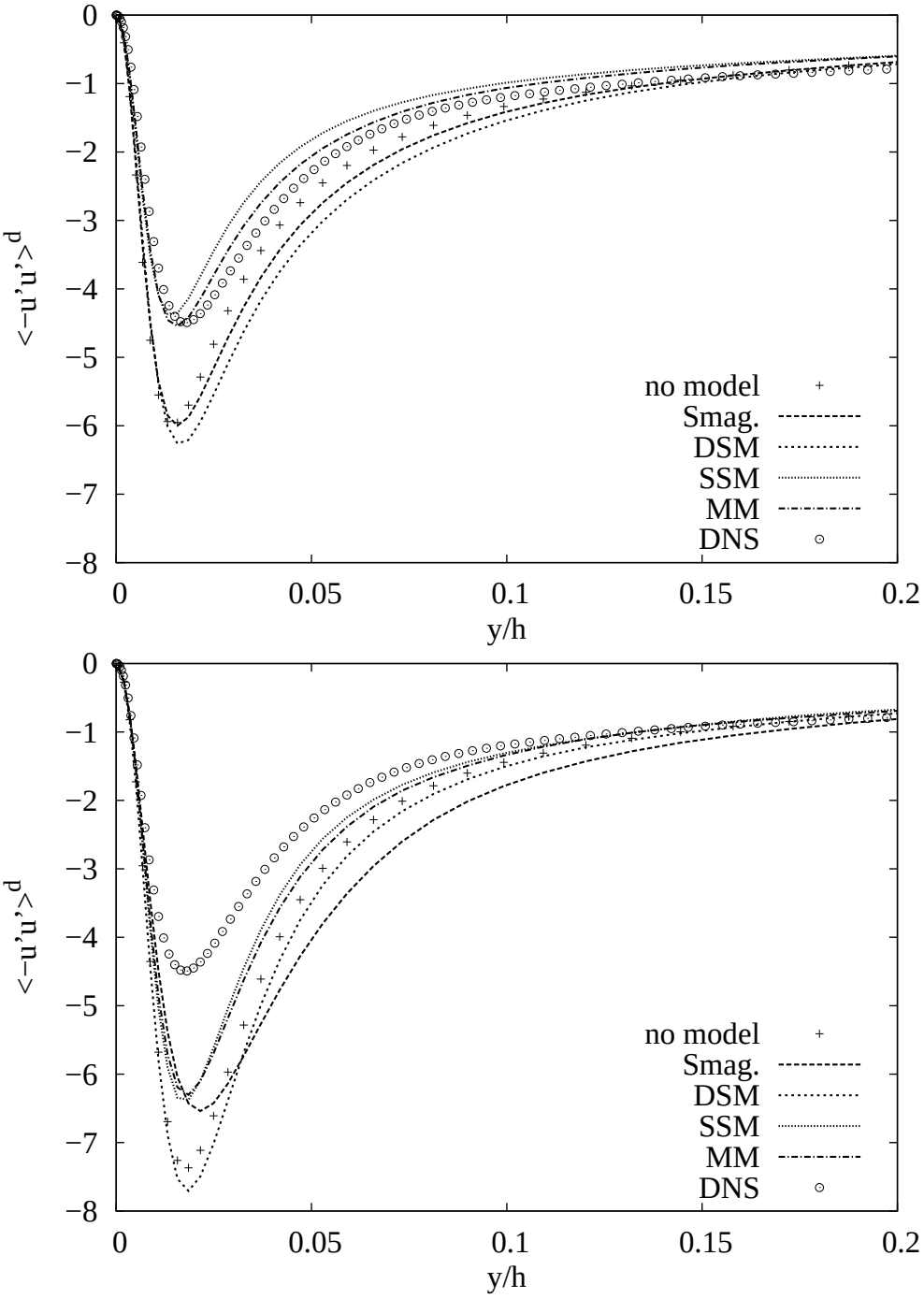

Figure 4.24: Resolved anisotropic streamwise Reynolds stress. Explicit filtering of the convection term with different SGS models. **Upper:** No explicit filtering. **Lower:** Explicit filtering with $\Delta_f = 2\Delta$.

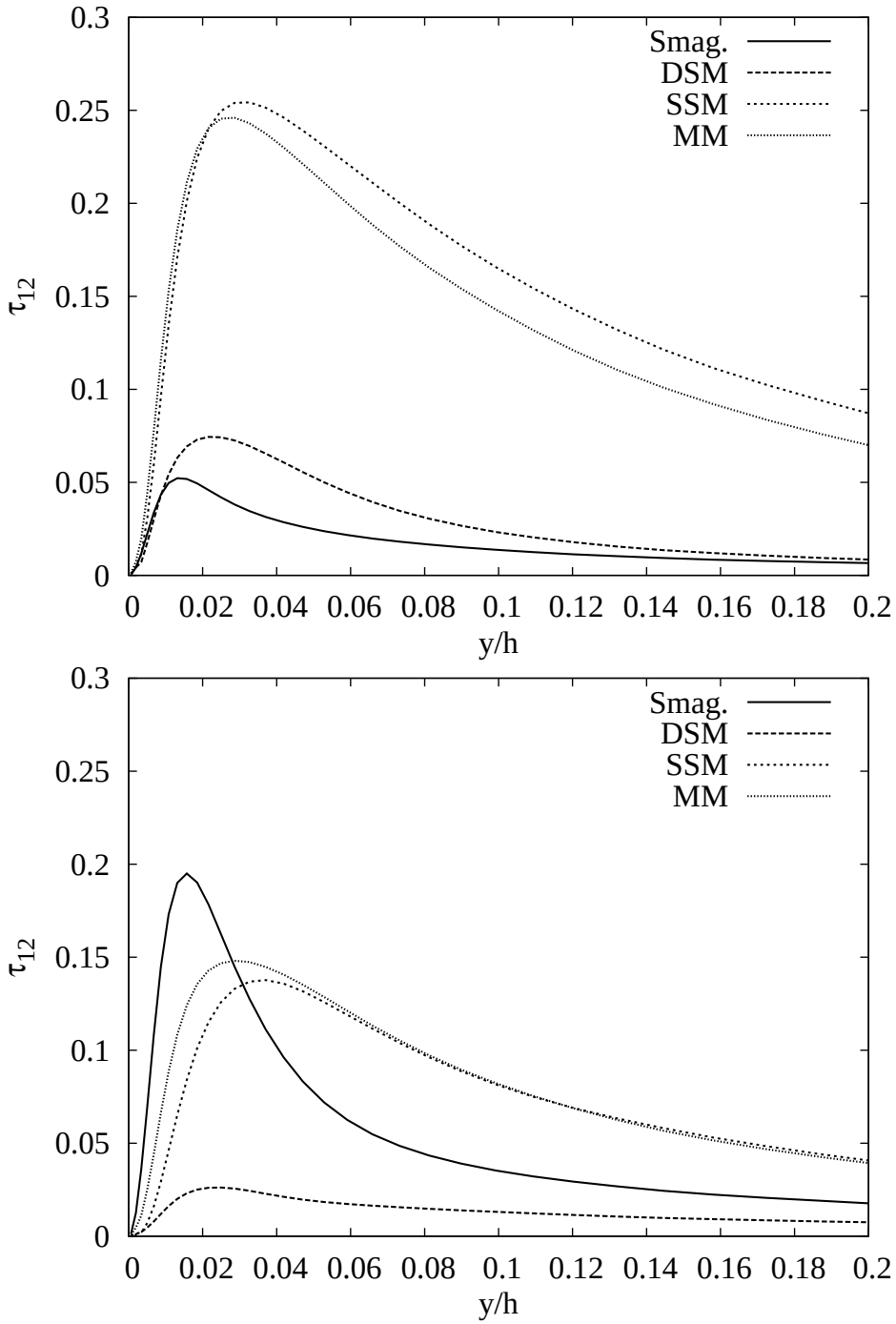

Figure 4.25: SGS or SFS shear stress. Explicit filtering of the convection term with different SGS models. **Upper:** No explicit filtering. **Lower:** Explicit filtering with $\Delta_f = 2\Delta$.

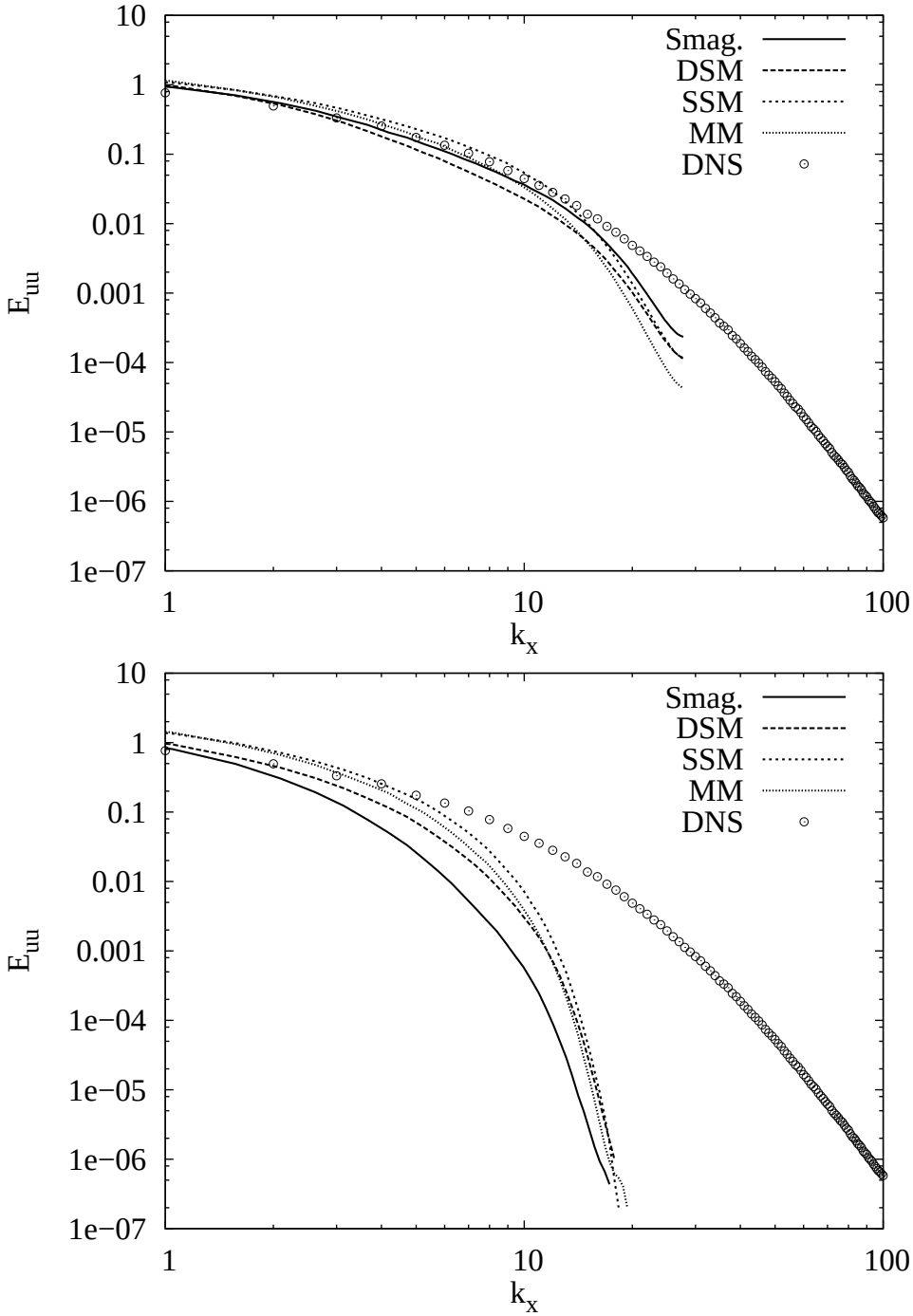

Figure 4.26: One-dimensional energy spectra at $y^+ \approx 5$. Streamwise direction. Explicit filtering of the convection term with different SGS models. **Upper:** No explicit filtering. **Lower:** Explicit filtering with $\Delta_f = 2\Delta$.

4.6 SFS Filtering versus Filtering of Convection Term

In the previous sections, we saw that explicit filtering of the non-linear convection term can have a large negative effect on the simulation results. In this section, we apply the approach of Carati et al. (2001) where filtering is performed via subfilter-scale (SFS) modelling (see Section 2.2.2, Equations (2.48)–(2.49)). The same models as applied in the previous section are applied here, and the aim is to compare filtering of the non-linear convection term to filtering via SFS modelling. As was discussed in Section 2.2, the equations being solved are different in different approaches to explicit filtering, and the definition of exact SGS or SFS tensor changes. Thus, the terms that the SGS and SFS models represent are also different in different approaches.

Here, modelling is first applied only to the SGS component of the shear stress using the Smagorinsky models, then only the SFS component is modelled using the scale-similarity model (SSM), and finally, both SFS and SGS stresses are modelled using SSM and a Smagorinsky model as a mixed model. Gullbrand and Chow (2003) showed that the modelling of the SFS stress is necessary, and to obtain improved results compared to the traditional approach, the dynamic reconstruction model of Stolz et al. (2001) had to be applied. Here, much simpler models are applied because the main goal is to compare the two approaches. In this section, the fourth-order commutative filters with the widths of two and four grid spacings are applied.

In the upper part of Figure 4.27, the mean-velocity profiles from the cases using a Smagorinsky model for the SGS stress are depicted. First, no extra filtering is provided via the model. The model length scale in the standard Smagorinsky model, Δ_S, is equal to the grid spacing, and the test filter in DSM, Δ_{test}, has the width of two grid spacings. Then, the model length scale in the standard Smagorinsky model is increased to two grid spacings and in DSM, the width of the test filter is increased to four grid spacings. This corresponds to a situation where the explicit filter has the width of two grid spacings. In the standard Smagorinsky model, the filtering provided by the model is actually implicit filtering since no filtering operation is made explicitly. In Figure 4.27, the larger model length scale in the standard Smagorinsky model increases the thickness of the viscous sublayer and makes the mean bulk velocity overpredicted. In the dynamic Smagorinsky model, increasing the test filter width has only a small effect on the velocity profile. The small effect of varying the test filter width was noticed previously by Lund (1997).

In the lower part of Figure 4.27, we have the velocity profiles from cases where SSM is used alone as an SFS model and as a mixed model together with Smagorinsky models to model both SGS and SFS stresses. The filter in SSM has the width

of two grid spacings, and when the mixed model is applied, the model parameter in the standard Smagorinsky model is proportional to the grid spacing, and the test-filter width in DSM is four grid spacings. As seen in Figure 4.27, the use of the mixed model improves the prediction of the viscous sublayer, which is too thin when only SSM is applied. DSM together with SSM produces the best profile. When compared to the cases with only an SGS model in the upper part of the figure, the mean bulk velocity is a bit low, but the thickness of the logarithmic layer is better predicted.

In Figure 4.27, the filtering provided by modelling does not change the slope of the velocity profile in the way that explicit filtering of the convection term did in Figure 4.23. In addition, the behaviour in the viscous sublayer improves, which does not happen in Figure 4.23.

The resolved deviatoric streamwise Reynolds stress from the different cases is plotted in Figure 4.28. In the upper part of the figure, we notice the typical behaviour of the standard Smagorinsky model as the model length scale is increased. The Reynolds stress becomes overpredicted and the distribution widens. When the dynamic model is applied, the increased test filter width has only a small effect on the Reynolds stress, and it becomes slightly more overpredicted. In the lower part of the figure, the use of SSM together with the standard Smagorinsky model produces the best Reynolds stress. However, the differences between the cases are small. By comparison of the upper and lower figures, we see that the use of SSM as an SFS model clearly improved the prediction of the Reynolds stress, as was found already by Gullbrand and Chow (2003). The results are similar for the other diagonal stress components. When compared to the case with explicit filtering of the non-linear convection term in Figure 4.24, the clear overprediction produced by the filtering is not visible in any of the cases in Figure 4.28.

In Figure 4.29, we have the SGS and SFS stresses from the different cases. As the model length scale is increased, the SGS shear stress of the standard Smagorinsky model is increased strongly. When the larger test filter of the width of four grid spacings is applied in DSM, the SGS shear stress inconsistently decreases. Thus, the improved results obtained using this test filter were probably due to the decreased effect of the model. In the lower part of figure, the SFS stress produced by SSM is much larger than the SGS stress produced by the Smagorinsky models. Thus, using the SFS model increases the effect of modelling.

The one-dimensional energy spectra are depicted in the streamwise direction in Figure 4.30. As can be expected, increasing the length scale of the Smagorinsky model damps down the whole spectrum. In the lower part of the figure, the mixed models affect the low frequencies less, and damp down the high frequencies better than the Smagorinsky models alone in the upper figure. However, the differences are rather small, and compared to the case with explicit filtering of the convection term in Figure 4.26, the damping of high frequencies is clearly not as efficient.

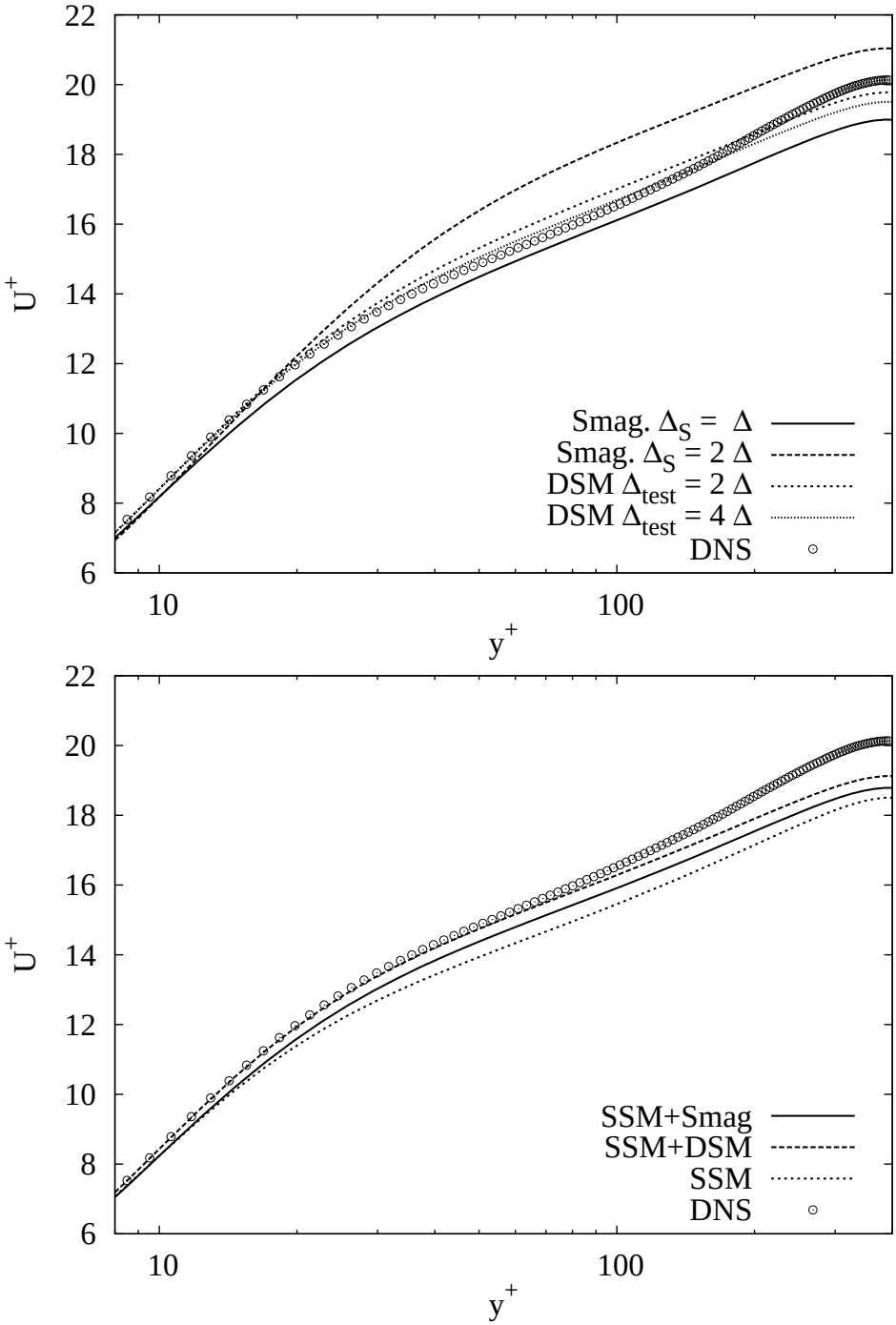

Figure 4.27: Mean-velocity profile. Filtering provided via the model. **Upper:** Only SGS stress is modelled. **Lower:** SFS or SFS and SGS stress are modelled.

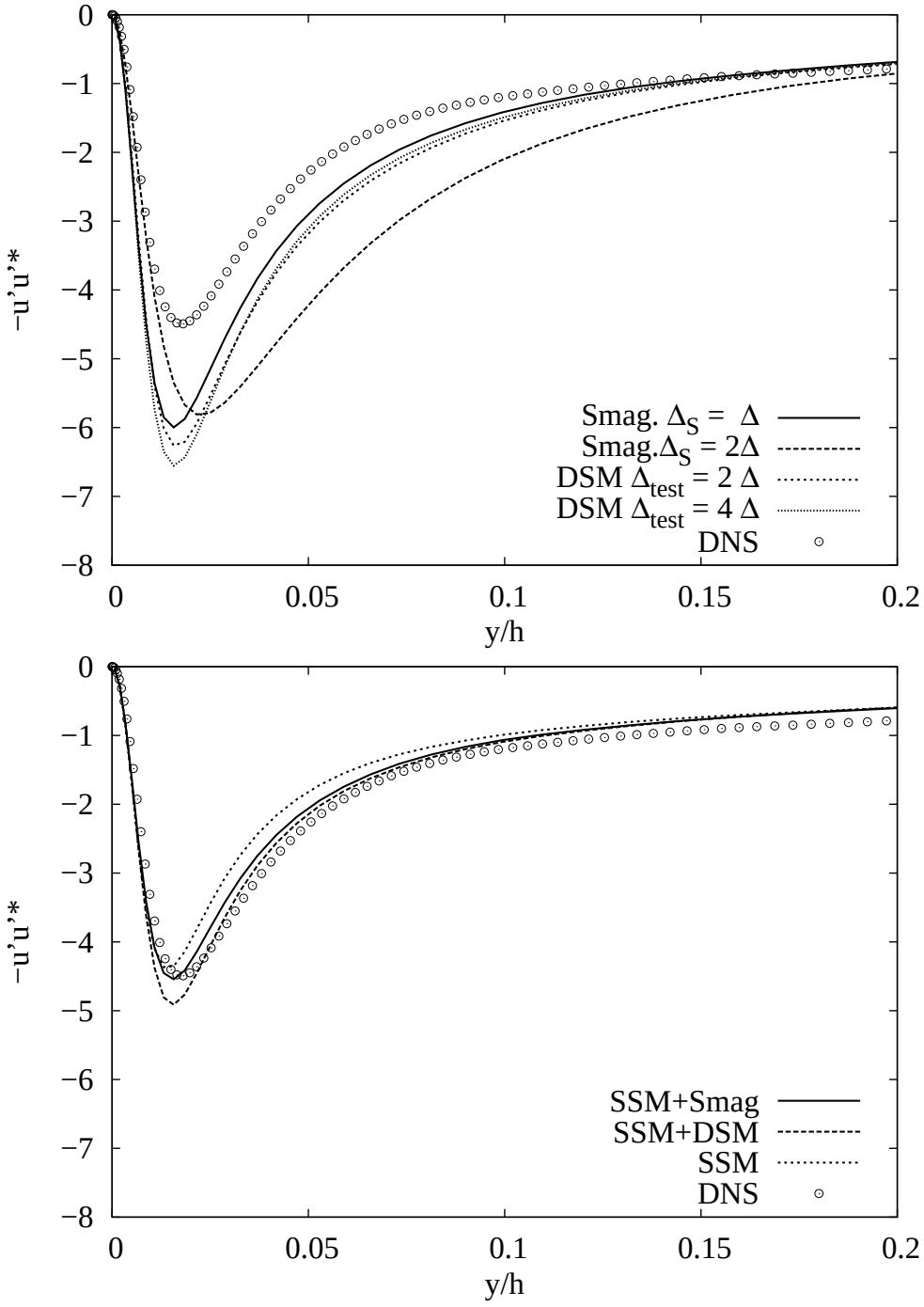

Figure 4.28: Resolved deviatoric streamwise Reynolds stress. Filtering provided via the models. **Upper:** Only SGS stress is modelled. **Lower:** SFS or SFS and SGS stress are modelled.

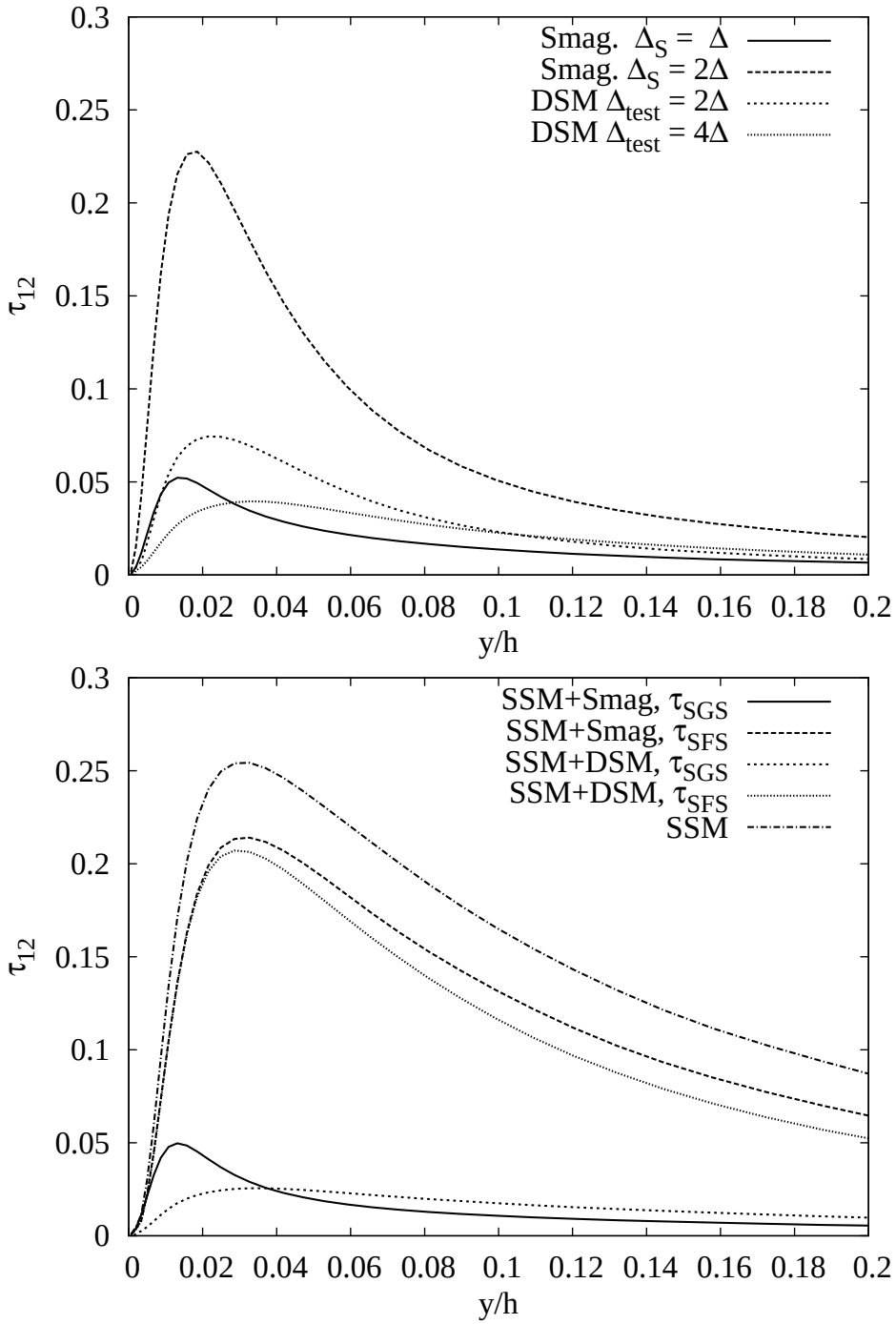

Figure 4.29: SGS and SFS shear stresses. Filtering provided via the models. **Upper:** Only SGS stress is modelled. **Lower:** SFS or SFS and SGS stress are modelled.

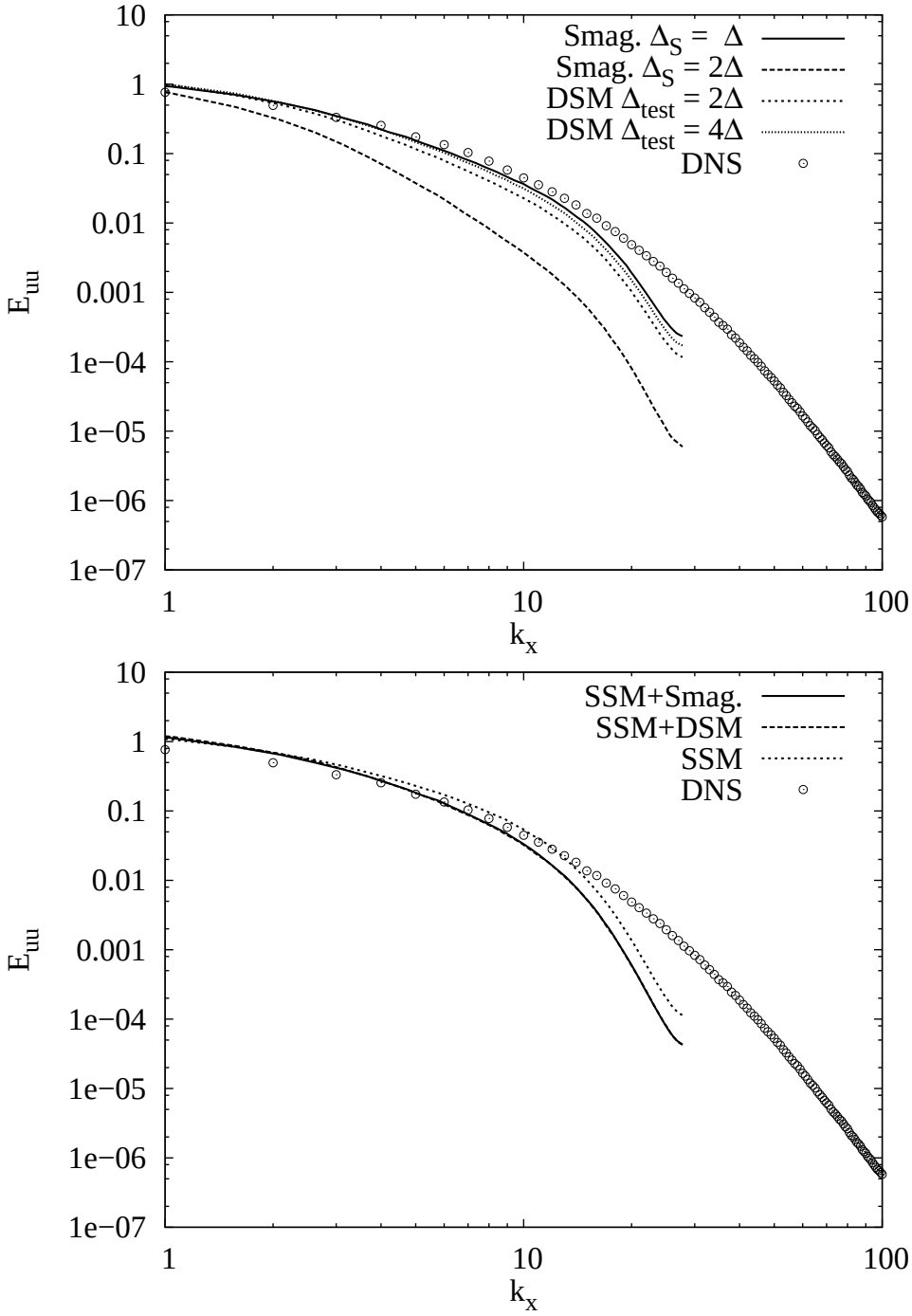

Figure 4.30: One-dimensional energy spectra at $y^+ \approx 5$. Streamwise direction. Filtering provided via the models. **Upper:** Only SGS stress is modelled. **Lower:** SFS or SFS and SGS stress are modelled.

4.7 Conclusions of Application of Explicit Filtering

In this chapter, explicit and implicit filtering has been applied in actual LES. The main new contributions are the comparisons between different filtering approaches and the demonstration of the rather large negative effect of explicit filtering with smooth filter functions. Despite the promising results of the a priori tests of the previous chapter, we have seen that explicit filtering of the non-linear convection term, or the change of the velocity field, does not improve the simulation results with the present grid resolution, SGS and SFS models and numerical methods. On the contrary, the total simulation error clearly increased when explicit filtering with a smooth filter was applied.

Some of the simulations were repeated using a finer grid to see if the applied grid resolution was too coarse for explicit filtering (not shown here), but it did not affect the conclusion – explicit filtering still increased the total error. Gullbrand and Chow (2003) applied both second- and fourth-order methods in their study, and when the grid resolutions were properly chosen, there were only small differences between the results. Since here increasing the grid resolution did not remove the negative effect of filtering, it can be assumed that it would remain also if a higher-order numerical scheme were applied.

In the majority of the chapter, only the Smagorinsky model, which actually provides no reconstruction for the subfilter scales, was applied. In Section 4.5, also the scale-similarity model and a mixed model, where a first-order reconstruction of SFS is provided, were applied. The main deficiencies noticed in the other parts of the chapter were also visible in these results. Thus, it seems difficult to compensate for the effect of explicit filtering of the convection term performed with a smooth filter via improved SGS or SFS modelling.

We also studied the use of different filter functions, and the commutative filters produced slightly better results than the trapezoidal and Simpson filters. It was concluded that the shape of the filter in the low-frequency area and the damping of the small frequencies is the important feature of the explicit filter function. However, the negative effect of filtering remained also with the commutative filters.

By comparing the simulation results with and without filtering to simulations with no SGS model, we saw that when explicit filtering was applied, modelling had a rather small effect on the simulation results, and the main part of the increased total error was caused by explicit filtering itself. When the results with SGS modelling and filtering were compared to the simulation with filtering but no model, we also saw some improvement in the simulation results when the model length scale was increased. Thus, there was some beneficial interaction of filtering and modelling although the total simulation error still remained large.

In Section 4.4, explicit filtering was compared to the implicit filtering provided by the standard Smagorinsky model. When large explicit filter widths were applied, some similarities in the behaviour of the mean-velocity profile and the Reynolds stress components were noticed. The main difference was that, while the Smagorinsky model affects all frequencies in a similar manner, explicit filtering damps down the high frequencies more than the low ones.

Finally, we applied the approach of Carati et al. (2001) to explicit filtering, and noticed that filtering via the SFS model does not have negative effect on the total error. Gullbrand and Chow (2003) already noticed that the use of the SFS model is necessary, and also here better results were obtained when SSM was used as an SFS model. However, we noticed that when filtering was provided by the SFS and SGS models, the small scales were not damped as strongly as when the convection term was filtered, and thus the filtering provided by the applied models is not the same as explicit limiting of the high frequencies. The use of mixed models improved the prediction of the spectra compared to using Smagorinsky models or SSM alone. If one considers the total simulation error and the computing time, this latter approach seems to be better than filtering of the non-linear convection term. However, the original reason for using explicit filtering was the large numerical error, and in the latter approach, it is not clear if this error was decreased.

In this chapter, only the total error in LES was studied, and thus we cannot state what the role of numerical error was in the present results. In the next chapter, the channel flow test case is studied a posteriori and both numerical and modelling error are evaluated. In addition, their role in the simulations with explicit filtering is studied.

Chapter 5

A Posteriori Tests on Numerical and Modelling Error in LES

*The results of Section 5.1 were published in Brandt (2007), the results of Section 5.2 in Brandt (2006*e*), and the results of Section 5.3 in Brandt (2006*c*).*

In this chapter, the numerical and modelling error in actual LES of the channel flow at $\mathrm{Re}_\tau = 395$ are separated from the total error. The aim is to explain the behaviour of the total error in LES via the error components. Different approaches are applied to a posteriori testing, and in addition to the clarification of the roles of the error components, the aim is to describe the differences between the approaches. In Section 5.1, the error components are studied using so-called implicit filtering, and we focus on cases with no explicit filtering. In Section 5.2, an approach using the Richardson extrapolation is studied. Finally, in Section 5.3, an approach using explicit filtering is applied in a posteriori testing, and the error components are compared to the effect of filtering.

In this chapter, the study is performed with the standard Smagorinsky model because two of the approaches applied to a posteriori testing are developed mainly for this model. In addition, in the previous chapter we saw that applying DSM, SSM or MM did not improve the results with explicit filtering.

5.1 A Posteriori Tests Using Implicit Filtering

In this section, we study LES of the channel flow using the standard Smagorinsky model and no explicit filtering. The aim is to evaluate a posteriori the numerical and modelling error in this case and to clarify the effect of the model parameters of the standard Smagorinsky model and the grid resolution on the error components.

5.1.1 Grid-independent LES Using Implicit Filtering

As suggested by Vreman et al. (1996), the numerical error involved in LES is defined here as the difference between the so-called grid-independent or fine-grid LES and the LES results, and modelling error as the difference between DNS and the grid-independent LES:

$$\begin{aligned} \varepsilon_{\text{numerical error}} &= \tilde{u} - \tilde{u}_{\text{grid-indep. LES}} \\ \varepsilon_{\text{modelling error}} &= \tilde{u}_{\text{grid-indep. LES}} - u_{\text{DNS}}, \end{aligned} \tag{5.1}$$

where $\tilde{u}$ refers to an LES solution and u to a DNS solution. The total error is the sum of these two: $\varepsilon_{\text{tot}} = \tilde{u} - u_{\text{DNS}}$. Here, the error is averaged over time and homogeneous flow directions. Since in the Smagorinsky model the built-in filter involved is not explicitly defined, the DNS solution instead of filtered DNS is applied in the definition of the modelling error. This choice was applied by Meyers et al. (2003).

The grid-independent LES means a solution of the LES equations where the grid resolution is increased to a level where the effect of numerical error is negligible while the effect of the model is preserved. When the effect of the model is kept constant as the grid is refined, the solution does not approach DNS as normally in LES. The effect of the model can be preserved either by applying an explicit low-pass filter to remove the high-frequency components as done by Vreman et al. (1996) and Gullbrand (2002), or by fixing the parameter in the SGS model which controls the size of the smallest resolved flow scales as done by Geurts and Fröhlich (2002) and Meyers et al. (2003). It is not suggested that grid-independent LES would be a way to perform practical LES. It is only a tool for error analysis.

In this section, the approach of Geurts and Fröhlich (2002) to obtaining the grid-independent LES is applied. Here, explicit filtering is not considered, and the equations being solved are those of implicit LES (Eq. 2.7). The approach is based on implicit filtering, which means that the smoothing provided by the SGS model is interpreted as filtering. For the standard Smagorinsky model, the grid-independent LES is approached by keeping the product of the model coefficient and model length scale $C_S\Delta_S$ in Equation (2.16) constant as the grid is refined. This relies on the interpretation of the LES equations as a set of differential equations with one externally defined parameter $C_S\Delta_S$. Traditionally, this parameter is fixed to grid resolution. When the Smagorinsky model is applied, the grid-independent solution has also been referred to as the grid-independent solution for the "Smagorinsky fluid", which means the smooth grid-independent solution of the LES equations and the Smagorinsky model (Muschinski 1996, Geurts and Fröhlich 2002).

Geurts and Fröhlich (2002) applied parameters called the SGS resolution and SGS activity parameter to describe the different combinations of the model length scale or width of the built-in filter and the grid resolution. The SGS resolution, r, is

defined as the ratio of the model length scale to the grid spacing $r = \Delta_S/\Delta$. When r is large, the numerical error has only a small effect on the solution and the solution approaches the grid-independent case. The SGS activity parameter, s, describes the amount of modelling in LES compared to DNS. It is defined as the ratio of the turbulent dissipation to the total dissipation as

$$s = \frac{\langle \epsilon_t \rangle}{\langle \epsilon_t \rangle + \langle \epsilon_\mu \rangle}, \tag{5.2}$$

where the brackets refer to average over homogeneous directions and time and the turbulent dissipation and the molecular dissipation are defined as

$$\epsilon_t = \tau_{ij}\frac{\partial \tilde{u}_i}{\partial x_j} = \mu_T 2\tilde{S}_{ij}\frac{\partial \tilde{u}_i}{\partial x_j} \quad , \quad \epsilon_\mu = \frac{1}{\mathrm{Re}_\tau}\tilde{S}_{ij}\frac{\partial \tilde{u}_i}{\partial x_j}, \tag{5.3}$$

respectively. In DNS, the value of s is zero, and the value of unity is approached in LES as the Reynolds number grows towards infinity. The value of s is related to the effective filter width, and it is almost independent of the grid resolution (Geurts and Fröhlich 2002). This was also noticed in the present simulations in the channel flow.

This approach using implicit filtering has been previously applied in a turbulent mixing layer (Geurts and Fröhlich 2002) and in homogeneous turbulence (Meyers et al. 2003). In this thesis, the fully developed turbulent channel flow is studied using the approach.

5.1.2 Applied Grid Resolutions

Four LES grids, which are labelled as grid 1, grid 2, grid 3 and grid 4 (see Table 5.1), are applied in this section. Grid 1 is a very coarse LES grid, and it is used only to study the effect of increasing grid resolution on the error components. Grid 2 has nearly the same resolution as the LES grids studied in the previous sections, and it is the base test case of this section. Grids 3 and 4 are applied to approach the grid-independent situation. The numerical error involved in DNS performed on grid 4 was studied in Section 2.4.2. Since using the SGS model further smooths the resolved flow field and thus decreases the numerical error, this resolution was considered as an adequate approximation for grid-independent LES. The DNS data applied in this section are that of Moser et al. (1999).

5.1.3 Effect of Varying Grid Resolution on Numerical and Modelling Error

In this section, we study LES results and the involved numerical and modelling error from the two coarsest grid resolutions – grid 1 and grid 2. Here, the subgrid-scale resolution is fixed to value 1, i.e. the model length scale Δ_S is set equal to

Table 5.1: Domain size and resolution of the applied LES grids. (x=streamwise, z=spanwise, y=wall-normal direction).

	grid 1			grid 2		
	x	z	y	x	z	y
extent of the domain / channel height	3.0	1.6	1.0	3.0	1.6	1.0
number of grid points	36	36	40	54	54	60
resolution in wall units (Δ^+)	70	37	3,...,41	44	23	2,...,27
	grid 3			grid 4		
extent of the domain / channel height	3.0	1.6	1.0	3.0	1.6	1.0
number of grid points	108	108	120	180	180	180
resolution in wall units (Δ^+)	22	12	1,...,14	13	7	0.7,...,9

wall units: $x^+ = \mathrm{Re}_\tau x$, where x is scaled by the channel half-height.

the grid spacing Δ (Eq. 2.17). The SGS activity parameter from the two cases is plotted in Figure 5.1. As the grid resolution is increased, the model length scale decreases, and also the SGS activity decreases.

The mean-velocity profiles from grid 1 and grid 2 cases are plotted in Figure 5.2. As the resolution is increased, the non-dimensional mean bulk velocity becomes less overpredicted and the prediction of the thickness of the viscous sublayer improves. If the grid resolution is increased further with $r = 1$, also the slope of the profile improves and the profile approaches the DNS result. The deviatoric diagonal streamwise Reynolds stress is plotted in Figure 5.3. As the grid resolution is increased, the total error in this quantity diminishes. The situation is similar for the spanwise and wall-normal Reynolds stresses. The SGS shear stress, τ_{12}, for the two cases is plotted in Figure 5.4. Since SGS resolution $r = \Delta_S/\Delta$ remains constant, the increase in grid resolution decreases the contribution of the SGS model.

Next, the model length scale is fixed and the grid resolution is increased for both grid 1 and grid 2 cases. The aim is to approach the grid-independent situation and to evaluate the numerical and modelling error involved with the two cases. The effect of increasing the grid resolution with a fixed model length scale on the SGS shear stress and energy spectra is studied in the next subsection, and here we concentrate only on the error components.

The mean-velocity profile from the grid 1 case and the corresponding results from the higher resolution cases with the model length scale of $\Delta_S = \Delta_{\text{grid 1}}$ are plotted in the upper part of Figure 5.5, where the difference between the DNS curve and the LES case with the highest resolution (grid 4) approaches the modelling error, and the difference between grid 4 and grid 1 approaches the numerical error. The

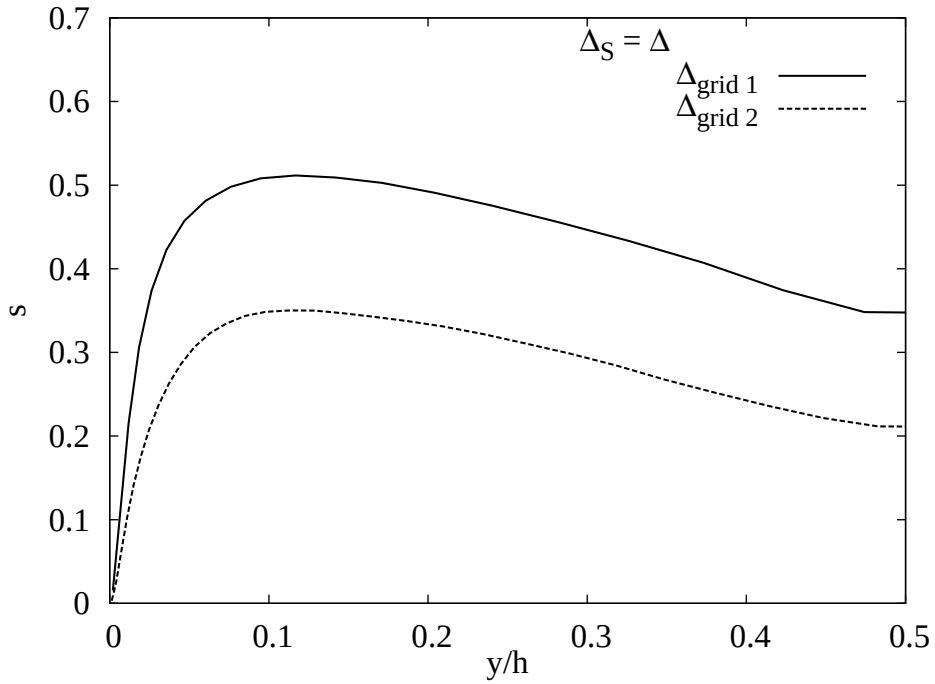

Figure 5.1: Subgrid-scale activity parameter. Grid resolution is varied and $r = \Delta_S/\Delta = 1$.

error components are plotted in the lower part of the figure. Also the numerical error from the simulation on grid 2 and $\Delta_S = \Delta_{\text{grid 1}}$ is included. We will use it in the next subsection. In the grid 1 case, the viscous sublayer is too long and thus, the slope of the profile is not correct. Neither one of the error components is constant in the logarithmic layer and thus, they both affect the error in the slope. Both the numerical and modelling error also affect the mean bulk velocity. The numerical and modelling error in the mean bulk velocity have different signs, and the modelling error is, by absolute value, actually larger than the total error. This type of counteraction of the error components was also noticed in the study of Geurts and Fröhlich (2002) in a turbulent mixing layer.

The mean-velocity profile from the grid 2 case together with the results from the higher-resolution cases with $\Delta_S = \Delta_{\text{grid 2}}$ are plotted in the upper part of Figure 5.6 and the numerical and modelling errors in the lower part of the figure. Here, the modelling error is clearly smaller than in the grid 1 case in Figure 5.5. However, the numerical error is not that much affected by the grid resolution, and it is almost the same here as it is in the grid 1 case in Figure 5.5. Because of the decreased modelling error, the total error changes its sign. Thus, the better prediction of the shape of the mean-velocity profile and the mean bulk velocity in the grid 2 case mainly results from the diminished effect of the SGS model.

The deviatoric streamwise Reynolds stress and the error components from the

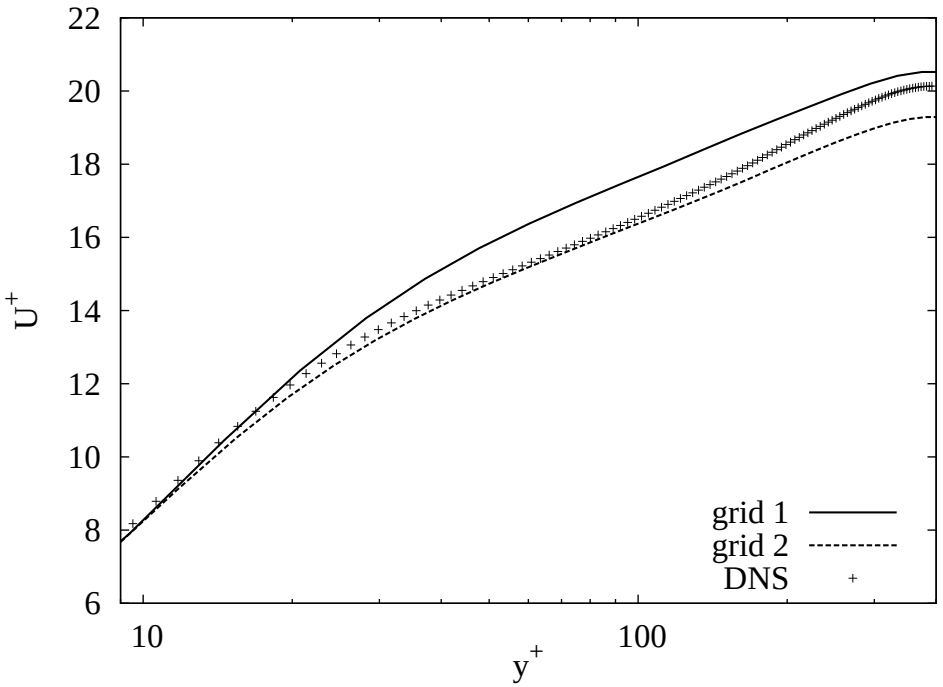

Figure 5.2: Mean-velocity profile. The grid resolution is varied and the SGS resolution is kept constant: $\Delta_S = \Delta$.

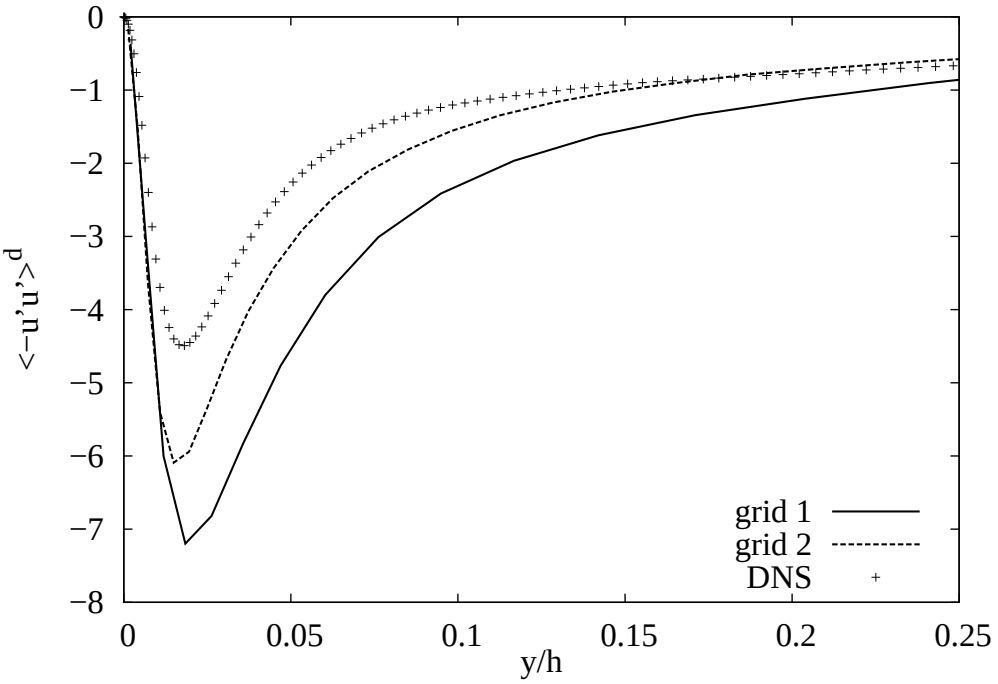

Figure 5.3: Deviatoric diagonal Reynolds stress. The grid resolution is varied and the SGS resolution is kept constant: $\Delta_S = \Delta$.

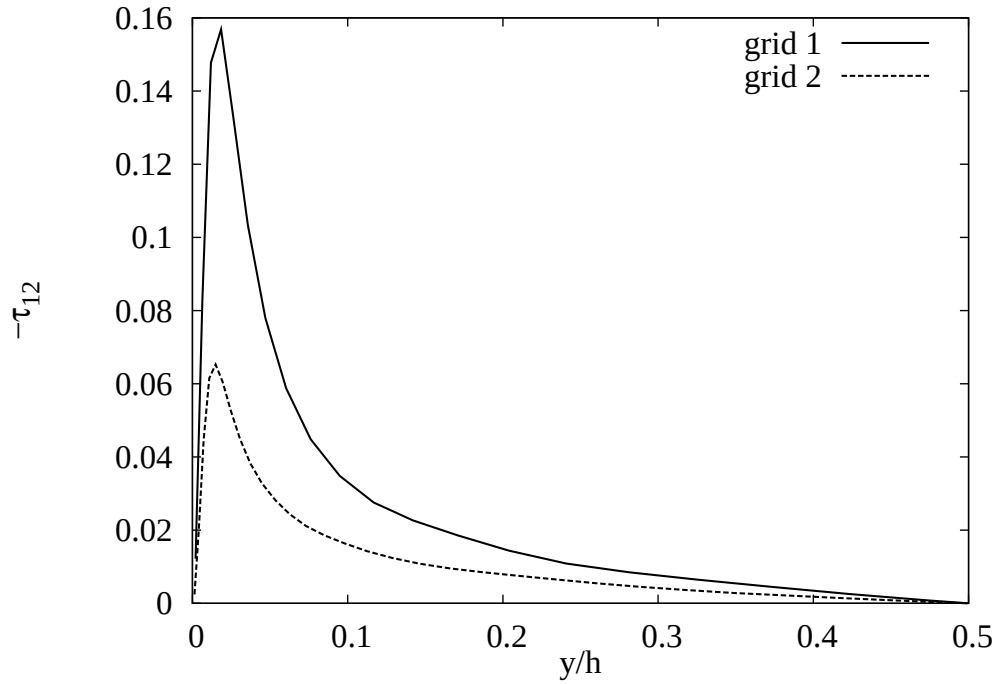

Figure 5.4: SGS shear stress. The grid resolution is varied and the SGS resolution is kept constant: $\Delta_S = \Delta$.

grid 1 case are plotted in Figure 5.7. Here, the modelling error dominates the numerical error in most parts of the channel. Numerical error is larger than the modelling error only in the near-wall region and in the middle of the channel. In the grid 1 case, the counteraction of the two error components occurs only in the area very close to the wall. In Figure 5.8, the deviatoric streamwise Reynolds stress is plotted from the grid 2 case with the model length scale set to $\Delta_S = \Delta_{\text{grid 2}}$. Here, the modelling error is clearly decreased compared to the grid 1 results in Figure 5.7. However, as seen by comparing Figures 5.8 and 5.7, the numerical error is only slightly affected when the grid resolution is varied and the SGS resolution is kept constant. The situation is similar for the other Reynolds stress components.

Based on the above findings, the improved results in Figures 5.2 and 5.3 that were obtained when the resolution was increased from grid 1 to grid 2 keeping the SGS resolution constant were mainly owing to the decreased modelling error. As the SGS resolution was kept constant, the model length scale and SGS activity decreased with increased grid resolution. Thus, the effect of the model was also decreased, which makes the decreasing of the modelling error natural. One would have assumed that increasing the resolution would also have decreased the numerical error. However, it had very little effect on the numerical error. This is probably owing to the SGS motions that became badly described resolved scales

as the grid resolution was increased. In addition, we saw that actually the numerical and modelling error were of the same size in the mean-velocity profile, and in the Reynolds stresses the modelling error even dominated the numerical one. Thus, the results of the a priori tests of Chapter 3 were too pessimistic regarding the role of the numerical error.

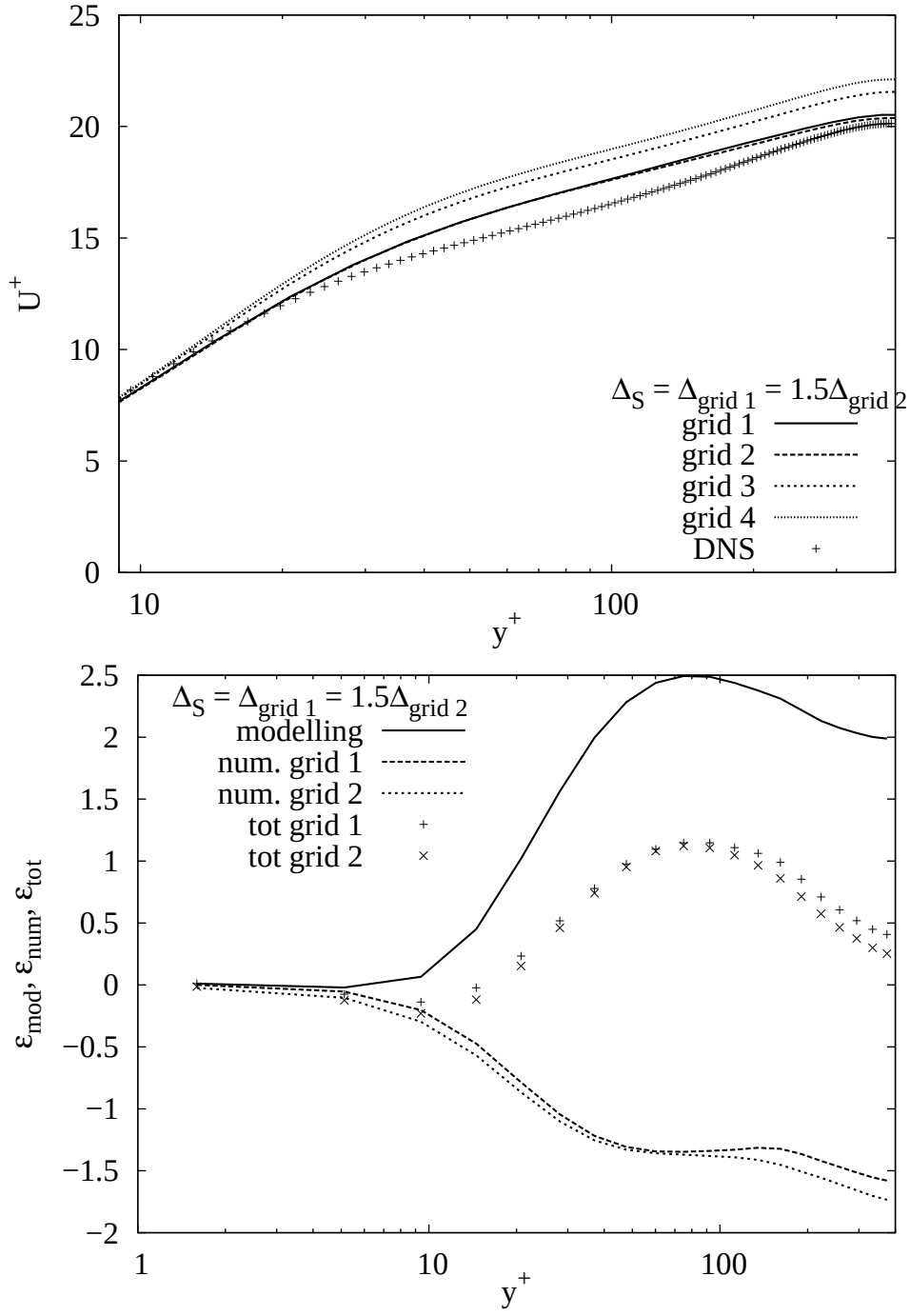

Figure 5.5: Upper: Mean-velocity profile in the wall coordinates. Model length scale is kept constant and the grid resolution increased. $\Delta_S = \Delta_{\text{grid 1}} = 1.5\Delta_{\text{grid 2}}$. **Lower:** Numerical and modelling errors involved in grid 1 and grid 2 cases.

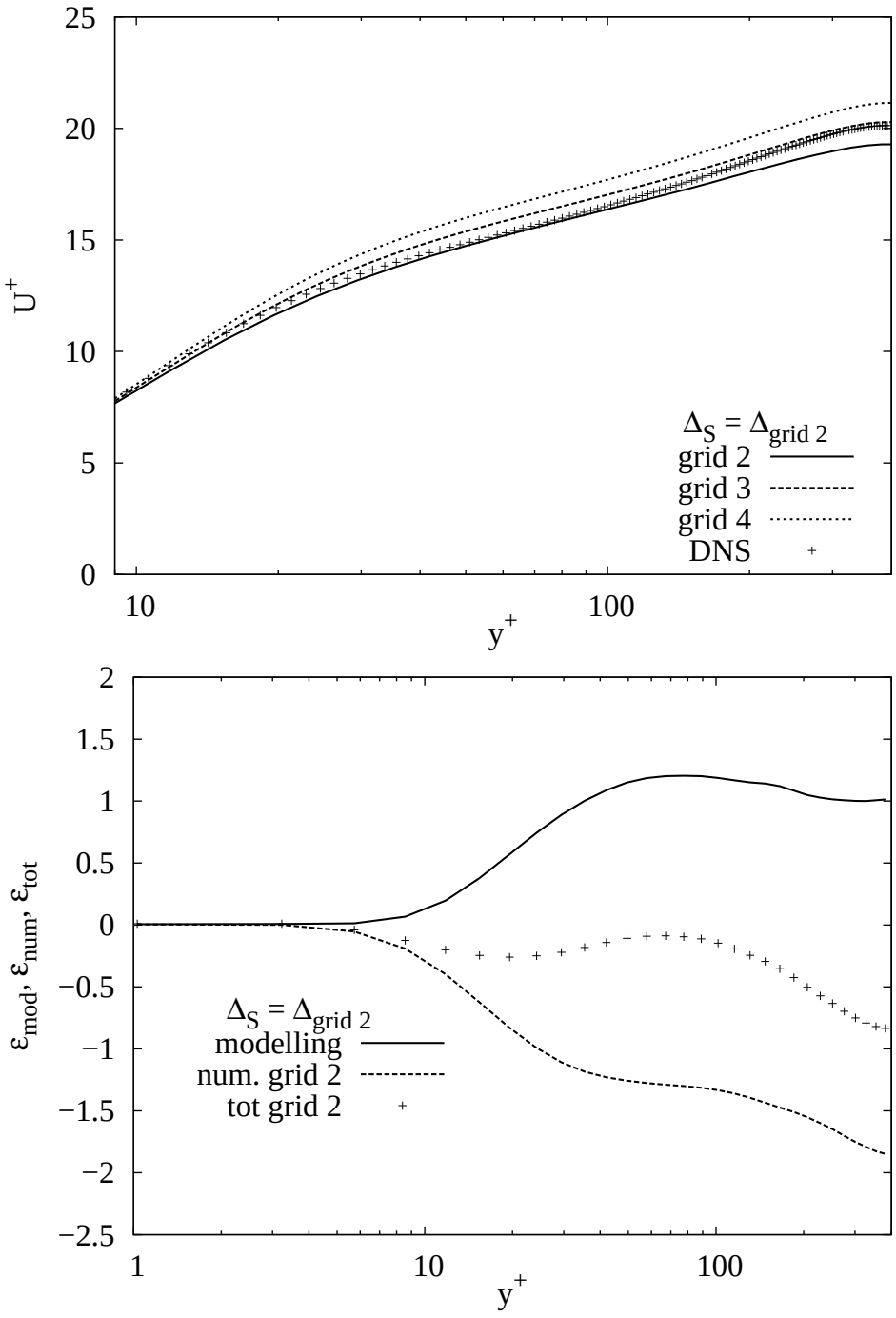

Figure 5.6: Upper: Mean-velocity profile in the wall coordinates. Model length scale is kept constant and the grid resolution increased. $\Delta_S = \Delta_{\text{grid 2}}$. **Lower:** Numerical and modelling errors involved in the grid 2 case.

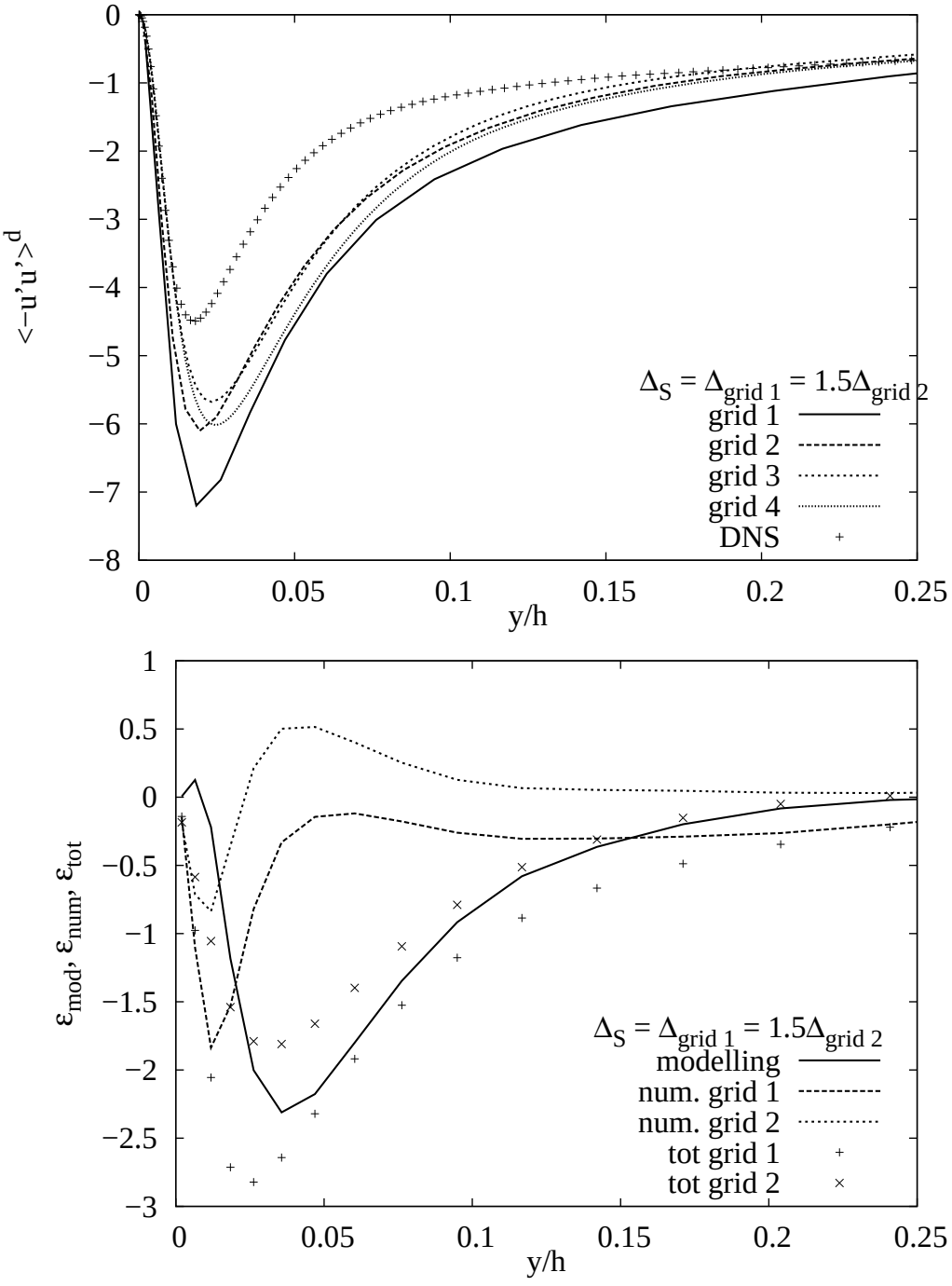

Figure 5.7: Upper: Deviatoric part of the streamwise Reynolds stress. Model length scale is kept constant and the grid resolution increased. $\Delta_S = \Delta_{\text{grid 1}} = 1.5\Delta_{\text{grid 2}}$. **Lower:** Numerical and modelling errors involved in the grid 1 and grid 2 cases.

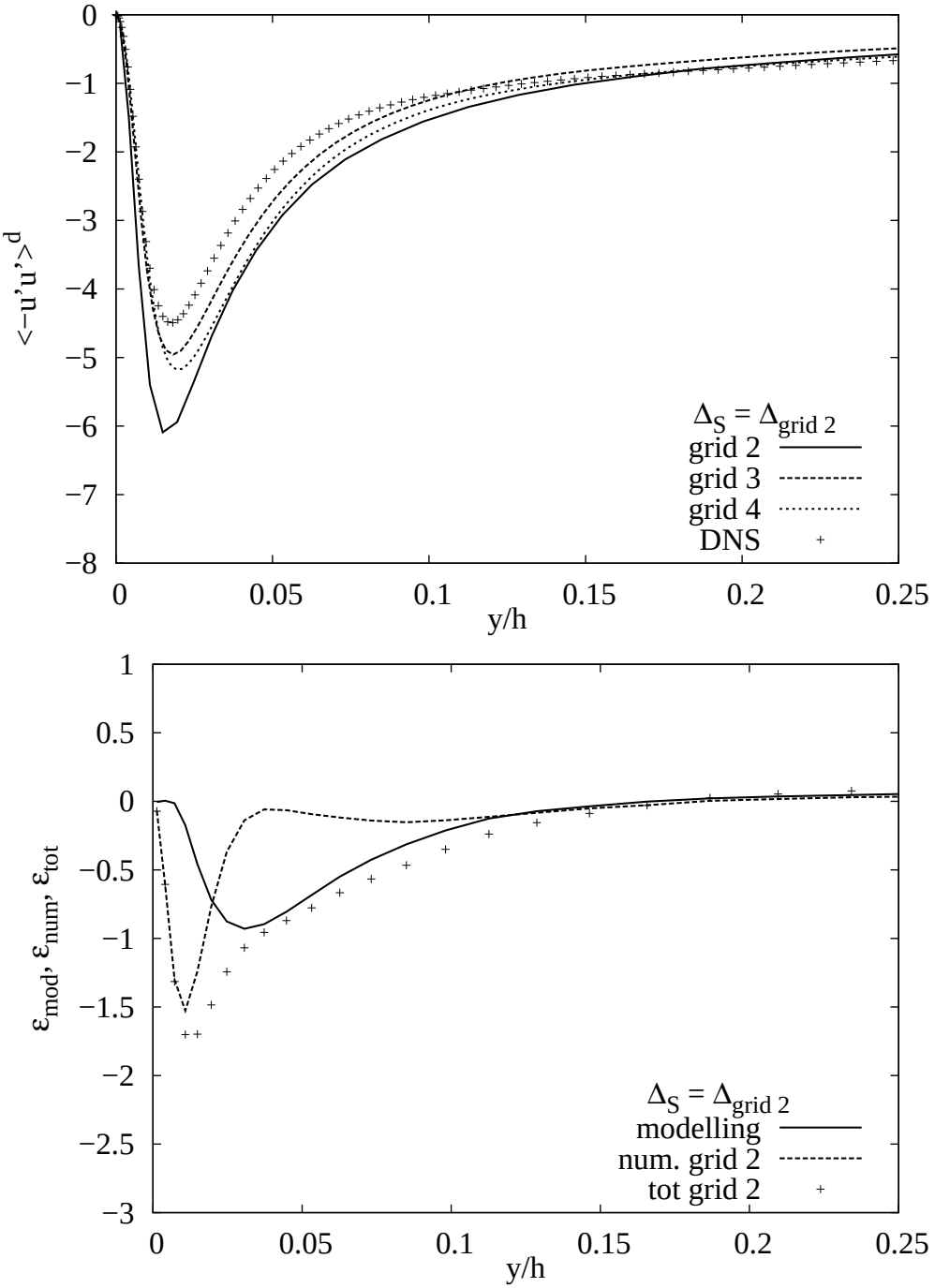

Figure 5.8: Upper: Deviatoric part of the streamwise Reynolds stress. Model length scale is kept constant and the grid resolution increased. $\Delta_S = \Delta_{\text{grid 2}}$. **Lower:** Numerical and modelling errors involved in the grid 2 case.

5.1.4 Effect of Varying Model Length Scale on Numerical and Modelling Error

In the previous chapter, we saw some examples of the effect of varying the model length scale or the width of the built-in filter of the standard Smagorinsky model. Here, we explain this behaviour by the error components.

The effect of the built-in filter width of the standard Smagorinsky model on the error components is studied using grid 2. The model length scales $\Delta_S = 0$ (no model), 0.5Δ, Δ and 1.5Δ are applied, and the corresponding SGS resolutions are $r = 0$, 0.5, 1 and 1.5, respectively. In the previous chapter, we also studied a case with the model length scale of 2Δ, but since the results with no explicit filtering were quite bad, the model length scale is not increased as much here. The SGS activity parameter s (Eq. 5.2) from these cases is depicted in Figure 5.9. The largest values ($s \approx 0.5$) are found in the case with the largest model length scale, and in the case with no model, s has the value of zero. The case with the largest model length scale $1.5\Delta_{\text{grid 2}}$ in grid 2 has the same SGS activity as the grid 1 case with $r = 1$ in Figure 5.1. These cases also have the same model length scales, and thus s seems to be rather independent of the grid resolution as has been previously noticed in the turbulent mixing layer (Geurts and Fröhlich 2002).

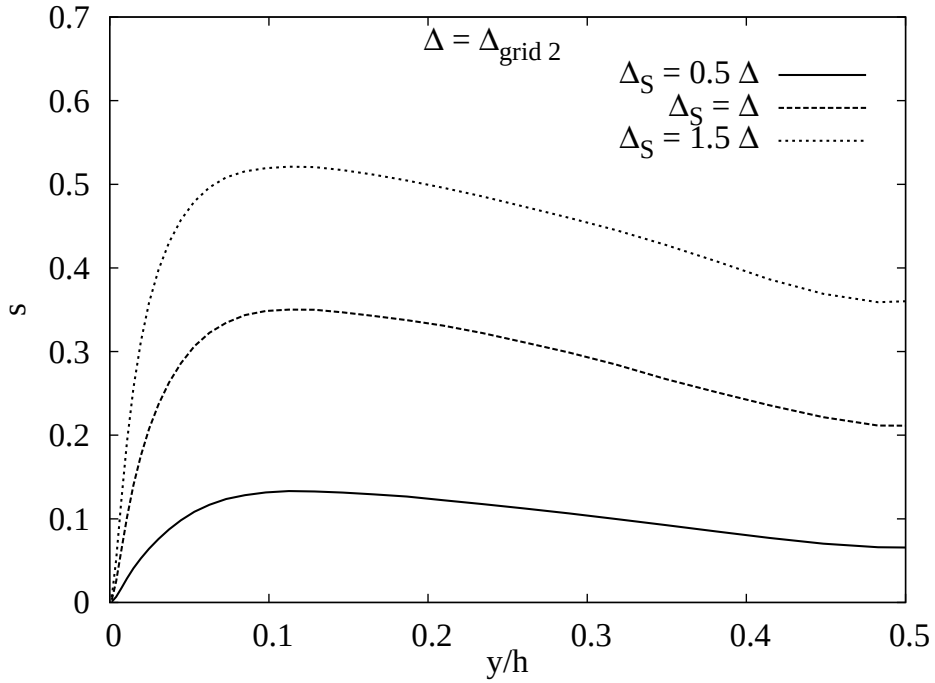

Figure 5.9: Subgrid-scale activity parameter. Grid resolution is constant (grid 2) and r is varied via the model length scale Δ_S.

The mean-velocity profiles from cases with different model length scales on grid 2

are plotted in Figure 5.10. If no SGS model is applied, i.e. $\Delta_S = 0$, the mean velocity is underpredicted. As the model length scale is increased, the situation first improves, but finally the mean velocity becomes overpredicted. In addition, as the model length scale is increased, the thickness of the viscous sublayer increases. In all cases, the slope of the velocity profile in the log-layer is too low, and applying the SGS model does not improve this. In Figure 5.11, we have the deviatoric diagonal streamwise Reynolds stress. The SGS model does not improve the prediction. When the model length scale is increased, the Reynolds stress becomes more overpredicted and the peak value starts to move towards the middle of the channel. The other Reynolds stress components show the same behaviour.

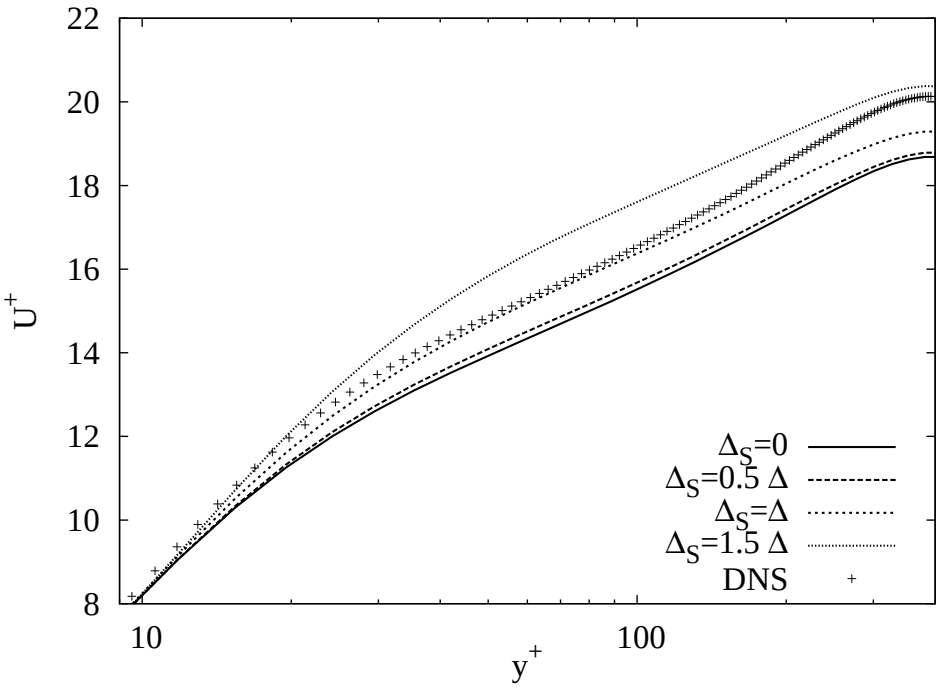

Figure 5.10: Mean-velocity profile in the wall coordinates. The grid resolution is constant (grid 2) and SGS resolution is varied via the model length scale Δ_S.

Next, the grid-independent situation corresponding to each Δ_S is approached by increasing the grid resolution for each case while keeping the model length scale constant. Before presenting the error components, the effect of increasing the grid resolution on the SGS shear stress and energy spectra is studied to see how well the different cases with different resolutions correspond to each other.

The SGS shear stresses for each case with different Δ_S is depicted in Figure 5.12 together with the plots from the corresponding higher-resolution cases. We notice that there is some variation in $\tau_{12} = -2\left(C_S\Delta_S\right)^2 |\tilde{S}|\, \tilde{S}_{12}$ (see Equation (2.16)) in each sub-figure. Since the product $C_S\Delta_S$ is a constant in each sub-figure, this

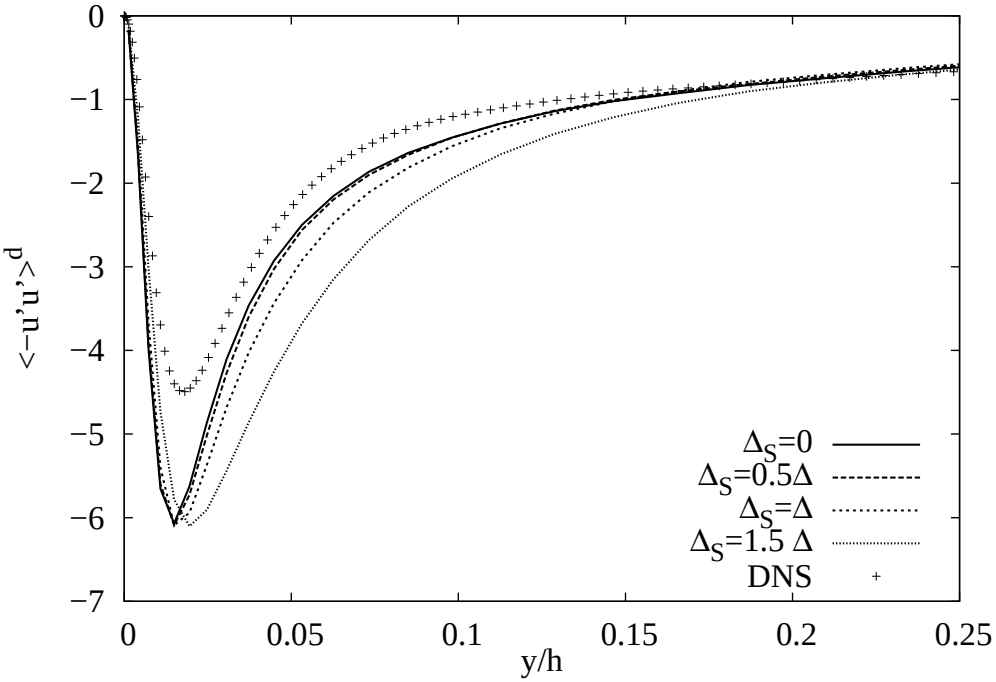

Figure 5.11: Deviatoric part of the streamwise Reynolds stress. The grid resolution is constant (grid 2) and SGS resolution is varied via the model length scale Δ_S.

variation is owing to changes in the strain rate tensor S_{ij}, and it appears because of the effect of numerics on the resolved velocity field. However, the variation between the subfigures, which is caused by varying the model length scale, is clearly larger than the effect of numerics. This verifies that the effect of the SGS model remains nearly constant when the grid resolution is varied independently of the model length scale. Thus, this approach to obtaining grid-independent LES is valid.

The one-dimensional energy spectra of the streamwise velocity component from the near-wall region are evaluated in the streamwise direction in Figure 5.13. The spectra from simulations with different grid resolutions and the same model length scale are quite close to each other but not exactly the same even at the low frequencies. Due to the resolution of the coarsest grid, the spectra from different grids are not evaluated exactly at the same points, which causes some of the variation. However, the variation with the grid resolution is weaker than the variation with the model length scale, which is seen by comparing the three figures. Thus, the shapes of the spectra are mainly determined by SGS modelling.

The corresponding spectra evaluated in the middle of the channel are depicted in Figure 5.14. Here we notice that increasing the grid resolution has a clear effect on the spectra. Smaller length scales are present in the simulations with the finest grid than with the coarser grids. Variation of the model length scale has only a

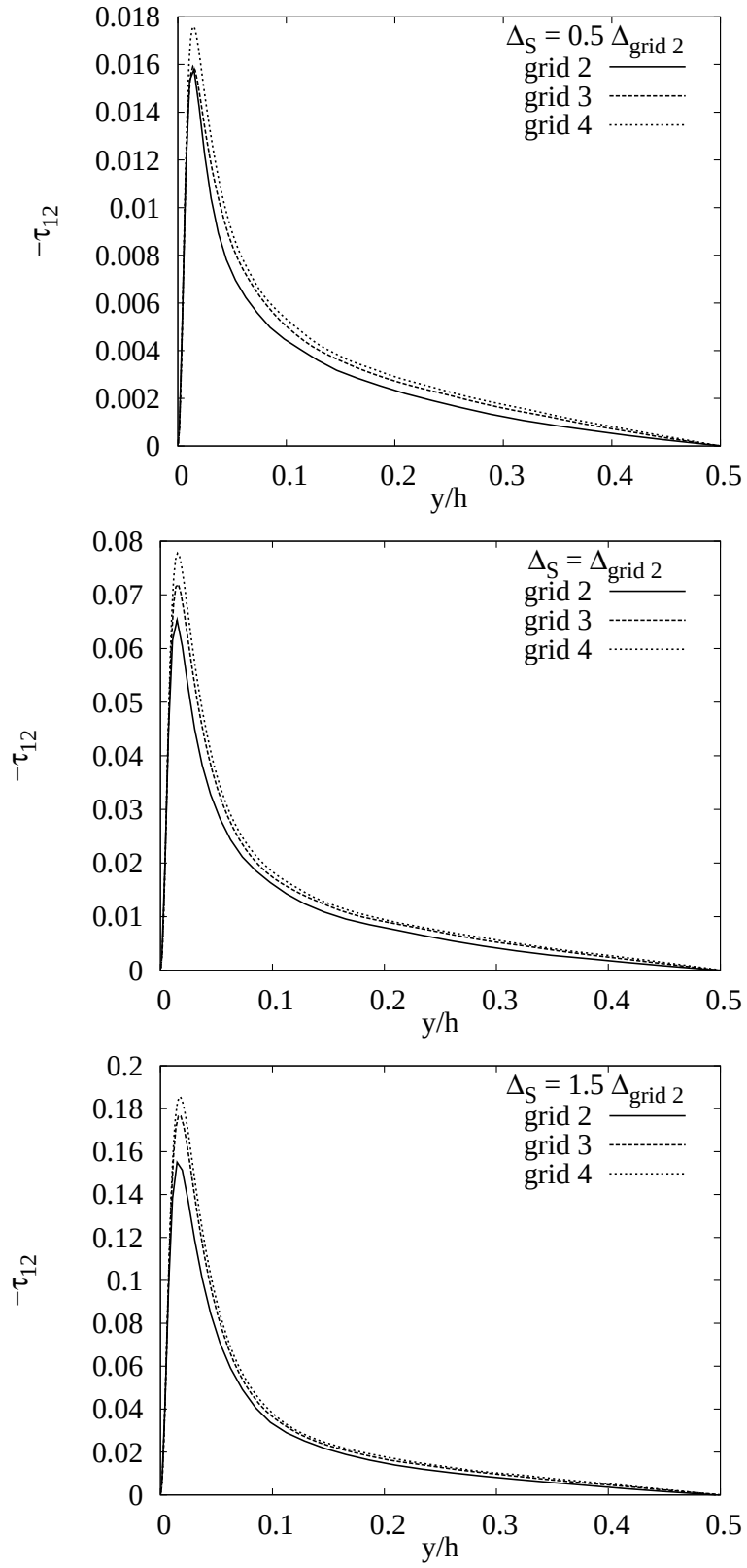

Figure 5.12: The SGS shear stress $-\tau_{12}$. The model length scale is varied between the sub-figures.

small effect on the spectra here. This suggests that, in the middle of the channel, the high frequencies are mainly damped down by the numerical error, whereas in the near-wall region modelling has a larger effect on the high frequencies. In the spanwise spectra (not shown here), neither the changing grid resolution nor the model length scale has a large effect on the spectra.

Next, the error components related to the mean-velocity profile and the Reynolds stress are evaluated. The mean-velocity profiles from cases with the model length scales equal to $\Delta_S = \Delta_{\text{grid 2}}$ and $\Delta_S = 1.5\Delta_{\text{grid 2}}$ have already been presented in Figures 5.6 and 5.5, respectively. Since the modelling error of the grid 2 case with the model length scale of $\Delta_S = 1.5\Delta_{\text{grid 2}}$ is the same as the modelling error of the grid 1 case with model length scale $\Delta_S = \Delta_{\text{grid 1}}$, the same discussion applies here for the differences between the modelling errors as in the previous subsection for the grid 1 and grid 2 cases with $\Delta_S = \Delta$. The modelling error decreases as the filter width is decreased. This error affects the shape of the profile and the value of the mean bulk velocity. The mean-velocity profile together with the error components from the case $\Delta_S = 0.5\Delta_{\text{grid 2}}$ are plotted in Figure 5.15, and we notice that the same trend continues.

The numerical error mainly affects the mean bulk velocity. It first remains almost constant when the model length scale is increased from $\Delta_{\text{grid 2}}$ to $1.5\Delta_{\text{grid 2}}$ (Figs. 5.6 and 5.5), and it seems to decrease slightly when the length scale $0.5\Delta_{\text{grid 2}}$ is applied (Fig. 5.15). This is not the behaviour one expects, since decreasing the model length scale should decrease the dissipation and there should thus be more badly described details in the resolved flow field. Since the grid-convergence rate seems to vary with the model length scale, this behaviour of the numerical error can arise from non-grid-converged mean bulk velocity. From the results of the grid-convergence study for the case with no model in Figure 2.17, we see that the numerical error in the mean bulk velocity on grid 4 in the case with no model was approximately 0.3. Since the error is probably of this size also when the low value of the model constant, $0.5\Delta_S$, is applied, the numerical error on grid 4 can explain the behaviour of the obtained numerical error on grid 2. It seems that varying the model length scale has only a small effect on the obtained numerical error.

The effect of the numerical error on the slope of the mean-velocity profile is the opposite to its effect on mean bulk velocity. The numerical error in the slope increases with decreasing model length scale as one would expect, and the incorrect slope in the $0.5\Delta_{\text{grid 2}}$ case is thus caused by numerics.

The deviatoric streamwise Reynolds stress obtained using model length scales $\Delta_S = \Delta_{\text{grid 2}}$ and $\Delta_S = 1.5\Delta_{\text{grid 2}}$ have already been depicted in Figures 5.8 and 5.7, respectively. The modelling error clearly increases as the model length scale is increased. In the near-wall region, the numerical error decreases as the model length scale is increased. However, around $y/h = 0.05$ it increases with

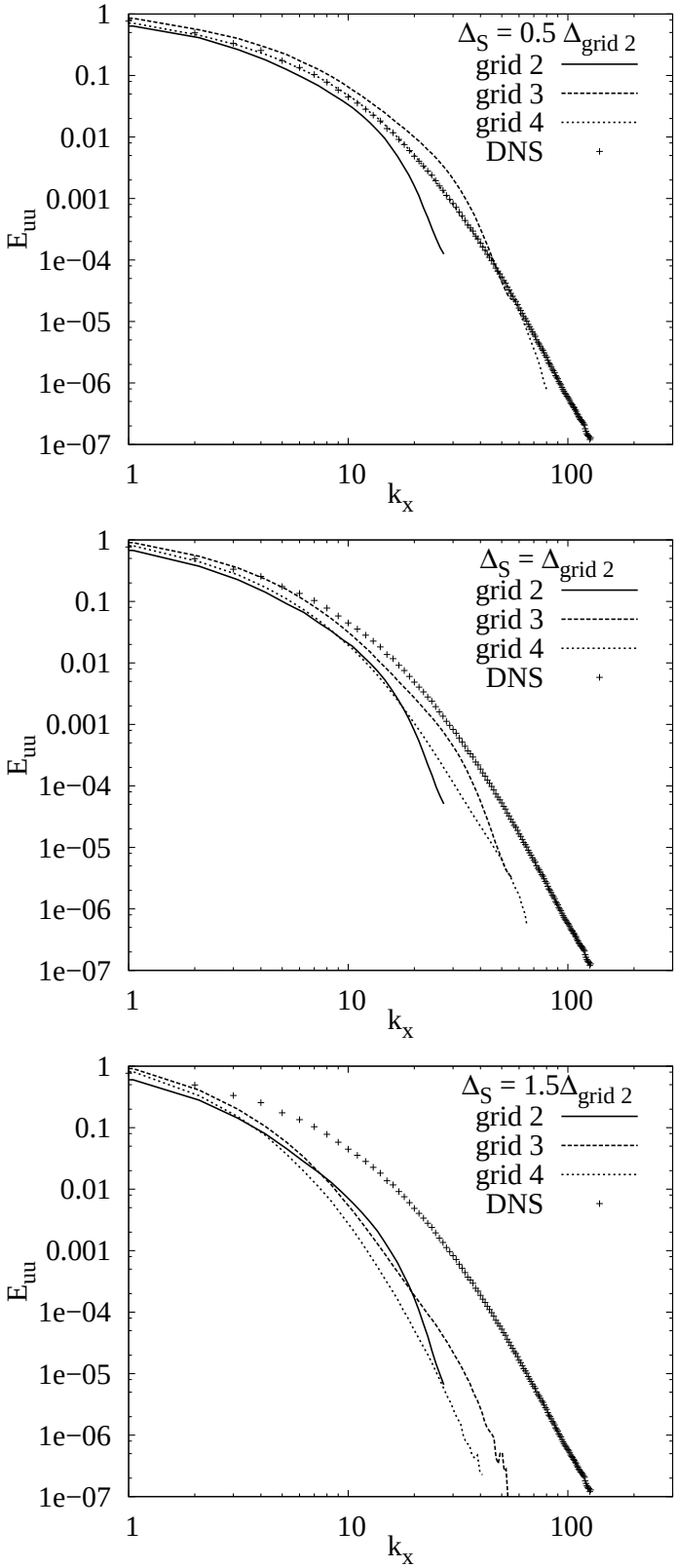

Figure 5.13: The streamwise one-dimensional spectra evaluated at $y^+ \approx 3$. The model length scale is varied between the sub-figures.

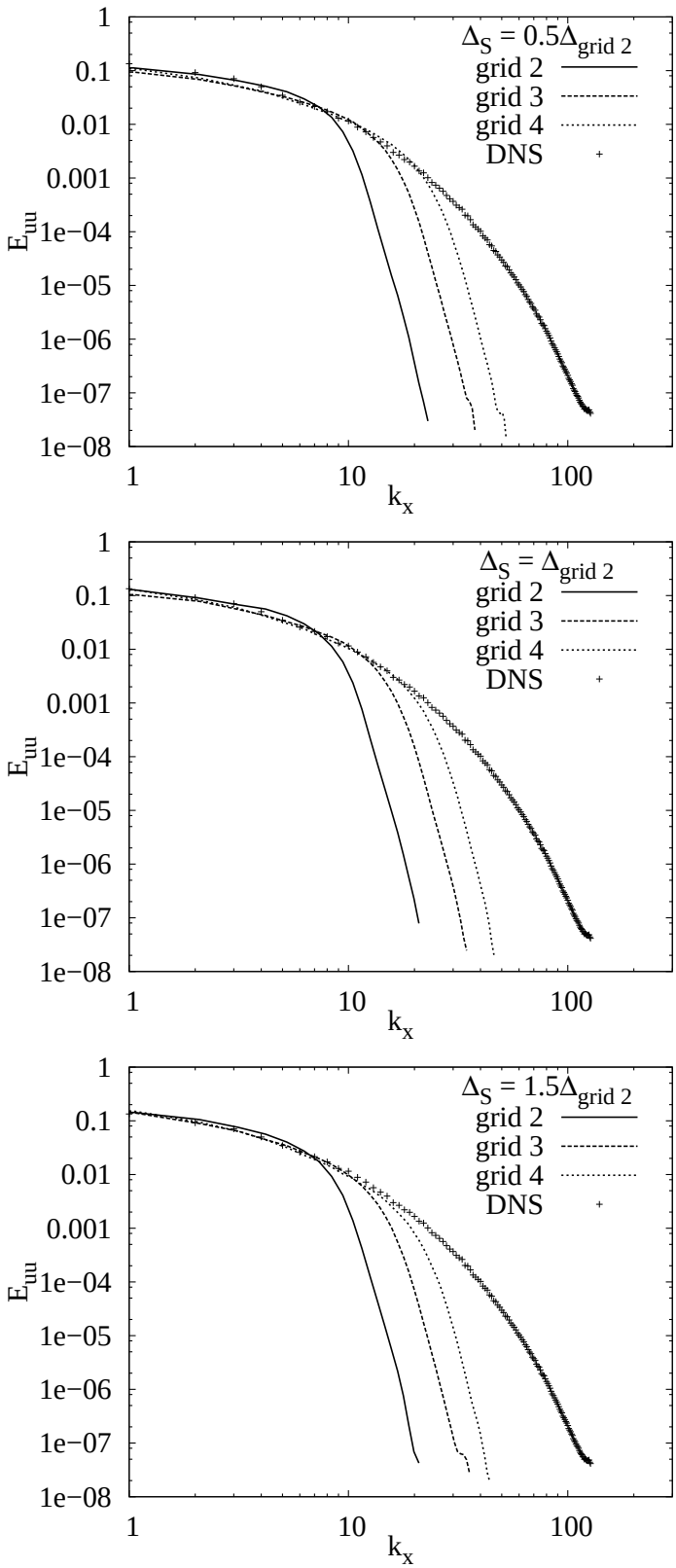

Figure 5.14: The streamwise one-dimensional spectra evaluated in the middle of the channel. The model length scale is varied between the sub-figures.

increasing model length scale. Again, this is not the behaviour one expects. The Reynolds stress and the error components from the case with the model length scale $\Delta_S = 0.5\Delta_{\text{grid 2}}$ are plotted in Figure 5.16, and there the overall trend continues, but the inconsistent behaviour of the numerical error is not visible. When the model length scale is decreased from $\Delta_S = \Delta_{\text{grid 2}}$ to $\Delta_S = 0.5\Delta_{\text{grid 2}}$, the numerical error increases everywhere in the channel.

In the mean bulk velocity, the grid-convergence became slower when the model length scale was decreased. In the Reynolds stress, the behaviour is the opposite: The grid-convergence becomes faster as the model length scale decreases. The grid-convergence study was presented for the case with no model in Figure 2.18, and there we saw that the numerical error at the resolution of grid 4 was at its maximum of 0.8 slightly below $y/h = 0.05$, and approximately 0.3 further away from the wall. Thus, the incomplete grid convergence can still change the conclusion about the numerical error on grid 2, especially in the $\Delta_S = 1.5\Delta$ case. The obtained inconsistency around $y/h \approx 0.05$ is probably caused by the incomplete grid convergence, and varying Δ_S has a larger effect on the modelling error than on the numerical error. The modelling error is clearly larger by absolute value, and the uncertainty on grid 4 is too small to affect the conclusion of this error component.

Based on the present results, one can say that the situation in Figure 5.11, where increasing the model length scale while keeping the grid resolution constant did not improve the prediction of the Reynolds stress, is caused by both numerical and modelling error. As the model length scale is increased, the numerical error is diminished, but at the same time the modelling error increases quite rapidly and the total error increases.

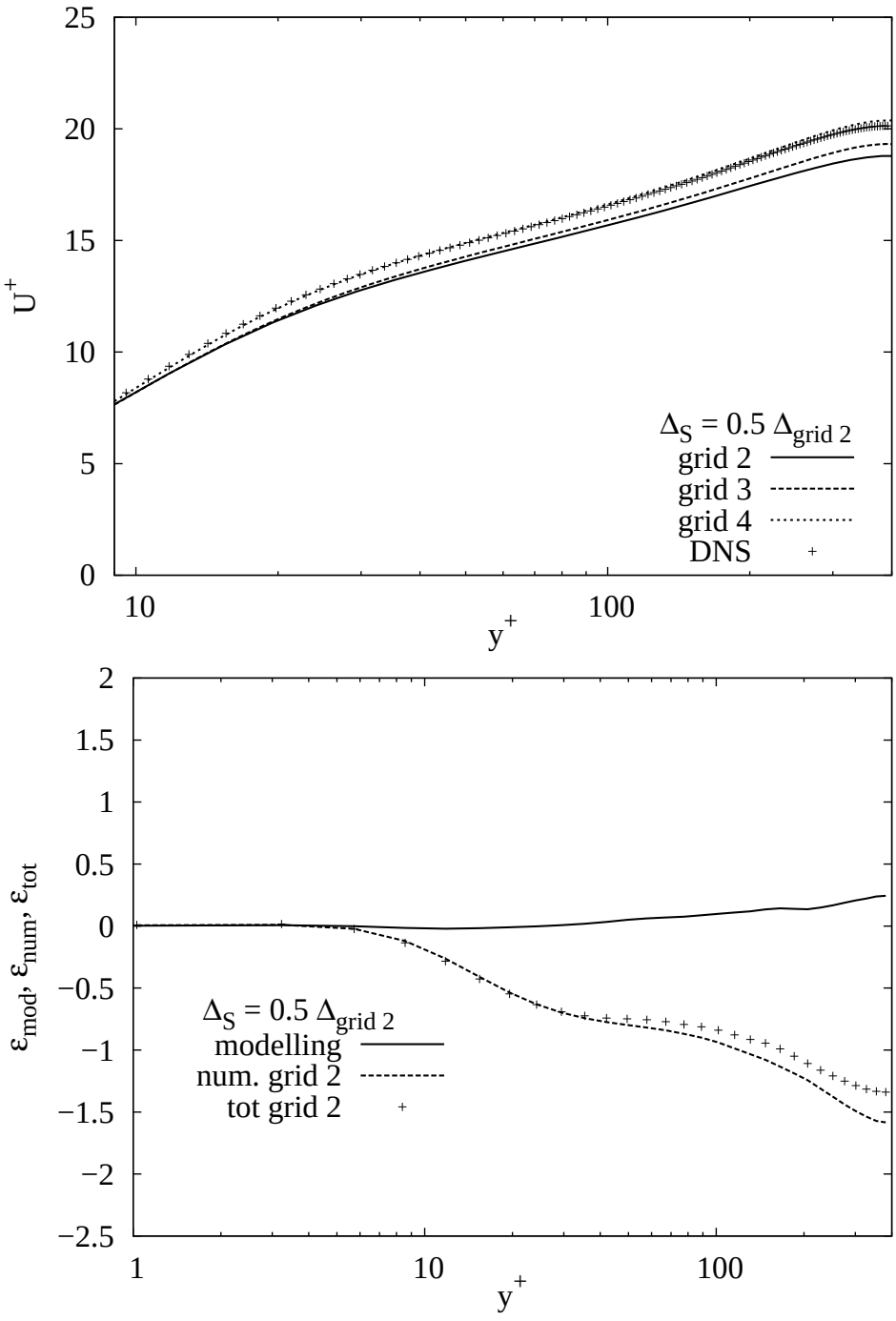

Figure 5.15: Upper: Mean-velocity profile in the wall coordinates. **Lower:** Numerical and modelling errors. The model length scale is constant $\Delta_S = 0.5\Delta_{\text{grid 2}}$.

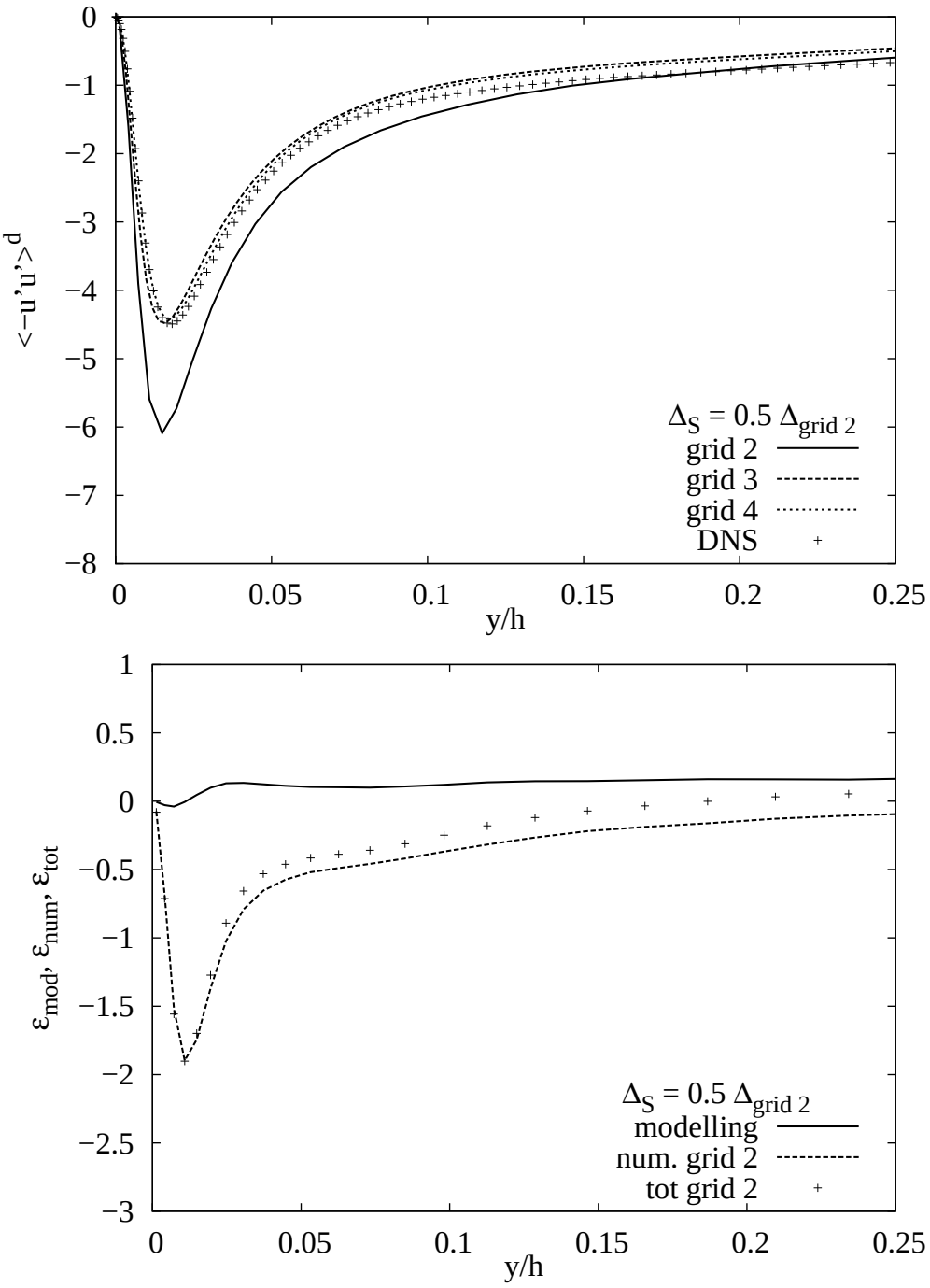

Figure 5.16: Upper: Deviatoric part of the streamwise Reynolds stress. **Lower:** Error components. The model length scale is constant $\Delta_S = 0.5\Delta_{\text{grid 2}}$.

5.1.5 Conclusions of Implicit a Posteriori Tests

In this section, the numerical and modelling errors in LES using the standard Smagorinsky model were studied applying the approach presented by Geurts and Fröhlich (2002). The aims of the section were to evaluate the error components, to clarify the reasoning behind the choice of the model constant $C_S\Delta_S$ of the standard Smagorinsky model in the channel flow by means of numerical and modelling error, and to describe the effect of the model length scale on the two error components.

In the a priori tests of Chapter 3, the numerical error in a simulation with no explicit filtering seemed to be larger than the effect of the SGS model. This behaviour was also noticed by, e.g. Ghosal (1996). However, based on the present a posteriori tests, the modelling error was at least of the same magnitude as the numerical error, and in the Reynolds stress components it even dominated the numerical error. The magnitudes of the error components were similar in the studies of Geurts and Fröhlich (2002) and Meyers et al. (2003) in a turbulent mixing layer and in homogeneous turbulence. This contradiction of the results of the a priori tests is probably caused by the effect of the SGS model on the flow field, which is not taken into account in the a priori testing.

We noticed that, when the grid resolution was increased from grid 1 to grid 2 while keeping the SGS resolution constant, the improvement of the results was almost entirely caused by the decreased modelling error, and increasing the grid resolution did not decrease the numerical error very efficiently. As the model length scale was varied in the grid 2 case, again the modelling error determined the greater part of the total error. Although increasing the model length scale decreased the numerical error, it increased the modelling error rapidly. Thus, controlling the numerical error via the built-in filter of the Smagorinsky model does not seem to be a very promising approach. The case with the smallest total error was a compromise between the two error components, and they were approximately of the same magnitude.

It has been previously noticed that the two error components can have different signs and they can partially cancel out each other (Geurts and Fröhlich 2002, Meyers et al. 2003). In the present study, this was noticed in the mean velocity in all the studied cases and in the Reynolds stress when a large value of the model coefficient was applied. This behaviour makes it difficult to draw conclusions from the total simulation error alone.

In the present study, the results on the finest grid were not totally grid-converged, and obtaining grid-converged results seems to require simulations with very large grids. When the model length scale was varied, there was some inconsistency in the behaviour of the numerical error, which was probably caused by the incomplete grid-convergence. The other option is that, since in this approach the

modelling error is not allowed to be affected by numerics, some of the effect of the SGS model is included in the numerical error. However, the uncertainty in grid-convergence can especially affect the obtained numerical error of the streamwise Reynolds stress on grid 2 because the numerical error on the finest grid with no model was about the same size as the obtained error on grid 2. Although this makes the quantitative comparison of the numerical errors of the different cases difficult, it does not change the overall conclusion. The modelling error is still clearly larger than the numerical one, and varying the model length scale or the grid resolution affects the model more than the numerical error.

If one considers the choice of the model length scale from the point of view of the two error components, the model length scale becomes dependent also on the chosen numerical method. Thus, from the point of view of this study, modelling and numerics are not two separate issues. If the numerical error is controlled via the implicit filtering of the model, the numerical scheme has to be taken into account when the model parameters are chosen.

Geurts and Fröhlich (2002) proposed two parameters, SGS activity, s, and SGS resolution, $r = \Delta_S/\Delta$, to quantify the different combinations of grid resolution and model length scale. The SGS activity turned out to be nearly independent of grid resolution and it characterised the effect of the SGS model. In the present test case, the modelling error was quite large already at values $s \approx 0.5$. Both SGS activity and SGS resolution characterised the numerical error. As r is increased, the numerical error diminishes, but as we saw, e.g. in Figures 5.16, 5.8 and 5.7, the grid-convergence rate depends on s.

5.2 Approach Using Richardson Extrapolation

In practical applications of LES, DNS data or fine-grid LES results are not usually available. To asses the quality of LES in these situations, Klein (2005) suggests a method based on the Richardson extrapolation. In the Richardson extrapolation, it is assumed that the grid resolution is fine enough for the numerical method to actually achieve its formal order. In this section, this approach is applied to the LES of the channel flow with no explicit filtering and we study the justification of the use of the method. In addition, we compare the obtained numerical and modelling error to the results of the previous sections.

5.2.1 Numerical and Modelling Error Using Richardson Extrapolation

Klein (2005) strongly objects to using the grid-independent LES in a posteriori testing because in LES the grid resolution is usually related to the effective filter width, and the main difference between Reynolds-averaged Navier–Stokes (RANS) calculations and LES is the coupling between the model and the filter width. Thus, Klein (2005) does not see it reasonable to interpret the model length scale of the standard Smagorinsky model as an external parameter that could be varied independently of the grid resolution. He proposes an alternative approach to a posteriori testing, where the difference between the exact solution, u, and a numerical LES solution, $\tilde{u}_\Delta$, obtained on a grid with resolution Δ, is approximated using the Taylor polynomial like in the Richardson extrapolation as

$$\tilde{u}_\Delta - u = c_n \Delta^n + c_m \Delta_S^m + \mathcal{O}\left(\Delta^{n+1}, \Delta_S^{m+1}\right) \tag{5.4}$$

where n is the order of the numerical method, m the order of modelling error, c_n and c_m are constants, Δ is the grid spacing and Δ_S the model length scale or filter width. For the numerical error, $\varepsilon_{\text{num}} = c_n \Delta^n$, the approach is equal to the Richardson extrapolation, and in Klein's (2005) approach, the same type of expansion is applied also to the effect of the SGS model, $\varepsilon_{\text{mod}} = c_m \Delta_S^m$. Since there are no cross terms, it is assumed that numerics and modelling are totally independent of each other.

Klein (2005) uses the approach with a second-order code, which has similar numerical methods as the code applied in this study and the standard Smagorinsky model. He assumes that both the obtained order of the numerical method in an actual simulation and the effect of the SGS model are of second order, i.e. $n = m = 2$. If the values for n and m are known, three simulations are required to evaluate the error components. If the model length scale is first varied by the factor α while keeping the grid resolution constant, and then the grid resolution

is varied by the factor β while keeping the model length scale equal to the grid spacing, the following equations can be written:

$$\begin{aligned} \tilde{u}_{\Delta,\Delta_S} - u &= c_n\Delta^n + c_m\Delta_S^m + \mathcal{O}\left(\Delta^{n+1}, \Delta_S^{m+1}\right) \\ \tilde{u}_{\Delta,\alpha\Delta_S} - u &= c_n\Delta^n + c_m\left(\alpha\Delta_S\right)^m + \mathcal{O}\left(\Delta^{n+1}, \Delta_S^{m+1}\right) \\ \tilde{u}_{\beta\Delta,\beta\Delta_S} - u &= c_n\left(\beta\Delta\right)^n + c_m\left(\beta\Delta_S\right)^m + \mathcal{O}\left(\Delta^{n+1}, \Delta_S^{m+1}\right) \end{aligned} \tag{5.5}$$

where u is the DNS solution, $\tilde{u}$ denotes an LES solution, Δ is the grid spacing of the original LES grid, Δ_S the model length scale of the original grid and subscripts of $\tilde{u}$ refer to simulations performed with different resolutions and different model length scales. Klein (2005) sets the model length scale equal to the grid spacing, $\Delta_S = \Delta$, and directly varies the effect of the SGS model and not the model length scale. However, in Equations (5.5), we allow the possibility of $\Delta_S \neq \Delta$ and thus Δ_S is visible in the equations. The difference is only in the power of α. If the high-order terms are assumed to be negligible as is usually done in the Richardson extrapolation, the error components of the studied case, $\varepsilon_{\text{num}} = c_n\Delta^n$ and $\varepsilon_{\text{mod}} = c_m\Delta_S^m$, can be solved from Equations (5.5).

Klein (2005) recommends decreasing the effect of the SGS model by a factor of two and reducing the grid resolution by a factor of two to approximate the error components and to report statistics from all three simulations in addition to the error components. In the present study, the approach is applied to the grid 2 case of Table 5.1 with the model length scale equal to the grid spacing. This is the same test case as applied in the study with implicit filtering in Section 5.1. To apply Equations (5.5), the model length scale is first varied by the factor of $\alpha = 0.5$ and then the grid resolution is decreased by the factor of $\beta = 1.5$, which corresponds to the grid 1 case of Table 5.1 with the model length scale equal to grid spacing. The grid resolution was not decreased by a factor of two because the obtained grid would have been too coarse for a reasonable LES.

The mean-velocity profiles from the present simulations are given in the upper part of Figure 5.17, and the obtained error components, $c_n\Delta^n$ and $c_m\Delta_S^m$, for the grid 2 case are depicted in the lower part of the figure. In addition, the true total error obtained as the difference of the grid 2 result from the DNS of Moser et al. (1999) is included. We notice that the sum of the modelling and numerical error is not even close to the true total error. This suggests that the resolution is not in the asymptotic range, and either one or both of the error components cannot be approximated with the first term of the Taylor series.

To study the effect of the grid resolution on the behaviour of the Richardson extrapolation, the study was repeated for grid 3 of Table 5.1 using grid 2 as the coarser grid, $\beta = 2$, and reducing the model length scale by 2, $\alpha = 0.5$. The mean-velocity profiles and the error components are depicted in Figure 5.18. On this finer grid, the prediction for the total error is somewhat better, but the difference from the true total error is still large. In addition, the estimates for

the total error do not behave in the same way as the true total errors when the grid resolution is varied. We notice that, somewhat surprisingly, the true total error increases when the grid is refined from grid 2 to grid 3. This can be caused by some interaction of the error components, but the error components predicted using the Taylor expansion do not explain this. The estimate for the modelling error diminishes as the grid is refined, which is consistent since the effect of the modelling is decreased. The estimate for the numerical error increases with the grid refinement. In principle, this could also be true. However, the sum of the two is not correct.

Klein (2005) applied the approach to the channel flow at the same Reynolds number as here and to a turbulent jet flow. There was some deviation from the true total error, but the results were not as bad as here. The resolution of the channel flow was finer than that of the present test case in the homogeneous directions but coarser in the wall-normal direction. Based on the results of this section, it seems that the total error obtained by the Richardson extrapolation does not necessarily behave in a similar manner as the true total error, and the success of the method can be very sensitive to the grid resolution. One possible explanation for this is that the simulation results are not in the asymptotic range. We will study this in the next subsection.

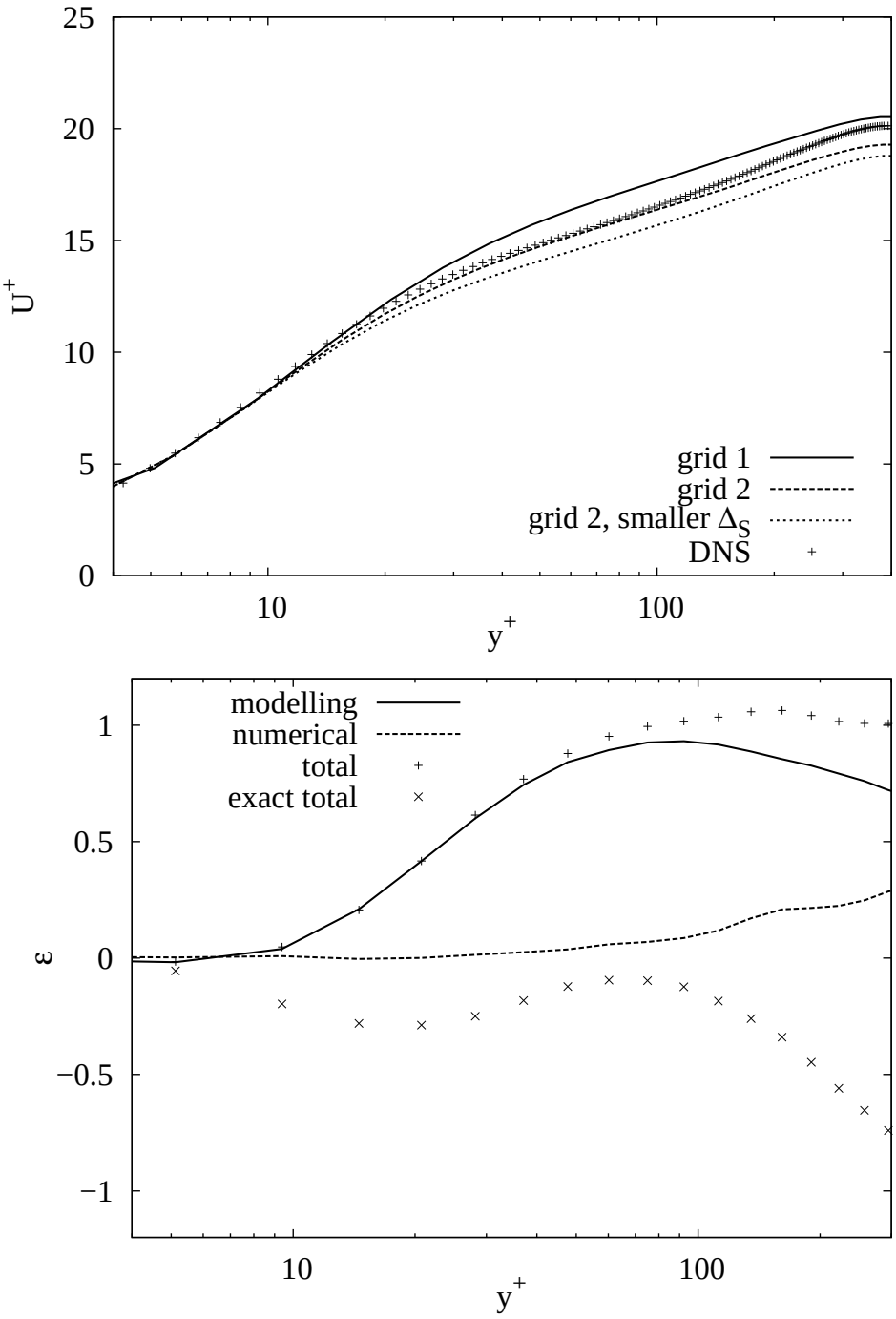

Figure 5.17: Evaluation of numerical and modelling error using Richardson extrapolation. Grid 2. **Upper:** Mean-velocity profiles. **Lower:** Obtained error components for the grid 2 case.

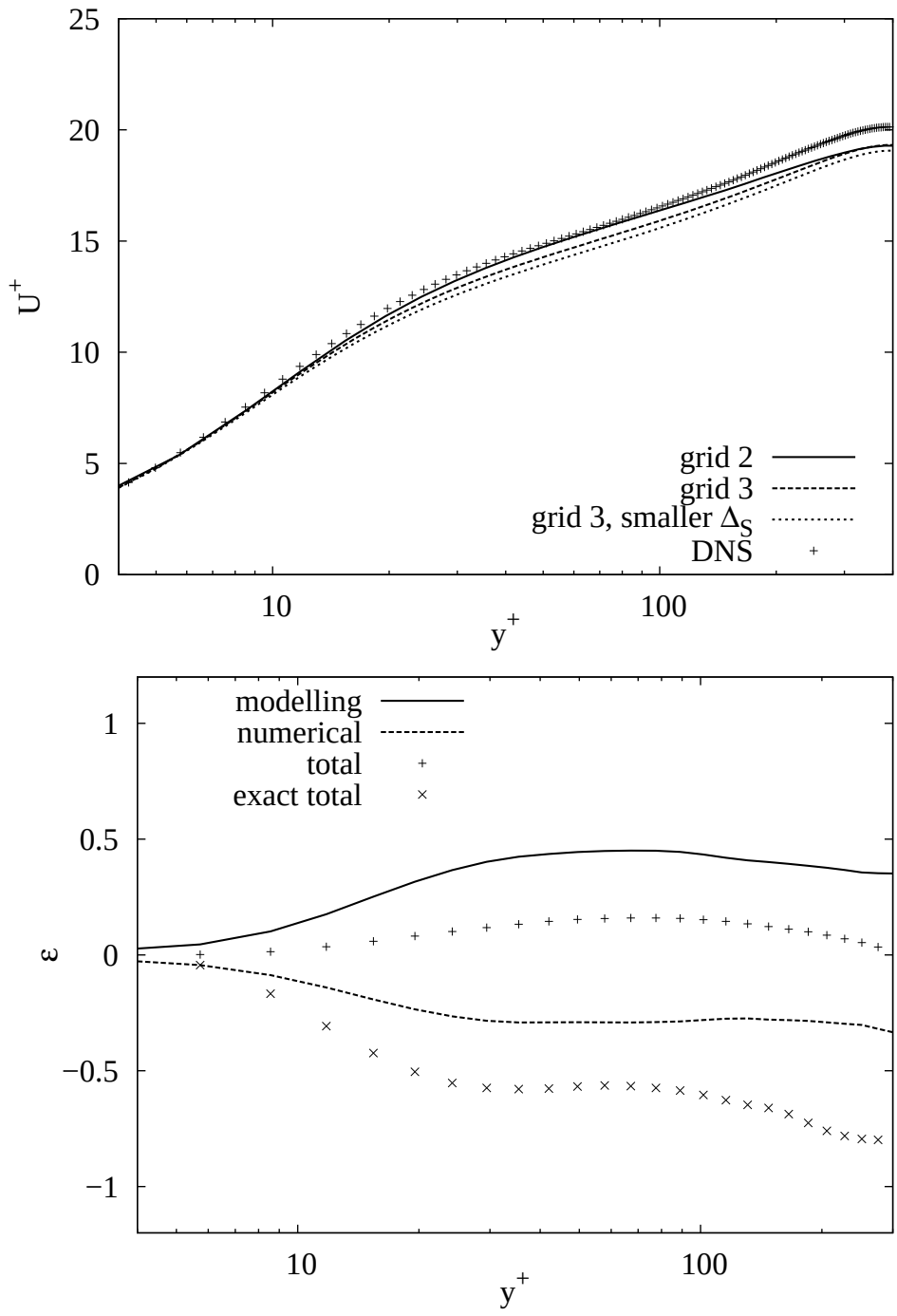

Figure 5.18: Evaluation of numerical and modelling error using Richardson extrapolation. Grid 3. **Upper:** Mean-velocity profiles. **Lower:** Obtained error components.

5.2.2 Order of Numerical and Modelling Error in Present LES

In the previous subsection, we assumed that both the numerical error involved in the simulations and the effect of modelling were in the asymptotic range, and that they are both of the second order, i.e. $n = m = 2$. In this section, we test the assumption.

The order of the modelling error, m, can be evaluated if three simulations are performed with the same grid resolution and by varying model length scale. These simulations were done on grids 2 and 3 with the model length scales of $\Delta_S = 0.5\Delta, \Delta, 2\Delta$. Using the Taylor expansion, the following equations can be written for the total error

$$\begin{aligned} \tilde{u}_{\Delta,0.5\Delta_S} - u &= c_n\Delta^n + c_m 0.5^m \Delta_S^m \\ \tilde{u}_{\Delta,\Delta_S} - u &= c_n\Delta^n + c_m \Delta_S^m \\ \tilde{u}_{\Delta,2\Delta_S} - u &= c_n\Delta^n + c_m 2^m \Delta_S^m \end{aligned} \tag{5.6}$$

where u again refers to the DNS solution and $\tilde{u}$ to the numerical LES solution. Both the order of the numerical error m and the constant c_m can be solved from these equations. The order of the modelling error for the mean-velocity profile is depicted for both grid resolutions in Figure 5.19. In the logarithmic region, the order of the error is close to the value $m = 2$, which was applied in the previous subsection. However, in the viscous sublayer, where the total error is almost zero, the modelling error is not in the asymptotic range, and m obtains even negative values. The area where the use of the Taylor expansion is possible is thicker for the resolution of grid 3. Since the order of the modelling error is quite close to the theoretical one in the logarithmic layer, the reason for the bad results for the total error obtained in the previous subsection has to be the numerical error.

The order of the numerical error can be evaluated in the same way as the order of the modelling error. It can be estimated using three simulations with the same absolute width of the model length scale. For this purpose, two simulations, grid 2b and grid 2c with grid resolutions of 1.5 and 1.5^2 times the resolution of grid 2 were performed. In these simulations, the model length scale was kept the same as in the grid 2 case. First, the model length scale was equal to the grid spacing of grid 2 and then it was increased to 1.5 times the grid spacing. This was done to see if the dissipation provided by the model had an effect on the obtained order of the numerical scheme. Using the three simulations results, the following equations can be written for the total error:

$$\begin{aligned} \tilde{u}_{\Delta,\Delta_S} - u &= c_n\Delta^n + c_m \Delta_S^m \\ \tilde{u}_{\Delta/1.5,\Delta_S} - u &= c_n \left(\Delta/1.5\right)^n + c_m \Delta_S^m \\ \tilde{u}_{\Delta/1.5^2,\Delta_S} - u &= c_n \left(\Delta/1.5^2\right)^n + c_m \Delta_S^m \end{aligned} \tag{5.7}$$

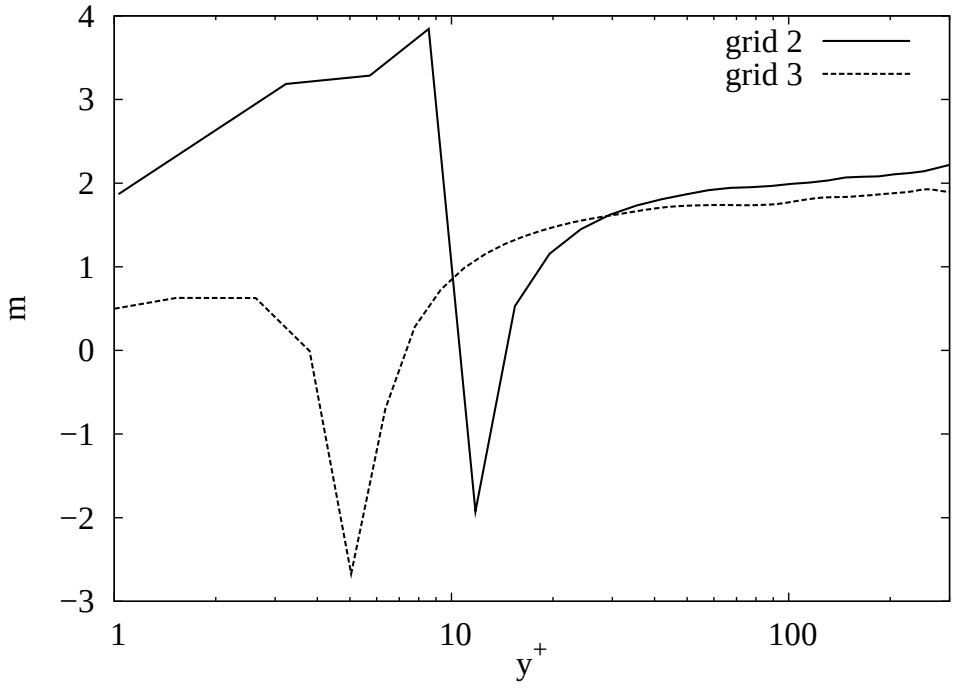

Figure 5.19: Order of SGS modelling by means of Richardson extrapolation.

Here Δ is the grid spacing of grid 2 and Δ_S is the model length scale that has the same absolute width in all three cases. The obtained order of numerical error, n, is plotted in Figure 5.20 for both cases. n has only negative values, which indicates that the applied resolutions are not in the asymptotic range, i.e. the method does not obtain its nominal order at this resolution, and thus the numerical error cannot be described by the first term of the Taylor expansion. The negative values are obtained for n because the difference between the two coarsest resolutions is smaller than the difference between the finer resolutions, and in the asymptotic range this should by the other way around. With the larger model length scale, the situation is somewhat better: the order of the numerical scheme remains constant through the logarithmic sublayer. However, it is still negative.

Since the numerical error cannot be described by the Richardson extrapolation, comparing Figures 5.17 and 5.18 to the results of the a posteriori tests of the previous section is not reasonable. However, since the modelling error can be described via the Taylor expansion in the logarithmic layer and we have the true total error, we can evaluate the numerical error as the difference between the true total error and the estimate for the modelling error.

The modelling, numerical and total errors obtained in the grid 2 cases with different model length scales are plotted in Figure 5.21, and the corresponding plots

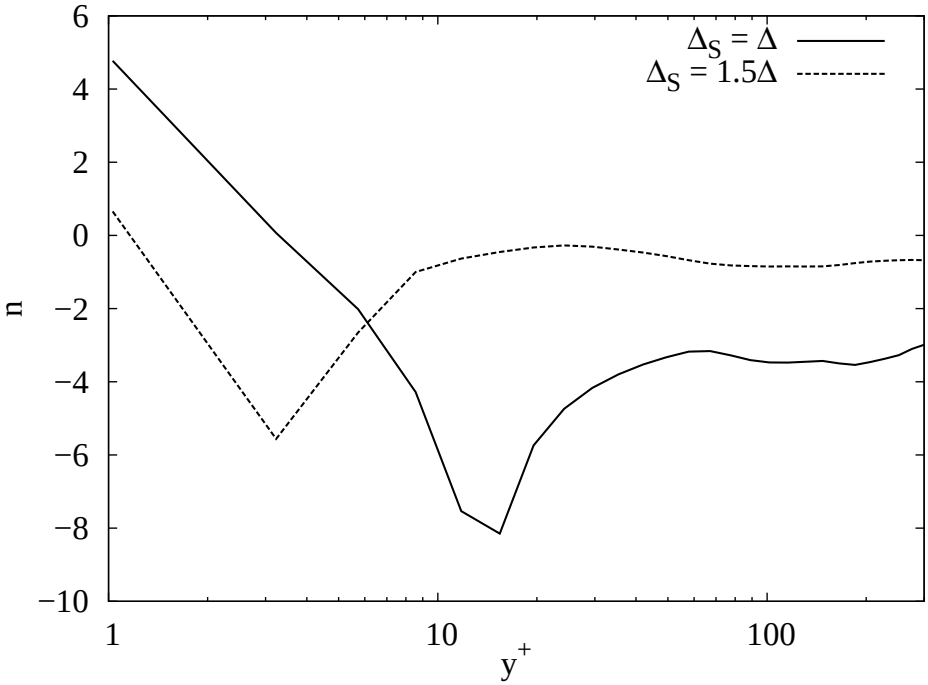

Figure 5.20: The order of the numerical error obtained using the Taylor expansion. Grid 2.

for the grid 3 cases are given in Figure 5.22. We can now compare the error components of the case $\Delta_S = \Delta$ to the ones of Figures 5.17 and 5.18 where constant values were applied for n and m. We notice that, for both grid resolutions, the obtained modelling error is nearly the same as the one obtained with constant m. This supports the conclusion that for the modelling error, the use of the Richardson extrapolation is reasonable at least in the logarithmic layer. The numerical error obtained here as the difference between the true total error and the modelling error is by absolute value larger than the one obtained with the Richardson extrapolation. By the applied definition, the numerical error is not dependent on the effect of modelling. We see this for grid 2 and grid 3 cases in Figures 5.21 and 5.22, respectively. Here, the change of the total error with the model length scale is caused entirely by the modelling error.

When the study of the applicability of Klein's (2005) approach was repeated for the diagonal Reynolds stress components, the results were more pessimistic than for the mean-velocity profile. Neither numerical nor modelling error could be evaluated using the Richardson extrapolation. The obtained order for the effect of modelling varied strongly as a function of the wall distance and it obtained both large positive and negative values. Thus, it seems that while the Richardson extrapolation produces reasonable results for the modelling error of the mean-velocity profile, the modelling error in the Reynolds stresses at the

applied resolutions cannot be explained using only the first term of the Taylor expansion of the truncation error. Celik, Cehreli and Yavuz (2005) proposed an approach for error assessment, which is based on approximating the resolved turbulent kinetic energy with the Richardson extrapolation. The problems in the applicability of the Richardson extrapolation are also visible in the turbulent kinetic energy, and this makes also the applicability of Celik, Cehreli and Yavuz's (2005) approach questionable.

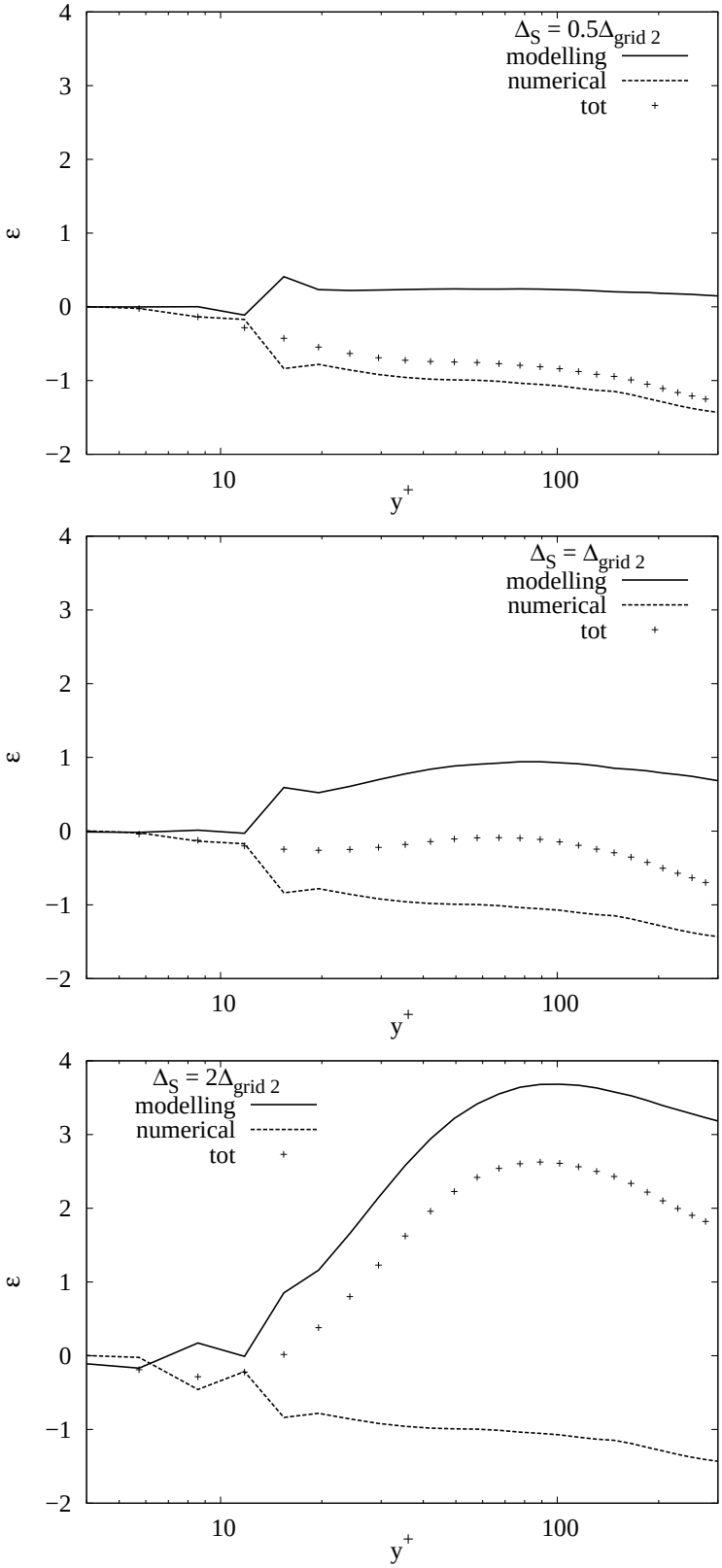

Figure 5.21: Modelling, numerical and total error of mean velocity in grid 2 cases with different model length scales.

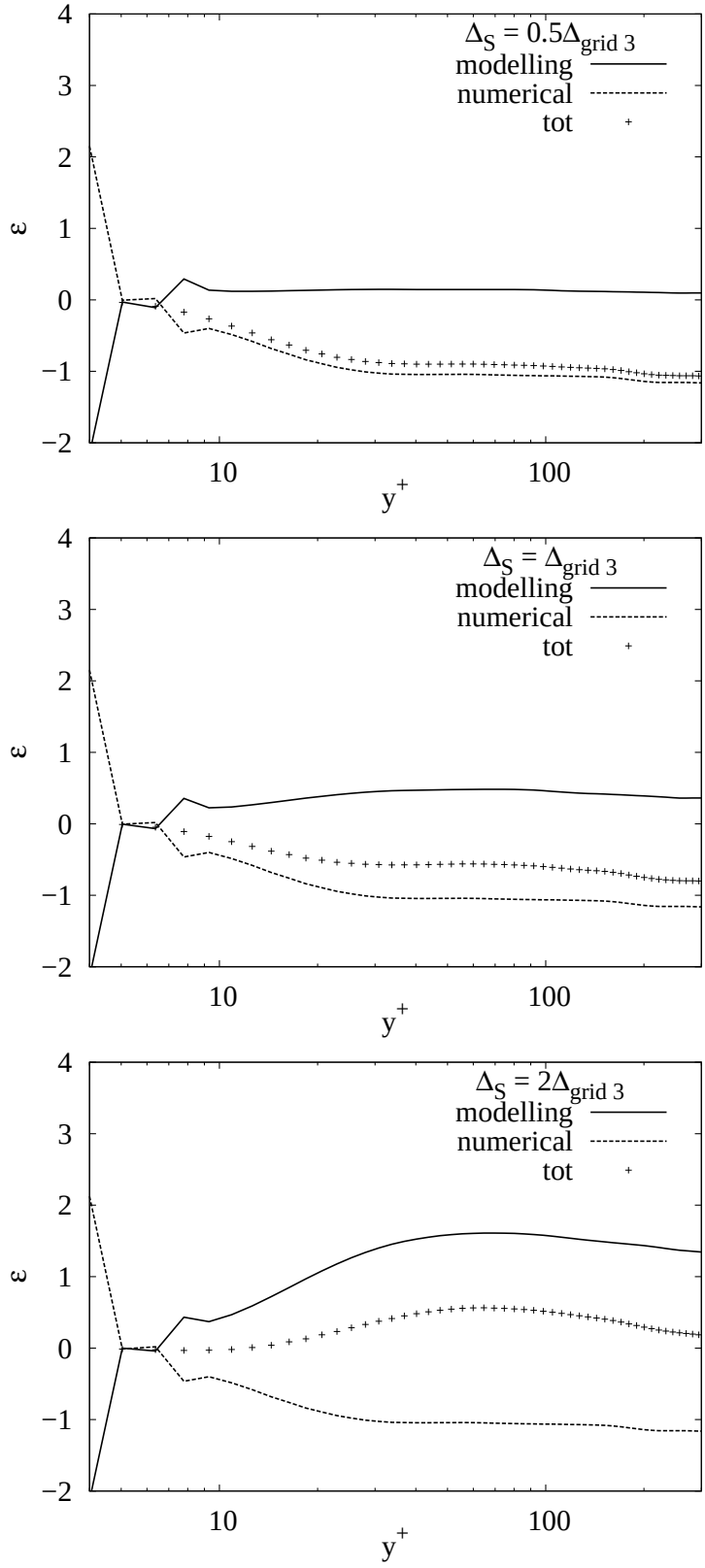

Figure 5.22: Modelling, numerical and total error of mean velocity in grid 3 cases with different model length scales.

5.2.3 Comparison to Tests with Implicit Filtering

One of the clear differences between the approaches of Geurts and Fröhlich (2002) and Klein (2005) is that in Klein's (2005) approach, the numerical error is by definition independent of modelling. In Geurts and Fröhlich's (2002) approach, the definition of the error components allows the control of the numerical error via the model parameters. However, in both the approaches, the modelling error is defined to be independent of numerics.

If we compare the error components obtained with different values of the model length scale using Klein's (2005) approach in Figure 5.21 or in Figure 5.22, we notice that the numerical error is indeed a constant although it was evaluated using the true total error. This indicates that Klein's (2005) definition for the modelling error actually describes the entire effect of the SGS modelling. In Geurts and Fröhlich's (2002) approach, the numerical error was allowed to vary with the model parameters, but the obtained variation in the previous section was rather small.

Similarly, as the numerical error seems to be independent of modelling in Klein's (2005) approach, the modelling error should be independent of numerics, and thus two simulations with different grid resolutions and the same model length scales should have the same modelling error. This, however, does not happen. The cases of grid 2 with $\Delta_S = \Delta_{\text{grid 2}}$ and grid 3 with $\Delta_S = 2\Delta_{\text{grid 3}}$ have the same model length scales, but the modelling error is larger in the grid 3 case. This is a clear difference to the approach of Geurts and Fröhlich (2002), where the modelling error was defined using the grid-independent LES and it was thus independent of grid resolution.

In the previous section in Figure 5.6, we had the error components from the grid 2 case with the model length scale equal to the grid spacing obtained using implicit filtering. If we compare these curves to the ones in the middle sub-figure of Figure 5.21 ($\Delta_S = \Delta_{\text{grid 2}}$), we notice that, despite the differences between the approaches to evaluating the error components, the obtained results for the modelling error are surprisingly close to each other. The modelling error predicted by implicit filtering is only slightly larger than the error predicted by the approach of Klein (2005). Making comparison between the numerical errors is not reasonable, since the numerical error in Figure 5.21 was obtained just as the difference between the true total error and the modelling error. The error components for the grid 2 case with $\Delta_S = 0.5\Delta$ obtained using implicit filtering have been presented in Figure 5.15. When this is compared to the upper sub-figure of Figure 5.21, the modelling errors obtained using the two approaches are again similar. Here, the error obtained using implicit filtering is slightly smaller. This difference is necessary, since the approach using implicit filtering allows the numerical error to change as the model length scale is varied.

5.2.4 Conclusions of Using the Richardson Extrapolation

Klein (2005) proposed the method discussed in this section be used for quality assessment in practical simulations where DNS data or measurements are not necessarily available. In addition, the aim was probably to propose a method that avoids the use of the concept of grid-independent LES. In this section, the method was applied in the same test case as the a posteriori tests using implicit filtering in the previous section. The main new findings were the similarity in the obtained modelling error with the approach of Klein (2005) and with the approach using grid-independent LES and the deficiency of the Richardson extrapolation in predicting the numerical error of LES.

Despite the clear difference between the approaches based on Richardson extrapolation and grid-independent LES, the modelling errors they predicted for the mean-velocity profile were close each other. Thus, also the approach using grid-independent LES gives a modelling error that is of the order Δ_S^2. However, the first term of the Taylor expansion did not describe the modelling error of streamwise Reynolds stress and the Richardson extrapolation did not work for this quantity.

Based on the present results in the channel flow, it seems that the use of the Richardson extrapolation and Klein's (2005) method for the numerical error are not always justified on LES grids. In LES, the smallest resolved flow scales are often of the same size as the grid resolution, and as also pointed out by Klein (2005), practical LES is always grid-dependent. In this case, the numerical method does not necessarily obtain its formal accuracy. Thus, before using this method for error analysis, one should verify that the resolution is actually in the asymptotic range.

5.3 A Posteriori Tests Using Explicit Filtering

5.3.1 Grid-Independent LES Using Explicit Filtering

In Section 5.1, we studied the numerical and modelling error in an LES with no explicit filtering, and in the a posteriori tests implicit filtering was applied to approach the grid-independent LES. In the derivation of the LES equations, there appears a filter, and thus one could ask if the grid-independent LES obtained by fixing the Smagorinsky length scale, as done in Section 5.1, actually approaches an LES solution or something else (Moin 2005). In this section, a posteriori tests are performed using explicit filtering. The aims are firstly to clarify the behaviour noticed with the explicit filtering in Chapter 4, and secondly to study the difference between the approaches to a posteriori testing using implicit and explicit filtering. Since explicit filtering of the non-linear convection term is applied here, the equations being solved are Equations (2.46).

The approach used here for separating the error components uses the grid-independent or fine-grid LES, as did the approach using implicit filtering. The difference is that here explicit filtering, instead of implicit filtering, is applied to approach the grid-independent situation. As the grid resolution is increased, the absolute width of the explicit filter is kept constant, i.e. the ratio of the explicit filter width to the grid spacing increases. A similar approach was also applied by Vreman et al. (1996) and Gullbrand (2002). Since there is no direct connection between the explicit filter and the standard Smagorinsky model, also the model length scale is kept constant when the grid-independent situation is approached. Thus, the only difference between the approaches of this section and Section 5.1 is the use of the explicit filter.

In Chapter 4, we noticed that the explicit filtering itself had a large effect on the simulation results. However, the role of numerical error on those results could not be determined by comparing them to the DNS results. Here, we divide the total simulation error into the numerical and modelling error and into the effect of the filter using the grid-independent LES and so-called filtered DNS as follows:

$$\begin{aligned} \varepsilon_{\text{numerical error}} &= \tilde{u} - \tilde{u}_{\text{grid-indep. LES}} \\ \varepsilon_{\text{modelling error}} &= \tilde{u}_{\text{grid-indep. LES}} - u_{\text{filtered DNS}} \\ \varepsilon_{\text{filtering}} &= u_{\text{filtered DNS}} - u_{\text{DNS}} \end{aligned} \tag{5.8}$$

Here, $\tilde{u}$ refers to an LES solution and u to a DNS solution. By filtered DNS, we mean here a simulation performed at the same resolution as grid-independent LES but with no SGS modelling. Thus, in filtered DNS, the explicit filtering of the non-linear convection term is included in the simulation while SGS modelling is not.

5.3.2 Applied Grid Resolutions

The applied grid resolutions of the base test case (grid 1) and the two finer grids (grid 2, grid 3), which are applied to approximate the grid-independent LES and filtered DNS, are given in Table 5.2. The finest applied grid is somewhat coarser in the streamwise and spanwise directions than the finest grid applied in the study with implicit filtering. However, here the use of explicit filtering makes the grid convergence faster, and the remaining numerical error is thus smaller. As the grid resolution was increased, the extent of the computational domain had to be reduced because the simulations became too heavy. However, at least at smaller resolutions, the flow statistics were not sensitive to the domain lengths.

Table 5.2: Domain size and resolution of the applied LES grids. (x=streamwise, z=spanwise, y=wall-normal direction).

	x	z	y
grid 1			
extent of the domain / channel height	6.0	3.2	1.0
number of grid points	108	108	90
size of the grid cell in wall units (Δ^+)	44	23	1, ..., 20
grid 2			
extent of the domain / channel height	6.0	1.6	1.0
number of grid points	216	108	180
size of the grid cell in wall units (Δ^+)	22	12	0.5, ..., 10
grid 3			
extent of the domain / channel height	3.0	1.6	1.0
number of grid points	162	162	180
size of the grid cell in wall units (Δ^+)	15	8	0.5, ..., 10

wall units: $x^+ = \mathrm{Re}_\tau x$, where x is scaled by the channel half-height.

In the grid 1 case, the applied explicit filter is the same three-dimensional fourth-order commutative filter with the width of two grid spacings which was applied in Chapter 4. On the finer grids, the absolute filter width is kept the same as that of grid 1, which means that the ratio of filter width to the grid spacing, Δ_f/Δ, is larger than in the grid 1 case. On grid 2, the explicit filter width was four grid spacings and on grid 3 six grid spacings in the homogeneous directions and four grid spacings in the wall-normal direction. These filters were discussed in Section 2.2.3, and the transfer functions were depicted in Figure 2.4. Filtering is applied to the non-linear convection term.

To verify that the grid-independent LES actually corresponds to the studied LES on grid 1, the effect of the SGS model on the turbulent shear stress and the energy

spectra were studied. The modelled turbulent shear stress from the different grid resolutions is plotted in Figure 5.23. Here we notice a small difference in the peak value of the stress. Since the product $C_S\Delta_S$ has the same value in each case, this difference must be due to variation in the strain rate tensor (see Equation (2.16)). The definition for the error components, Equation (5.8), allows the numerics to affect the SGS model, and thus we can have numerical error in the SGS model. The difference between the simulations with different resolutions is sufficiently small to be caused by the numerical error. The one-dimensional energy spectra for the streamwise velocity component evaluated in the streamwise direction from the simulations with different resolutions are depicted in Figure 5.24. Here we see that the spectra from the different resolutions coincide. This indicates that the SGS model produces similar damping in all cases. The shape of the spectra at the low frequencies is actually mainly determined by the shape of the filter and the numerics has only a small effect on it. The situation is similar in the middle of the channel and for the spanwise spectra.

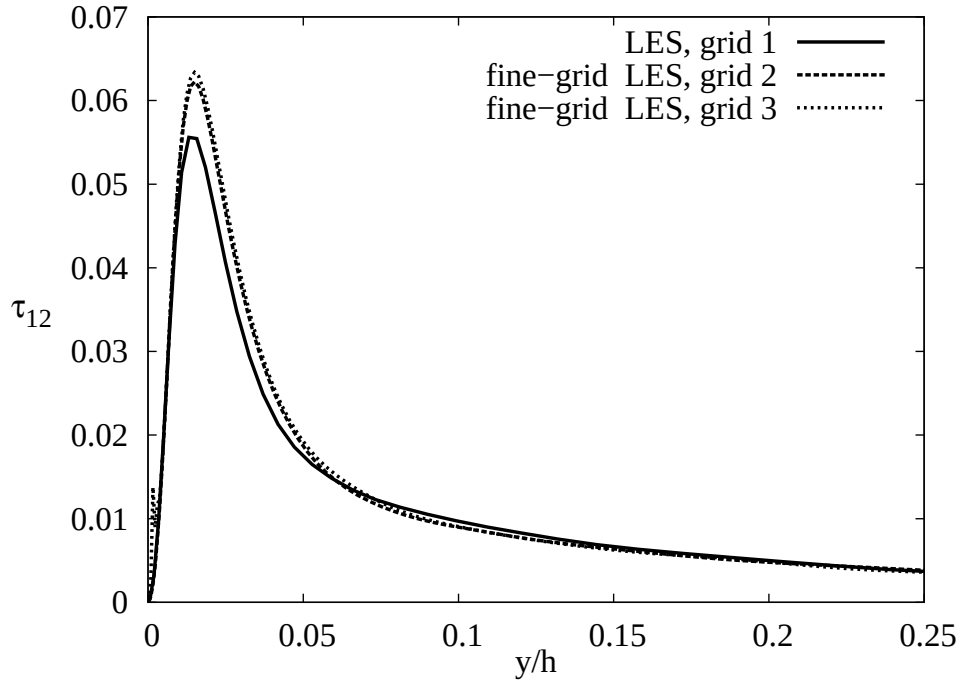

Figure 5.23: Turbulent shear stress from LES with different resolutions.

5.3.3 Error Components and Effect of Filtering

In the upper part of Figure 5.25, we have the mean-velocity profile obtained from simulation on grid 1 and the corresponding finer-grid cases. In addition, the DNS of Moser et al. (1999) and the grid 3 case with filtering but no SGS model, which

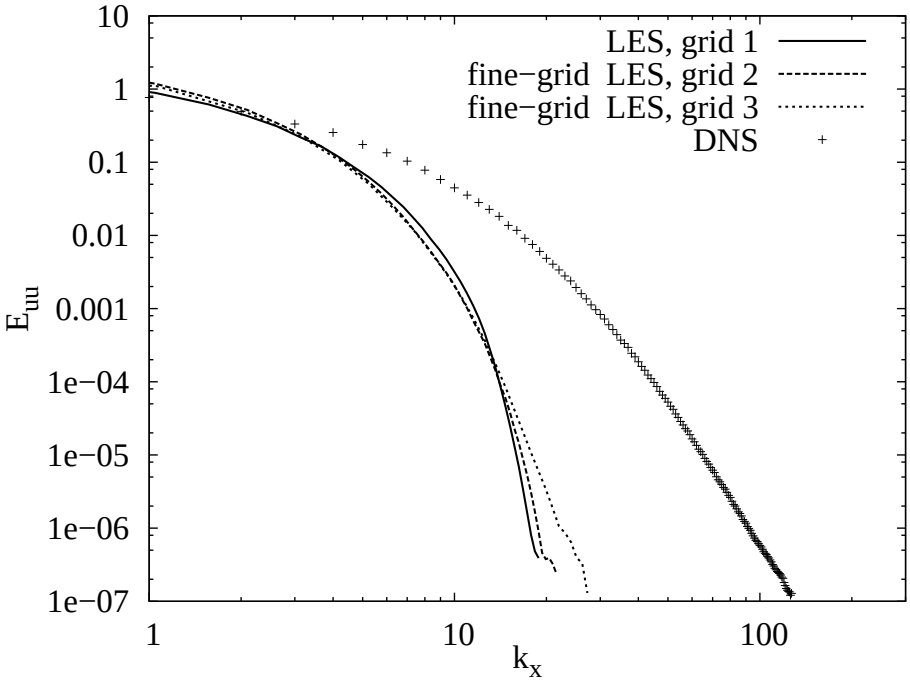

Figure 5.24: One-dimensional streamwise energy spectra of the streamwise velocity component from the near-wall region $y^+ \approx 5$.

approximates a filtered DNS, are included. The difference between grid 2 and grid 3 results is small, and thus the grid 3 result is a fair approximation to grid-independent LES. The error components (5.8) evaluated using these results are depicted in the lower part of the figure. In all the simulations with filtering, the shape of the velocity profile is almost the same, and it differs from the DNS result. Since the change is visible already in the filtered DNS, the shape of the profile is caused by filtering and not by the modelling or numerics. The large effect of filtering is also visible in the lower part of the figure where the effect of filtering is larger than the total simulation error. The difference between the grid 3 case and the filtered DNS is small, which indicates that the effect of SGS modelling is small and this is visible also in the small modelling error. Both the modelling and numerical errors are visible mainly in the mean bulk velocity, and the error components are thus nearly constants in the logarithmic layer. In addition, the numerical and modelling errors are of the opposite sign and they partially cancel out each other.

In Section 5.1 in the study using implicit filtering, similar interaction of the numerical and modelling errors was noticed, and there the numerical and modelling errors were approximately of the same magnitude. In the present results, both the error components are smaller, which is probably partly owing to explicit filtering, since it reduces the effect of the Smagorinsky model, as we saw earlier in

Section 4.3, and partly owing to different resolutions in the wall-normal direction.

In Figure 5.26, the corresponding plots are given for the deviatoric streamwise Reynolds stress. Here, the effect of modelling is even smaller than in the mean-velocity profile, and the greater part of the error is caused by explicit filtering. The numerical error is again of the opposite sign to the modelling error and thus, they partially cancel out each other. The error components are similar for the other diagonal Reynolds stresses. In the study with implicit filtering, the obtained modelling error was larger than here, the distribution of the numerical error somewhat different, and the interaction of the error components was not visible there.

In Section 4.3, it was noticed that as the length scale of the Smagorinsky model is increased, the results with explicit filtering slightly improve. Here, the a posteriori tests are repeated using a model length scale which was set proportional to the filter width, i.e. it has twice the value compared to the first test case discussed above. The plots depicting the mean-velocity profile and the involved error components are given in Figure 5.27. Increasing the model constant naturally increases the effect of modelling compared to the curves of Figure 5.25. In the mean-velocity profile, this is visible in the increased mean bulk velocity and increased thickness of the viscous sublayer. The change in the viscous sublayer also slightly improves the slope of the profile. As the model length scale is increased, the total error in the mean-velocity profile decreases in the middle of channel and in the end of the viscous sublayer. However, in the lower part of the logarithmic layer, it increases. In the lower part of Figure 5.27, we see that this is caused by the interaction of numerical and modelling error. The increased model length scale affects mainly the modelling error. Since the two error components are of the different sign, this leads to decreased total error in some parts of the channel. The effect of the increased model length scale on the numerical error is small, and in some parts of the channel the numerical error even appears to increase slightly when compared to Figure 5.25 although the SGS model should smooth out the resolved flow field. Similar behaviour was also visible in the previous section with implicit filtering.

The corresponding plots for the streamwise deviatoric Reynolds stress are given in Figure 5.28. Here, the grid convergence is not as fast as with the lower model length scale in Figure 5.26. Increasing the model length scale improves the prediction of the peak value of the Reynolds stress, but at the same time, it widens the distribution. This is also visible in the total error which decreases in the near-wall region but increases after the peak of the Reynolds stress compared to the case with the lower model constant in Figure 5.26. However, changes in the total error are mainly caused by the interaction of the numerical and modelling error. Increasing the model length scale increases the effect of modelling and the modelling error, and now, the modelling error is larger than the numerical error, but they are still of different sign. Compared to the case with the smaller model

length scale, the numerical error clearly increases, and the increase is stronger than in the mean-velocity profile. Similar behaviour was noticed in the study with implicit filtering. However, there the numerical error of the Reynolds stress increased, as it should, also when the model length scale was reduced to 0.5Δ.

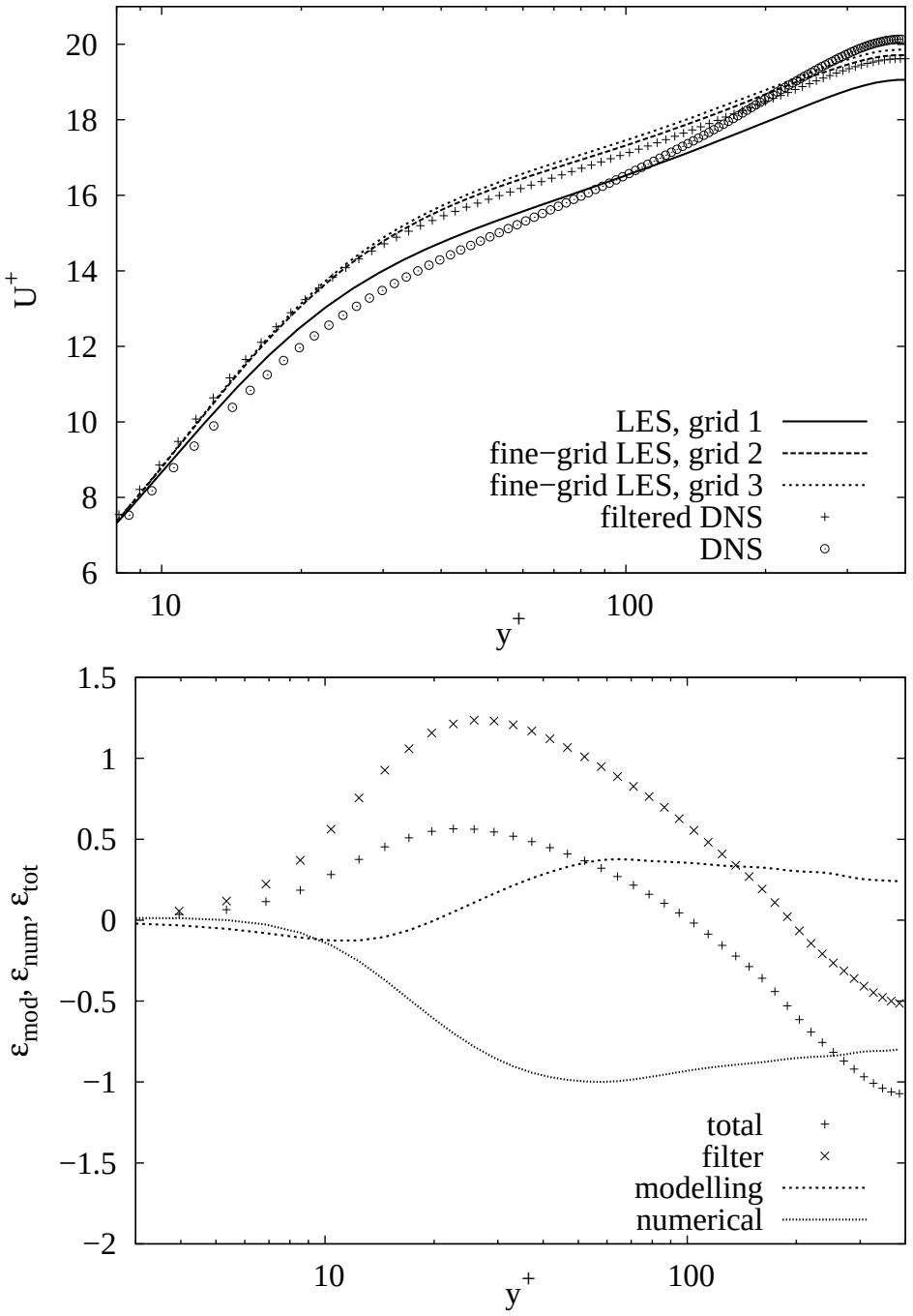

Figure 5.25: Upper: Mean-velocity profile, $\Delta_S = 0.5\Delta_f = \Delta_1$. **Lower:** Error components ΔU^+ related to grid 1 case.

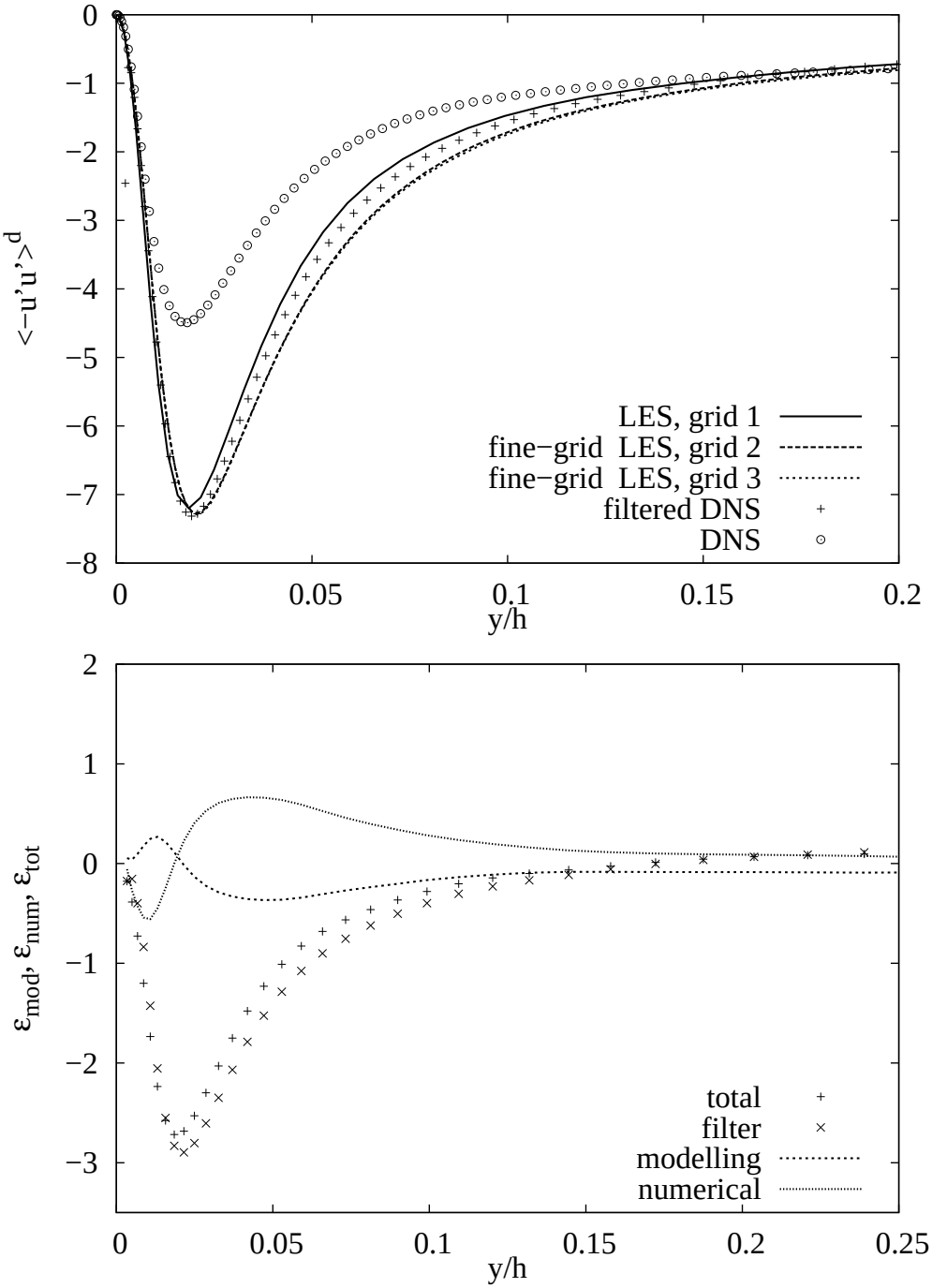

Figure 5.26: Upper: Deviatoric Reynolds stress, $\Delta_S = 0.5\Delta_f = \Delta_1$ **Lower:** Error components related to grid 1 case.

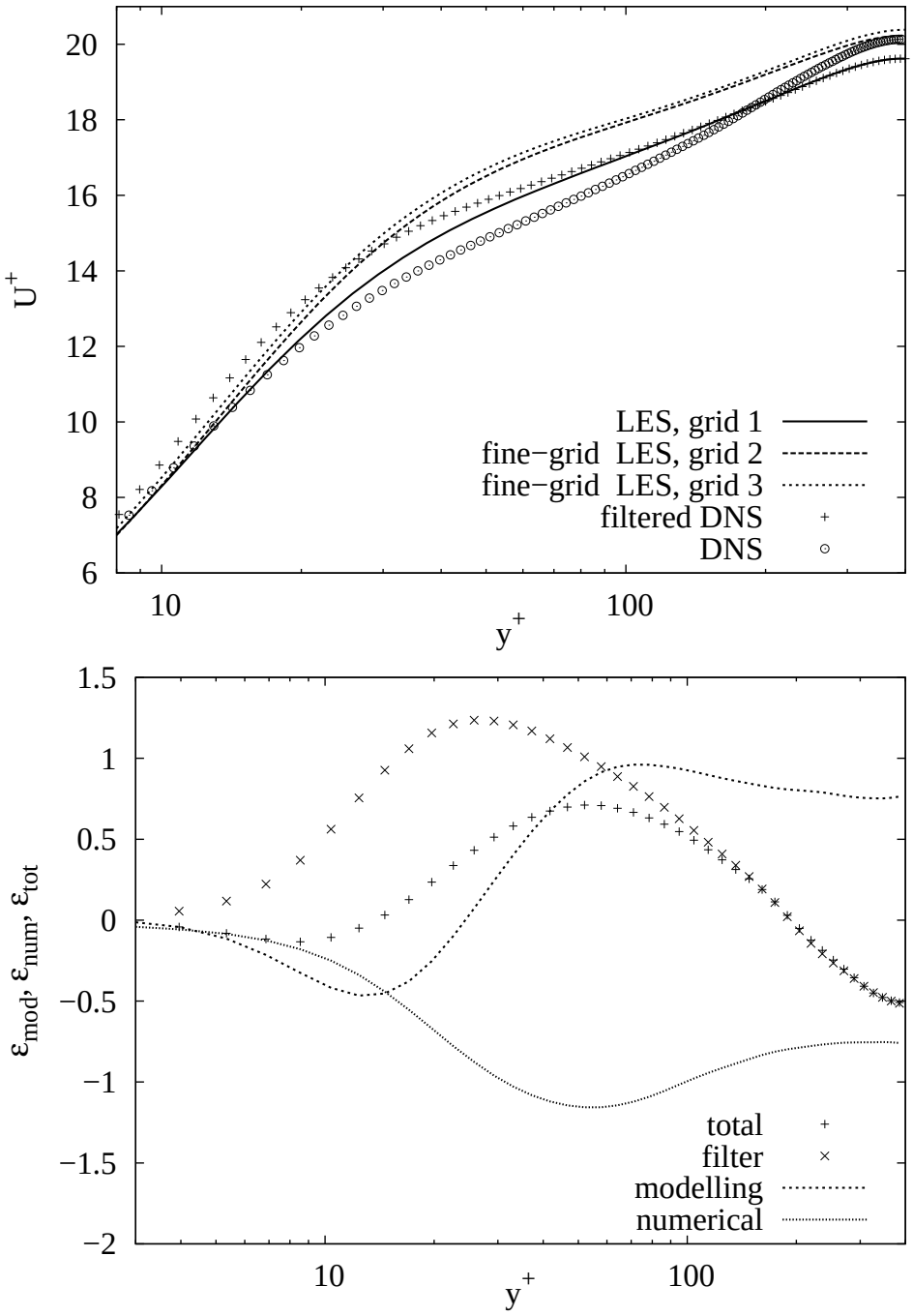

Figure 5.27: Upper: Mean-velocity profile, $\Delta_S = \Delta_f = 2\Delta_1$ **Lower:** Error components related to grid 1 case.

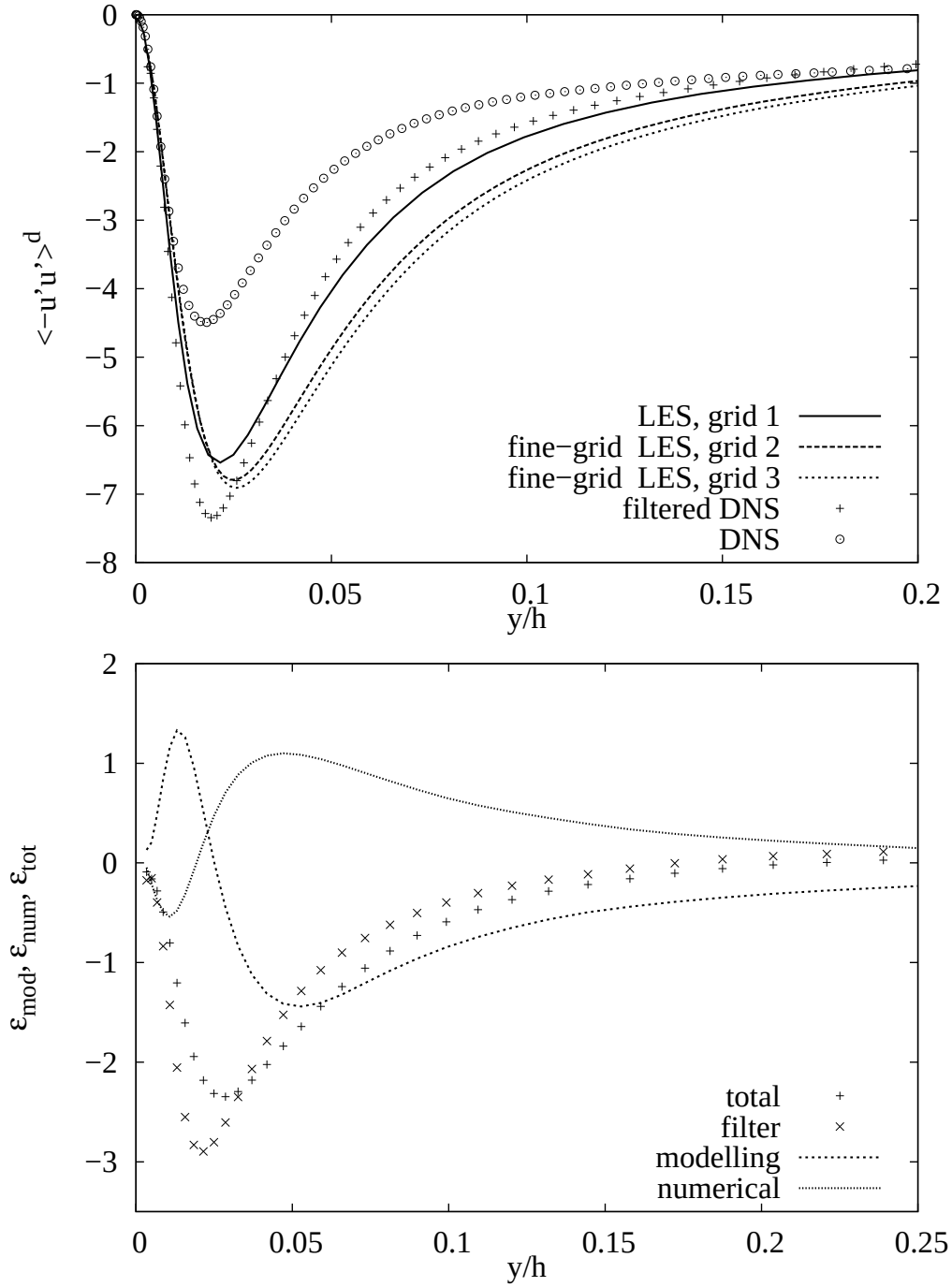

Figure 5.28: Upper: Deviatoric Reynolds stress, $\Delta_S = \Delta_f = 2\Delta_1$ **Lower:** Error components related to grid 1 case.

5.3.4 Conclusions of a Posteriori Studies with Explicit Filtering

In this section, the a posteriori tests were performed using explicit filtering. The main new findings were the large effect of explicit filtering of the non-linear convection term in grid-independent LES, and the similarity between the results of a posteriori tests performed with explicit and implicit filtering. The first finding removes the uncertainty of the effect of numerics in the results of Section 4.3 where this effect was noticed on a normal-resolution LES grid. The second finding verifies that the missing explicit filter in the approach to a posteriori testing using implicit filtering does not make the results unphysical.

The numerical error related to the second-order scheme and the modelling error of the standard Smagorinsky model were approximately of the same size and of different sign. When compared to results obtained with implicit filtering, the results were similar except for the effect of explicit filtering itself. In addition, filtering reduced both error components.

The a posteriori tests were repeated with a larger model length scale. This showed that the slight improvement of simulation results with this model length scale that was noticed in Section 4.3 was caused by the interaction of error components. The increased modelling error cancelled out the numerical error.

In the study with implicit filtering, some increase of numerical error with increasing model length scale was visible in the mean-velocity profile and in the Reynolds stresses, and this trend was noticed also here. This behaviour suggests that in these a posteriori studies, part of the effect of modelling is included in the numerical error as the model length scale is increased.

Chapter 6

Summary and Conclusions

In this thesis, the numerical and modelling error were studied using both a priori and a posteriori testing. These studies were performed using the second-order central-difference scheme and mainly with the standard Smagorinsky model. In addition, the use of explicit filtering and some factors affecting its behaviour, like filter function, model length scale and filtering approach, were studied a priori, in actual simulations and a posteriori. The main results of this thesis can be divided into two groups: differences of the applied error assessment methods, and the applicability of explicit filtering in practical LES and the reasons behind the bad behaviour of filtering.

As noticed also in a priori tests of other authors (Vreman et al. 1994*a*, Ghosal 1996, Chow and Moin 2003), in Chapter 3 we saw that with the second-order discretization, the numerical error appears to be larger than the effect of the SGS terms, and explicit filtering seems a promising approach to decreasing it. The new results in a priori testing of this thesis were related to explicit filtering of the non-linear convection term of the Navier–Stokes equations, and to comparison of this approach to the traditional filtering of the whole velocity field. In the present a priori tests, this approach reduced the numerical error efficiently and it did not lead to unphysical diminishing of the exact SGS term like filtering of the whole velocity field did. Thus, it seemed a promising approach to controlling the numerical error in LES.

In Chapter 4, explicit filtering was applied in an actual LES simulation using the second-order central-difference scheme. The new contributions of this chapter were the demonstration of the large effect of explicit filtering and comparison between different filtering approaches. In contrast to the promising results of the a priori studies, it was noticed that the total error in simulations with explicit filtering was much larger than in simulations without filtering, and increasing the filter width only increased the total error. This behaviour occurred also with the dynamic Smagorinsky model and with the scale-similarity and mixed

models which include a reconstruction for the subfilter-scale stresses. It has been suggested that a filter with the width of four grid spacings should be used together with a second-order scheme (Vreman et al. 1994*a*, Chow and Moin 2003), but in the present simulations, even using the filter with a width of two grid spacings leads to bad simulation results. Gullbrand and Chow (2003) also noticed some difficulties in improving results using explicit filtering, but the results were not as clearly affected by the explicit filtering as the present results.

The simulations with explicit filtering were repeated using no SGS modelling, and it was noticed that the negative effect of filtering was already present in these simulations and the SGS models had a very small effect on the simulation results. Filtering also decreased the effect of SGS modelling. Increasing the model length scale of the Smagorinsky model slightly improved the simulation results compared to the cases with smaller model length scales, but the large negative effect of filtering remained. Even including an SSM model to reconstruct the subfilter scales did not remove the negative effect. In addition, the effect of the chosen filter function was studied, and we saw that the closer the filter was to the spectral cutoff at the low frequencies, the smaller the negative effect was. However, with all the applied filters, the negative effect of filtering was large.

The large effect of explicit filtering was verified in the a posteriori tests of Section 5.3 of Chapter 5. There, the total error was divided into the effect of the filter, numerical error and modelling error. The effect of the filter was clearly larger than the error components also in the grid-independent case, which verifies that the large effect of filtering is not caused by numerics. The effect of increasing the model length scale was also studied a posteriori, and it turned out that the improved results stemmed from the interaction between the two error components. They were of different sign, and when increasing the model length scale increased the modelling error, the total error was diminished. This demonstrates the difficulty of validating the simulation results based on the total error.

The difference between explicit and implicit filtering was studied in Sections 4.3, 4.4 and 4.6. It was noticed that there are some similarities between the effect of a smooth explicit filter and a Smagorinsky model on the large resolved scales. However, explicit filtering damps the high-frequency components more effectively than implicit filtering via a Smagorinsky model. When implicit filtering was included via an SFS model, the simulation results improved. However, also with these models the high-frequency components were not damped, and thus the effect on the numerical error is probably not very large.

The numerical and modelling errors were studied in Chapter 5 using altogether three approaches, two of which were based on using the so-called grid-independent LES and one on the Richardson extrapolation. The main new contributions were the clarification of the differences between these approaches and further explanation of the results of the previous chapter in terms of the error components.

None of the performed a posteriori studies supported the conclusion on the large numerical error predicted by the a priori tests. With all the approaches, the numerical error related to the second-order scheme and the modelling error related to the standard Smagorinsky model were approximately of the same magnitude.

Based on the present results of the a priori and a posteriori tests, one can say that the results of the a priori tests regarding the numerical error are too pessimistic compared to the behaviour of actual simulations or the error components obtained in the a posteriori tests. This same type of overly pessimistic results has been noticed in a priori testing of the SGS stress predicted by different SGS models (Ferziger 1996). In the a priori tests, the interaction of the SGS model and numerics is not included, and probably, to obtain more realistic results with a priori tests, one should approximate the length and the shape of the implicit filter involved with the applied model instead of filtering the DNS data with the filter with a width equal to the LES grid spacing. Clearly, e.g. in the present a priori tests, the resolved flow field predicted from the DNS data was not as smooth as in the actual simulations. However, in many models, such as the standard Smagorinsky, the built-in filter involved with the model is not explicitly defined and thus, predicting its shape or width is not straightforward.

In addition to the pessimistic results for the numerical error, the behaviour of explicit filtering in the a priori tests is too optimistic. The negative effect of filtering with smooth filters is not shown in the a priori tests, and although filtering decreases the numerical error, it also decreases the effect of SGS modelling. This is probably caused by the dynamics of the simulation that cannot be described a priori.

The first applied approach in the a posteriori tests is based on implicit filtering (Geurts and Fröhlich 2002, Meyers et al. 2003). In this approach, the grid resolution is increased while keeping the model length scale constant. It was first verified that the SGS shear stress remains almost constant in this process, and thus the cases with different resolutions and the same model length scale actually correspond to each other and the method is valid.

Besides quantifying the error components in the channel flow, the aim in the present study was to clarify the effect of grid refinement and the model parameters of the standard Smagorinsky model on the error components in the channel flow. Because the smallest resolved scales in LES are of the same size as the grid resolution, increasing the grid resolution does not necessarily decrease the numerical error of all the resolved scales. In addition, it has been noticed that applying an SGS model does not necessarily improve the simulation results (Majander and Siikonen 2002), and the same behaviour was noticed here in the Reynolds stress components. In the a posteriori tests, it was noticed that both varying the grid resolution and model length scale mainly affected the modelling error, which increased rapidly with increasing model length scale. The increasing model length

scale makes the filtering via the model not a feasible approach to control the numerical error. It was also noticed that the combination of the model parameters, which was previously noticed to give good results in the present code, can be interpreted as a compromise between the error components. In situations where applying modelling does not improve the simulation results, the modelling error increases rapidly.

In the second applied approach to a posteriori testing, filtering was applied also explicitly. Including this filtering makes the approach more compatible with the LES equations, where the filter is present, and one aim here was to compare the approaches using implicit and explicit filtering. However, including filtering in the physical space also includes the negative effect of filtering. In the present study, the effect of filtering was separated from the modelling error, and after this the results for numerical and modelling error were similar to the ones obtained with implicit filtering. In both studies, some uncertainty remained in the prediction of the numerical error because of the slow grid convergence of the results. The inconsistent decrease of the numerical error obtained when the model length scale was increased was either owing to this or to definitions of the error components, which does not allow the modelling error to vary with grid resolution.

Klein (2005) criticised the use of the concept of grid-independent LES and proposed a method based on the Richardson extrapolation. However, when this approach was applied to the modelling error of the mean-velocity profile in Section 5.2, similar results as in the a posteriori tests using implicit filtering were obtained and the effect of modelling was approximately of the order of Δ_S^2 in both approaches. Nevertheless, the first term of the Taylor expansion did not explain the behaviour of the modelling error of the streamwise Reynolds stress component. In addition, the use of the Richardson extrapolation was not justified for the numerical error, since the applied grid resolutions were not in the asymptotic range where the numerical method obtains its formal accuracy. Thus, before applying this approach to error assessment of LES, one should verify that the applied grid resolution is sufficient for this approach. The possibilities for obtaining LES results from the asymptotic range does not seem straightforward, since the smallest resolved scales are always of the same size as the grid resolution, and practical LES is always grid-dependent. In Section 2.4, we saw that even obtaining DNS results from the asymptotic range requires rather high resolution.

Based on the present study, the most reliable approaches to error assessment in LES are a posteriori tests where grid-independent LES is applied. These approaches are only applicable when DNS results and fine-grid LES are available, and thus they cannot be applied directly to error assessment in complex geometries or at high Reynolds numbers. However, results of tests performed in simpler test cases can be used to interpret the behaviour of total error in a more complex application.

References

Amiri, A. E., Hannani, S. K. and Mashayek, F. (2005), 'Evaluation of a fourth-order finite-volume compact scheme for LES with explicit filtering', *Numerical Heat Transfer, Part B* **48**, 147–163.

Bardina, J., Ferziger, J. H. and Reynolds, W. C. (1980), 'Improved subgrid scale models for large eddy simulation', *AIAA-80-1357* .

Bogey, C. and Bailly, C. (2005), 'Decrease of the effective Reynolds number with eddy-viscosity subgrid-scale modeling', *AIAA Journal* **43**(2), 437–439.

Bogey, C. and Bailly, C. (2006), 'Large eddy simulations of round free jets using explicit filtering with/without dynamic Smagorinsky model', *International Journal of Heat and Fluid Flow* **27**, 603–610.

Brandt, T. (2004), Studies on numerical errors in large eddy simulation, Licentiate's thesis, Helsinki University of Technology. ISBN 951-22-7192-3.

Brandt, T. (2006*a*), 'A priori tests on numerical errors in large eddy simulation using finite differences and explicit filtering', *International Journal for Numerical Methods in Fluids* **51**(6), 635–657. Published Online: 20 Dec 2005.

Brandt, T. (2007), *A posteriori* study on modelling and numerical error in LES applying the Smagorinsky model, *in* S. Kassinos, C. Langer, G. Iaccarino and P. Moin, eds, 'Complex Effects in Large Eddy Simulations', Vol. 56 of *Lecture Notes in Computational Science and Engineering*, Springer, pp. 185–202. ISBN: 978-3-540-34233-5.

Brandt, T. T. (2006*b*), Study of large eddy simulation and Smagorinsky model using explicit filtering, *in* '36th AIAA Fluid Dynamics Conference and Exhibit', San Francisco, California. AIAA-2006-3541.

Brandt, T. T. (2006*c*), Study on numerical and modelling error in LES of a channel flow using explicit filtering, *in* H. Deconinck and E. Dick, eds, 'Computational Fluid Dynamics 2006: Proceedings of the Fourth International Conference on Computational Fluid Dynamics', ICCFD4, Springer. To appear.

Brandt, T. T. (2006*d*), Use of explicit filtering, second-order scheme and SGS models in LES of turbulent channel flow, *in* P. Wesseling, Y. Oñate and J. Périaux, eds, 'European Conference on Computational Fluid Dynamics', ECCOMAS CFD 2006, Egmond aan Zee, The Netherlands.

Brandt, T. T. (2006*e*), Use of Richardson extrapolation in error estimation of LES, *in* O. Dahlblom, L. Fuchs, K. Persson, M. Ristimaa, G. Sandberg and I. Svensson, eds, 'Proceedings of the 19th Nordic Seminar on Computational Mechanics', Lund, Sweden, pp. 143–146.

Brethouwer, G. (2002). Private communication.

Carati, D., Winckelmans, G. S. and Jeanmart, H. (2001), 'On the modelling of the subgrid-scale and filtered-scale stress tensors in large-eddy simulation', *Journal of Fluid Mechanics* **441**, 119–138.

Celik, I. B., Cehreli, Z. N. and Yavuz, I. (2005), 'Index of resolution quality for large eddy simulations', *Journal of Fluids Engineering* **127**, 949–958.

Celik, I., Li, J., Hu, G. and Shaffer, G. (2005), 'Limitations of Richardson extrapolation and some possible remedies', *Journal of Fluids Engineering* **127**, 795–805.

Chow, F. K. and Moin, P. (2003), 'A further study of numerical errors in large-eddy simulations', *Journal of Computational Physics* **184**, 366–380.

Clark, R. A., Ferziger, J. H. and Reynolds, W. C. (1979), 'Evaluation of subgrid-scale models using an accurately simulated turbulent flow', *Journal of Fluid Mechanics* **91**, 1–16.

Deardorff, J. (1970), 'A numerical study of three-dimensional turbulent channel flow at large Reynolds numbers', *Journal of Fluid Mechanics* **41**(Part 2), 453–480.

Eggels, J. G. M., Unger, F., Weiss, M. H., Westerweel, J., Adrian, R. J., Friedrich, R. and Nieuwstadt, F. T. M. (1994), 'Fully developed turbulent pipe flow: a comparison between direct numerical simulation and experiment', *Journal of Fluid Mechanics* **268**, 175–209.

Ferziger, J. H. (1996), Large eddy simulation, *in* T. Gatski, M. Y. Hussain and J. Lumley, eds, 'Simulation and modeling of turbulent flows', Oxford University Press, New York (NY).

Ferziger, J. H. and Peric, M. (1999), *Computational methods for fluid dynamics*, 2 edn, Springer.

Germano, M. (1986), 'A proposal for a redefinition of the turbulent stresses in the filtered Navier–Stokes equations', *Physics of Fluids* **29**(7), 2323–2324.

Germano, M. (1992), 'Turbulence: the filtering approach', *Journal of Fluid Mechanics* **238**, 325–336.

Germano, M., Piomelli, U., Moin, P. and Cabot, W. H. (1991), 'A dynamic subgrid-scale eddy viscosity model', *Physics of Fluids A* **3**(7), 1760–1765.

Geurts, B. J. and Fröhlich, J. (2002), 'A framework for predicting accuracy limitations in large-eddy simulation', *Physics of Fluids* **14**(6), L41–L44.

Ghosal, S. (1996), 'An analysis of numerical errors in large-eddy simulations of turbulence', *Journal of Computational Physics* **125**, 187–206.

Ghosal, S. and Moin, P. (1995), 'The basic equations for the large eddy simulation of turbulent flows in complex geometry', *Journal of Computational Physics* **118**, 24–37.

Gullbrand, J. (2001), 'Explicit filtering and subgrid-scale models in turbulent channel flow', *Center for Turbulence Research, Annual Research Briefs* pp. 31–42. Stanford University.

Gullbrand, J. (2002), 'Grid-independent large-eddy simulation in turbulent channel flow using three-dimensional explicit filtering', *Center for Turbulence Research, Annual Research Briefs* pp. 167–179. Stanford University.

Gullbrand, J. (2004), 'Dynamic modeling in large-eddy simulation of turbulent channel flow, investigation of two-dimensional versus three-dimensional test filtering', *International Journal of Numerical Methods for Heat & Fluid Flow* **14**(4), 467–492.

Gullbrand, J. and Chow, F. K. (2003), 'The effect of numerical errors and turbulence models in large-eddy simulations of channel flow, with and without explicit filtering', *Journal of Fluid Mechanics* **495**, 323–341.

Harlow, F. H. and Welch, J. E. (1965), 'Numerical calculation of time-dependent viscous incompressible flow of fluid with free surface', *Physics of Fluids* **8**(12), 2182–2189.

Jiménez, J. (2003), 'Computing high-Reynolds-number turbulence: will simulations ever replace experiments?', *Journal of Turbulence* **4**.

Klein, M. (2005), 'An attempt to assess the quality of large eddy simulations in contex of implicit filtering', *Flow, Turbulence and Combustion* **75**, 131–147.

Kravchenko, A. G. and Moin, P. (1997), 'On the effect of numerical errors in large eddy simulations of turbulent flows', *Journal of Computational Physics* **131**, 310–322.

Kreyszig, E. (1993), *Advanced Engineering Mathematics*, 7 edn, Wiley.

Leonard, A. (1974), 'Energy cascade in large-eddy simulations of turbulent fluid flows', *Advances in Geophysics A* **18**, 237–299.

Lilly, D. K. (1992), 'A proposed modification to the Germano subgrid-scale closure method', *Physics of Fluids A* **4**(3), 633–635.

Liu, S., Meneveau, C. and Katz, J. (1994), 'On the properties of similarity subgrid-scale models as deduced from measurements in a turbulent jet', *Journal of Fluid Mechanics* **275**, 83–119.

Lund, T. S. (1997), 'On the use of discrete filters for large eddy simulation', *Center for Turbulence Research, Annual Research Briefs* pp. 83–95. Stanford University.

Lund, T. S. and Kaltenbach, H.-J. (1995), 'Experiments with explicit filtering for LES using a finite-difference method', *Center for Turbulence Research, Annual Research Briefs* pp. 91–105. Stanford University.

Lundbladh, A., Berlin, S., Skote, M., Hildings, C., Choi, J., Kim, J. and Henningson, D. (1999), An efficient spectral method for simulation of incompressible flow over a flat plate, Technical Report 11, Royal Institute of Technology, Department of Mechanics, Stockholm, Sweden.

Magnient, J.-C. and Sagaut, P. (2001), 'A study of built-in filter for some eddy viscosity models in large-eddy simulation', *Physics of Fluids* **13**(5), 1440–1449.

Mahesh, K., Constantinescu, G. and Moin, P. (2004), 'A numerical method for large-eddy simulation in complex geometries', *Journal of Computational Physics* **197**, 215–240.

Majander, P. and Siikonen, T. (2002), 'Evaluation of Smagorinsky-based subgrid-scale models in a finite-volume computation', *International Journal for Numerical Methods in Fluids* **40**, 735–774.

Majander, P. and Siikonen, T. (2004), Large-eddy simulation of a round jet in a crossflow, *in* P. Neittaanmäki, T. Rossi, K. Majava and O. Pironneau, eds, 'European Congress on Computational Methods in Applied Sciences and Engineering', ECCOMAS 2004, Jyväskylä, Finland.

Mason, P. and Callen, N. (1986), 'On the magnitude of the subgrid-scale eddy coefficient in large-eddy simulations of turbulent channel flow', *Journal of Fluid Mechanics* **162**, 439–462.

Mathew, J., Foysi, H. and Friedrich, R. (2006), 'A new approach to LES based on explicit filtering', *International Journal of Heat and Fluid Flow* **27**, 594–602.

Mathew, J., Lechner, R., Foysi, H., Sesterhenn, J. and Friedrich, R. (2003), 'An explicit filtering method for large-eddy simulation of compressible flows', *Physics of Fluids* **15**(8), 2279–2289.

Meyers, J., Geurts, B. J. and Baelmans, M. (2003), 'Database analysis of errors in large-eddy simulation', *Physics of Fluids* **15**(9), 2740–2755.

Meyers, J., Geurts, B. J. and Baelmans, M. (2005), 'Optimality of the dynamic procedure for large-eddy simulation', *Physics of Fluids* **17**.

Moin, P. (2005). Private communication.

Moin, P. and Kim, J. (1980), 'On the numerical solution of time-dependent viscous incompressible fluid flows involving solid boundaries', *Journal of Computational Physics* **35**, 381–392.

Moin, P. and Kim, J. (1982), 'Numerical investigation of turbulent channel flow', *Journal of Fluid Mechanics* **118**, 341–377.

Moin, P. and Mahesh, K. (1998), 'Direct numerical simulation: A tool in turbulence research', *Annual Reviews of Fluid Mechanics* **30**, 539–578.

Morinishi, Y., Lund, T. S., Vasilyev, O. V. and Moin, P. (1998), 'Fully conservative higher order finite difference schemes for incompressible flow', *Journal of Computational Physics* **143**, 90–124.

Moser, R. D., Kim, J. and Mansour, N. N. (1999), 'Direct numerical simulation of turbulent channel flow up to $\mathrm{Re}_\tau = 590$', *Physics of Fluids* **11**(4), 943–945.

Muschinski, A. (1996), 'A similarity theory of locally homogeneous and isotropic turbulence generated by a Smagorinsky-type LES', *Journal of Fluid Mechanics* **325**, 239–260.

Najjar, F. M. and Tafti, D. K. (1996), 'Study of discrete test filters and finite difference approximations for the dynamic subgrid-scale model', *Physics of Fluids* **8**(4), 1076–1088.

Orszag, S. A. (1969), 'Numerical methods for the simulation of turbulence', *Physics of Fluids* **12**(12), II–250–II–257.

Piomelli, U., Moin, P. and Ferziger, J. H. (1988), 'Model consistency in large eddy simulation of turbulent channel flow', *Physics of Fluids* **31**(7), 1884–1891.

Piomelli, U., Zang, T. A., Speziale, C. G. and Hussaini, M. Y. (1990), 'On the large-eddy simulation of transitional wall-bounded flows', *Physics of Fluids A* **2**(2).

Pope, S. T. (2000), *Turbulent flows*, Cambridge University Press.

Rogallo, R. S. and Moin, P. (1984), 'Numerical simulation of turbulent flows', *Annual Reviews in Fluid Mechanics* **16**, 99–137.

Sagaut, P. (2001), *Large eddy simulation for incompressible flows*, Springer.

Schumann, U. (1975), 'Subgrid scale model for finite-difference simulations of turbulent flows in plane channels and annuli', *Journal of Computational Physics* **18**, 376–404.

Smagorinsky, J. S. (1963), 'General circulation experiments with the primitive equations, part I: The basic experiment', *Monthly Weather Review* **91**, 99–152.

Stolz, S., Adams, N. A. and Kleiser, L. (2001), 'An approximate deconvolution model for large-eddy simulation with application to incompressible wall-bounded flows', *Physics of Fluids* **13**(4), 997–1015.

Tennekes, H. and Lumley, J. (1972), *A First Course on Turbulence*, 8 edn, The MIT Press.

van der Bos, F. and Geurts, B. J. (2005), 'Lagrangian dynamics of commutator errors in large-eddy simulation', *Physics of Fluids* **17**.

Vasilyev, O. V., Lund, T. S. and Moin, P. (1998), 'A general class of commutative filters for LES in complex geometries', *Journal of Computational Physics* **146**(1), 82–104.

Visbal, M. R. and Rizzetta, D. P. (2002), 'Large-eddy simulation on curvilinear grids using compact differencing and filtering schemes', *Journal of Fluids Engineering* **124**, 836–847.

Vreman, B., Geurts, B. and Kuerten, H. (1994*a*), 'Discretization error dominance over subgrid terms in large eddy simulation of compressible shear layers in 2D', *Communications in Numerical Methods in Engineering* **10**, 785–790.

Vreman, B., Geurts, B. and Kuerten, H. (1994*b*), 'On the formulation of the dynamic mixed subgrid-scale model', *Physics of Fluids* **6**(12), 4057–4059.

Vreman, B., Geurts, B. and Kuerten, H. (1995), 'A priori tests of large eddy simulation of the compressible plane mixing layer', *Journal of Engineering Mathematics* **29**, 299–327.

Vreman, B., Geurts, B. and Kuerten, H. (1996), 'Comparison of numerical schemes in large-eddy simulation of the temporal mixing layer', *International Journal for Numerical Methods in Fluids* **22**, 297.

Vreman, B., Geurts, B. and Kuerten, H. (1997), 'Large-eddy simulation of the turbulent mixing layer', *Journal of Fluid Mechanics* **339**, 357–390.

Winckelmans, G. S., Jeanmart, H. and Carati, D. (2002), 'On the comparison of turbulence intensities from large-eddy simulation with those from experiment or direct numerical simulation', *Physics of Fluids* **14**(5), 1809–1811.

Winckelmans, G. S., Wray, A. A., Vasilyev, O. V. and Jeanmart, H. (2001), 'Explicit-filtering large-eddy simulation using the tensor-diffusivity model supplemented by a dynamic Smagorinsky term', *Physics of Fluids* **13**(5), 1385–1403.

Zang, Y., Street, R. L. and Koseff, J. (1993), 'A dynamic mixed model and its application to turbulent recirculating flows', *Physics of Fluids A* **5**(12), 3186–3196.

ISBN 978-951-22-8634-8
ISBN 978-951-22-8635-5 (PDF)
ISSN 1795-2239
ISSN 1795-4584 (PDF)